INFORMATION TO USERS

This manuscript has been reproduced from the microfilm master. UMI films the text directly from the original or copy submitted. Thus, some thesis and dissertation copies are in typewriter face, while others may be from any type of computer printer.

The quality of this reproduction is dependent upon the quality of the copy submitted. Broken or indistinct print, colored or poor quality illustrations and photographs, print bleedthrough, substandard margins, and improper alignment can adversely affect reproduction.

In the unlikely event that the author did not send UMI a complete manuscript and there are missing pages, these will be noted. Also, if unauthorized copyright material had to be removed, a note will indicate the deletion.

Oversize materials (e.g., maps, drawings, charts) are reproduced by sectioning the original, beginning at the upper left-hand corner and continuing from left to right in equal sections with small overlaps. Each original is also photographed in one exposure and is included in reduced form at the back of the book.

Photographs included in the original manuscript have been reproduced xerographically in this copy. Higher quality 6" x 9" black and white photographic prints are available for any photographs or illustrations appearing in this copy for an additional charge. Contact UMI directly to order.

UMI

A Bell & Howell Information Company
300 North Zeeb Road, Ann Arbor MI 48106-1346 USA
313/761-4700 800/521-0600

THE UNIVERSITY OF OKLAHOMA

GRADUATE COLLEGE

PART I. KINETIC STUDIES OF THE COMPLEXATION REACTIONS OF NICKEL(II) WITH HYDROXAMIC ACIDS IN AQUEOUS MEDIUM

PART II. KINETIC STUDIES OF THE FORMATION AND DISSOCIATION REACTIONS OF IONOMYCIN AND 2,6-DIMETHYLHEPTANE-3,5-DIONE WITH NICKEL(II) AND MAGNESIUM(II) IN 80% METHANOL-WATER MEDIUM

A DISSERTATION SUBMITTED TO THE GRADUATE FACULTY

in partial fulfillment of the requirements for the

degree of

DOCTOR OF PHILOSOPHY

BY

NEERAJ KHANNA

Norman, Oklahoma

1997

PART I. KINETIC STUDIES OF THE COMPLEXATION REACTIONS OF NICKEL(II) WITH HYDROXAMIC ACIDS IN AQUEOUS MEDIUM

PART II. KINETIC STUDIES OF THE FORMATION AND DISSOCIATION REACTIONS OF IONOMYCIN AND 2,6-DIMETHYLHEPTANE-3,5-DIONE WITH NICKEL(II) AND MAGNESIUM(II) IN 80% METHANOL-WATER MEDIUM

A DISSERTATION

APPROVED FOR THE DEPARTMENT OF CHEMISTRY AND BIOCHEMISTRY

BY

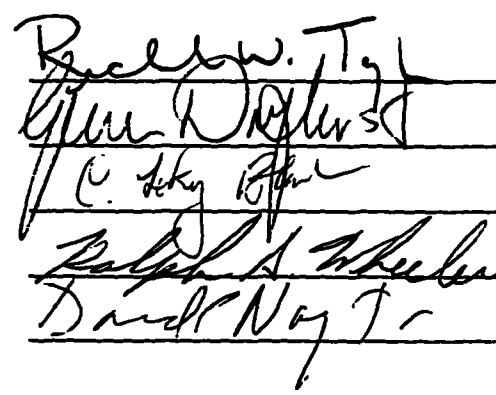

ACKNOWLEDGMENTS

This project was possible with the direct and indirect help of a great many people. Foremost, I would like to express my sincere gratitude to my research advisor Dr. Richard W. Taylor, who provided the essential motivation required to drive this project. I appreciate his guidance, which shaped this project and helped me avoid pitfalls. He taught me to think like a scientist and helped me to discover talents which had before been hidden. I would also like to thank the other members of my graduate committee, Drs. L. C. Blank, G. Dryhurst, D. Nagle and R. W. Wheeler for their valuable suggestions and encouragement, and their cooperation in scheduling committee meetings.

Analytical Services provided vital help with this project. I thank, Dr. Eric Enwall for his meticulous training on the 500 MHz NMR machine, John Laing for doing the preliminary work on the hydroxamic acid project, Tom Karns for his expertise as a mass spectroscopist, and Allen Rees for helping resolve problems in data transfer from one operating system to another.

I am grateful for the financial assistance from the Department of Chemistry and Biochemistry in the form of teaching assistantship. Part of the hydroxamic acid project was funded by the University of Oklahoma. The funding for the ionomycin project was provided by the National Institutes of Health.

All my labmates are to be commended for providing a congenial working environment in the lab, and for making my stay at OU a memorable and enjoyable experience. I am indebted to Laura Haley and Kay Bjornen for helping me believe in myself in moments of crisis, and for enlightening me on American culture.

Carlos Rodriguez deserves special thanks for graciously helping me with computer problems. I would also like to acknowledge Drs. Tim Thomas, Don Simmons and Dorota Inerowicz for the insight I obtained from their work and the possibilities they helped me see.

Last, but certainly not the least, I would like to thank my parents whose unconditional love and care, throughout my life, has supported and encouraged me in this endeavor. They gave me the greatest gift parents can give a child, which is the confidence to believe in myself and my dreams. I love them very much and could never have accomplished this degree without their influence and faith.

TABLE OF CONTENTS

CHAPTER page

PART II. Complexation Reactions of Ionomycin with Divalent Metal Ions

LIST OF TABLES

Page

Page

Page

LIST OF ILLUSTRATIONS

Page

Page

Page

Page

Page

LIST OF ABBREVIATIONS

BHA	Benzohydroxamic acid
PNBHA	*para*-nitrobenzohydroxamic acid
PMBHA	*para*-methoxybenzohydroxamic acid
1-NHA	1-Naphthohydroxamic acid
N-PBHA	*N*-phenylbenzohydroxamic acid
t-CHA	*trans*-Cinnamoylhydroxamic acid
DMHD	2,6-Dimethyl-3,5-heptanedione
TEAP	Tetraethylammonium perchlorate
MES	4-Morpholinoethanesulphonic acid
HEPES	4-(2-hydroxyethyl)-1-piperazineethanesulphonic acid
EPPS	4-(2-hydroxyethyl)-1-piperazinepropanesulfonic acid
CHES	2-(cyclohexylamino)ethanesulphonic acid
PIPES	1,4-piperazinebis-(ethanesulphonic acid)
TEEDA	*N,N,N'N'*-Tetraethylethylenediamine
TEPDA	*N,N,N'N'*-Tetraethylpropanediamine

ABSTRACT

Two biologically relevant systems have been explored that involve the reactions of divalent metal ions with multidentate ligands that coordinate through oxygen atoms. The first part of the study involved kinetic investigations of the reactions of nickel(II) with a variety of hydroxamic acids ($R_1C(O)N(OH)R_2$) with different steric and electronic properties where, R_1=C_6H_5, 4-$NO_2C_6H_4$, 4-$CH_3OC_6H_4$, *trans*-C_6H_5CH=CH, 1-$C_{10}H_7$; R_2=H and R_1=R_2=C_6H_5. These reactions were studied in aqueous medium using the stopped-flow technique. The kinetic data is consistent with a mechanism in which the protonated and unprotonated forms of the ligands react with Ni(II) by a parallel path mechanism. The rate constants for these pathways are reported.

The second part of the study involved the reactions of nickel(II) and magnesium(II), with the ionophore ionomycin and the model compound 2,6-dimethyl-3,5-heptanedione (DMHD). A detailed analysis of the kinetic data for these reactions required information about the keto-enol isomerism exhibited by these ligands. These studies were conducted using NMR spectroscopy, pH-jump and rapid dilution experiments. It was observed that the keto-enol interconversion of ionomycin and DMHD is catalyzed by buffers. The buffer independent rate constants for the enolization and ketonization for ionomycin are approximately two orders of magnitude higher than those of DMHD. An intramolecular base-catalyzed mechanism is proposed for the isomerization of ionomycin. The enol/keto ratios for ionomycin and DMHD were determined to be 7.33 and 2.84, respectively, from the NMR experiments. The kinetic data obtained for the reactions of ionomycin and DMHD with Ni(II) is consistent with a mechanism in which the enol form of the ligand reacts with the metal ion. The formation

reactions of ionomycin with Mg(II) in presence of buffers proceed by a mechanism in which a protonated metal-ligand precursor complex is formed. These reactions are catalyzed by the basic form of the buffers. The dissociation of the Mg(II)-ionomycin complex is catalyzed by the acid form of the buffer.

CHAPTER I

INTRODUCTION

Research in the field of bio-inorganic chemistry has significantly contributed to the understanding of the biological processes. The primary impetus behind the growth in this area of research has been the need to understand the metal-ligand interactions of biological importance. In the study reported here, we have attempted to explore two biologically relevant systems involving the reactions of divalent metal ions with multidentate ligands that coordinate through oxygen atoms. Chapters I to IV present the first part of the study, investigations of the reactions of a variety of hydroxamic acids with nickel(II).

The coordination chemistry of nickel has recently attracted a lot of attention because of the recognition of nickel as an essential trace element for animals, plants and bacteria.[1-3] Deficiency of nickel in animals results in complications such as growth depression, anemia, liver malfunction and impaired reproduction.[4] Nickel deprivation in plants, results in the necrosis of leaflet tips due to urea accumulation.[5] Four bacterial and plant enzymes have been found to be nickel dependent;[6] they are: methyl-S-coenzyme-M methylreductase, carbon monoxide dehydrogenase, hydrogenase and urease. These enzymes contain nickel atoms at their active sites. Significant efforts have been made to understand how the different ligand environments, coordination geometries, and oxidation states of the nickel atoms in these enzyme active sites facilitate the catalysis of a wide range of reactions.[3] Attempts have been made towards synthetic modeling of the active sites of the nickel-containing enzymes.[7]

Designing inhibitors for the nickel-containing enzymes, is another area of considerable practical interest.[8-12] Hydroxamic acids are a group of compounds that serve as efficient inhibitors for these enzymes. Fundamental understanding of the process of complex formation between Ni(II) and hydroxamic acids will facilitate the development of efficient inhibitors. Furthermore, this information will also be helpful in understanding the mechanism of metal chelation by naturally occurring hydroxamic acids in biological systems.[13] The study reported here was performed with the objective to elucidate the complexation mechanism of hydroxamic acids with Ni(II).

A. General Background on Hydroxamic Acids

Hydroxamic acids are the N-acyl derivatives of hydroxylamine that were first reported by Lossen in 1869.[14] The general structure of these compounds is shown in Figure 1.1.

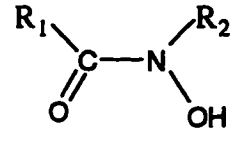

Figure 1.1. Hydroxamic acid with substituents R_1 and R_2.

The substituents R_1 and R_2 can be varied to obtain a wide variety of these compounds offering different steric, electronic and acid/base properties. Hydroxamic acids behave as weak organic acids and can form complexes with a variety of transition metals. Because of their complexing abilities, numerous applications of these compounds were developed in the field of analytical chemistry.[15,16] These compounds exhibit large signal changes on complexation with the metal ions and therefore, they serve as excellent ligands for

probing the environment and the function of metal ions that are located in the active site of an enzyme.[17]

i) Isomers of hydroxamic acids

Hydroxamic acids contain carbonyl and hydroxylamine functionalities present adjacent to each other. There are several possibilities for these compounds to form different kinds of isomers. When there is no substitution of the proton adjacent to the nitrogen, there is a possibility for the hydroxamic acids to exhibit keto/enol tautomerism. Furthermore, when the rotation about the C-N bond is restricted, the keto forms of hydroxamic acids can exhibit geometrical isomerism (also referred to as *cis-trans* isomerism). Figure 1.2 summarizes the various possibilities for the isomerization of hydroxamic acids.[18] The assignment of geometrical isomers is based on *E* and *Z* system. According to this system, if both the oxygen atoms are on the same side of the C-N bond, the isomer is designated as *Z*; conversely, if the oxygen atoms are on the opposite sides of the C-N bond, the isomer is designated as *E*.

The presence of *E* and *Z* isomers has been detected experimentally. For acetohydroxamic acid, *Z*- and *E*- forms exist in a ratio of 10:1 in DMSO. This conclusion was made from the results of an NMR experiment which shows two different sets of peaks for *Z*- and *E*- forms.[19] *ab initio* MO calculations for hydroxamic acids indicate that the *Z*-keto isomer is the most stable form in aqueous solvents.[20] The X-ray crystal structure of acetohydroxamic acid hemihydrate[21] shows that it does, in fact, exist in the *Z*-keto form. In this dissertation the hydroxamic acids are represented by their *Z*-keto form.

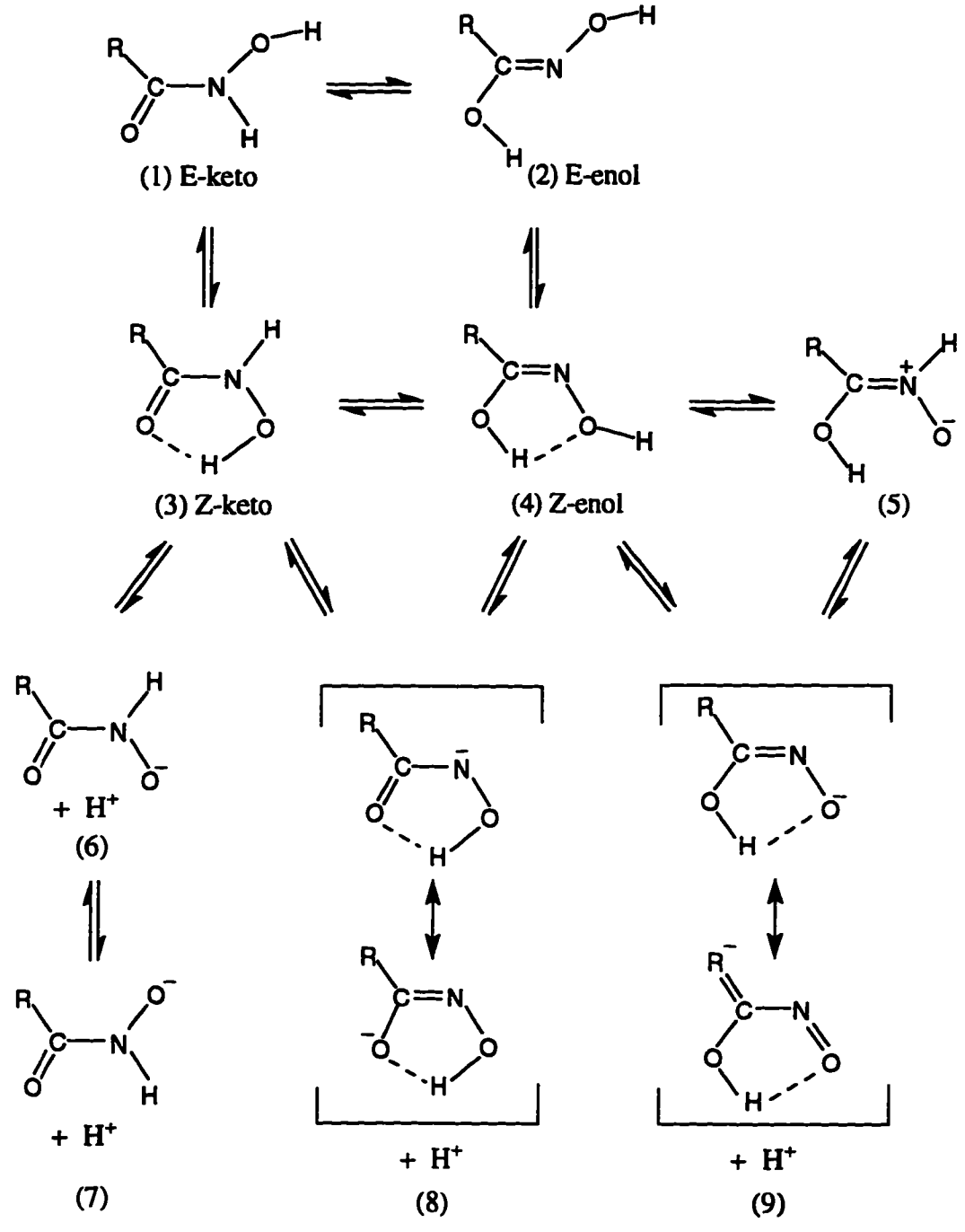

Figure 1.2. Different forms of hydroxamic acids.

ii) Site of ionization on hydroxamic acids

Although the ionization behavior of hydroxamic acids has been studied by many groups,[22-25] it is still not completely understood. The possibility for the existence of different isomeric forms of hydroxamic acids, as illustrated in Figure 1.2, provides several possibilities for the mode of proton dissociation from the ligand. However, so far the only evidence is in favor of the Z-keto isomer.[19,22-25] This isomer can behave as a N-acid or an O-acid.

Exner *et al.*[22-24] concluded from UV and IR data, that in dioxane as well as in 50% methanol-water solutions, benzohydroxamic acid and its alkyl derivatives exclusively exist as N-acids (structure 8 or 9 in Figure 1.2). However, the investigations of Stinberg *et al.*[25] show that in aqueous solutions they exist as O-acids, consisting of two species in equal concentration (structures 6 and 7 in Figure 1.2). These findings are supported by the *ab initio* MO calculations performed by Dannenberg *et al.*[26] that suggest that in aqueous solutions hydroxamic acids are more prone to behave as O-acids rather than N-acids. Further evidence for the O-acid behavior of hydroxamic acids in aqueous solution comes from studies of the temperature-dependent acid dissociation constant of these compounds[27] and NMR investigations.[28]

According to Exner, the existence of different monoionic forms of hydroxamic acids is a property of the ligand as well as the solvent.[29] Decreased acid strength of the ligand (for example, substitution of a methoxy group on the aromatic ring of benzohydroxamic acid, see Figure 1.3), and high-polarity solvents, favor O-acidity. On the other hand, increased acid strength of the ligand (substitution of a nitro group on the aromatic ring of benzohydroxamic acid) and low polarity solvents, favor N-acidity.

iii) Complexes of monohydroxamic acids

Monohydroxamic acids behave as bidentate donors towards various metal ions.[30] Spectroscopic studies indicate that the metal-ligand coordination takes place via two oxygen atoms.[31,32] The IR spectrum of monohydroxamic acid complexes of Cu(II), Fe(III) and Ni(II) shows bands for the metal-oxygen in the region of 250-600 cm^{-1} which compare with the calculated values.[31] The NMR spectra of acetohydroxamic acid exhibits signals for both NH and OH protons, whereas the sodium complex of this compound displays the signal for only the NH proton. These results indicate that the sodium ion replaces the proton on the oxygen atom. The X-ray structures of the complexes of benzohydroxamic acid with Fe(III) and Cr(III) show coordination of the oxygen atoms of the ligand in a bidentate fashion.[33,34]

The stability constants for the transition metal complexes of a wide variety of hydroxamic acids have been summarized.[18,35] The complexes of hydroxamic acids with transition metals are fairly strong. It is interesting to note that the stability constants for the nickel(II)hydroxamate complexes are about the same or somewhat lower than those of the respective Zn(II) species which is in contrast to the trend predicted by Irving and Williams.[36]

iv) Hydroxamic acids chosen for this study

The choice of hydroxamic acids was based on differences in their steric, electronic, and acid/base properties. The different hydroxamic acids studied are shown in Figure 1.3. Benzohydroxamic acid (BHA) and its two substituted forms, *para*-nitrobenzohydroxamic acid (PNBHA) and *para*-methoxybenzohydroxamic acid (PMBHA), were chosen as examples of ligands having similar steric properties but different basicity. 1-Naphthohydroxamic acid (1-NHA) and *N*-phenylbenzohydroxamic acid (*N*-PBHA) were chosen in order to study the effect of steric bulk and *N*-substitution, respectively, by comparing their Ni(II)-complexation rate constants with

that of BHA. *trans*-Cinnamoylhydroxamic acid (*t*-CHA) was chosen because it has been used for studies with the nickel-containing enzyme urease.[17]

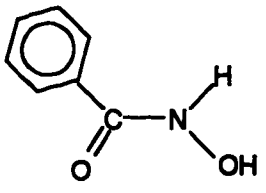

benzo-HA

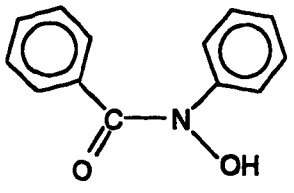

N-phenylbenzo-HA

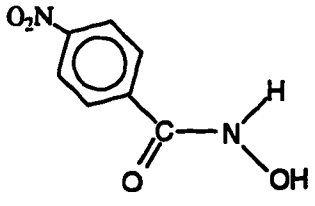

para-nitrobenzo-HA

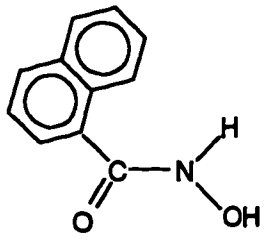

1-naphtho-HA

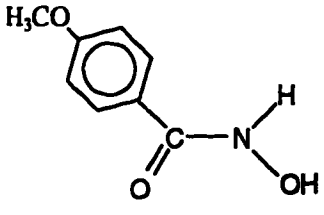

para-methoxybenzo-HA

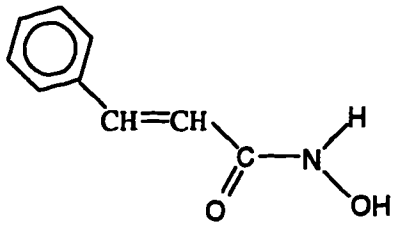

trans-cinnamoyl-HA

Figure 1.3. Structures of the different hydroxamic acids used in this study.

B. General Mechanism for the Reactions of Ni(II)

Among the labile group of divalent transition metal ions, Ni(II) is the easiest to study experimentally due to its low reactivity.[37] In aqueous solutions Ni(II) exists as octahedral $Ni(H_2O)_6^{2+}$.[37,38] The reactions of $Ni(H_2O)_6^{2+}$ with a wide range of ligands have been reviewed by Wilkins[37] and Margerum *et al.*[39] It was observed that most reactions of Ni(II) with unidentate ligands proceed via a dissociative interchange (I_d) mechanism.[40] In this mechanism the ligand forms an outer-sphere complex with the solvated metal ion which is followed by the rate-determining loss of the solvent molecule from the inner coordination sphere of the metal ion. Finally, rapid formation of the metal-ligand bond takes place. For multidentate ligands the rate-determining step may shift from the expulsion of the solvent molecule to some later step depending on the nature of the ligand.

Monohydroxamic acids behave as bidentate ligands which may be represented as $(L\text{-}L)^{n-}$. For these ligands one can extend the I_d mechanism in a way illustrated in Scheme 1.1. The formation of the outer-sphere complex $(H_2O)_6Ni\cdot(L\text{-}L)^{2-n}$ is followed by the formation of the inner-sphere complex $(H_2O)_5Ni\text{-}L\text{-}L^{2-n}$ with one end of the ligand free. The free end then coordinates to the metal ion resulting in the final chelate complex $(H_2O)_4NiL_2$.

Scheme 1.1

$$Ni(H_2O)_6^{2+} + (L\text{-}L)^{n-} \underset{k_{-1}}{\overset{k_1}{\rightleftharpoons}} Ni(H_2O)_6 \cdot (L\text{-}L)^{2-n} \qquad (1.4)$$

$$Ni(H_2O)_6 \cdot (L\text{-}L)^{2-n} \underset{k_{-2}}{\overset{k_2}{\rightleftharpoons}} [(H_2O)_5Ni\text{-}L\text{-}L]^{2-n} + H_2O \qquad (1.5)$$

$$[(H_2O)_5Ni\text{-}L\text{-}L]^{2-n} \underset{k_{-3}}{\overset{k_3}{\rightleftharpoons}} \left[(H_2O)_4\,Ni\begin{smallmatrix} L \\ | \\ L \end{smallmatrix}\right]^{2-n} + H_2O \qquad (1.6)$$

If step 1.4 is very rapid compared with step 1.5, and steady-state conditions are applied for the intermediates, the rate for chelate formation is given by equation 1.7.[37]

$$\frac{d[(H_2O)_4Ni(L_2)]}{dt} = k_f[(H_2O)_6Ni\cdot(L\text{-}L)^{2-n}] - k_d[(H_2O)_4Ni(L_2)] \qquad (1.7)$$

where $k_f = \dfrac{k_1 k_2 k_3}{k_{-1}(k_{-2} + k_3)}$ and $k_d = \dfrac{k_{-2} k_{-3}}{k_{-2} + k_3}$

If $k_3 >> k_{-2}$, the overall rate of complex formation will be determined by the rate of formation of the $(H_2O)_5Ni\text{-}L\text{-}L^{2-n}$ intermediate and therefore,

$$k_f = \frac{k_1 k_2}{k_{-1}} \qquad (1.8)$$

If the equilibrium constant for the formation of outer-sphere complex, K_{os} ($= k_1/k_{-1}$), is substituted in equation 1.8 then,

$$k_f = K_{os}\, k_2 \qquad (1.9)$$

For the complexation reactions of a wide range of metal ions and ligands that follow the dissociative mechanism, the values of k_2 were found to be in good agreement with the rate constants of water exchange, k^{M-H_2O}, of the cations measured by NMR.[39] Thus, equation 1.9 can be written as

$$k_f = K_{OS} k^{M-H_2O} \tag{1.10}$$

The factors which control the formation of $(H_2O)_5Ni\text{-}L\text{-}L^{2-n}$ are the same as those applicable in the case of a unidentate ligand. The value of K_{OS} can be determined theoretically by using the expression derived independently by Eigen[41] and Fuoss[42]. For the cases where a bidentate ligand reacts, Rorabacher *et al.*[43,44] have modified the expression to equation 1.11.

$$K_{OS} = \frac{4}{3}\pi N a^3 \times 10^{-3} \exp -\left[\frac{Z_M Z_L e_0^2}{a' D k_b T} - \frac{Z_M Z_L e_0^2 \kappa}{D k_b T (1 + \kappa a')}\right] \tag{1.11}$$

where a (cm) is the center-to-center distance between the metal ion and the coordinating site of the ligand, a ' (cm) is the distance from the center of the metal ion to the ligand atom bearing the charge, N is Avogadro's number, Z_M and Z_L are the formal charges on the metal and ligand, e_0 (esu) is the electronic charge, D is the dielectric constant of the solvent, k_b (ergs) is the Boltzmann constant, T is the absolute temperature, and κ is the Debye-Huckel ion atmosphere parameter. κ is a function of ionic strength *I* and is given by

$$\kappa = \left(\frac{8\pi N e_0^2 I}{1000 D k_b T}\right)^{1/2} \tag{1.12}$$

Thus, it is seen that the estimation of the values of the formation rate constants is possible in cases where the complex formation takes place via a dissociative interchange mechanism. It is common practice to compare the theoretically calculated values with those obtained experimentally to gain insight into the mechanism of a reaction. If the calculated and the observed values of the rate constants for a reaction agree within a factor of 2 to 3, the dissociative interchange mechanism is a strong possibility, especially for reactions involving the second half of the first row divalent transition elements.[39]

C. Significance of the Kinetics of Ni(II) with Hydroxamic Acids

i) Need for inhibitors for urease

More information about the reactions of hydroxamic acids with Ni(II) is required because these systems serve as simple models for the inhibition of enzymes containing divalent metal ions. One such enzyme that has recently drawn a lot of attention is urease.[8,45,46] This enzyme plays important role in the growth of bacteria and plants.[47,48] However, when produced in unwanted locations such as agricultural fields or human body, it is a cause for several problems. Therefore, efficient inhibitors for this enzyme are required. The general background on this enzyme and the results of some inhibition studies are discussed below.

Found in plants, bacteria and some invertebrates, urease catalyzes the hydrolysis of urea to give ammonium and carbamate ions (equation 1.13).[49] The carbamate degrades spontaneously *in vivo* to give ammonia and bicarbonate (equation 1.14), resulting in an overall reaction which may be represented by equation 1.15.

$$H_2N(CO)NH_2 + H_2O \text{ ----> } NH_4^+ + H_2NCO_2^- \quad (1.13)$$

$$H_2NCO_2^- + H_2O \text{ -------> } NH_3 + HCO_3^- \quad (1.14)$$

$$H_2N(CO)NH_2 + H_2O \text{ ---> } 2\,NH_3 + CO_2 \quad (1.15)$$

In agricultural fields, where urea is added as an external source of nitrogen, the concomitant presence of urease causes rapid hydrolysis of urea. The resultant ammonia adversely affects the crops. Furthermore, uncontrolled urea hydrolysis by soil-urease causes environmental pollution and the loss of fertilizer. Studies show that only 25 to 35% of applied urea is utilized by the crops.[50] For the efficient use of urea fertilizers, several compounds have been evaluated as urease inhibition in the soil.[51-56] However, the knowledge of the mechanistic information for urease inhibition can facilitate the efforts for the design of more efficient and economical inhibitors.

The need for a urease inhibitor is also required in the field of medicine. Urease is known to cause the formation of stones in the human body that results in the origin of diseases such as pyelnonephritis, ammonia encephalopathy, hepatic coma, urinary catheter encrustation, and peptic ulcer.[57] The stone formation occurs due to the *in vivo* urea hydrolysis caused by bacterial urease. The increase in pH leads to supersaturation of normally soluble polyvalent ions that give rise to infection stones such as struvite ($MgNH_4PO_4.6H_2O$). Conventional therapy involves surgical removal of the stones, nevertheless, in 50% of the cases recurrent formation of stones occurs.[58] It was shown that the stone formation could be significantly reduced by the oral administration of acetohydroxamic acid.[59,60] However, the oral administration of this drug causes side-effects such as hemolytic anemia and thrombophlebitis.[61,62] Thus, there is a wide interest for developing new urease inhibiting drugs having lesser side effects.

ii) Inhibition of urease by hydroxamic acids

Urease is known to contain two Ni(II) ions in its active site. It is believed that the inhibition of urease by hydroxamic acids is caused by complexation of one or both of these metal ions.[7] Several groups have investigated the reactions of urease with hydroxamic acids.[17,63,64] The reaction of acetohydroxamic acid (AHA) with urease was observed to be biphasic in nature.[65] The two processes are assigned to: (i) formation of an initial urease-AHA complex and (ii) slow transformation of the intermediate to give the final product. The second order rate constant for process (i) was measured to be 17 $M^{-1}s^{-1}$. The value of this rate constant is much smaller than the value of the rate constant for the complexation of AHA with free aquo-nickel which was measured to be 717 $M^{-1}s^{-1}$.[66] The difference in the values of these rate constants may be because of the following reasons: (i) the amino acid residue(s) on the Ni(II) center in urease have to dissociate for the ligand to bind, (ii) the incoming ligand faces electrostatic repulsions or steric hinderance that may be caused by the charged amino acid residues present at the active site and/or (iii) the ligand may bridge between the two nickel ions in which case the reaction mechanism is quite different than the mechanism of ligand binding with aquo Ni(II). The overall inhibition constant (K_i) for the urease-hydroxamate complex, was measured to be 4 μM.

Figure 1.4 illustrates some proposed structures for urease-hydroxamic complexes. Structure (i) was proposed by Hausinger *et al.*[63] in which a tetrahedral hydroxamate-oxygen adduct bridges the two Ni(II) ions. Structure (ii) was proposed by Pecoraro *et al.*[64] who based it on a nickel dimer [Ni_2(Hshi)(H_2shi)-(pyridine)$_4$(OAc)] (where H_2shi = salicylichydroxamic acid), in which the *N*-hydroxyl oxygen of Hshi bridges the two Ni(II) ions. Structure (iii) was proposed by Dixon *et al.*;[17] in this structure hydroxamate anion forms a bidentate chelate with one of the Ni(II) ions. Although there are reasonable justifications in favor of structures (i), (ii) and (iii), a bridging

structure (iv), in which the hydroxamate coordinates to the two nickel ions separately through the carbonyl and *N*-hydroxyl oxygen atoms, can not be ruled out.

Pecoraro *et al.*[64] also proposed a mechanism for inhibition of urease. In this mechanism, the monodentate carbonyl oxygen first coordinates with the tricoordinated Ni(II). Deprotonation of the oxime oxygen takes place next. The oxime oxygen then binds with the tricoordinate Ni(II) resulting in a chelate where it simultaneously bridges the pentacoordinate Ni(II). With the exception of bridging hydroxamate oxygen atom, the structure of the model compound $[Ni_2(Hshi)(H_2shi)(pyridine)_4(OAc)]$, is nearly identical to the proposed structure of the hydroxamate coordinated enzyme active site.

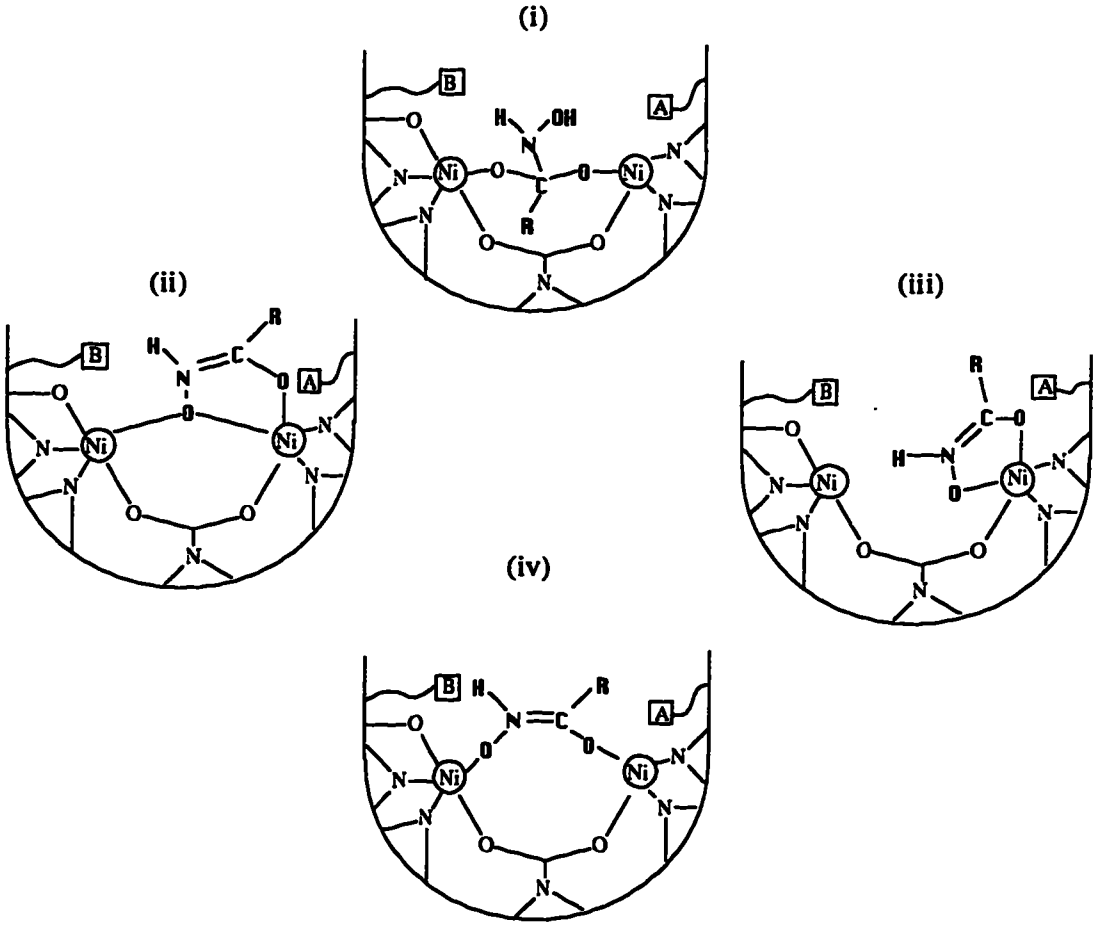

Figure 1.4. Possible structures of urease-hydroxamic acid complexes.

Inhibition of urease was studied by Kumaki *et al.*[55] who related the structure and activity of the hydroxamic acids with their inhibition power. It was concluded that electronic factors did not influence the structure-activity relationship of hydroxamic acids on urease inhibition; however, steric factors were shown to play a role. Ortho-substituted derivatives of benzohydroxamic acid were markedly less inhibitory than meta- and para-substituted derivatives.

Detailed studies of the reaction of hydroxamic acids with urease-nickel(II) may give some insight about the mechanism of inhibition. Before investigating the reaction of hydroxamic acids with urease-nickel(II), the investigation of the reaction of a series of hydroxamic acids with aquo-nickel(II) is required. Comparison of the rate constants obtained for the Ni-hydroxamate complexation reactions with the rate constants obtained from urease-hydroxamates may reveal information about the electronic and steric properties of the active site. For example, if the active site of urease is sterically hindered, a hydroxamic acid with bulky substitutent such as a naphtho group may not react as rapidly with urease as it reacts with aquo-Ni(II). Similarly, substituents with different electronic properties may produce different results on the inhibition reaction of urease.

Beside urease, hydroxamic acids are known to inhibit a number of zinc and iron containing metalloenzymes. The list of enzymes includes peroxidase from horseradish,[67] fructose-bisphosphate aldolase (class II) from *Saccharomyces cerevisiae*,[68] thermolysin from *B. thermoproteolyticus*,[69] adenylosuccinate synthetase from *Escherichia coli*,[70] tyrosinase from mushroom,[71] and collagenase from human skin fibroblast.[72] Studies also report that hydroxamic acids inhibit these enzymes by a mechanism other than binding the metal ion.[73-75]

iii) Rate determining step in the Ni-hydroxamate complex formation

As stated earlier, the reactions of Ni(II) with hydroxamic acids are of great biological importance. Nevertheless, the kinetics of these reactions have not received much attention. There is only one study reported on the reaction of Ni(II) with acetohydroxamic acid.[66] The reaction was studied using the temperature-jump method and the rate constants for the formation and the dissociation of the Ni-hydroxamate complex have been resolved for the pathways involving the protonated (HA) and the deprotonated (A^-) form of the ligand. The experimental value of the formation rate constant ($3.25 \times 10^4\ M^{-1}s^{-1}$) for the reaction of the deprotonated ligand with Ni(II) is very close to that predicted from the I_d mechanism ($5 \times 10^4\ M^{-1}s^{-1}$; see chapter IV for the calculations). Therefore, it is proposed that the rate-determining step in this pathway is the expulsion of the water molecule from the inner coordination sphere of the metal ion. However, for the pathway involving the protonated form of the ligand the value for the experimental rate constant ($7.2 \times 10^2\ M^{-1}s^{-1}$) is an order of magnitude smaller than that of the predicted value ($4 \times 10^3\ M^{-1}s^{-1}$). The reason for the smaller value of the rate constant is attributed to the shift in the rate-determining step from expulsion of water to proton dissociation.

If the expulsion of a water molecule is the rate-determining step in the case of the complex formation through the protonated ligand, it would be expected that the acidity of the ligand will play a role in controlling the rate. That is, a greater value for the proton dissociation constant of the ligand would be expected to result in a greater value of the formation rate constant. In the study reported here, the reactions of Ni(II) were performed with a series of hydroxamic acids with changing acid/base properties. The results obtained support an alternative mechanism for the complexation of the protonated form of the ligand.

iv) Need to obtain information regarding the reactivity of the deprotonated form of the ligand

As found by Dominey *et al.*,[66] for the reactions of Ni(II) and Co(II) with acetohydroxamic acid, the rate constants for the formation of metal hydroxamate complexes are approximately an order of magnitude higher for the pathway involving the deprotonated form of the ligand compared to that involving the protonated form of the ligand. The present study investigated whether this behavior is generally true for various hydroxamic acid systems. It is hoped that this information will provide a basis for a detailed elucidation of mechanism of binding of hydroxamic acids with metal ions present in biological systems. One such system of considerable interest is the interaction of Fe(III) with hydroxamic acids. Kinetic studies for this system are conducted with the interest of analyzing hydroxamic acids as potential therapeutic agents to remove iron from patients suffering from iron overload.[13] These studies were performed at low pH (< 2), to avoid the formation of metal hydroxide species (log K for $(FeOH)^{2+}$ = 11.8). However, under these conditions the information regarding the pathway involving the deprotonated form of the ligand could not be obtained because of the very low concentration of this form of the ligand. On the other hand, since the hydroxide formation for Ni(II) occurs at much higher pH values (log K for $(NiOH)^{+}$ = 4.1), kinetic studies with this metal ion could be performed at a much higher pH values without complications due to metal hydroxides. From the analysis of the data obtained under these conditions, the values for the rate constants for the pathway involving the deprotonated form of the ligand could be extracted.

D. Summary of Studies

The study reported here was designed to provide fundamental mechanistic information about the pathways involving the protonated as well as the deprotonated forms of the ligand in the complexation reactions of hydroxamic acids with aquo-Ni(II). The effects of various substituents that alter the electronic and steric properties of the ligand were examined. Six different hydroxamic acids were used in this study; BHA, PNBHA, PMBHA, 1-NHA, *N*-PBHA and *t*-CHA. The abbreviations and the structures have been described in section A (iv) of this Chapter. The reactions were studied in aqueous medium at 25.0 °C, using a stopped-flow technique of rapid mixing. Pseudo-first-order conditions were employed i) by taking $[Ni^{2+}]$ in excess and ii) by performing the reactions at fixed $[H^+]$ using a buffer (5mM MES). The ionic strength was maintained at $I = 0.10$ M using $NaClO_4$.

Based on the kinetic data, a mechanism for complexation is proposed and the rate constants for the individual steps are calculated. The mathematical model used to deconvolute the individual rate constants required the values for the protonation constants (K_H) for the all the ligands. These values were determined spectrophotometrically and for 1-NHA the value of K_H was also determined potentiometrically. The conditions used in these experiments were similar to those used for the kinetic runs.

The information about the rate-determining step was obtained by comparing the empirical results with theoretical calculations based on I_d mechanism. This study provides a fundamental basis for the understanding of the inhibition mechanism of urease by hydroxamic acids.[8] Furthermore, this study provides information about the pathway involving the deprotonated form of the ligand in the metal-hydroxamate complexation reactions. This information cannot be directly obtained for the biologically important systems which involve the reactions of hydroxamic acids with Fe(III).

REFERENCES

1) Thauer, R. K.; Diekert, G.; Schonheit, P. *Trends Biochem. Sci.* **1980**, *5*, 304-306.

2) Sunderman, F. W. *Nickel in the Human Environment*; Oxford University Press: New York, 1985.

3) Lancaster, J. R., Jr. *The Bioinorganic Chemistry of Nickel*; VCH: Deerfield Beach, FL, 1988, pp 141-332.

4) Mertz, W. *Science* **1981**, *213*, 1332-1338.

5) Eskew, D. L.; Welch, R. M.; Cary, E. E. *Science* **1983**, *222*, 621-623.

6) Hausinger, R. P. *Microbiol. Rev.* **1987**, 22-42.

7) Halcrow, M. A.; Christou, G. *Chem. Rev.* **1994**, *94*, 2421-2481.

8) Lipkin, R. *Science News* **1995**, *147*, 310.

9) Kistiakowsky, G. B.; Shaw, W. H. R. *J. Am. Chem. Soc.* **1953**, *75*, 866-871.

10) Dixon, N. E.; Gazzola, C.; Asher, C. J.; Lee, D. S. W.; Blakeley, R. L.; Zerner, B. *Can. J. Biochem.* **1980**, *58*, 474-480.

11) Blakeley, R. L.; Hinds, J. A.; Kunze, H. E.; Webb, E. C.; Zerner, B. *Biochemistry* **1969**, *8*, 1991-2000.

12) Holmes, M. A.; Matthews, B. W. *Biochemistry* **1981**, *20*, 6912-6920.

13) Monzyk, B.; Crumbliss, A. L. *J. Am. Chem. Soc.* **1979**, *101*, 6203-6213.

14) Lossen, H. *Justus Liebigs Ann. Chem.* **1869**, *150*, 314-320.

15) Davidson, D. *J. Chem. Ed.* **1940**, *17*, 81-83.

16) Bass, V. C.; Yoe, J. H. *Talanta* **1966**, *13*, 735-744.

17) Dixon, N. E.; Hinds, J. A.; Fihelly, A. K.; Gazzola, C.; Winzor, D. J.; Blakeley, R. L.; Zerner, B. *Can. J. Biochem.* **1980**, *58*, 1323-1334.

18) Kurzak, B.; Kozlowski, H.; Farkas, E. *Coord. Chem. Rev.* **1992**, *114*, 169-200.

19) Brown, D. A.; Glass, W. K.; Mageswaran, R.; Girmay, B. *Mag. Res. Chem.* **1988**, *26*, 970-973.

20) Fitzpatrick, N. J.; Mageswaran, R. *Polyhedron* **1989**, *8*, 2255-2263.

21) Bracher, B. H.; Small, R. W. H. *Acta Crystallogr. Sect. B* **1970**, *26*, 1705-1709.

22) Exner, O.; Kakac, B. *Collect. Czech. Chem. Commun.* **1962**, *27*, 1656-1663.

23) Exner, O.; Holubek, J. *Collect. Czech. Chem. Commun.* **1965**, *30*, 940-951.

24) Exner, O.; Simon, W. *Collect. Czech. Chem. Commun.* **1965**, *30*, 4078-4093.

25) Steinberg, G. M.; Swidler, R. *J. Org. Chem.* **1965**, *30*, 2362-2365.

26) Ventura, O. N.; Rama, J. B.; Turi, L.; Dannenberg, J. J. *J. Am. Chem. Soc.* **1993**, *115*, 5754-5761.

27) Monzyk, B.; Crumbliss, A. L. *J. Org. Chem.* **1980**, *45*, 4670-4675.

28) Bagno, A.; Comuzzi, C.; Scorrano, G. *J. Am. Chem. Soc.* **1994**, *116*, 916-924.

29) Exner, O.; Hradil, M.; Mollin, J. *Collect. Czech. Chem. Commun.* **1993**, *58*, 1109-1121.

30) Anderegg, V. G.; L' Eplattenier, F.; Schwarzenbach, G. *Helv. Chim. Acta* **1963**, *46*, 1409-1421.

31) Brown, D. A.; Dervilla, M.; Glass, W. K. *Inorg. Chim. Acta* **1979**, *35*, 57-60.

32) Brown, D. A. *Inorg. Chem.* **1983**, *22*, 2199-2202.

33) Lindner, H. J.; Goettlicher, S. *Acta Crystallogr., Sect. B* **1969**, *25*, 832-842.

34) Abu-Dari, K.; Ekstrond, J. D.; Freyburg, D. P.; Raymond, K. N. *Inorg. Chem.* **1979**, *18*, 108-112.

35) Chatterjee, B. *Coord. Chem. Rev.* **1978**, *26*, 281-303.

36) Irving, H.; Williams, R. J. P. *J. Am. Chem. Soc.* **1975**, *156*, 3192-3210.

37) Wilkins, R. G. *Acc. Chem. Res.* **1970**, *3*, 408-416.

38) Swift, T. J.; Weinberger, J. *J. Am. Chem. Soc.* **1968**, *90*, 2023-2026.

39) Margerum, D. W.; Cayley, G. R.; Weatherburn, D. C.; Pagenkopf, G. K. In *Kinetics and Mechanisms of Complex Formation and Ligand Exchange*; Martell, A. E., Ed.; ACS: Washington, D. C., 1978; Vol. 174, pp 1-221.

40) Eigen, M. In *Advances in the Chemistry of the Coordination Compounds*; Kirschner, S., Ed.; Macmillan: New York, 1962, p 371.

41) Eigen, M.; Kruse, W.; Maass, G.; DeMaeyer, L. *Progr. Reac. Kinet.* **1964**, *2*, 287-318.

42) Fuoss, R. M. *J. Am. Chem. Soc.* **1958**, *80*, 5059-5061.

43) Rorabacher, D. B.; Turan, T. S.; Defever, J. A.; Nickels, W. G. *Inorg. Chem.* **1969**, *8*, 1498-1506.

44) Lin, C. T.; Rorabacher, D. B. *Inorg. Chem.* **1973**, *12*, 2402-2410.

45) Lippard, S. J. *Science* **1995**, *268*, 996-997.

46) Jabri, E.; Carr, M. B.; Hausinger, R. P.; Karplus, P. A. *Science* **1995**, *268*, 998-1004.

47) Klucas, R. V.; Hanus, F. J.; Russell, S. A.; Evans, H. J. *Proc. Natl. Acad. Sci. USA* **1983**, *80*, 2253-2257.

48) Eskew, D. L.; Welch, R. M.; Norvell, W. A. *Plant Physiol.* **1984**, *76*, 691-693.

49) Andrews, R. K.; Blakeley, R. L.; Zerner, B. In *Urea and urease*; Eichhorn, G. L.; Marzilli, L. G., Eds.; Elsevier: New York, 1984; Vol. 6, pp 245-283.

50) Byrnes, B. H.; Savant, N. K.; Craswell, E. T. *Soil Sci. Soc. Am. J.* **1983**, *47*, 270-274.

51) Bremner, J. M.; Mulvaney, R. L. In *Urease Activity in Soils*; Burns, R. G., Ed.; Academic Press: London, 1978, pp 149-196.

52) Bremner, J. M.; Krogmeier, M. J. *Proc. Natl. Acad. Sci. USA* **1988**, *85*, 4601-4604.

53) Liao, C. F.-H.; Raines, S. G. *Plant and Soil* **1985**, *85*, 149-152.

54) Kobashi, K.; Hase, J. *Biochim. Biophys. Acta* **1962**, *65*, 380-383.

55) Kumaki, K.; Tomioka, S.; Kobashi, K.; Hase, J. *Chem. Pharm. Bull.* **1972**, *20*, 1599-1606.

56) Park, J.-B.; Imamura, L.; Kobashi, K.; Itoh, H.; Miyazaki, T.; Horisaki, T. *Biol. Pharm. Bull.* **1995**, *18*, 208-213.

57) Mobley, L. T.; Hausinger, R. P. *Microbiol. Rev.* **1989**, *53*, 85-108.

58) Griffth, D. P. *Urol. Res.* **1979**, *7*, 215-221.

59) Martelli, A.; Buli, P.; Cortecchia, V. *Eur. Urol.* **1981**, *7*, 291-293.

60) Griffth, D. P. *Kidney International* **1978**, *13*, 372-382.

61) Sim, E.; Jones, A.; Stanley, L. *Acta. Pharmacol. Toxicol.* **1985**, *42*, 89-96.

62) Griffith, D. P. *Urological Research* **1979**, *7*, 215-221.

63) Todd, M. J.; Hausinger, R. P. *J. Biol. Chem.* **1989**, *264*, 15835-15842.

64) Stemmler, A. J.; Kampf, J. W.; Kirk, M. L.; Pecoraro, V. L. *J. Am. Chem. Soc.* **1995**, *117*, 6368-6369.

65) Dixon, N. E.; Riddles, P. W.; Gazzola, C.; Blakeley, R. L.; Zerner, B. *Can. J. Biochem.* **1980**, *58*, 1335-1344.

66) Dominey, L. A.; Kustin, K. *Inorg. Chem.* **1984**, *23*, 103-108.

67) Schonbaum, G. R. *J. Biol. Chem.* **1973**, *248*, 502-511.

68) Collins, K. D. *J. Biol. Chem.* **1974**, *249*, 136-142.

69) Nishino, N. *Biochemistry* **1979**, *18*, 4340-4347.

70) Shigeura, H. T.; Gordon, C. N. *J. Biol. Chem.* **1962**, *237*, 1937-1940.

71) Rich, P. R.; Wiegand, N. K.; Blum, H.; Moore, A. L.; Bonner, W. D., Jr. *Biochim. Biophys. Acta* **1978**, *525*, 325-337.

72) Grobelney, D.; Poncz, L.; Galardy, R. E. *Biochemistry* **1992**, *31*, 7152-7154.

73) Summers, J. B.; Kim, K. H.; Mazdiyasni, H.; Holms, J. H.; Ratajczyk, J. D.; Stewart, A. O.; Dyer, R. D.; Carter, G. W. *J. Med. Chem.* **1990**, *33*, 992-998.

74) Summers, J. B.; Mazdiyasni, H.; Holms, J. H.; Ratajczyk, J. D.; Dyer, R. D.; Carter, G. W. *J. Med. Chem.* **1987**, *30*, 574-580.

75) Brand, L. M.; Harper, A. E. *Biochemistry* **1976**, *15*, 1814-1821.

CHAPTER II

EXPERIMENTAL

A. Reagents

Nickel Perchlorate. $Ni(ClO_4)_2$ was prepared earlier in this laboratory by Thomas,[1] by reacting $NiCO_3$ (Aldrich or Baker and Adamson, > 99.99%) with a slight excess of $HClO_4$ followed by recrystallization from hot water. The stock solutions of $Ni(ClO_4)_2$ were standardized by titration with EDTA using murexide indicator (Fisher Scientific Co.).[2] The indicator for the titration was prepared by grinding 0.1 g murexide with 10 g of potassium nitrate and about 50 mg of solid mixture was used for each titration. At the end-point, murexide changed color from yellow to violet. The titration was performed at pH ~10, that was controlled using ammonium chloride/ammonia buffer.

Sodium Perchlorate. $NaClO_4 \cdot H_2O$ (Aldrich) was recrystallized from acetone.[3] The crystals were filtered and dried under vacuum at 150 °C to remove solvent of crystallization.[4]

Sodium Hydroxide. NaOH was prepared by diluting the commercial concentrate (Dilut-it, J.T.Baker, Phillipsburg, NJ); The solutions were standardized by the titration with potassium hydrogen phthalate (primary standard, Mallinckrodt or Fisher Scientific, A. C. S. reagent grade) using phenolphthalein as the indicator.

Perchloric Acid. The stock solutions of $HClO_4$ were made from concentrated acid (EM Science, Cherry Hill, NJ). The solutions were standardized against NaOH using phenolphthalein as the indicator.

Ethylenediaminetetraacetic acid. H_4EDTA and Na_2H_2EDTA (Aldrich, >99% pure) were dried in the oven at 80 °C for two hours and were cooled over P_2O_5 in the dessicator prior to use.[5]

Buffers. 4-Morpholinoethanesulphonic acid monohydrate, 98% (MES); 1,4-piperazinebis-(ethanesulphonic acid), 98% (PIPES); 4-(2-hydroxyethyl)-1-piperazineethanesulphonic acid, 99% (HEPES); and 2-(cyclohexylamino)ethanesulphonic acid 99% (CHES) buffers, were purchased from Sigma Chemical Co. (St. Louis, MO) and were used as provided.

Preparation of solutions. All solutions were prepared using double-distilled water. The second distillation was performed using a Corning Megapure (model MP-3A) glass distillation apparatus.

Hydroxamic acids. 1-NHA and NPBHA were purchased from ICN pharmaceuticals, Inc. (Plainview, N.Y). BHA was purchased from Aldrich Chemical Co., Inc. (Milwaukee, WI). *t*-CHA was synthesized according to the procedure described in section B of this chapter. PNBHA and PMBHA were synthesized earlier in this laboratory, by other workers according to the procedure described in the literature.[6,7]

Thin-layer chromatography (TLC) and melting point determinations were used to check the purity for all the hydroxamic acids used in this study. The analysis of hydroxamic acids by reversed phase TLC (Whatman, KC_{18}) in 80% propanol-water

solvent sysem, showed single bands under UV light. The melting point determinations were made on a Thomas-Hoover apparatus and the values were found to be consistent with those in the literature, as summarized in Table 2.1.

Table 2.1 Melting Point (°C) Values for Hydroxamic Acids

	observed	literature	reference
i) PNBHA	174-175	174-175	8
ii) *t*-CHA	118.5	118.4-118.6	9
iii) 1-NHA	191.7	191-192	8
iv) BHA	129.0	128	10
v) PMBHA	163.0	163	10

B. Synthesis of *trans*-Cinnamoylhydroxamic Acid

2.3 g of sodium metal was cleaned with ethanol and then dissolved in 50 mL of the same solvent. The resultant $NaOC_2H_5$ solution, was added dropwise to an equal volume of 2M cold hydroxylamine hydrochloride (Aldrich) solution in ethanol. The reaction mixture was filtered and the filtrate (containing free NH_2OH) was stirred with 50 mL of a 2 M solution of ethyl *trans*-cinnamate (Aldrich) in ethanol. The stirring was performed for three hours, in an ice bath under N_2 atmosphere. To the stirred solution, another equivalent of NaOEt prepared in 50 mL of ethanol was added. The resultant solution was stirred again under N_2, at room temprature for 15 hrs. After the stirring was complete, the solvent was removed by filtration and the sodium salt of *t*-CHA was acidified with HCl to get *t*-CHA. *t*-CHA was purified by recrystallization from

chloroform and then from hot water. The yield after recrystallization was 0.9 gram.

The mass spectrum (70ev, DIP) for the product ($C_9H_9NO_2$) showed a peak for the parent ion at m/e = 163.0 (theory, 163.2). The proton NMR spectrum in $CDCl_3$ showed two doublets centered at 7.75 and 6.36 ppm with the coupling constant of ~17 Hz each, which is characteristic of *trans* olefinic protons.[11] The UV-VIS spectrum and the melting points were consistent with the results reported in the literature.[9]

C. pH Measurements

The pH values for the metal ion and the ligand solutions were adjusted immediately before each experiment using conc. NaOH and conc. $HClO_4$. Corning model 125 or Fisher model 825MP pH meters, with an Orion Ross sure-flow semi-micro pH-electrode were used to measure the pH. 3M KCl (Orion 81-00-07) was used as internal filling solution for the electrode. The pH-meter/electrode system was calibrated using standard buffers (Gram-Pac®, Fisher) of nominal pH values 4.01, 6.86 and 9.18. The solutions for the 9.18 buffer were prepared in CO_2 free water and were stored under N_2.

D. Kinetic Measurements

All reactions were rapid and were studied using a Durrum-Dionex stopped-flow system interfaced to a Cromemco Z2-D microprocessor. A schematic diagram of this instrument is shown in Figure 2.1. With this instrument, often there is a time difference between the initiation of the reaction and the beginning of the data acquisition. This time difference is referred to here as "time-offset". It arises due to the limitation in starting the clock exactly at the initiation of the reaction. The time-offset for the instrument was measured by performing a reaction on it that involved the mixing of 0.01 M $Fe(NO_3)_3$ (in 0.1 N H_2SO_4) with 0.01 M NaSCN ($t_{1/2}$ = 40 ms).[12] These solutions are colorless; however when mixed, they form a colored complex $Fe(SCN)^{2+}$ that absorbs at λ_{max} = 466 nm. The data were acquired for 10 ms to record only some initial part of the reaction. The values for the time-offset were determined by fitting the time versus absorbance data to a second order polynomial expression and then extrapolating the theoretical fit to a value of Absorbance = 0.0.

The reaction kinetics for the formation of Ni(II)-hydroxamates was studied by monitoring the appearance of the charge-transfer bands that are produced as a result of complexation of nickel with hyrdoxamic acids. Since the output of the photomultiplier tube is proportional to the transmittance, the wavelengths (λ_{obs}) chosen for monitoring the reaction were at the positions where transmittance changes for the reactions were maximum. The values of λ_{obs} are summarized in Table 2.2 .

The formation rates of nickel-hydroxamate complexes were measured in the pH range 5.30 to 6.70. Reactions were carried out with at least a 10-fold excess of Ni(II) to ensure pseudo first-order conditions, and to minimize the formation of 1:2 and 1:3 nickel hydroxamate complexes. The ionic strength of each solution was maintained at 0.10 M with $NaClO_4$. At each pH value, the reactions were initiated by mixing a solution of

hydroxamic acid (0.12-0.30 mM HA, 5mM MES) with an equal volume of a solution of Ni(II) (2-30 mM Ni(II), 5mM MES). The temperature of the reactants and the observation cell was maintained at 25.0 °C with a circulating constant temperature bath. The details about fitting the absorbance-time data are described in Chapter III.

Table 2.2. λ_{obs} and Total Ligand Concentrations used for Kinetic Studies of Ni(II) with Hydroxamic Acids (HA).

HA	λ_{obs} (nm)	$[HA]_{tot} \times 10^4$, M[a]
PNBHA	330	0.60
t-CHA	320	0.60
1-NHA	315	1.50
BHA	280	0.60
PMBHA	298	0.60

[a]After mixing concentrations

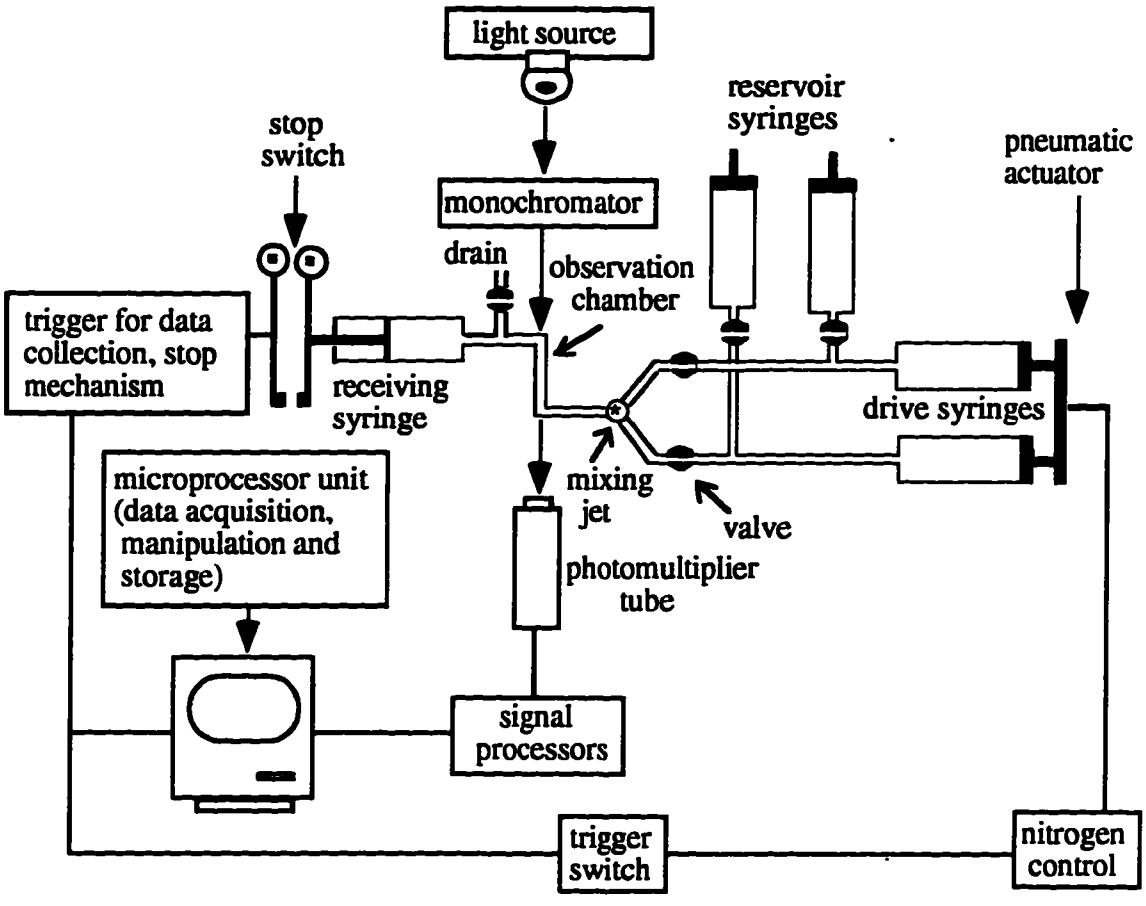

Figure 2.1. Diagram of the Durrum-Dionex stopped-flow system.

E. Determination of Protonation Constants (K_H) of Hydroxamic Acids

i) Spectophotometric method

The values for the protonation constants (K_H) were determined from the UV-VIS spectrophotometric data that were obtained as a function of pH in the range 4 to 12. The pH of the solution was adjusted in a thermo-jacketed cell. The spectra were recorded from 190 nm to 800 nm on a Hewlett Packard 8452A diode array spectrophotometer. The wavelength accuracy of the spectrophotometer was checked using standard holmium oxide filter. To obtain a spectrum, an aliquot (~3 mL) of solution was transfered to a 1 cm quartz cuvette using a Pasteur pipet and, after the recording the spectrum, the solution was poured back into the cell and adjusted to another pH value. The cell and the cuvette holder were connected to the external flow circuits of the temperature bath which were maintained at 25.0 °C.

The titrations were performed by adding conc. NaOH to the solution initially containing the protonated form of the ligand. For each ligand, spectra were recorded over the pH range 4.5 to 12.0. The ligand concentrations used for the titration were: [BHA] = 0.24 mM; [PNBHA] = 0.12 mM; [PMBHA] = 0.12 mM; [1-NHA] = 0.16 mM and [t-CHA] = 0.28 mM. The solutions were made with 3 mM each of MES (or PIPES), HEPES and CHES buffers. EDTA (0.5 mM) was added to all solutions to chelate any metal ion impurities. The ionic strength was controlled at $I = 0.10$ M with $NaClO_4$.

ii) Potentiometric method

In addition to the spectrophotometric determination the log K_H value for 1-NHA was also obtained by potentiometric method. 20.0 mL of 0.81 mM of the protonated form of 1-NHA was titrated with 8.0 mM NaOH. The ionic strength of the ligand

solution and the titrant was controlled at $I = 0.1$ M with $NaClO_4$.

Titrations were performed using a Metrohm model 655 digital buret and a Fisher 825MP pH meter controlled by a Zenith 158-42 computer. The details on the operation of the automated titration system are described elsewhere.[13] The value of K_H was obtained from the pH versus volume of NaOH data using the program PKAS.[14,15]

REFERENCES

1) Thomas, P. T. *Ph.D. Thesis* **1991**, The University of Oklahoma, Norman, OK.

2) Vogel, A. I. *Textbook of Quantitative Chemical Analysis*; 5th ed.; Longman: Essex, England, 1989, p 327.

3) Perrin, D. D.; Armarego, W. L. F. *Purification of Laboratory Chemicals*; 3rd ed.; Pergamon Press: New York, 1992, p 350.

4) Schilt, A. A. *Perchloric Acid and Perchlorates*; Fredrick Smith: Columbus, Ohio, 1979, pp 36-37.

5) Vogel, I. A. *A Textbook of Quantitative Inorganic Analysis*; 3rd ed.; Wiley: New York, 1961, p 432.

6) Gupta, V. K.; Tandon, S. G. *J. Indian Chem. Soc.* **1969**, *46*, 831-834.

7) Monzyk, B.; Crumbliss, A. L. *J. Org. Chem.* **1980**, *45*, 4670-4675.

8) Summers, J. B.; Mazdiyasni, H.; Holms, J. H.; Ratajczyk, J. D.; Dyer, R. D.; Carter, G. W. *J. Med. Chem.* **1987**, *30*, 574-580.

9) Dixon, N. E.; Hinds, J. A.; Fihelly, A. K.; Gazzola, C.; Winzor, D. J.; Blakeley, R. L.; Zerner, B. *Can. J. Biochem.* **1980**, *58*, 1323-1334.

10) Dutt, N. K.; Seshadri, T. *Bull. Chem. Soc. Jpn.* **1967**, *40*, 2280-2283.

11) Silverstein, R. M.; Bassler, G. C.; Morrill, T. C. *Spectrophotometric Identification of Organic Compounds*; Wiley: New York, 1991, pp 192-193.

12) Mieling, G. E.; Taylor, R. W.; Hargis, L. G.; English, J.; Pardue, H. L. *Anal. Chem.* **1976**, *48*, 1686-1993.

13) Craig, M. E. *Ph.D. Thesis* **1990**, The University of Oklahoma, Norman, OK.

14) Motekaitis, R. J. *Can. J. Chem.* **1982**, *60*, 168-173.

15) Martell, A. E.; Motekaitis, R. J. *Determination and Use of Stability Constants*; 2nd ed.; VCH: New York, 1992.

CHAPTER III

RESULTS

A. Protonation Constants for Hydroxamic Acids

The absorbance versus pH data obtained from the spectrophotometric titrations of hydroxamic acids, are consistent with the ionization of a single proton, as shown by equation.

$$A^- + H^+ \rightleftharpoons HA; \qquad K_H = \frac{[HA]}{[H^+]\,[A^-]} \tag{3.1}$$

The absorbance value (A_i) for a mixture of A^- and HA is given by the relationship,[1]

$$A_i = \frac{A_{HA} K_H\,[H^+] + A_{A^-}}{1 + K_H\,[H^+]} \tag{3.2}$$

where, A_{A^-} and A_{HA} are limiting absorbance values for the acidic and the basic forms of hydroxamic acid, respectively, K_H is the protonation constant, and $[H^+]$ is the hydrogen ion concentration. The values of $[H^+]$ were calculated from the measured pH values using the set of equations 3.3 to 3.5.

$$a_{H^+} = 10^{-pH} \tag{3.3}$$

$$[H^+] = \frac{a_{H^+}}{\gamma} \tag{3.4}$$

$$-\log \gamma = 0.5\,(Z_x)^2 \left(\frac{\sqrt{I}}{1+\sqrt{I}} - 0.30\,I\right) \tag{3.5}$$

Equation 3.5 is known as Davies equation[2] and it is used to calculate the activity coefficient (γ) of an ion with charge Z_x in a solution of ionic strength I.

Figures 3.1-3.6 show the results of the spectrophotometric pH titrations of hydroxamic acids. In each of these figures, Part (a) shows the UV-VIS spectra of hydroxamic acids as a function of pH (for clarity, only the spectra at selected pH values are shown). Part (b) of these figures show plots of A_i versus pH. The estimates for the parameters A_i, A_{A^-}, and A_{HA} were obtained from fitting the A_i, $[H^+]$ data to equation 3.2, by using a non-linear least-squares method based on Marquardt strategy.[3,4] The solid lines in part (b) of the Figures 3.1-3.6 represent the theoretical fits to equation 3.2. The log values for the protonation constants (K_H) are summarized in Table 3.1.

With the exception of 1-NHA, all hydroxamic acids showed at least one isosbestic point at wavelengths greater than 230 nm. At the ligand concentrations used for these experiments, the absorbance values were too high to be meaningful in the wavelength region below 230 nm. Moreover, in this region, the absorbance due to buffers became significant. Therefore, isosbestic points in the wavelength region below 230 nm could not be seen. The characteristics of the UV-VIS absorption spectra for the hydroxamic acids are summarized in Table 3.2.

Table 3.1. Log K_H Values for Hydroxamic Acids[a]

HA	1st set[b]	2nd set[b]	mean
PNBHA	7.854 ± 0.001	7.878 ± 0.002	7.87
t-CHA	8.399 ± 0.007	8.390 ± 0.001	8.39
1-NHA	8.440 ± 0.020	8.540 ± 0.002[c]	8.49
BHA	8.672 ± 0.002	8.650 ± 0.010	8.66
PMBHA	8.795 ± 0.004	8.845 ± 0.004	8.82
N-PBHA	8.060 ± 0.008	8.132 ± 0.006	8.10

[a]Determined at 25.0 °C and I = 0.10 M. [b]The reported uncertainties are the errors in the nonlinear least-squares fitting of the data to equation 3.2. [c]Determined potentiometrically.

Table 3.2. Values for Isosbestic Points and λ_{max} for Acidic and Basic forms of Hydroxamic Acids.

HA	λ_{max} (nm) (HA)	λ_{max} (nm) (A^-)	Isosbestic point(s), nm
PNBHA	270	344	250, 298
t-CHA	274	268, 305	256, 295
1-NHA	282	280	-
BHA	228	268	247
PMBHA	248	280[a]	241, 266
N-PBHA	256[a]	290	240, 280

[a]shoulder

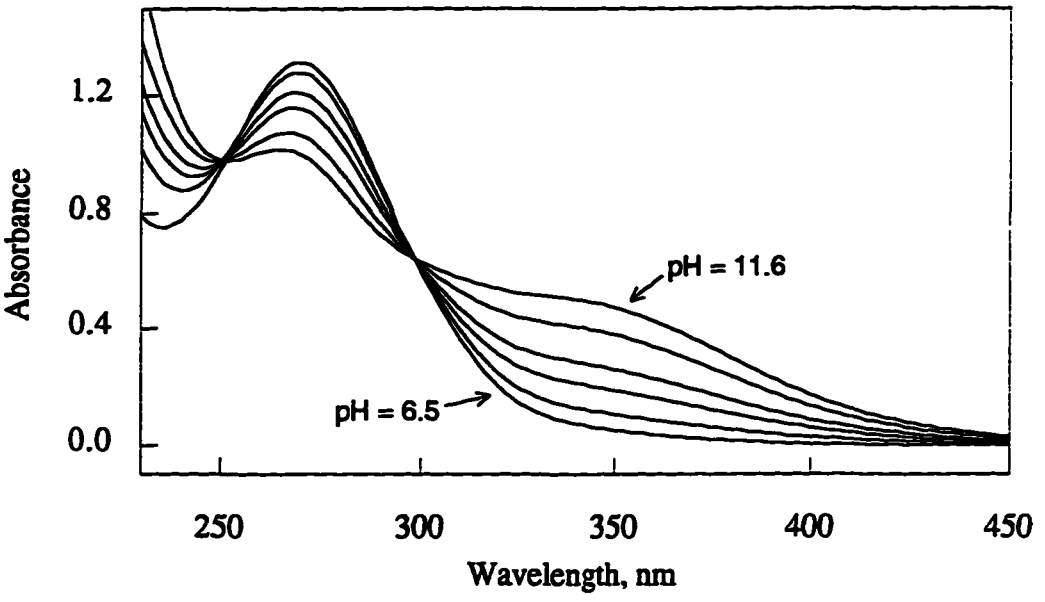

Figure 3.1 (a). UV-VIS spectra of PNBHA as a function of pH.

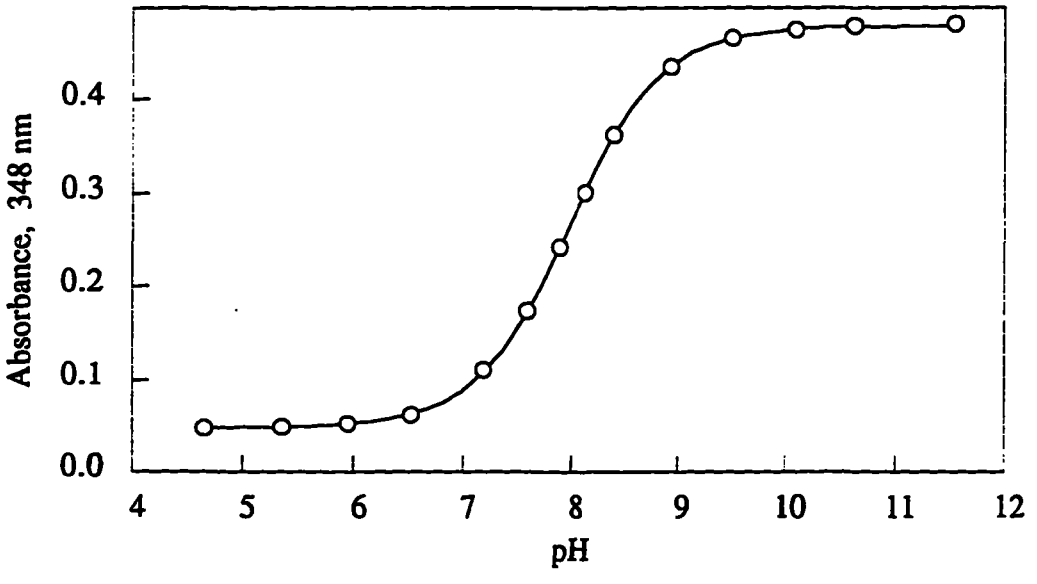

Figure 3.1 (b). pH titration of PNBHA. The solid line represents the theoretical fit.

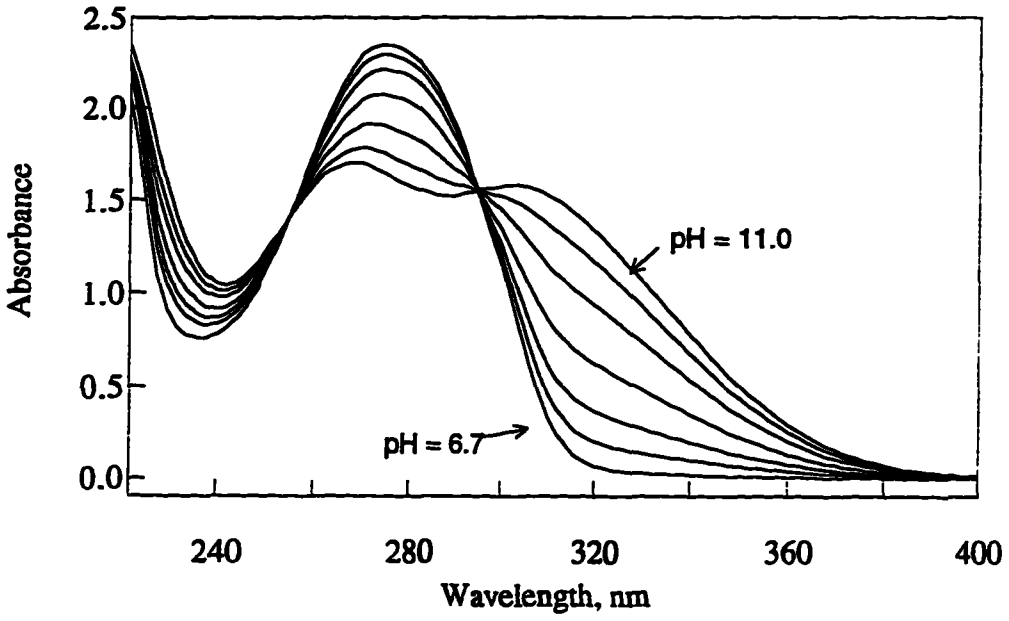

Figure 3.2 (a). UV-VIS spectra of t-CHA as a function of pH.

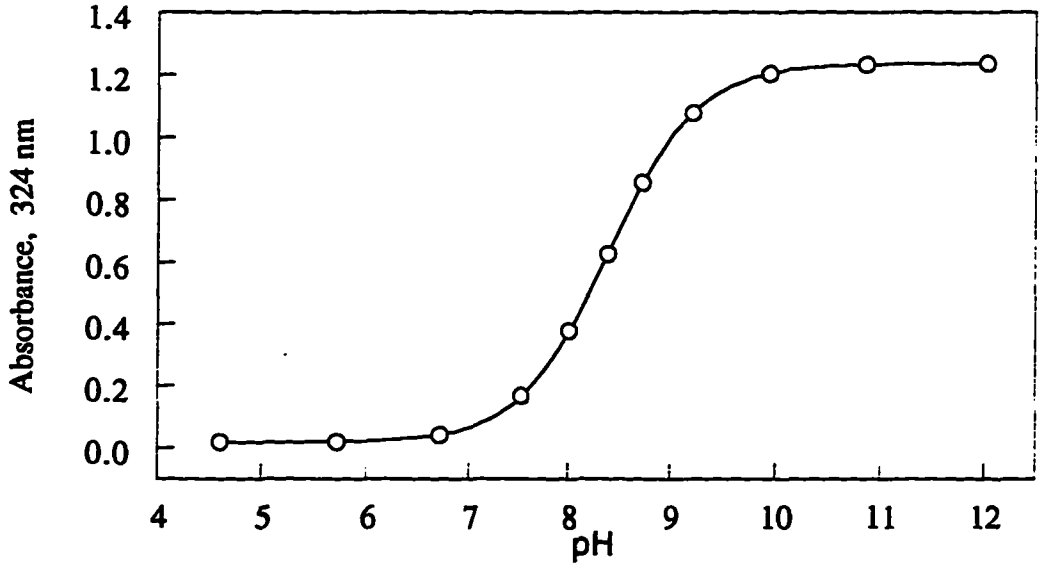

Figure 3.2b. pH titration of t-CHA. The solid line represents the theoretical fit

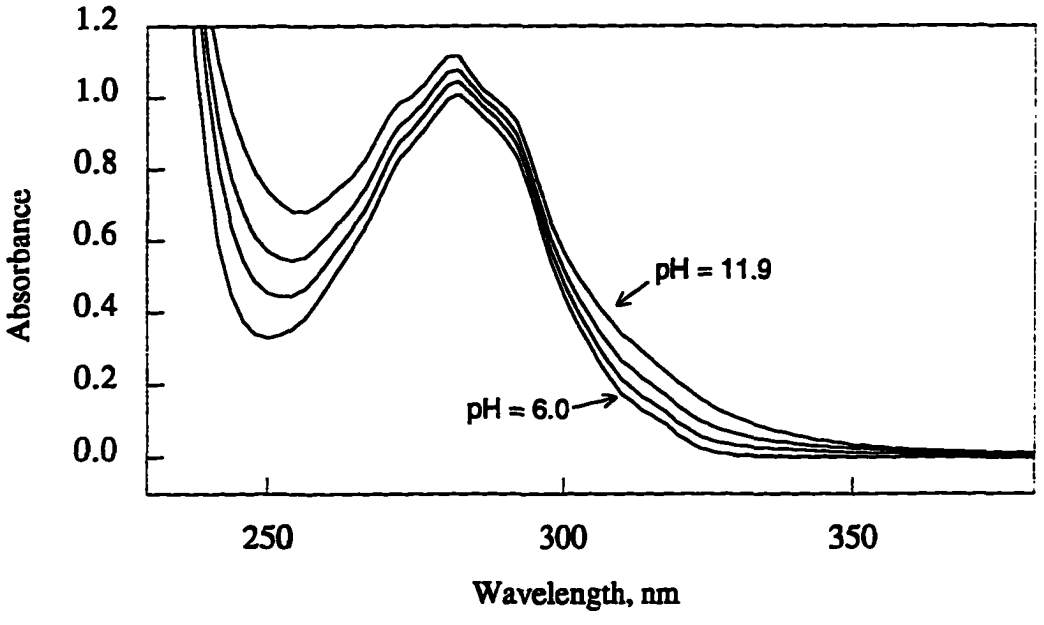

Figure 3.3 (a). UV-VIS spectra of 1-NHA as a function of pH.

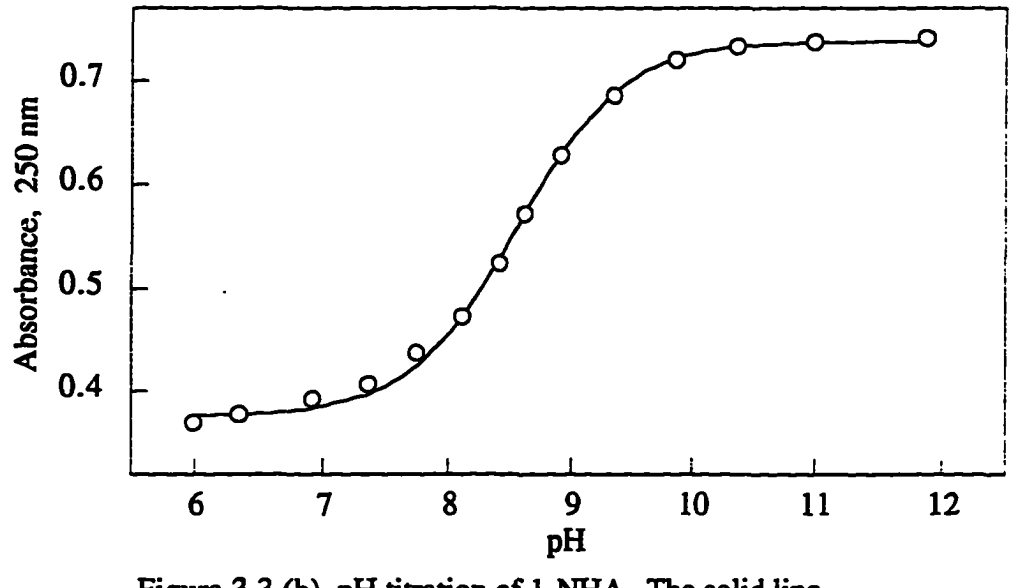

Figure 3.3 (b). pH titration of 1-NHA. The solid line represents the theoretical fit to equation 3.2.

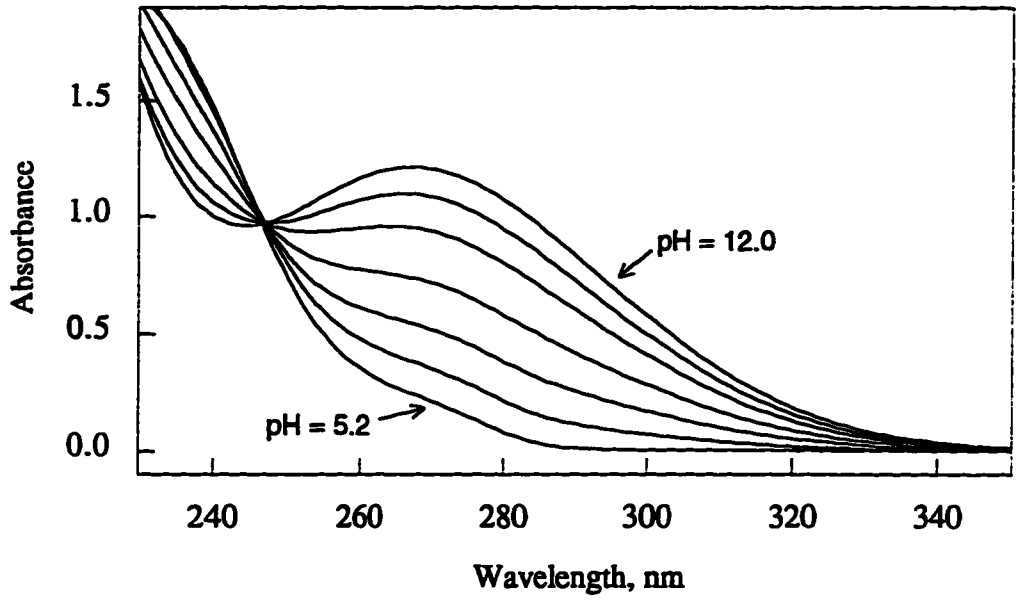

Figure 3.4 (a). UV-VIS spectra for BHA as a function of pH.

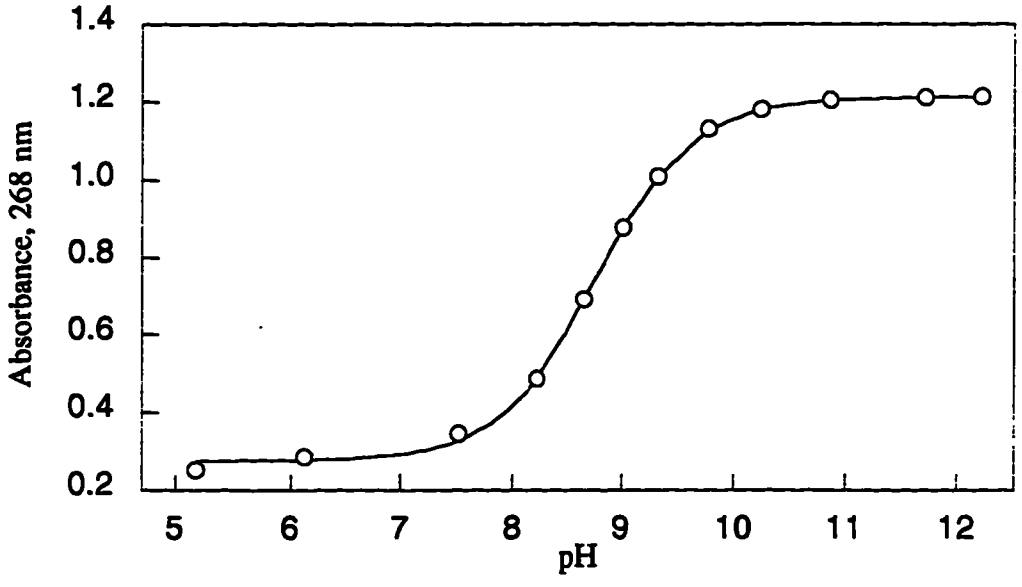

Figure 3.3 (b). pH titration of BHA. The solid line represents the theoritical fit to equation 3.2.

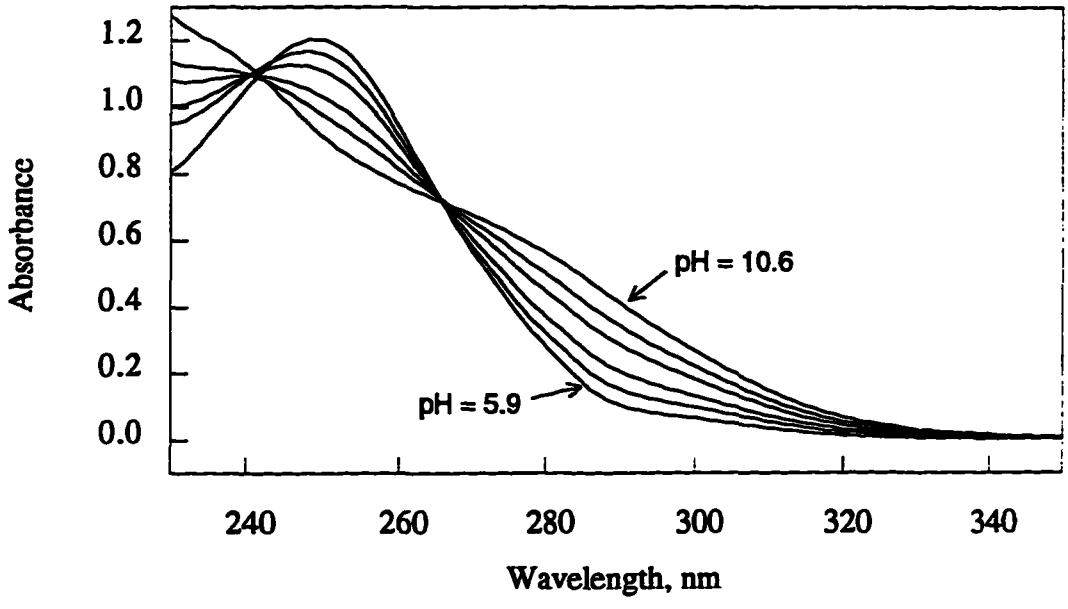

Figure 3.5 (a). UV-VIS spectra of PMBHA as a function of pH.

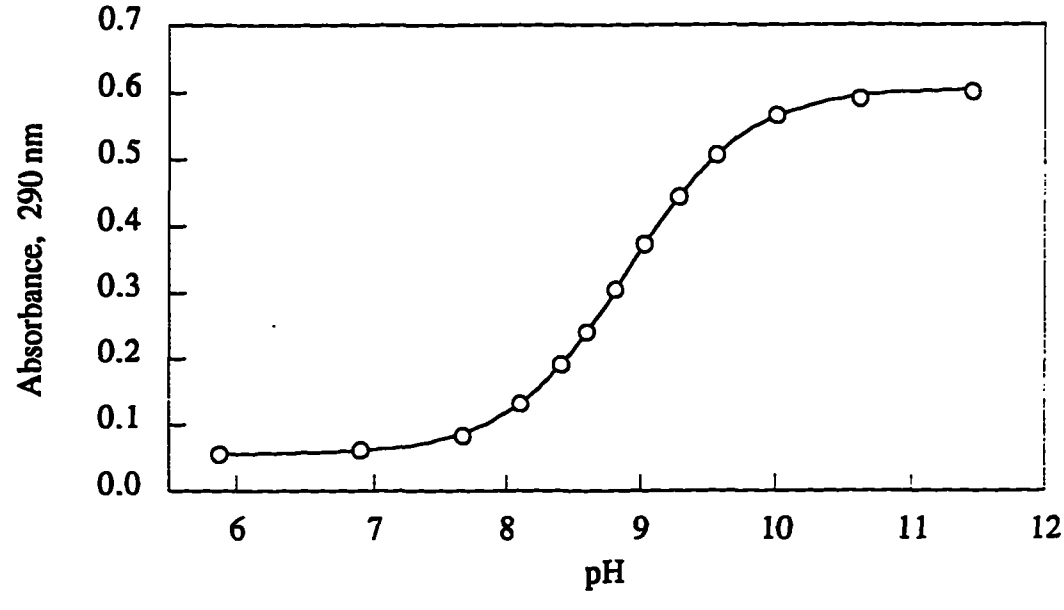

Figure 3.5 (b). pH titration of PMBHA. The solid line represents the theoritical fit to equation 3.2.

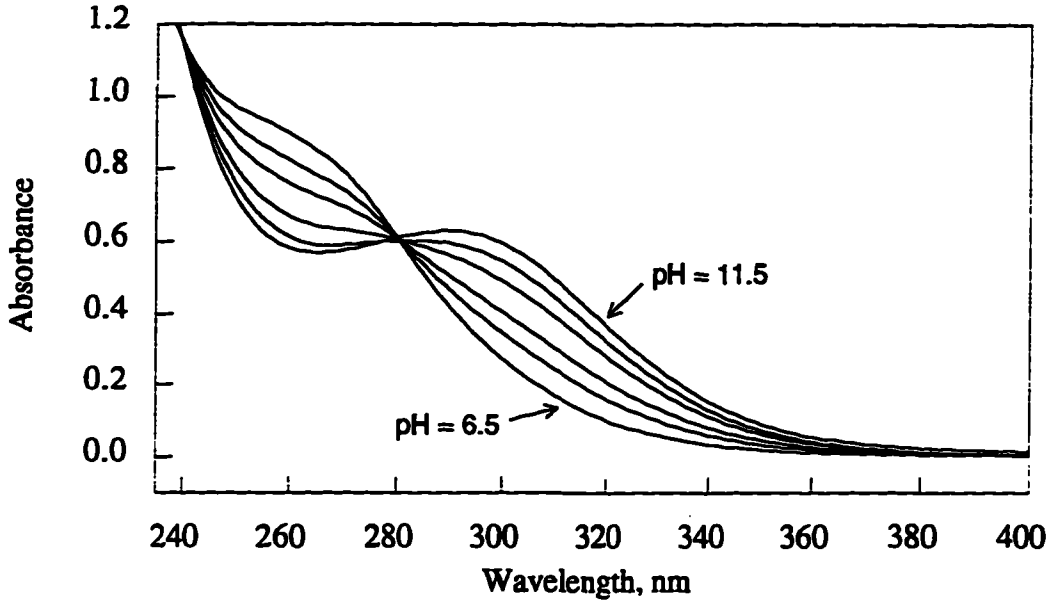

Figure 3.6 (a). UV-VIS spectra of N-PBHA as a function of pH.

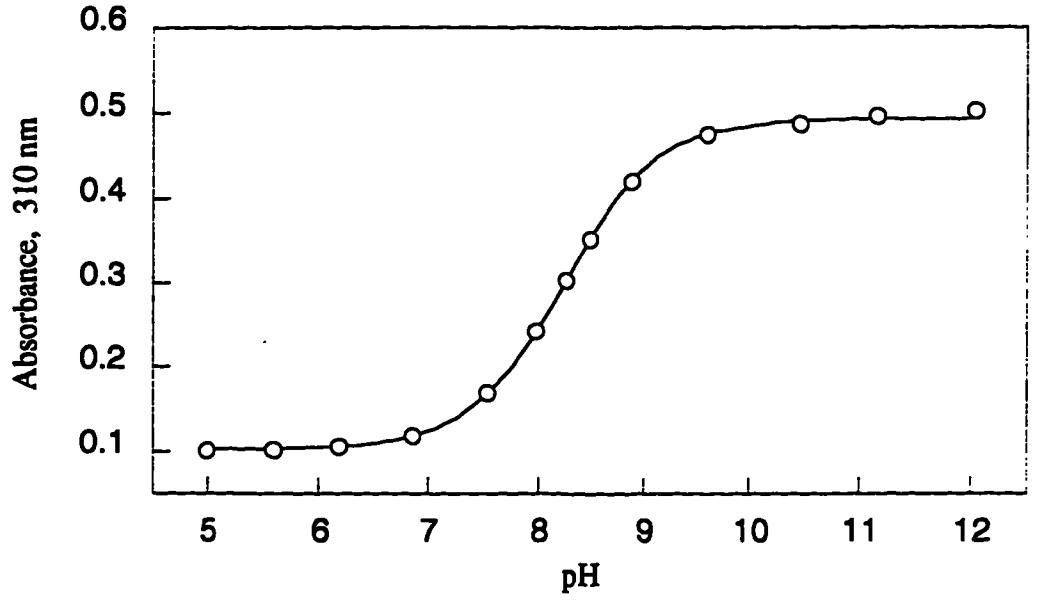

Figure 3.6 (b). pH titration of N-PBHA. The solid line represents theoretical fit.

B. Kinetic Studies of the Nickel(II)-hydroxamate Complexation

The complexation of Ni(II) with each hydroxamic acid produced a large metal-to-ligand charge transfer band in the wavelength region 280-350 nm. Figure 3.7 shows the the charge-transfer band for Ni(II)-(*t*-CHA) which appears at λ_{max} = 300 nm.

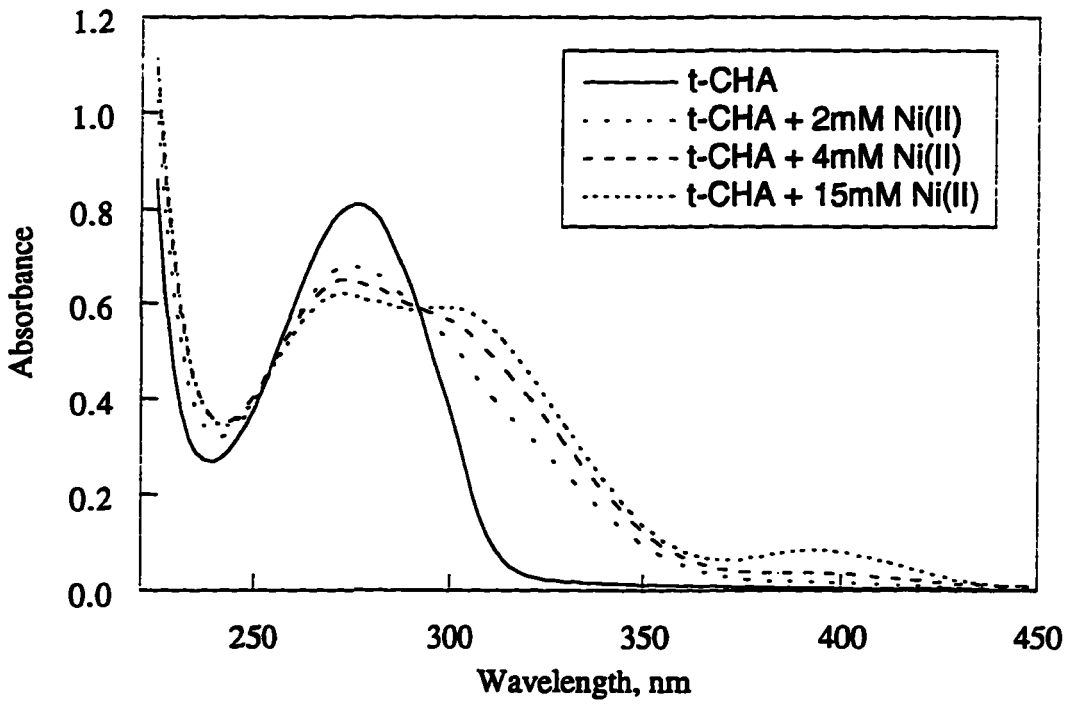

Figure 3.7. UV-Vis spectra of 3 x 10^{-5} M *t*-CHA with increasing concentration of added Ni(II), displaying the complex formation. The peak at 395 nm is due to the absorbance by Ni^{2+}.

The kinetics for all the reactions were studied using at least a ten-fold excess of Ni(II). All reactions displayed first-order behavior. A typical absorbance versus time curve for the reaction of Ni(II) with hydroxamic acids is shown in Figure 3.8 in which,

A_0 and A_∞ are the initial and final values of the absorbance, respectively, and ΔA is the total absorbance change. If A_i is the instantaneous value for the absorbance at any time t, equation 3.6 can be derived (see Appendix I for derivation).

$$\ln [A_i - A_\infty] = \ln [A_0 - A_\infty] - k_{obs}\, t \qquad (3.6)$$

A linear least-squares analysis of the absorbance-time data was performed using equation 3.6 to obtain the values of k_{obs}. The value of k_{obs} is given by the slope of the ln $[A_i - A_\infty]$ versus time plot. The intercepts of these plots gave the values for ln $[A_0 - A_\infty]$. Since $\Delta A = A_\infty - A_0$, the value of ΔA was calculated by evaluating the inverse ln of the intercept values obtained from the linear least-squares fits.

The value of absorbance used for the A_∞ for each run was the average of 50 points taken after 99.6% (8 half-lives) of the reaction was complete. The value of A_0 was calculated using the relationship $A_0 = A_\infty - \Delta A$. The kinetic data for the reactions of Ni(II) with selected hydroxamic acids are compiled in Appendix II. The reported values of k_{obs}, ΔA, A_∞ and A_0 represent the averages of at least four determinations. The errors in their values represent one standard deviation form the mean value. For the reaction with very small signal changes such as the formation of nickel-napthohydroxamate complex, greater number of kinetic runs were performed for the purpose of averaging.

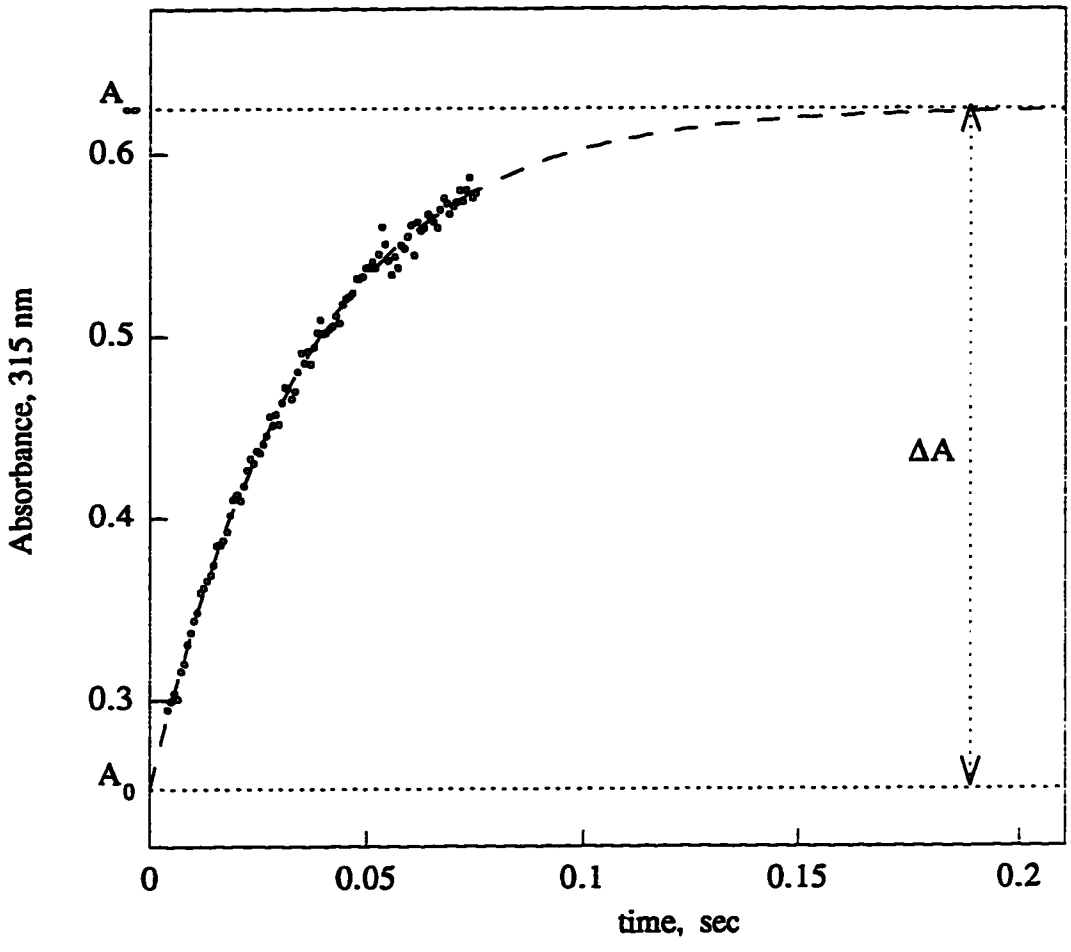

Figure 3.8. Absorbance versus time curve obtained for the complexation of nickel napthohydroxamate at pH = 5.43, [Ni(II)] = 15 mM; [1-NHA] = 1.2 x 10^{-4} M and I = 0.1M. The dashed line represents the nonlinear least-squares fit to the equation $A_i = A_\infty - \Delta A \exp(- k_{obs} t)$, which is a rearranged form of equation 3.6 when $A_\infty > A_0$.

C. Mechanism, Rate Law and Resolution of the Individual Rate Constants

For the reactions of hydroxamic acids with excess Ni(II) at a given pH, the plots of k_{obs} versus $[Ni^{2+}]$ gave straight lines indicating the first-order dependence of k_{obs} on $[Ni^{2+}]$. The kinetic behavior observed in these plots may be represented by equation 3.7, where k_f and k_d represent the slope and the intercept, respectively.

$$k_{obs} = k_f [Ni^{2+}] + k_d \qquad (3.7)$$

Figure 3.9 shows plots of k_{obs} versus $[Ni^{2+}]$ at different pH values, obtained for the formation of Ni(II)-PNBHA complex. These plots show the linear dependence of k_{obs} on $[Ni^{2+}]$. Similar plots were obtained for all other hydroxamic acids used in this study and two common features were noticed: i) the slopes increased with an increase in pH, and ii) the values for the intercepts decreased with an increase in pH. Such behavior is consistent with a mechanism shown in Scheme 3.1.

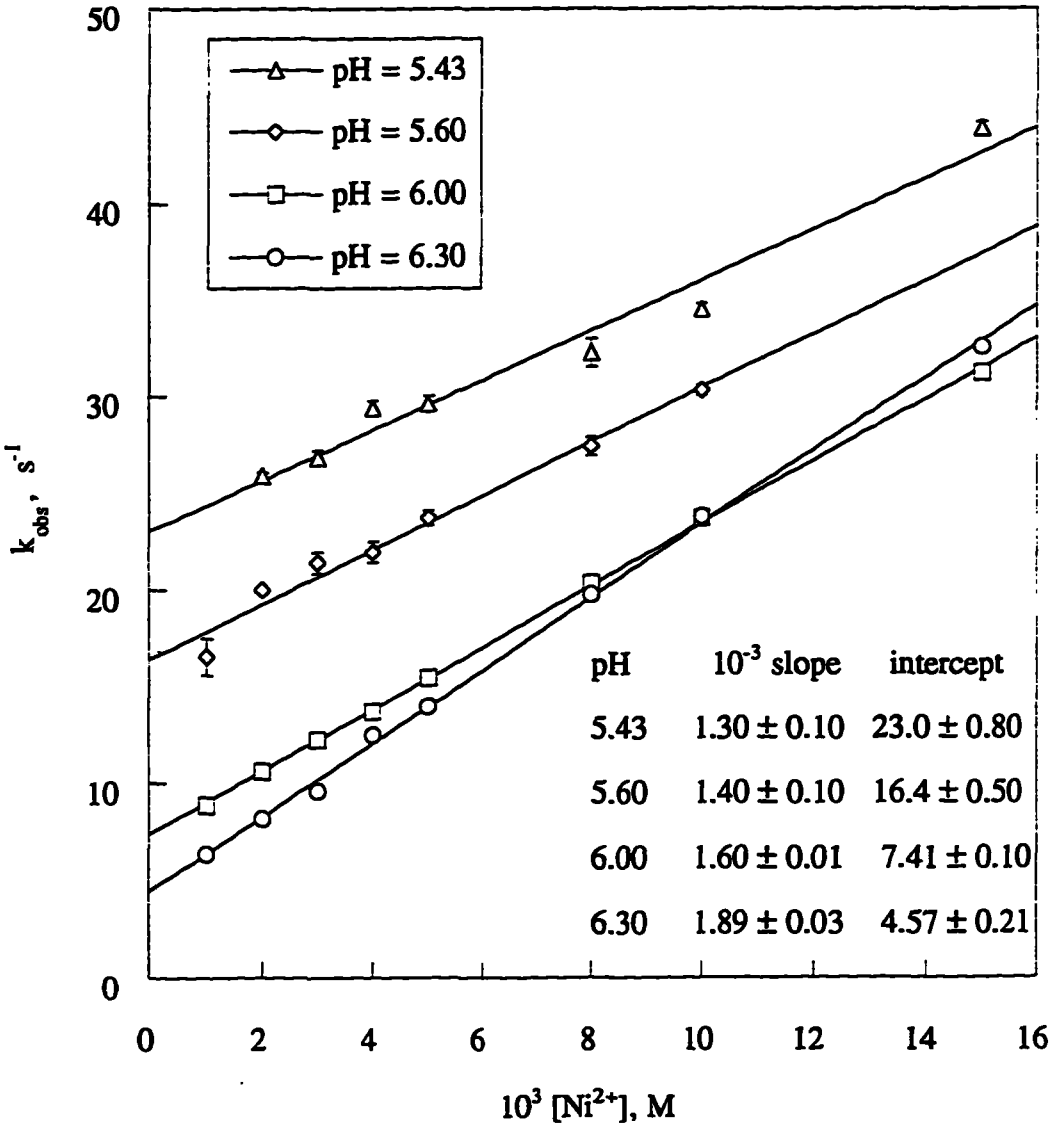

Figure 3.9 Dependence of k_{obs} on $[Ni^{2+}]$ and pH for the formation of nickel para-nitrobenzohydroxamate complex at 25.0 °C and I = 0.10 M ($NaClO_4$).

Scheme 3.1

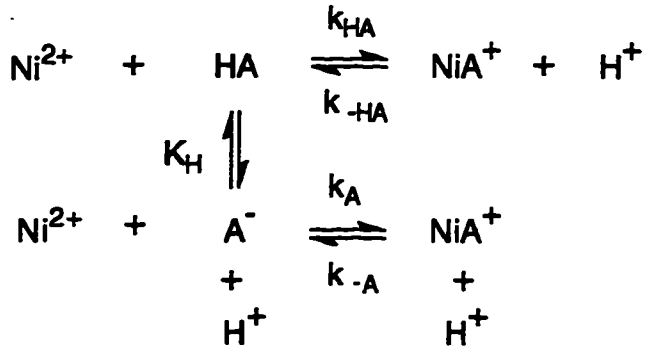

If $[HA]_{tot}$ is the concentration of the free ligand (HA + A^-), the rate law for its disappearance according to Scheme 3.1 is given by the expression shown by equation 3.8. This expression is derived in Appendix I.

$$\frac{-d[HA]_{tot}}{dt} = \left[\frac{(k_A + k_{HA} K_H [H^+])[Ni^{2+}]}{1 + K_H [H^+]} + k_{-A} + k_{-HA} [H^+] \right] ([HA]_{tot} - [HA]_{tot,\infty}) \tag{3.8}$$

or,

$$\frac{-d[HA]_{tot}}{dt} = k_{obs} ([HA]_{tot} - [HA]_{tot,\infty}) \tag{3.9}$$

where,

$$k_{obs} = \frac{(k_A + k_{HA} K_H [H^+])[Ni^{2+}]}{1 + K_H [H^+]} + k_{-A} + k_{-HA} [H^+] \tag{3.10}$$

From equations 3.7 and 3.10,

$$k_f = \frac{(k_A + k_{HA} K_H [H^+])}{1 + K_H [H^+]} \tag{3.11}$$

and

$$k_d = k_{-A} + k_{-HA} [H^+] \tag{3.12}$$

After rearrangement, expression 3.11 may be written in the form

$$k_f\{1+K_H[H^+]\} = k_A + k_{HA} K_H [H^+] \tag{3.13}$$

Equations 3.11 and 3.12 describe the expressions for the slope (k_f) and the intercept (k_d), respectively, of the k_{obs} versus $[Ni^{2+}]$ plot. The expression for the slope contains the quantities, k_A and k_{HA}, which represent the individual formation rate constants for the unprotonated and the monoprotonated ligand species, respectively, and the expression for k_d contains the quantities, k_{-A} and k_{-HA}, which represent the individual dissociation rate constants . Thus, the slope represents the overall complex formation rate constant and the intercept represents the overall complex dissociation rate constant.

In accordance with equations 3.12 and 3.13, when $k_f\{1+K_H[H^+]\}$ and k_d were plotted against $[H^+]$, straight lines were obtained. From the slopes and intercepts of these plots the individual rate constants k_A, k_{HA}, k_{-A}, and k_{-HA} were extracted. In the plots of $k_f\{1+K_H[H^+]\}$ versus $[H^+]$, the slopes are equal to $k_{HA} \cdot K_H$ and the intercepts are equal to k_A; in the plots of k_d versus $[H^+]$ the slopes are equal to k_{-A} and the intercepts are equal to k_{-HA}. The k_f and k_d values required to obtain these replots were calculated from the k_{obs} versus $[Ni^{2+}]$ plots. Figure 3.10 shows the replots for the complexation of Ni(II)-PNBHA.

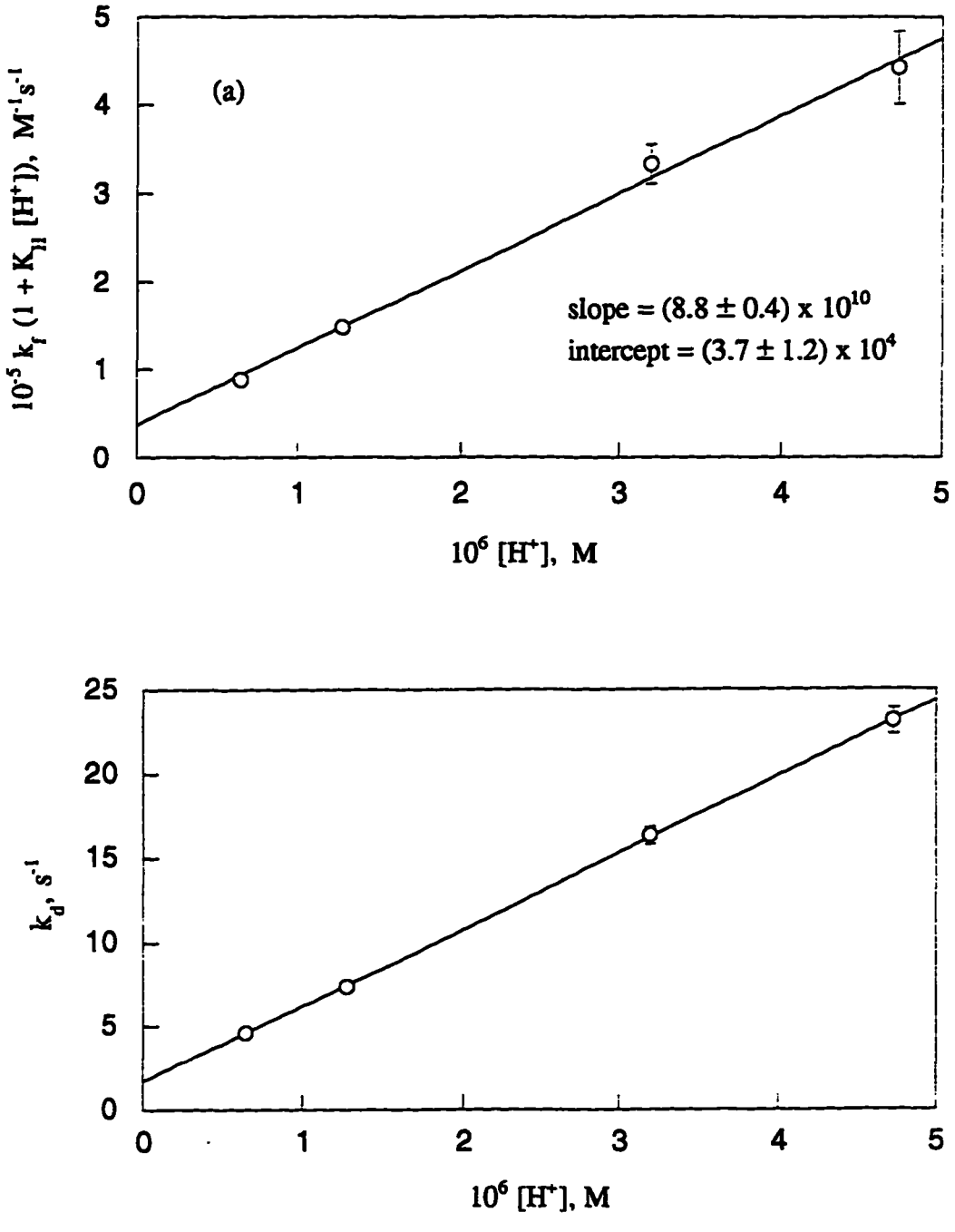

Figure 3.10 Plots of (a) $k_f\{1+K_H[H^+]\}$ versus $[H^+]$ and (b) k_d versus $[H^+]$ for the nickel para-nitrobenzohydroxamate complex formation kinetics. The values for k_f and k_d were obtained from the analysis of the data shown in Figure 3.9.

D. Nonlinear Least-Squares Method for Obtaining the Individual Rate Constants

A second method was used to resolve the individual rate constants for the formation of nickel(II)-hydroxamate complexes as shown in Scheme 3.1. This method involved fitting the k_{obs}-[Ni^{2+}]-[H^+] data to equation 3.10 using a nonlinear least-squares routine.[3,4] The program calculated the estimates for the parameters k_A, k_{HA}, k_{-A} and k_{-HA}.

Figures 3.11 to 3.16 show the plots of k_{obs} versus [Ni^{2+}] for all the hydroxamic acids studied. In these plots, the values used for [Ni^{2+}] are those attained after mixing of the reagents in the stopped-flow cell. The solid lines represent the calculated rate constants, k_{calc}, obtained from non-linear least-squares fit to equation 3.10.

Figures 3.17 to 3.22 show the plots of $k_f\{1+K_H[H^+]\}$ and k_d, versus [H^+]. The dotted lines in these plots represent the linear-least squares fits to the $k_f\{1+K_H[H^+]\}$, [H^+] and k_d, [H^+] data to equation 3.10 and the dashed lines represent the calculated values using the parameters obtained from non-linear least-squares fit. These plots show the agreement between the two methods used to resolve the rate constants in Scheme 3.1 for the formation of Ni(II)-hydroxamates.

The values of the resolved rate constants obtained from the nonlinear least-squares (NLLSQ) and the linear least-squares (LLSQ) methods are summarized in Table 3.3.

Table 3.3. Resolved Rate Constants for the Formation Kinetics of Nickel(II)-hydroxamate Complexes at 25.0 °C and at $I = 0.10$ M

HA	method[a]	$10^{-4} k_A$ $M^{-1}s^{-1}$	$10^{-3} k_{HA}$ $M^{-1}s^{-1}$	k_{-A} s^{-1}	$10^{-6} k_{-HA}$ $M^{-1}s^{-1}$
PNBHA	NLLSQ	2.86 ± 0.09	1.30 ± 0.01	1.66 ± 0.09	4.53 ± 0.03
	LLSQ	4 ± 1	1.22 ± 0.06	1.9 ± 0.4	4.6 ± 0.1
t-CHA	NLLSQ	6.2 ± 0.1	1.72 ± 0.01	2.0 ± 0.1	4.68 ± 0.03
	LLSQ	5.9 ± 0.9	1.69 ± 0.01	1.96 ± 0.01	4.623 ± 0.006
1-NHA	NLLSQ	8.7 ± 0.7	1.02 ± 0.03	2.1 ± 0.2	6.9 ± 0.1
	LLSQ	9 ± 2	1.03 ± 0.04	2 ± 1	2.1 ± 0.2
BHA	NLLSQ	6 ± 2	1.48 ± 0.03	3.4 ± 0.3	6.4 ± 0.1
	LLSQ	7 ± 3	1.46 ± 0.03	3 ± 1	6.6 ± 0.7
PMBHA	NLLSQ	5 ± 2	1.50 ± 0.04	2.4 ± 0.2	9.0 ± 0.2
	LLSQ	9 ± 1	1.41 ± 0.01	2.1 ± 0.7	9.3 ± 0.3
N-PBHA	NLLSQ	2.85 ± 0.09	0.67 ± 0.02	1.2 ± 0.2	0.833 ± 0.007
	LLSQ	1.9 ± 0.6	0.751 ± 0.002	1.3 ± 0.1	0.73 ± 0.4
AHA[b]	-	3 ± 1	0.72 ± 0.01	0.163	8.03

[a]NLLSQ refers to the method in which the rate constants were obtained by fitting the data to equation 3.10 using nonlinear least-squares program. LLSQ refers to the method in which the rate constants were obtained by fitting the data to linear expressions (equations 3.11 and 3.12).

[b]Values for acetohydroxamic acid (AHA) at 20 °C [5].

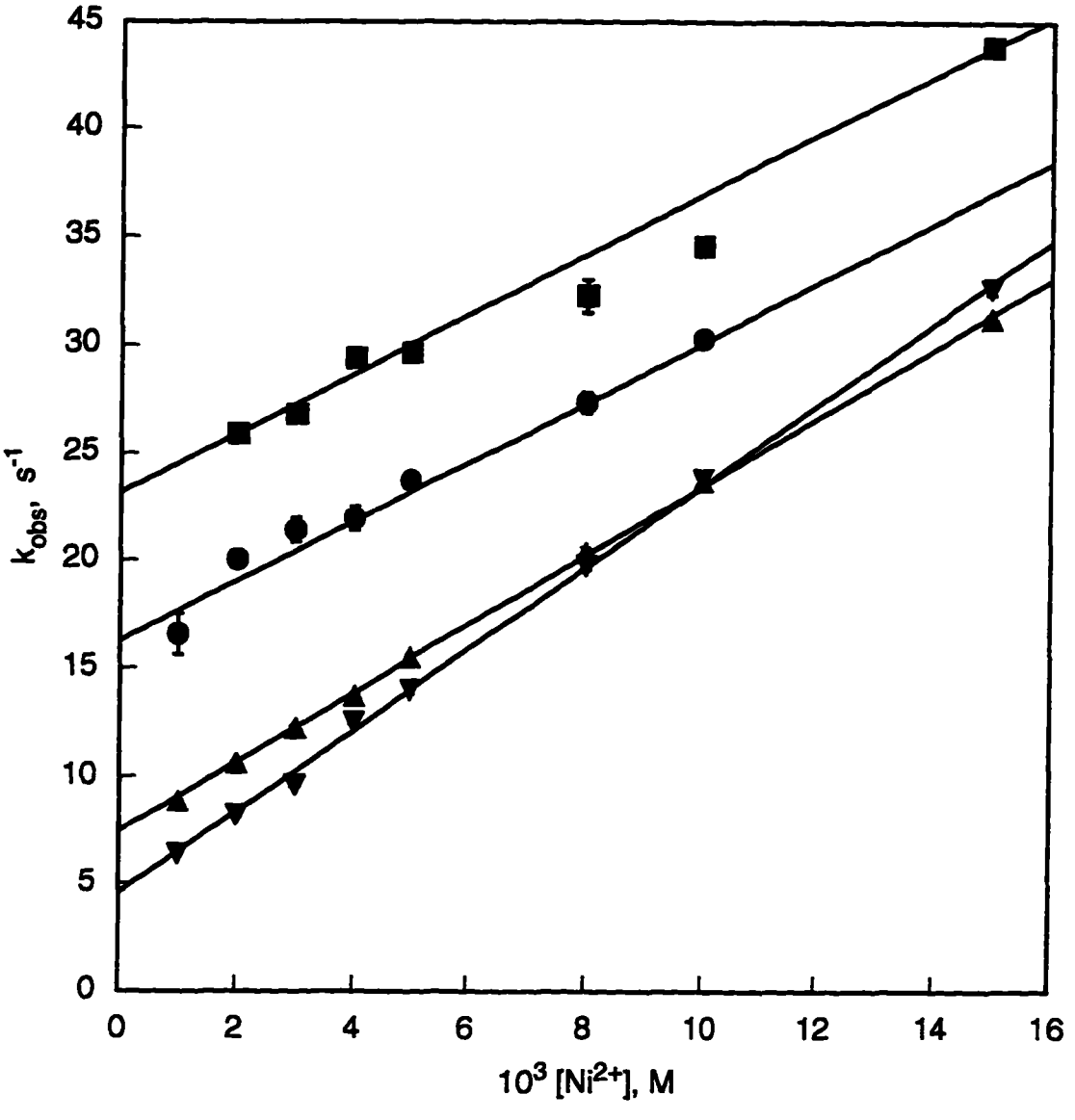

Figure 3.11. Plot of k_{obs} versus [Ni^{2+}] for PNBHA. pH 5.43 = (■); pH 5.60 = (●); pH=6.00 = (▲); pH 6.30 = (▼). The solid lines represents the nonlinear least-squares fit to equation 3.10.

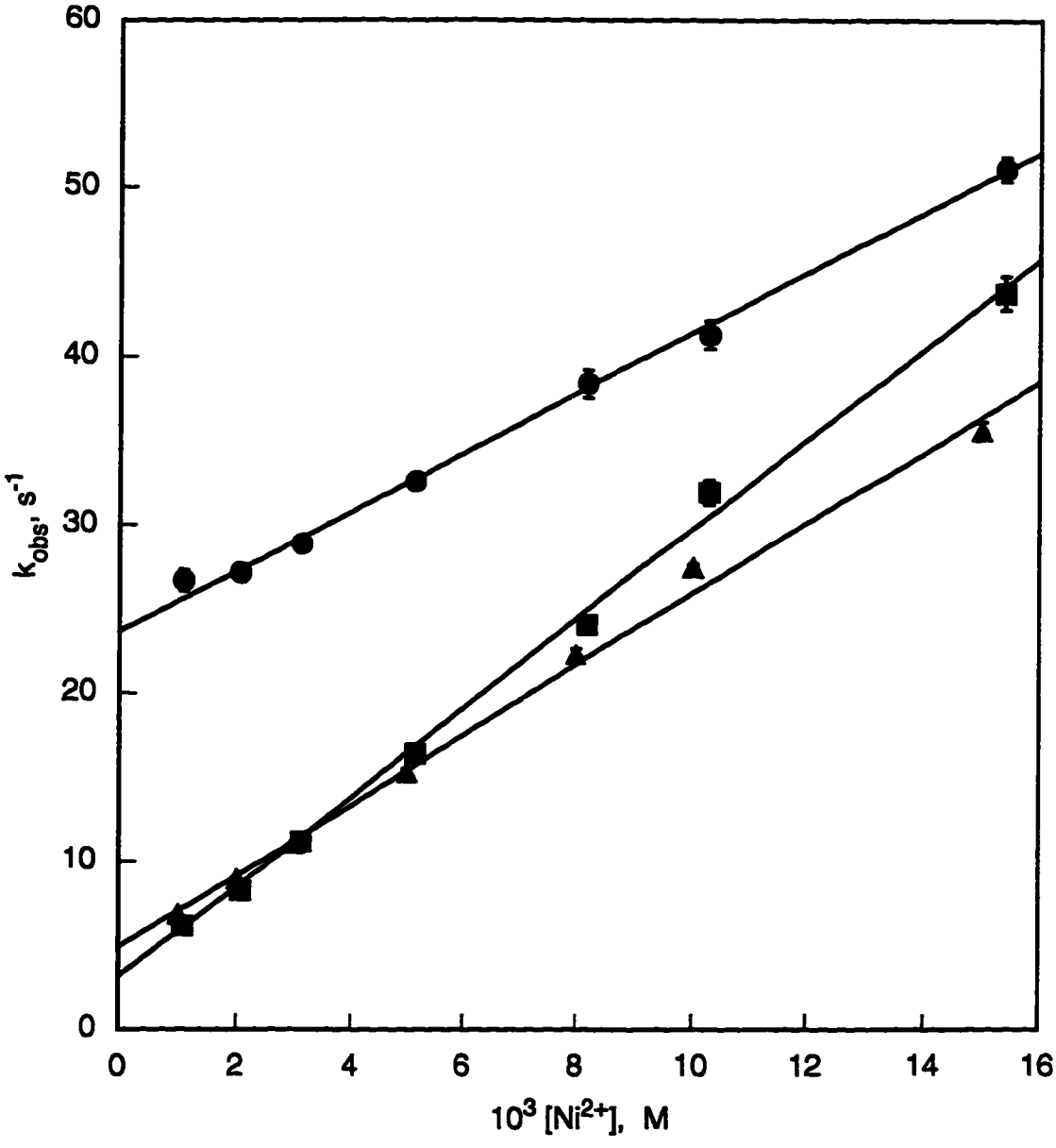

Figure 3.12. Plot of k_{obs} versus [Ni^{2+}] for *t*-CHA as a function of pH. pH 5.43 = (■); pH 6.30 = (●); pH 6.70 = (▲). The solid lines represents the nonlinear least-squares fit to equation 3.10.

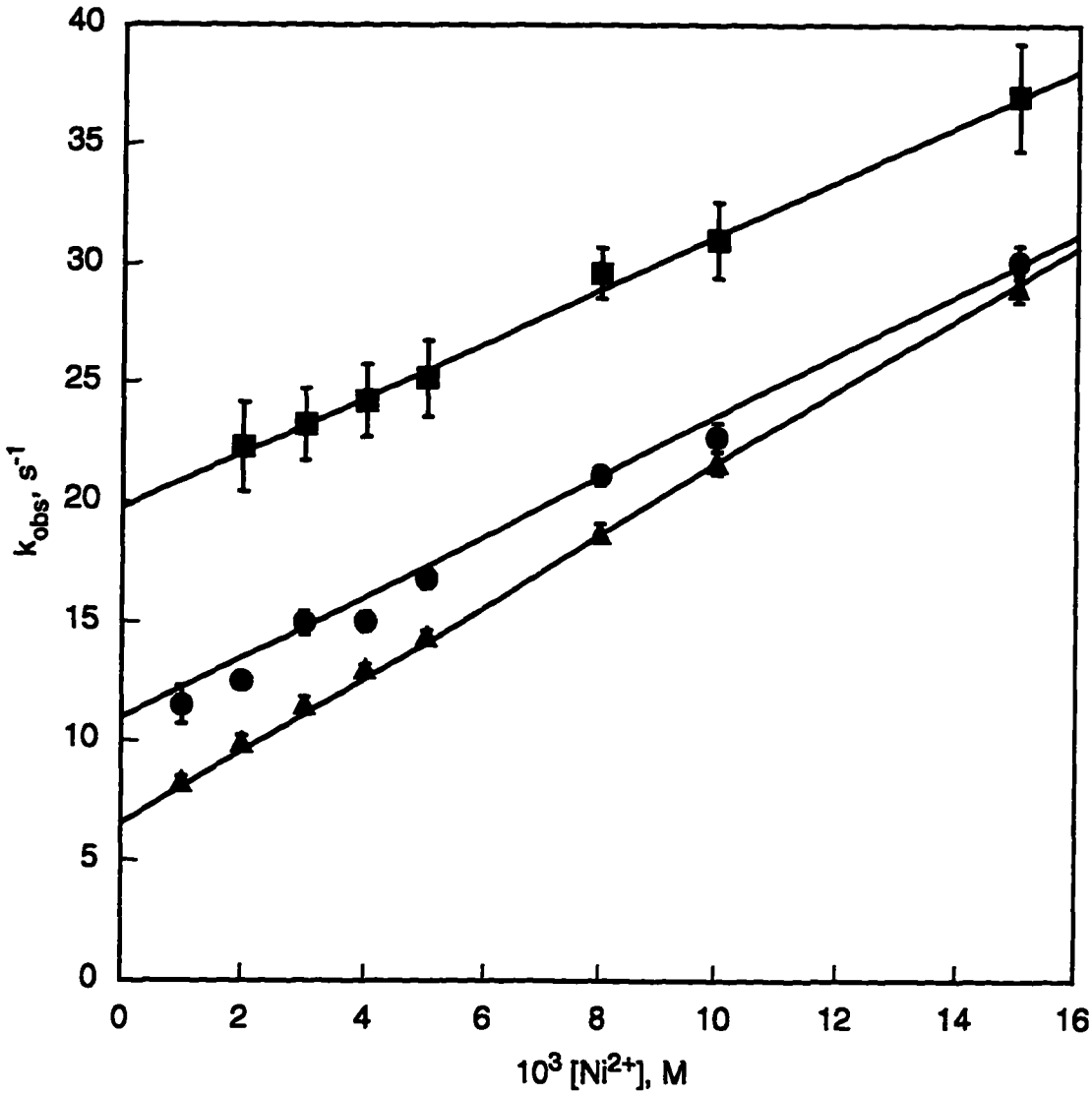

Figure 3.13. Plot of k_{obs} versus [Ni^{2+}] for 1-NHA as a function of pH. pH 5.70 = (■); pH 6.00 = (●); pH 6.30 = (▲). The solid lines represents the nonlinear least-squares fit to equation 3.10.

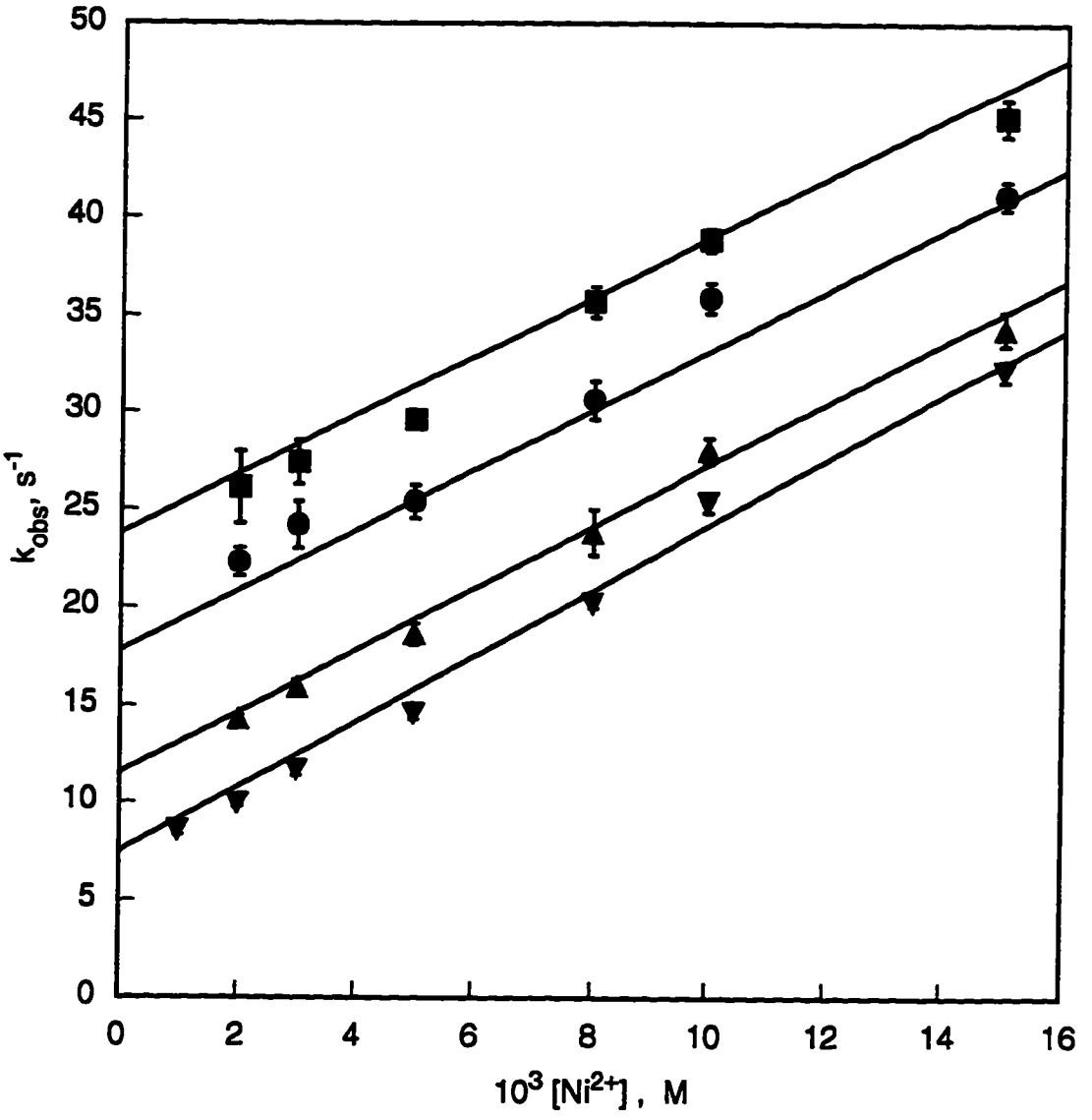

Figure 3.14. Plot of k_{obs} versus [Ni^{2+}] for BHA. pH 5.60 = (■); pH 5.75 = (●); pH 6.00 = (▲); pH 6.3 = (▼). The solid lines represents the nonlinear least-squares fit to equation 3.10.

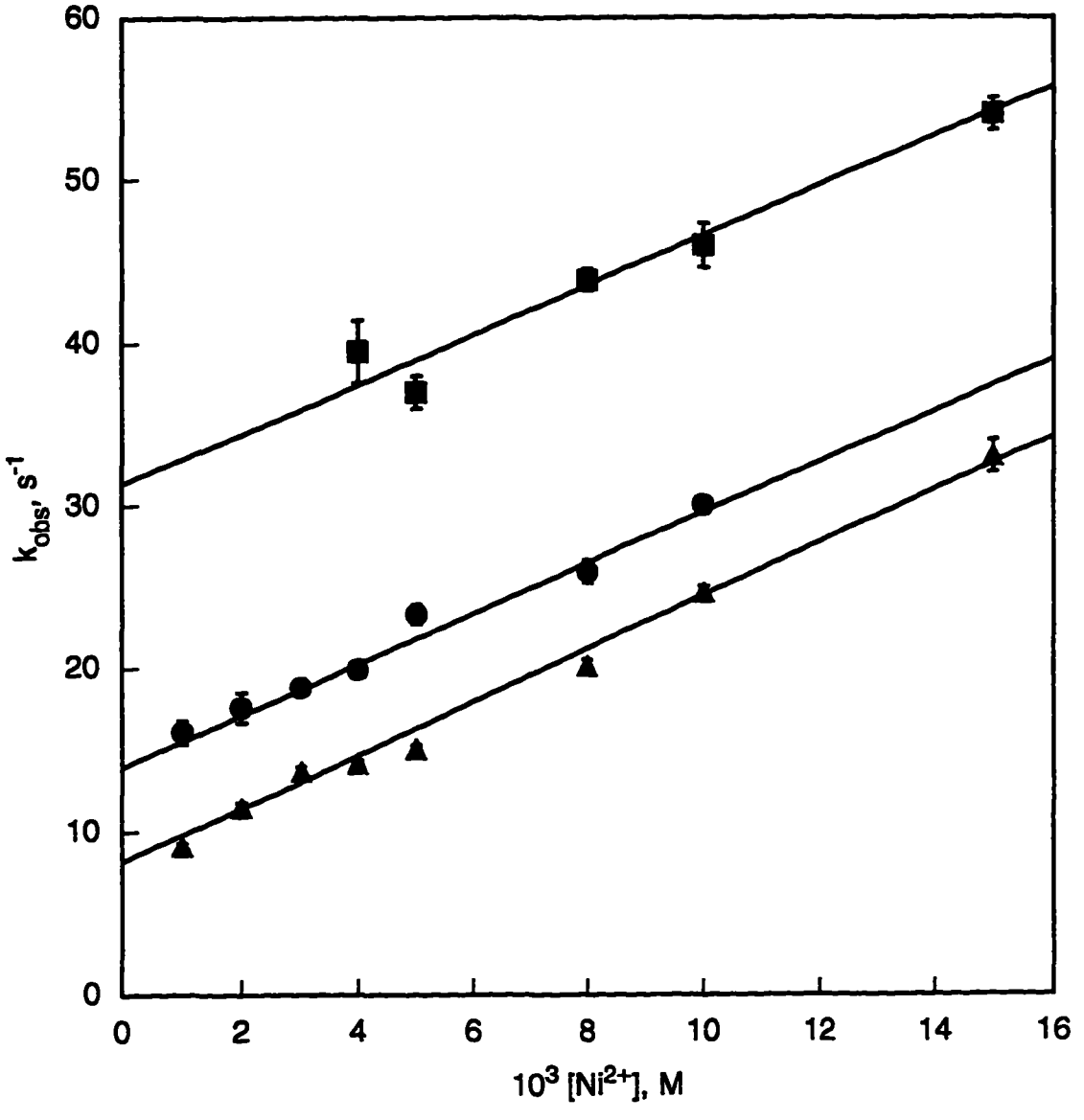

Figure 3.15. Plot of k_{obs} versus [Ni^{2+}] for PMBHA. pH 5.60 = (■); pH 6.00 = (●); pH 6.30 = (▲). The solid lines represents the nonlinear least-squares fit to equation 3.10.

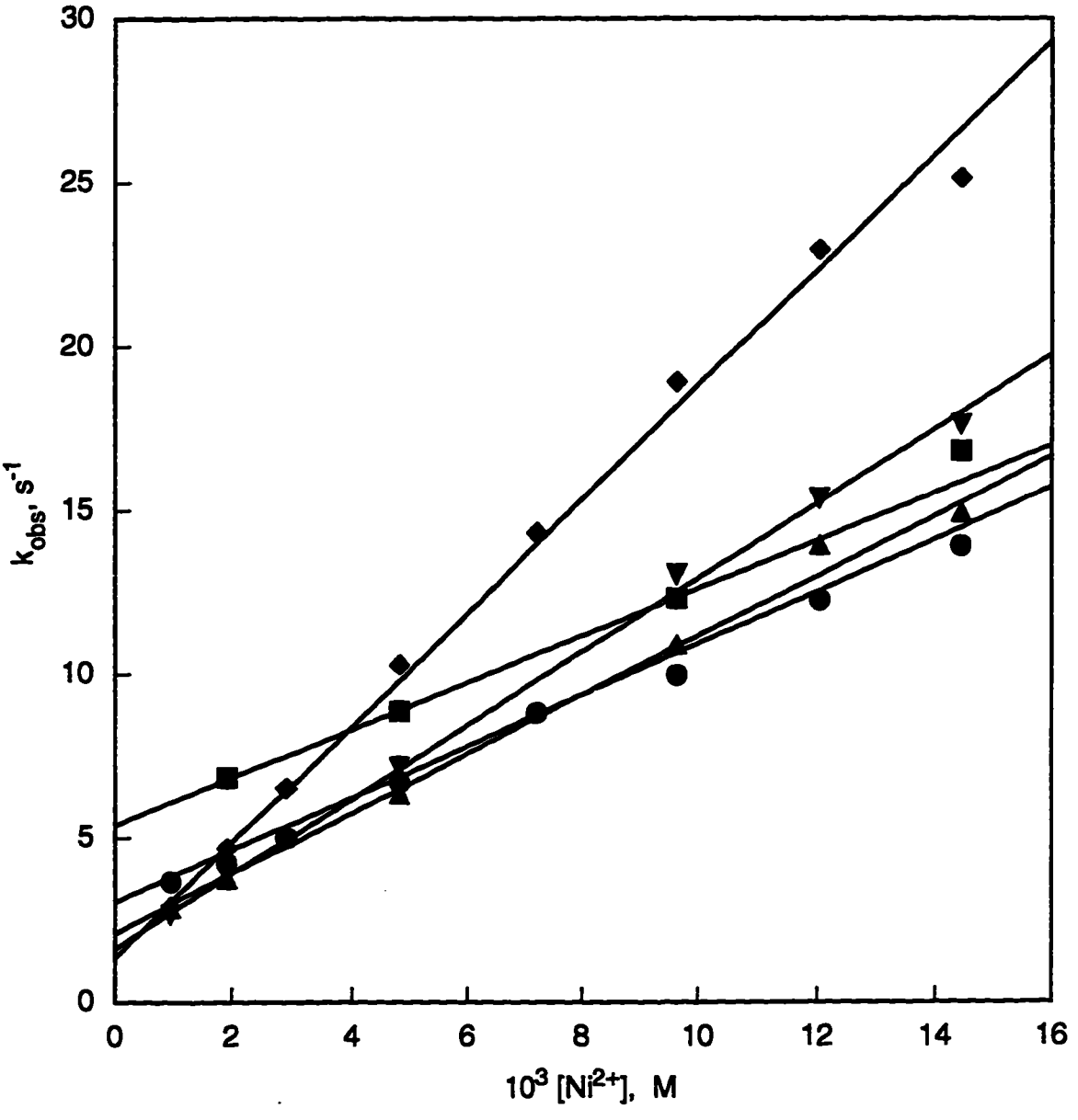

Figure 3.16. Plot of k_{obs} vs [Ni^{2+}] for N-PBHA as a function of pH. pH 5.40 = (■); pH 5.75 = (●); pH 6.05 = (▲); pH 6.34 = (▼); pH 6.72 = (◆). The solid lines represents the nonlinear least-squares fit to equation 3.10.

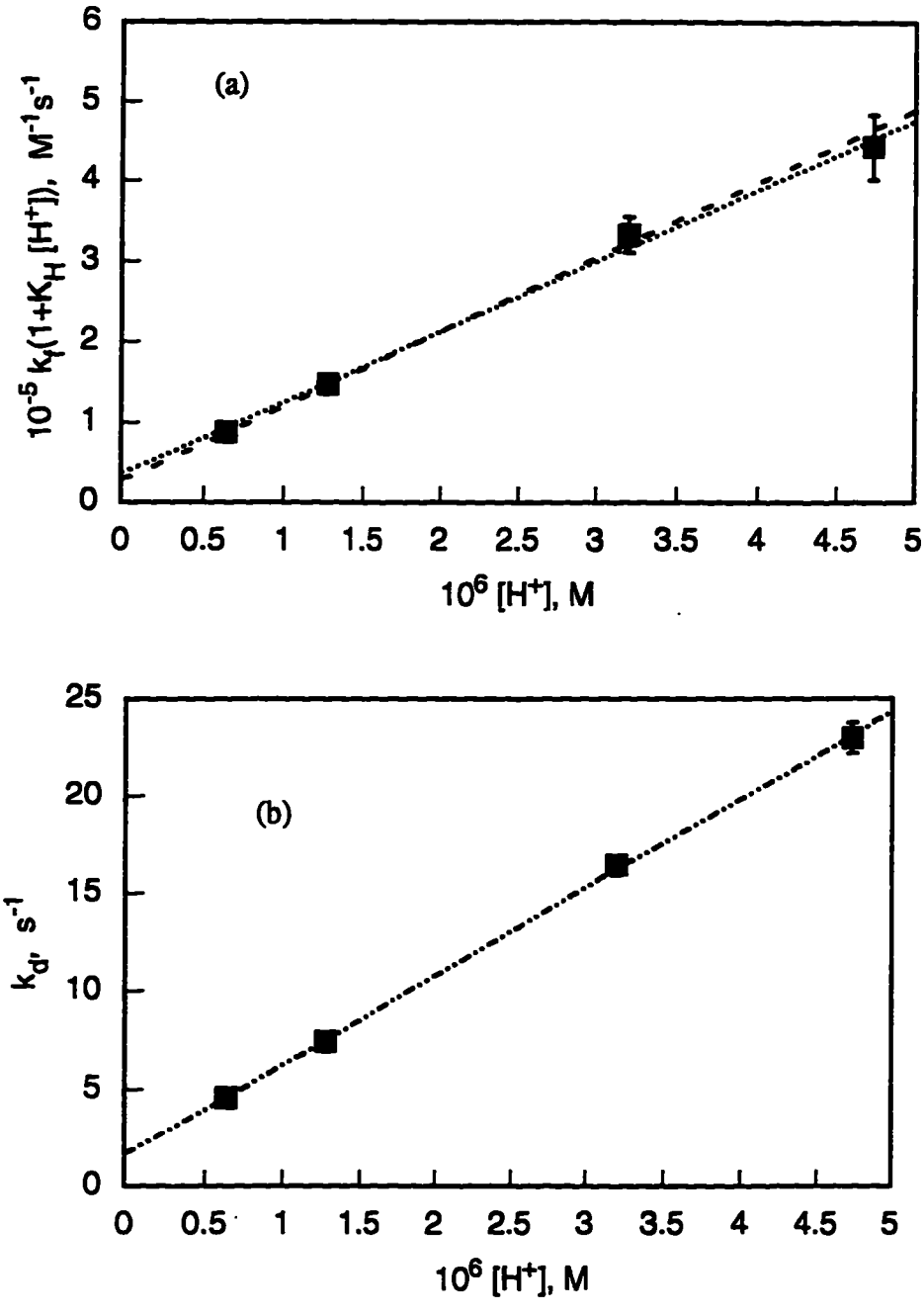

Figure 3.17. (a) slope and (b) intercept replots for PNBHA. The dotted lines represent the linear least-squares fit to the points calculated from the experimental data and the dashed lines represent the theoretical nonlinear least-squares fit to equation 3.10 .

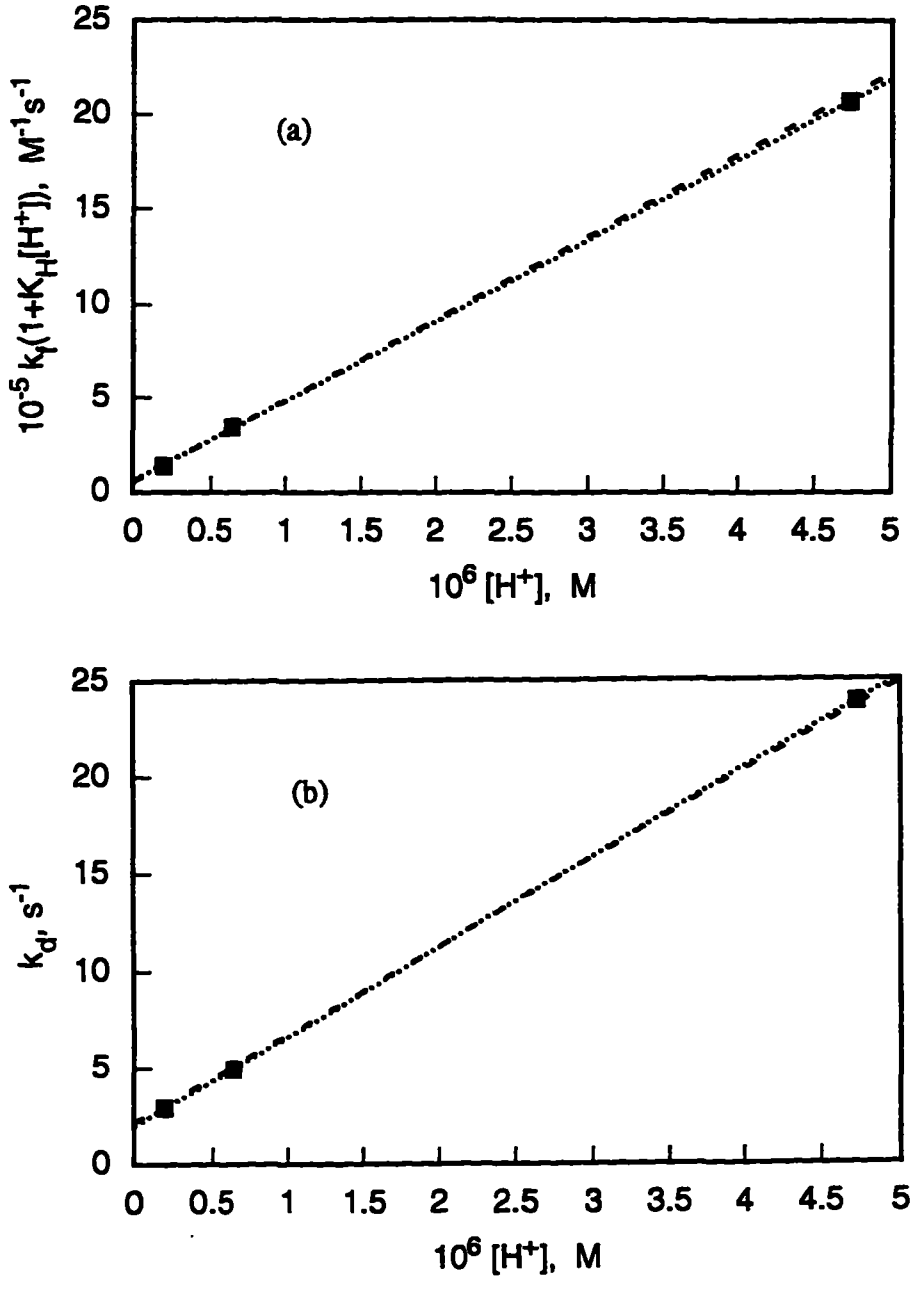

Figure 3.18. (a) Slope and (b) intercept replots for *t*-CHA. The dotted lines represent the linear least-squares fit to the points calculated from the experimental data and the dashed lines represent the theoretical nonlinear least-squares fit to equation 3.10 .

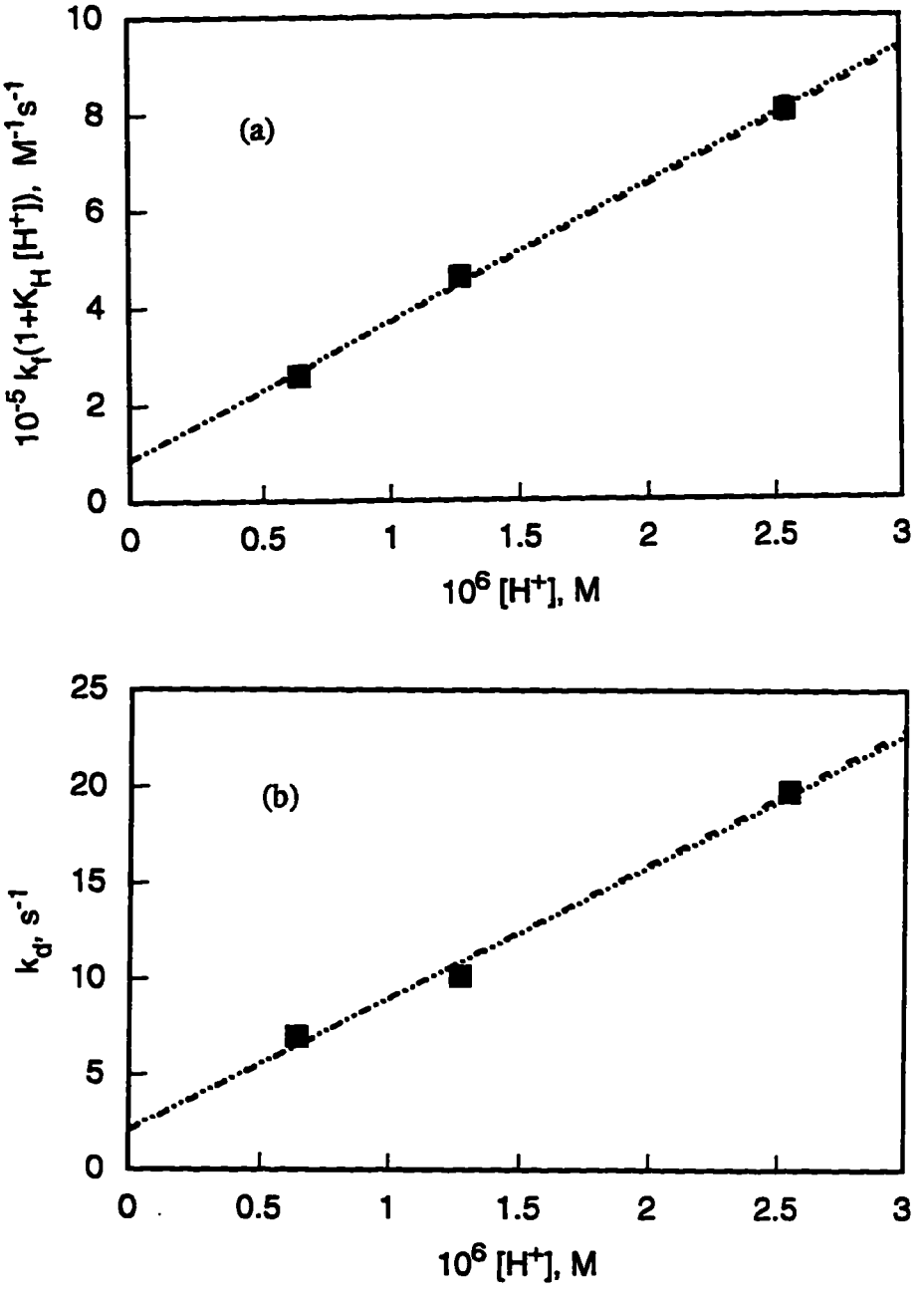

Figure 3.19. (a) slope and (b) intercept replots for 1-NHA. The dotted lines represent the linear least-squares fit to the points calculated from the experimental data and the dashed lines represent the theoretical nonlinear least-squares fit to equation 3.10.

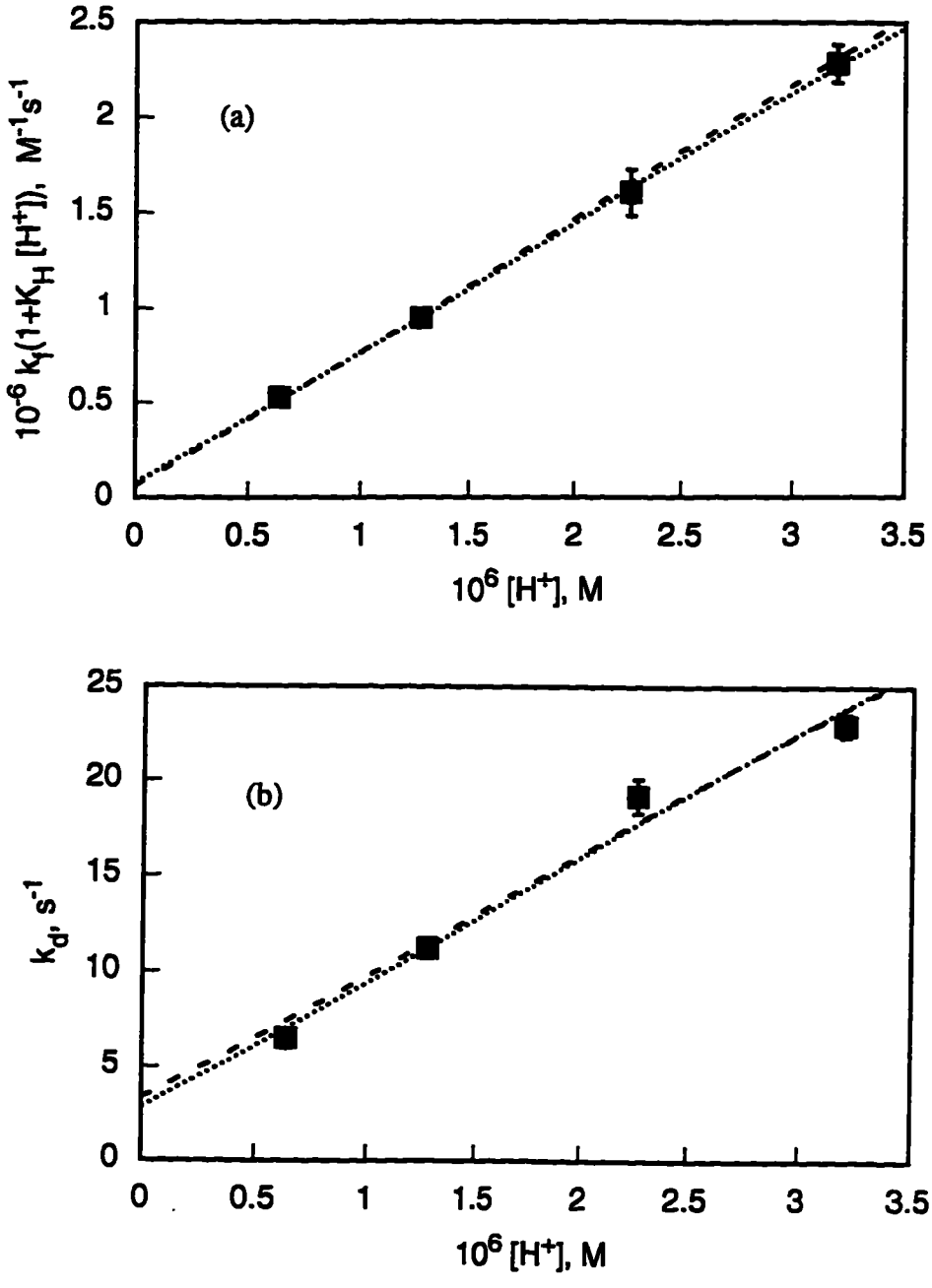

Figure 3.20. (a) slope and (b) intercept replots for BHA. The dotted lines represent the linear least-squares fit to the points calculated from the experimental data and the dashed lines represent the theoretical nonlinear least-squares fit to equation 3.10 .

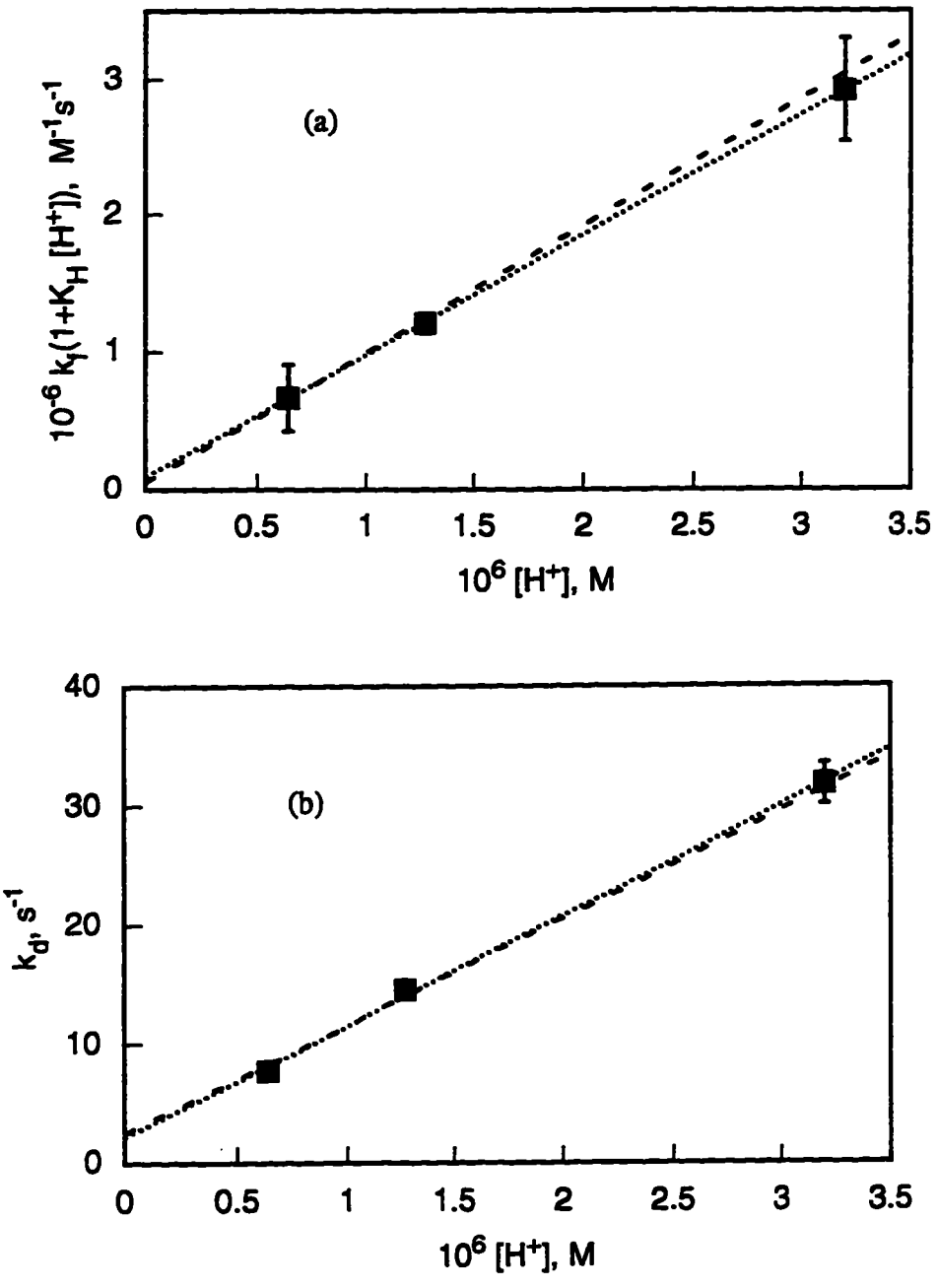

Figure 3.21. (a) slope and (b) intercept replot for PMBHA. The dotted lines represent the linear least-squares fit to the points calculated from the experimental data and the dashed lines represent the theoretical nonlinear least-squares fit to equation 3.10 .

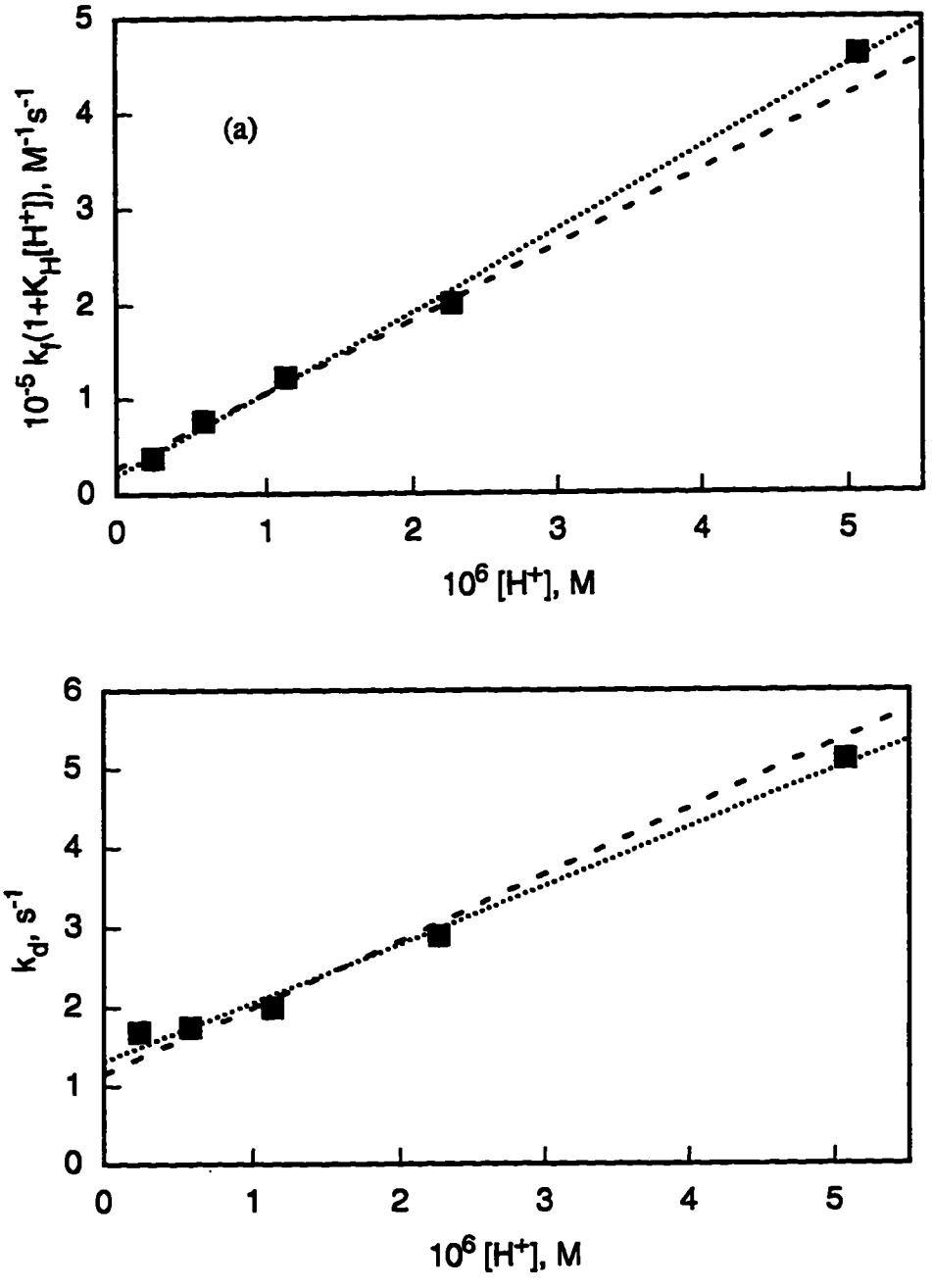

Figure 3.22. (a) slope and (b) intercept replot for *N*-PBHA. The dotted lines represent the linear least-squares fit to the points calculated from the experimental data and the dashed lines represent the theoretical nonlinear least-squares fit to equation 3.10 .

E. Determination of Stability Constants for Ni(II)-Hydroxamates

The absorbance data obtained from the stopped-flow kinetic studies were used to calculate the stability constants for nickel hydroxamate complexes. It follows from the proposed Scheme 3.1, that the reactions of hydroxamic acids with Ni(II) are reversible, and, the amount of Ni(II)-hydroxamate formed is a function of $[Ni^{2+}]$ and $[H^+]$. Since the reactions do not go to completion under the conditions chosen for our studies, the conditional stability constants for 1:1 Ni(II)-hydroxamate complex can be calculated from the acquired data. At a given pH value the conditional stability constant, K'_{NiA}, is defined as

$$K'_{NiA} = \frac{[NiA^+]_\infty}{[Ni^{2+}]_\infty [HA]_{tot,\infty}} \tag{3.14}$$

where $[HA]_{tot,\infty} = [A^-]_\infty + [HA]_\infty$, and the subscript ∞ is refers to the equilibrium concentration of a species. The values of K'_{NiA} were obtained from the relationship given by equation 3.15 which is derived in Appendix I, part B.

$$\Delta A_{Ni} = \frac{\Delta A_{sat} K'_{NiA} [Ni^{2+}]_\infty}{1 + K'_{NiA} [Ni^{2+}]_\infty} \tag{3.15}$$

In equation 3.15, ΔA_{Ni} is the value of the total absorbance change for a reaction at a given $[Ni^{2+}]$, and ΔA_{sat} is the value of the limiting absorbance change for the reaction with high Ni(II) concentration.

It is described in Section B of this chapter, how the values for ΔA (subscript Ni is omitted for a general case) were calculated from the absorbance versus time data. The ΔA_{Ni} value for a reaction is directly proportional to the amount of the product formed. The

amount of product formed in a reaction, according to Scheme 3.1, would increase with increasing $[Ni^{2+}]$ or pH and it is evident from the data shown in Appendix II, that ΔA_{Ni} shows this trend. The ΔA_{Ni}, $[Ni^{2+}]$ data for each pH value, were fitted to equation 3.15 using a non-linear least-squares method[3.4] to obtain estimates of the parameters ΔA_{sat} and K'_{NiA}.

It is worthwhile to note that the values of K'_{NiA} may also be obtained by fitting $A_{\infty, Ni}$, $[Ni^{2+}]$ data to a similar expression given by equation 3.16 (see Appendix I for derivation).

$$A_{\infty, Ni} = \frac{A_0 + A_{sat} K'_{NiA} [Ni^{2+}]_\infty}{1 + K'_{NiA} [Ni^{2+}]_\infty} \qquad (3.16)$$

However, the procedure for evaluating K'_{NiA}, from $A_{\infty, Ni}$, $[Ni^{2+}]$ data obtained on the stopped-flow instrument, is subject to greater error. The error is introduced because of the frequent voltage drifts in the main electricity power-line, from which the electricity is drawn for the operation of the stopped-flow instrument. If a voltage-drift occurred during the course of an experiment, the values of $A_{\infty, Ni}$ are affected because of the reasons described below.

The values of $A_{\infty, Ni}$ are calculated using equation 3.17.

$$A_{\infty, Ni} = - \log \left(\frac{v_\infty}{v_{ref}} \right) \qquad (3.17)$$

where v_{ref} and v_∞ are the voltage values recorded by the photomultiplier tube, at 100% transmittance and at 99.6% completion of the reaction, respectively. If a voltage drift occurs after the value of v_{ref} has been recorded, equation 3.17 will yield an incorrect

value of $A_{\infty, Ni}$ because of the value of v_{ref} is no longer valid.

The voltage drifts affect the values of ΔA_{Ni} less because these values are obtained by evaluating the expression,

$$\Delta A_{Ni} = A_{\infty, Ni} - A_0 \tag{3.18}$$

and substitution of the expressions for $A_{\infty, Ni}$ and A_0 in equation 3.18 will yield,

$$\Delta A_{Ni} = -\log\left(\frac{v_\infty}{v_{ref}}\right) + \log\left(\frac{v_0}{v_{ref}}\right) \tag{3.19}$$

Now taking a common log for both the terms on right hand side of the equation 3.19 will yield an expression,

$$\Delta A_{Ni} = -\log\left(\frac{v_0}{v_\infty}\right) \tag{3.20}$$

which is independent of the quantity v_{ref}. Therefore, using an incorrect value of v_{ref} in equation 3.19 would not effect the value of ΔA_{Ni}.

Figure 3.21 shows a plot of A_0, ΔA_{Ni} and $A_{\infty, Ni}$ as a function of $[Ni^{2+}]$ for the formation of Ni(II)-1-NHA at pH = 6.30. It can be seen in this plot that the values for A_0 remain constant and the values for ΔA_{Ni} and $A_{\infty, Ni}$ show a saturation type of behavior, when plotted against $[Ni^{2+}]$. All hydroxamic acids showed similar trends in this type of plot.

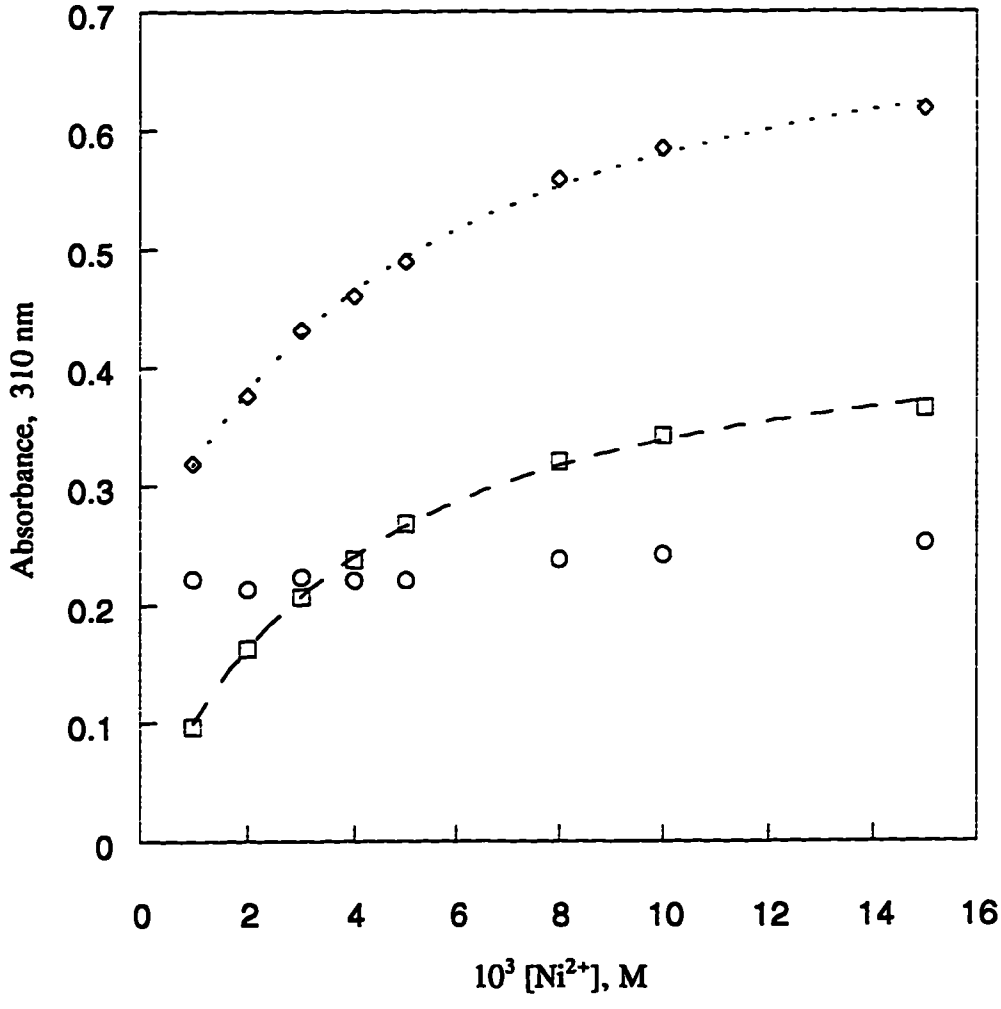

Figure 3.23. Plot of $A_{\infty, Ni}$ = (◇), ΔA_{Ni} = (□) and A_0 = (O) versus absorbance as a function of [Ni^{2+}] for the formation of the Ni(II)-1-NHA complex at pH = 6.30, I = 0.10 M and T = 25.0 °C. The dashed and the dotted curves are theoretical fits to equations 3.15 and 3.16, respectively.

F. Calculation of pH-Independent Values of Stability Constants

The pH-independent values of the stability constants, K_{NiA}, which is defined by equation 3.21, were also obtained.

$$K_{NiA} = \frac{[NiA^+]}{[Ni^{2+}]\,[A^-]} \tag{3.21}$$

Using equations 3.1, 3.14 and 3.21, the following expression for K_{NiA} may be derived. This expression was used to calculate the values of K_{NiA} from the values of K'_{NiA}.

$$K_{NiA} = K'_{NiA}(1+K_H[H^+]) \tag{3.22}$$

The value of K_{NiA} can also be obtained by using the values of rate constants, k_{HA} and k_{-HA}. From Scheme 3.1, equation 3.23 can be written. Using equations 3.1, 3.21 and 3.23, the expression for K_{NiA} can be derived as shown by equation 3.24.

$$\frac{k_{HA}}{k_{-HA}} = \frac{[NiA^+]\,[H^+]}{[Ni^{2+}]\,[HA]} \tag{3.23}$$

$$K_{NiA} = \frac{K_H\, k_{HA}}{k_{-HA}} \tag{3.24}$$

The stability constants are summarized in Table 3.4. It can be seen that there is good agreement between binding constant calculated from, the ΔA_{Ni}, $[Ni^{2+}]$ data, and from the rate constants.

Table 3.4. Values of Log K_{NiA}[a] for Selected Hydroxamic Acids Obtained from Thermodynamic and Kinetic Data

HA	pH	From ΔA_{Ni}, $[Ni^{2+}]$ data		From rate constants
		Log K'_{NiA}	Log K_{NiA}[b]	Log ($K_H k_{HA}/k_{-HA}$)
PNBHA	5.43	1.76	4.34	4.32
	5.60	2.00		
	6.00	2.43		
	6.30	2.70		
t-CHA	5.43	1.96	5.00	4.97
	6.30	2.85		
	6.70	3.16		
1-NHA	5.70	1.84	4.68	4.66
	6.00	2.21		
	6.30	2.43		
BHA	5.75	2.03	5.00	5.03
	6.00	2.23		
	6.30	2.47		
PMBHA	5.60	1.53	4.87	4.89
	6.00	1.95		
	6.30	2.35		
N-PBHA	5.75	2.43	4.89	5.01
	6.05	2.74		
	6.34	3.11		
	6.72	3.57		

[a]Determined at 25.0 °C and at $I = 0.10$ M ($NaClO_4$).

[b]Values represent the log of mean K_{NiA} values calculated from the values of K'_{NiA} using equation 3.22.

REFERENCES

1) Stiles, M. K.; Craig, M. E.; Gunnell, L. N.; Pfeiffer, D. R.; Taylor, R. W. *J. Biol. Chem.* **1991**, *266*, 8336-8341.

2) Davis, C. W. *Ion Association*; Butterworths: London, 1962, p 60.

3) Christian, S. D.; Tucker, E. E. *Am. Lab. (Fairfield, Conn)* **1982**, *14*, 31-34.

4) Christian, S. D.; Tucker, E. E. *Am. Lab. (Fairfield Conn)* **1982**, *14*, 36-41.

5) Dominey, L. A.; Kustin, K. *Inorg. Chem.* **1984**, *23*, 103-108.

CHAPTER IV

DISCUSSION

A. Ligand Protonation Constants (K_H)

The values of the complex formation rate constant k_A, obtained from the least-squares analysis of the data using equations 3.10 and 3.13, depended significantly on the input values used for K_H. Therefore, the values of K_H for the hydroxamic acids were determined under conditions similar to those used for the kinetic experiments, i.e., I = 0.10 M adjusted with $NaClO_4$ and 25.0 °C. Although the values of K_H for the hydroxamic acids used in this study have been reported in the literature,[1-3] these values were not obtained at I = 0.10 M. The literature values of K_H were corrected from their thermodynamic values (K_H^t) using the relationship described by equation 4.1. In this equation, a_{H^+}, a_{A^-} and a_{HA} are the activities of H^+, A^- and HA, respectively, and since HA is a neutral molecule a_{HA} = [HA]. The activity coefficients used for the correction were calculated using the Davies equation (equation 3.5, Chapter III).

$$K_H^t = \frac{a_{HA}}{a_{H^+}\, a_{A^-}} = \frac{[HA]}{[H^+]\,[A^-]\,\gamma_{H^+}\,\gamma_{A^-}} = \frac{K_H}{\gamma_{H^+}\,\gamma_{A^-}} \qquad (4.1)$$

The experimentally determined values and the corrected literature values are summarized in Table 4.1. It can be seen that the corrected literature values of K_H compare well with the experimentally determined values at I = 0.10 M.

Table 4.1. Log K_H Values of Hydroxamic Acids and their Carboxylic Acid Analogs

Substituents		$R_1C(O)N(OH)R_2$		$R_1C(O)OH$
R_1	R_2	this work[a]	literature[b]	literature[c]
para-nitrobenzo	H	7.87	7.92[d]	3.27
trans-cinnamo	H	8.40	8.35[e]	4.27
1-naphtho	H	8.49	-	3.70[b]
benzo	H	8.66	8.57[f], 8.70[d]	4.00
para-methoxybenzo	H	8.82	8.75[f], 8.94[d]	4.26[b]
benzo	benzo	8.10	8.06[f], 8.15[c]	-
methyl	H	-	9.35[g]	4.76

[a]Determined at 25.0 °C and $I = 0.10$ M. [b]Corrected from the thermodynamic values (K_H^I) to the K_H values at $I = 0.10$ M. [c]From ref (5). [d]From ref (1). [e]From ref (2). [f]From ref (3). [g]At 20 °C, from ref (6).

Of the set of hydroxamic acids studied, PNBHA is the least basic whereas, PMBHA was found to be the most basic. The log K_H values for the selected hydroxamic acids ranged from 7.87 to 8.82. From these values it can be concluded that at the physiological pH, these hydroxamic acids exist predominantly in the protonated form. The trend observed in the log K_H values is consistent with the electronic behavior of the substituents. The values for PNBHA, *N*-PBHA, *t*-CHA and 1-NHA are lower than that of BHA. This is because the anion form of these ligands is stabilized by the inductive electron withdrawing effect of the substituents.[4] On the other hand, the presence of an electron donating methoxy group (CH_3O-) on the benzene ring increases

the log K_H value.

Table 4.1 shows that the log K_H values of the carboxylic acid analogs of the selected hydroxamic acids are approximately 4.5 log units smaller than the corresponding hydroxamic acid. The higher acid strength of the former can be attributed to the more stable anionic form resulting from the delocalization of the negative charge on the two oxygens of the carboxyl group. An interesting fact about the data in Table 4.1 comes from the comparison of the analogs with benzo substituent with that of *trans*-cinnamo substituents. The log K_H value of *t*-CHA is less than that of BHA, whereas the corresponding value for *trans*-cinnamic acid is greater than that of benzoic acid. This means that the replacement of the benzo group by the *trans*-cinnamo group on hydroxamic acid makes the removal of the proton easier, whereas on the carboxylate analog a similar replacement makes the removal of proton more difficult. The reason for this anomaly is not clear. Substitution on the benzene ring in all other hydroxamic acids listed in Table 4.1 leads to variation in the log K_H value in a similar manner as it does in the carboxylic acid analogs.

B. Mechanism of Complex Formation

The kinetic data obtained for the reaction of Ni(II) with hydroxamic acids is consistent with the mechanism shown in Scheme 4.1. According to this scheme, both the protonated (HA) and the unprotonated (A^-) forms of the ligand react with the metal ion by a parallel path mechanism. The protonation equilibrium for the ligand is expected to be very rapid compared to the complexation reactions.[6,7] Under pseudo-first-order conditions of excess [Ni^{2+}] and buffered [H^+], the expression for the k_{obs} for the proposed mechanism is given by equation 4.2.

Scheme 4.1.

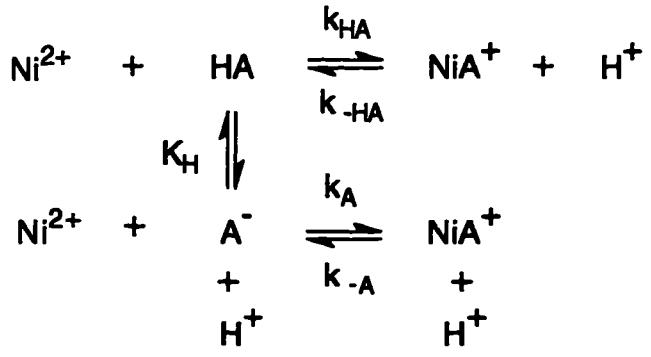

$$k_{obs} = \frac{(k_A + k_{HA} K_H [H^+])[Ni^{2+}]}{1 + K_H [H^+]} + k_{-A} + k_{-HA}[H^+] \qquad (4.2)$$

It is shown in Chapter III, that the plots of k_{obs} versus $[Ni^{2+}]$ are linear and that the slope and the intercept of these plots represent the formation and the dissociation of the NiA^+ complex, respectively. With an increase in pH, the slope increases and the value of the intercept decreases. This behavior is consistent with the proposed mechanism. The rate constants obtained from the nonlinear least-squares analysis of the kinetic data are summarized in Table 4.2.

Table 4.2. Resolved Rate Constants for the Formation Kinetics of Nickel(II)-hydroxamate Complexes at 25.0 °C and $I = 0.10$ M

HA	$10^{-4} k_A$ $M^{-1}s^{-1}$	$10^{-3} k_{HA}$ $M^{-1}s^{-1}$	k_{-A} s^{-1}	$10^{-6} k_{-HA}$ $M^{-1}s^{-1}$
PNBHA	2.9 ± 0.1	1.30 ± 0.01	1.66 ± 0.09	4.53 ± 0.03
t-CHA	6.2 ± 0.1	1.72 ± 0.01	2.0 ± 0.1	4.68 ± 0.03
1-NHA	8.7 ± 0.7	1.02 ± 0.03	2.1 ± 0.2	6.9 ± 0.1
BHA	6 ± 2	1.48 ± 0.03	3.4 ± 0.3	6.4 ± 0.1
PMBHA	5 ± 2	1.50 ± 0.04	2.4 ± 0.2	9.0 ± 0.2
N-PBHA	2.8 ± 0.1	0.67 ± 0.02	1.2 ± 0.2	0.83 ± 0.01
AHA[a]	3 ± 1	0.72 ± 0.01	0.163	8.03

[a]Values for acetohydroxamic acid (AHA) at 20 °C; from ref(6)

To hypothesize the intermediate steps for the formation of NiA^+, one may consider the structure of the acidic and basic forms of the ligand shown in Figure 4.1. It can be seen that in the acidic form of the ligand, the carbonyl oxygen is comparatively more basic than the *N*-hydroxyl oxygen. However, in the basic form of the ligand the situation is reversed.

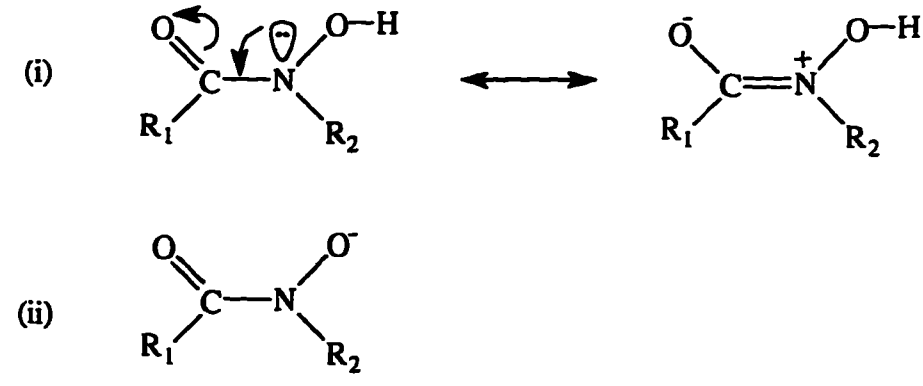

Figure 4.1. (i) Acidic and (ii) basic forms of hydroxamic acid.

Based on the above argument, an extension of Scheme 4.1 may be considered where the formation of the complex is considered in a stepwise fashion as shown in Scheme 4.2.

Scheme 4.2

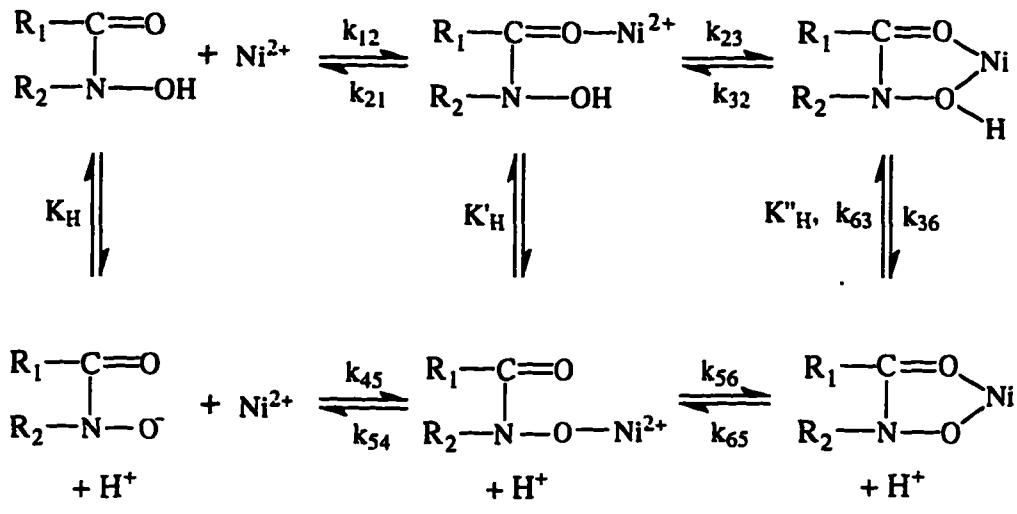

In this mechanism, it is assumed that the first bond formation of the unprotonated form of the ligand with the metal ion occurs through the oxygen adjacent to the nitrogen. Whereas, the first bond formation of the protonated form of the ligand occurs through the carbonyl oxygen. Some evidence for this mechanism comes from the comparison of the kinetic data for 1-NHA with BHA that is shown in Table 4.2. Within the experimental error, the value of k_A is the same for both ligands; whereas, the value of k_{HA} is a factor of 1.5 times smaller for 1-NHA. Lower value of k_{HA} for the binding of the acidic form of 1-NHA is expected due to the steric hinderance caused by the bulky naphtho group on the carbon atom. When the reacting ligand species is unprotonated, the initial binding is expected to occur via the oxygen atom bound to the nitrogen and the steric hinderance is negligible. Based on the kinetic studies of the reaction of Fe(III) with protonated forms of monohydroxamic acids, Crumbliss *et al.*[7] have proposed the intermediate where the metal ion is bound to the carbonyl oxygen.

The two pathways involving the protonated and the unprotonated form of the ligand are discussed below in greater detail.

i) Pathway involving the unprotonated form of the ligand (A^-)

The values of the rate constants for the complex formation of A^- with Ni(II), k_A, range from 2.8×10^4 to 8.7×10^4 $M^{-1}s^{-1}$. To gain an insight into the bond formation process between the metal and the ligand, the observed rate constants may be compared with those estimated for a dissociative interchange (I_d) mechanism.[8] The general procedure for the calculation of rate constants for I_d mechanism is described in Chapter I. The reaction of Ni(II) with A^- involves ion pair charge type (2+, 1-). Assuming that the center to center distance between the metal ion and the ligand oxygen in the outer-sphere complex is 5 Å, the value of equilibrium constant for this complex (K_{OS}) is calculated to be 2 M^{-1}. The water-exchange rate constant (k_{ex}) as determined from ^{17}O NMR line

broadening is 2.8 x 10^4 s^{-1}.[8] Using these values for K_{OS} and k_{ex}, the value of k_A is calculated to be 5 x 10^4 $M^{-1}s^{-1}$.

It can be seen that the calculated value of k_A differs from those observed, by factors ≤ 2. This observation suggests that the rate-limiting step for the reaction of A^- with Ni(II), is the first bond formation. A similar mechanism has been proposed by Kustin *et al.*[6] for the formation of nickel acetohydroxamate complex. The value of k_A reported in that study was 3 x 10^4 $M^{-1}s^{-1}$ which lies within the range of values for k_A found for the hydroxamic acids in this investigation.

ii) Pathway involving the protonated form of the ligand (HA)

The values for the rate constants for the complex formation of HA with Ni(II), k_{HA}, range from 670 to 1720 $M^{-1}s^{-1}$. For comparison, the predicted value for k_{HA} from dissociative interchange mechanism may be calculated. The reaction involves species with charge type (+2, 0), for which the K_{OS} value is calculated to be 0.16 M^{-1}. Using this value of K_{OS}, the value for the rate constant is calculated to be 4.5 x 10^3 $M^{-1}s^{-1}$. This value is larger than the experimentally determined values of k_{HA} by factors 3 to 7. This observation suggests that for the complexation of HA and Ni(II), the first bond formation is not the rate-determining step.

It is expected that the rate-determining step in this case is shifted to a later step. Some of the possibilities are: a) the proton transfer from the metal-ligand complex to the solvent (shown as step k_{36} in Scheme 4.2), b) expulsion of second water from the coordination sphere of Ni(II), or c) the ring closure (shown as step k_{23} in Scheme 4.2). These possibilities are discussed as follows.

a) Proton transfer as the rate-determining step

For the reaction of AHA with Ni(II), Kustin *et al.*[6] have proposed that proton

transfer is the rate-determining step. If this is true, then, assuming that the rate constant for the proton loss from the uncomplexed ligand and from the monobonded intermediate are related, one would expect the values of k_{HA} to be dependent on the acidity of the ligand. The results from our study show that this is not the case. To understand this, consider Scheme 4.3 which shows proton transfer from the ligand to the solvent. This scheme may be used to estimate the rate constant for proton dissociation (k_{-H}), that is defined by equation 4.3.

Scheme 4.3

$$H_2O + HL \underset{k_H}{\overset{k_{-H}}{\rightleftharpoons}} H_3O^+ + L^-$$

$$k_{-H} = 55.5\ K_a\ k_H \qquad (4.3)$$

In equation 4.3, k_H is the rate constant for the protonation process, K_a is the acid dissociation constant and 55.5 is the concentration of water (in molar units). The value of k_H may be assumed equal to that of a diffusion controlled process i.e., $k_H \cong 5 \times 10^{10}$ $M^{-1}s^{-1}$). Using the values of K_a (calculated from the values of K_H listed in Table 4.3), the values for k_{-H} are calculated for all the hydroxamic acids. These values, along with the experimentally determined values of k_{HA}, are shown in the Table 4.3. It can be seen that no correlation exists between the two values.

It is expected that the actual values of k_{-H} for the proton loss from the monobonded intermediate are much greater than the calculated values reported for the loss of proton from the free acid. According to Kustin *et al.*,[6] two effects are responsible for the enhancement of the proton loss in the former case: i) the metal-proton repulsion and

ii) the decrease in the electron density on the molecule due to inductive electron flow into the electron deficient metal center.

Table 4.3. Comparison of Calculated Rate Constants for Deprotonation of Ligand with k_{HA}

HA	log K_H (= pK_a)	10^{-3} k_{-H} $M^{-1}s^{-1}$	10^{-3} k_{HA} $M^{-1}s^{-1}$
PNBHA	7.87	37.4	1.30 ± 0.01
N-PBHA	8.10	21.9	0.67 ± 0.02
t-CHA	8.40	11.1	1.72 ± 0.01
1-NHA	8.49	8.88	1.02 ± 0.03
BHA	8.66	5.83	1.48 ± 0.03
PMBHA	8.82	4.16	1.50 ± 0.04
AHA	9.35	1.11	0.72 ± 0.01

Jorden *et al.*[9] have presented arguments that further support the fact that proton transfer is not the rate-determining step in the reaction of HA with Ni(II). They analyzed the data of Kustin *et al.*[6] that is shown in Table 4.4. Jorden *et al.* assumed that a direct correlation exists between the acidities of the monobound metal-ligand intermediate and the stability constants (K_{ML}) of the bidentate complex. If proton transfer is the rate determining step, a correlation is expected between the values of K_{ML} and k_{HA} obtained for different metal-ligand complexes. However, such a correlation was not observed for

the complexes of Ni(II), Co(II) and Fe(II) with AHA. The value of K_{ML} for Co(II) complex is a factor of 1.6 smaller than that of Ni(II) complex, whereas the value of k_{HA} for the Co(II) is 50 times larger. Furthermore, the value of K_{ML} for the monobound Fe(II) complex is less than that of monobound Ni(II) complex by a factor of 3.2 but the rate constant for Fe(II) is two orders of magnitude higher.

Table 4.4. Stability Constants (K_{ML}) and Formation Rate Constants (k_{HA}) for Group VIIIB metal Complexes of Acetohydroxamic Acid[a]

metal ion	$K_{ML} \times 10^{-4}$ (M^{-1})	k_{HA} ($M^{-1}s^{-1}$)
Ni(II)	20.0	7.17×10^2
Co(II)	12.6	3.59×10^4
Fe(II)	6.31	6.69×10^4

[a]At 20.0 °C, from ref (6)

Another argument presented by Jorden *et al.* that shows the improbability of the proton transfer step to be rate determining involves the analysis of Scheme 4.2. In this scheme, the rate constant for the protonation of the metal-ligand complex, k_{63}, is given by equation 4.2, where k_l and k_b are the rate constants for the acid and the buffer catalyzed pathways, respectively, and [HB] is the concentration of the acid form of the buffer.

$$k_{63} = k_l[H_3O^+] + k_b[HB] \qquad (4.2)$$

If proton transfer step is assumed to be rate-determining, then $k_{32} >> k_{36}$, and expression 4.3 can be derived.[9]

$$\frac{k_{12}}{k_{21}} \geq \frac{(k_1 + k_b K_{Hb}[B^-])K_{ML}}{K_H k_{23}} \qquad (4.3)$$

where, k_{12}, k_{21} and k_{23} are the rate constants for the steps shown in Scheme 4.2, K_H is the protonation constant for the ligand, K_{Hb} is the protonation constant for the buffer, $[B^-]$ is the concentration of the base form of the buffer, and K_{ML} is the stability constant for nickel hydroxamate complex. Under the limiting condition of the absence of buffer, equation 4.3 simplifies to equation 4.4.

$$\frac{k_{12}}{k_{21}} \geq \frac{k_1 K_{ML}}{K_H k_{23}} \qquad (4.4)$$

The values of K_H and K_{ML} for all the hydroxamic acids have been determined (Table 4.3, and Table 3.4 in Chapter III). The value of k_1 is expected to be close to the diffusion-control limit ~5 x 10^{10} $M^{-1}s^{-1}$. The value of k_{23} is estimated to be the same as the solvent exchange rate ~3 x 10^4 s^{-1}. Substitution of these values in equation 4.2 gave values for the equilibrium constant (k_{12}/k_{21}) for the monobound intermediate which lie in the range of 150 to 1025 M^{-1} for the selected hydroxamic acids. These values are much larger than expected for the complexation of Ni(II) with the carbonyl oxygen of the neutral ligand. For example, the value of the equilibrium constant for the complexation of Ni(II) with acetate ion is ~10 M^{-1} at $I = 0.10$ M and 25 °C.[10,11]

b) Expulsion of second water as the rate-determining step

The step that involves the expulsion of the second water molecule from the coordination sphere of the metal ion is also ruled out to be rate-limiting. It is expected

that the value of k_{ex} for the monodentate metal-ligand intermediate will be at least as high as that for the unbound ligand, i.e., $3 \times 10^4\ s^{-1}$.

c) Rate-determining step for the pathway involving the protonated ligand is ring closure

It is proposed that the rate-determining step for the pathway involving reaction of protonated form of hydroxamic acid with Ni(II) is ring closure. Assuming that the reopening of the chelate is very slow as compared to its formation, equation 4.5 could be derived for the mechanism in Scheme 4.2.

$$k_{HA} = \frac{k_{12}k_{23}}{k_{21} + k_{23}} \tag{4.5}$$

Rearrangement of the above expression yields equation 4.5

$$\frac{k_{12}}{k_{21}} = \frac{k_{HA}k_{12}}{k_{12}k_{23} + k_{HA}k_{23}} \tag{4.6}$$

where k_{12} is estimated from the I_d mechanism to be $\sim 3 \times 10^3\ M^{-1}s^{-1}$ and the value of k_{23} could be as large as k_{ex} for the solvent exchange, i.e., $3 \times 10^4\ s^{-1}$. Substituting the values for k_{12}, k_{23} and the experimentally determined values of k_{HA}, gives values for the equilibrium constants (k_{12}/k_{21}) for the monobound intermediates. The calculated values are summarized in Table 4.5. These values of the equilibrium constants are consistent with the expected values for the complexation of Ni(II) with the carbonyl oxygen of the neutral ligand.

Table 4.5. Equilibrium Constants for Monobound Intermediates

HA	$10^{-3}\ k_{HA}$ ($M^{-1}s^{-1}$)	$10^{2}\ k_{12}/k_{21}$ (M^{-1})
PNBHA	1.3	7.6
N-PBHA	0.67	2.9
t-CHA	1.72	13.4
1-NHA	1.02	5.2
BHA	1.48	9.7
PMBHA	1.50	10.0
AHA	0.72	3.2

From Table 4.2 it can be seen that the value of k_{HA} for *N*-PBHA is approximately a factor of two smaller than the other hydroxamic acids. The reason for this observation may be ascribed to the slower ring closure in the case of the former due to the steric hinderance caused by the *N*-phenyl group.

The value of k_{HA} for PNBHA is $1.30 \times 10^{3}\ M^{-1}s^{-1}$, whereas for BHA it is $1.48 \times 10^{3}\ M^{-1}s^{-1}$. The difference in the values of the two rate constants may be explained based on the nitro substituent in the former. Due to the electron withdrawing nature of the nitro group, it is expected that the electron density on the carbonyl oxygen of PNBHA is less than that of BHA. Therefore, due to the lower electrostatic attraction for the metal ion, the breaking of the Ni-O bond in the monobound intermediate (the step denoted by k_{21} in Scheme 4.2), is faster for PNBHA. Consequently, the value of k_{HA} is

lower for PNBHA. The values of k_{HA} for PMBHA and for BHA are not significantly different. This is in line with the fact that the difference in the log K_H values of these two ligands is small compared to the that of BHA and PNBHA. The lower value of k_{HA} for 1-NHA as compared with BHA may be attributed to the steric bulk on the former which causes hinderance in the first bond formation.

Based on the results of our study, it is expected that the value of k_{HA} for AHA should be at least a factor of two greater than the values reported by Kustin *et al.*[6] This anomaly may be due to the differences in the experimental conditions. The studies reported by Kustin *et al.* were performed at 20 °C and in the absence of buffers; whereas, our studies were performed at 25 °C and in the presence of 5 mM MES.

C. Conclusion

The log K_H values for the selected hydroxamic acids ranged from 7.87 to 8.82. It can be concluded that at the physiological pH, these hydroxamic acids exist predominantly in the protonated form. However, since the conjugate base form of the ligands reacts approximately an order of magnitude faster, the fraction of the conjugate base form present at the physiological pH will significantly contribute towards the metal complexation. For example, in the case of Ni-PNBHA complex formation at pH 7, the pathway involving the conjugate base form of the ligand will carry more than half of this reaction.

It is established that the unprotonated form of hydroxamic acids undergoes dissociative interchange mechanism with Ni(II) where the first bond formation occurs at the *N*-hydroxyl oxygen. The protonated form of ligand on the other hand undergoes complexation via a mechanism where the ring closure is the rate-determining step. In this

case the first bond formation occurs at the carbonyl oxygen. We have determined the rate constants for the reaction of Ni(II) with a variety of hydroxamic acids with different steric, electronic and acid/base properties. The stability constants for the nickel hydroxamte complexes have also been determined. This information can be utilized to study the inhibition mechanism of urease by hydroxamic acids.

REFERENCES

1) Agrawal, Y. K.; Shukla, J. P. Z. *Phys. Chemie, Leipzig* **1974**, *5*, S. 889-894.

2) Dixon, N. E.; Hinds, J. A.; Fihelly, A. K.; Gazzola, C.; Winzor, D. J.; Blakeley, R. L.; Zerner, B. *Can. J. Biochem.* **1980**, *58*, 1323-1334.

3) Fields, A. R.; Daye, B. M.; Christian, R. *Talanta* **1966**, *13*, 929-937.

4) Carey, F. A.; Sundberg, R. *Advance Organic Chemistry*; Plenum: New York, 1990; Vol. 1, pp 11-19.

5) Smith, R. M.; Martell, A. E. *Critical Stability Constants*; Plenum Press: New York, 1974-1981; Vol. 3, 5, 6.

6) Dominey, L. A.; Kustin, K. *Inorg. Chem.* **1984**, *23*, 103-108.

7) Monzyk, B.; Crumbliss, A. L. *J. Am. Chem. Soc.* **1979**, *101*, 6203-6213.

8) Margerum, D. W.; Cayley, G. R.; Weatherburn, D. C.; Pagenkopf, G. K. In *Kinetics and Mechanisms of Complex Formation and Ligand Exchange*; Martell, A. E., Ed.; ACS: Washington, D. C., 1978; Vol. 174, pp 1-221.

9) Dasgupta, P.; Jorden, R. B. *Inog. Chem.* **1985**, *24*, 2717-2720.

10) Linder, P. W.; Torrington, R. G.; Seemann, U. A. *Talanta* **1983**, *30*, 295-298.

11) Yasuda, M.; Yamasaki, K.; Ohtaki, H. *Bull. Chem. Soc. Japan* **1960**, *23*, 1067-1079.

CHAPTER V

INTRODUCTION

The development of tools plays a critical role in the progress of experimental science. The discovery of ionophores as tools to study metabolic processes in animals and plants started a new era in biological sciences. Fundamental understanding of the functioning of these tools would help reveal their advantages and limitations, which in turn will allow us to utilize their full potential. Such an endeavour is presented in Chapters V to VIII of this dissertation which describe the study of the properties of a biological tool known as ionomycin.

Ionomycin is a naturally-occurring antibiotic, which is capable of selectively transporting divalent metal ions across hydrophobic bilayers. Thus, it is defined as an "ionophore", which is a term generally used for substances with the ability to promote the transfer of ions from an aqueous medium into a hydrophobic phase.[1] Of primary interest among the ion transfer phenomena, is the transport of cations across cell membranes facilitated (or catalyzed) by ionophores.

A. General Background on Ionophores

Nigericin, X-206 and lasalocid-A were the first representatives of the ionophore family of compounds that were isolated from *Streptomyces* cultures by Berger in 1951.[2] Within the next decade and a half, several new ionophores (e.g; valinomycin, nonactin,

monensin, dianemycin) were reported. Owing to their antimicrobial activity, these ionophores were evaluated as potential antibiotic medicines. However, because of their high toxicity and low solubility in water, this application was not practical. In 1968 the selective ion transport properties of ionophores were discovered[3] attracting the attention of numerous investigators. Since then, several applications for these compounds have been discovered, and many details learned about their structures, complex formation properties, and the physiological activity.

Ionophores have extensive chemical applications.[1] The selective ion transport properties of ionophores have played an important part in the investigations of important biological processes such as mitochondrial activity[4] and photophosphorylation.[5] Some ionophores have been studied to evaluate their potential for the stimulation of cardiovascular response in humans as a treatment for sudden heart failure.[6] Ionophores are potential agents for the distribution of radioisotopes at specific sites in the human body for the treatment of tumors.[7] For several years, ionophores such as monensin have been used as a growth-promoters, and as anticoccidial agents for cattle and poultry.[8] The cation selectivity of ionophores has led to their use in the ion-selective electrodes for alkali and alkaline-earth cations.[9] Attempts to mimic the properties of ionophores led to the synthesis of compounds which behaved similarly.[10-12] Some examples of synthetic ionophores are crown ethers[13], cryptands[14] and chirality-recognizing polyethers.[15] The availability of these molecules led to the rapid development of the fields of phase- transfer catalysis and host-guest chemistry.[15]

Naturally occurring ionophores can be classified into two broad categories: channels and carriers. Although both types are organic molecules of moderate molecular weight (~200–2000), the basis for their classification is the difference in the mechanism by which they catalyze the diffusion of ions across the hydrophobic membrane. The channel type ionophores (also sometimes referred to as quasi-ionophores) span the

membrane and create a pore whose interior is lined with polar functional groups. Through this hydrophilic pore ions can pass selectively at the rate of 10^6 to 10^9 ions/second.[16] Among a few known examples of channels are gramicidin[17] and alamethicin[18].

B. Carrier Ionophores

The mechanism of ion transport by carriers and their three-dimensional structures have been studied in great detail.[1,19-22] The general architectural features and the molecular properties of this class of ionophore are discussed here.

As implied by their name, carrier ionophores selectively "carry" the ions across the membranes by forming inclusion complexes with them. In most cases, the transported ions are monvalent or divalent cations. The complexation process involves replacement of the solvation sphere of the cation by the donor atoms of the surrounding ionophore molecule. The ligating sites of the ionophore are generally composed of oxygen donor atoms which are arranged strategically on the backbone in such a way that they can form a central cavity to enclose the cation. In this respect, the structures of these complexes are closely similar to those of the complexes of synthetic ionophores.[23] The cation is shielded by the outer surface of the ionophore which comprises hydrophobic groups. Since the membrane medium is also hydrophobic, it can dissolve the complex. The driving force for the transport processes is usually a concentration gradient or the membrane potential.[12,16]

Two types of carrier ionophores have been reported; they are: i) neutral and ii) carboxylic acids. Neutral ionophores are primarily cyclic molecules containing ester or peptide linkages in the molecular ring. Examples of these types are nonactin[24] and

valinomycin[25], respectively. A neutral ionophore is preferentially partitioned in the membrane and diffuses to the aqueous-membrane interface to bind with the cation. The complex then diffuses from the interface to the interior of the membrane and translocates to the opposite membrane interface where the cation is released. Since the metal-ion complexes of neutral ionophores are charged, their transport across the membrane creates a transmembrane electrical potential. This type of transport which induces a charge across the membrane is termed as electrogenic.[26] It is governed by two factors: i) preexisting transmembrane electrical potential and ii) the concentration gradient of ions across the membrane. Electrogenic transport may cause complications in the study of biological systems because it interferes with the preexisting membrane potentials which play an important role in the cell function. The ideal ionophores for studying the cell activities thus would be those which do not alter the transmembrane electrical potentials. The carboxylic acid class of ionophores satisfy this condition. Their properties are discussed in the following section.

C. Carboxylic Acid Ionophores

Interestingly, all the known carboxylic acid ionophores contain cyclic ether moieties, and therefore, they are also known as polyether ionophores. The ether moieties consist of substituted furan and pyran rings. The ionophores have open-chain structures, with a carboxyl group at one end and one or two hydroxyl groups at the other end. The presence of the carboxyl group enables them to form charge-neutral complexes with cations. The cation-ionophore complex is formed at the aqueous-membrane interface and the cation is released at the opposite interface following translocation across the membrane. Due to their hydrophobic nature, the ionophore and its complexes partition strongly in the lipid membrane. Translocation of these complexes across the membrane

does not alter the membrane potential and therefore this type of transport is termed as electroneutral.[26]

Carboxylic acid ionophores are widely used to explore the cellular biochemistry and physiology where the electroneutral regulation of cations plays an important role.[27] These ionophores are used to manipulate ion gradients across natural or model cell membranes.[12] Some of the most commonly used carboxylic acid ionophores are monensin, nigericin, lasalocid A, A23187 and ionomycin.[28] Their structures are shown in Figures 5.1 and 5.2.

Due to the low solubility of ionophores in water, studies with them are performed in organic or mixed organic/aqueous solvents. Among these solvents methanol and methanol-water mixtures are widely used. Determination of the pH in the mixed solvent system is possible using the methods developed by de Ligny and Gelsema.[29-31] These methods are discussed in detail in the following chapter. Generally, for mixed solvents, the term pH is written as pH* which is used in the same manner as the term pH for an aqueous solution.[32] In this part of the dissertation we will use the term pH* to denote $-\log a^*_{H^+}$, where $a^*_{H^+}$ represents the activity of the hydrogen ion in the mixed solvent, 80% methanol-water (w/w).

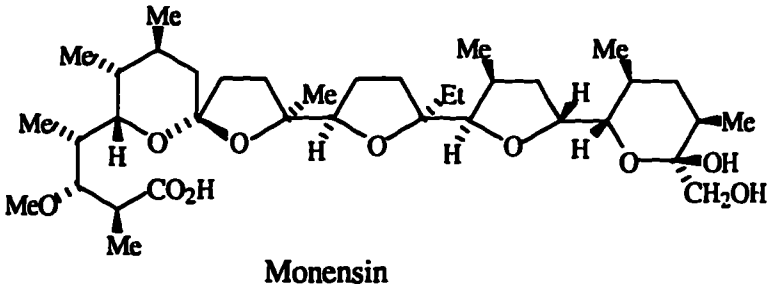

Monensin

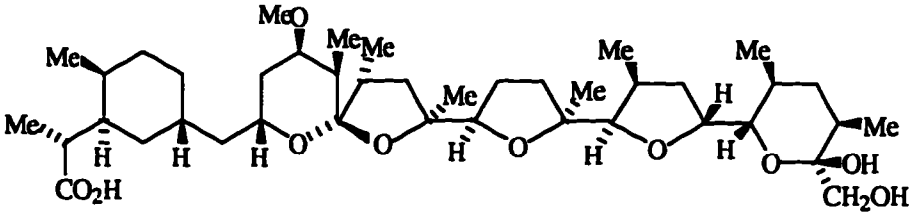

Nigericin

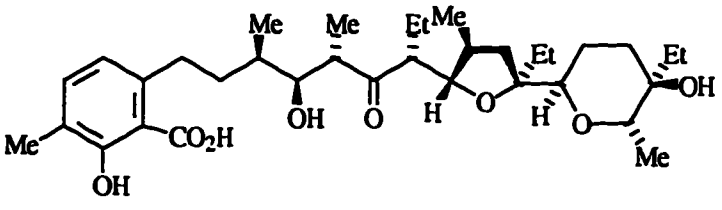

Lasalocid A

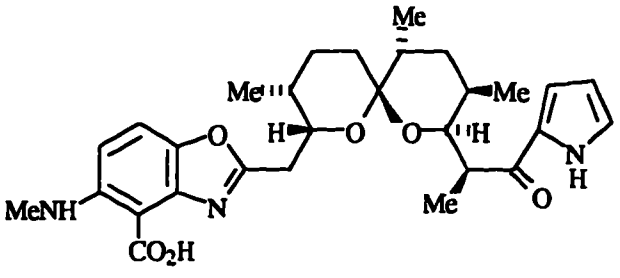

A23187

Figure 5.1. Structures of commonly used carboxylic acid ionophores[22]

D. Ionomycin

Among the broad class of carboxylic acid ionophores, ionomycin is unique because of its ability to form charge neutral 1:1 metal-ligand complexes with divalent metal ions. It is isolated from the organism *Streptomyces conglobatus sp. nov. Trejo.* and was first reported by Liu *et al.*[33,34] in 1978. In 1979, Toeplitz *et al.*[35] reported the crystal structures of the complexes of ionomycin with Ca(II) and Cd(II). The molecular conformations of the Ca(II) and Cd(II) complexes of ionomycin are very similar, both showing the coordination geometry of the cations to be octahedral. In both crystal forms, two molecules are joined in pairs by intermolecular hydrogen bonds to form dimeric globular structures having the lipophilic groups exposed to the outside. A stereoview of these structures is shown in Figure 5.2. The figure also shows the open chain structure of the ionomycin molecule in which the six oxygen atoms that are involved in bonding with the cation are marked with asterisks (*).

The solution conformation of the complexes in $CDCl_3$ as studied by ^1H NMR was found to be identical with that observed in the solid state.[36] The backbone of the ionomycin molecule is a chain of 32 carbon atoms containing three alcoholic groups, two furan rings, a carboxylate group and a β-diketone group. The carboxylic group is present on one end of the chain. The other end is terminated by an alcoholic group. The presence of β-diketone moiety makes this ionophore unique in that it provides an additional site, beside a carboxylic group, for deprotonation. The compound has a molecular weight of 709.0 based on its empirical formula $C_{41}H_{72}O_9$. Recently, the total synthesis of ionomycin was accomplished by two different groups.[37,38]

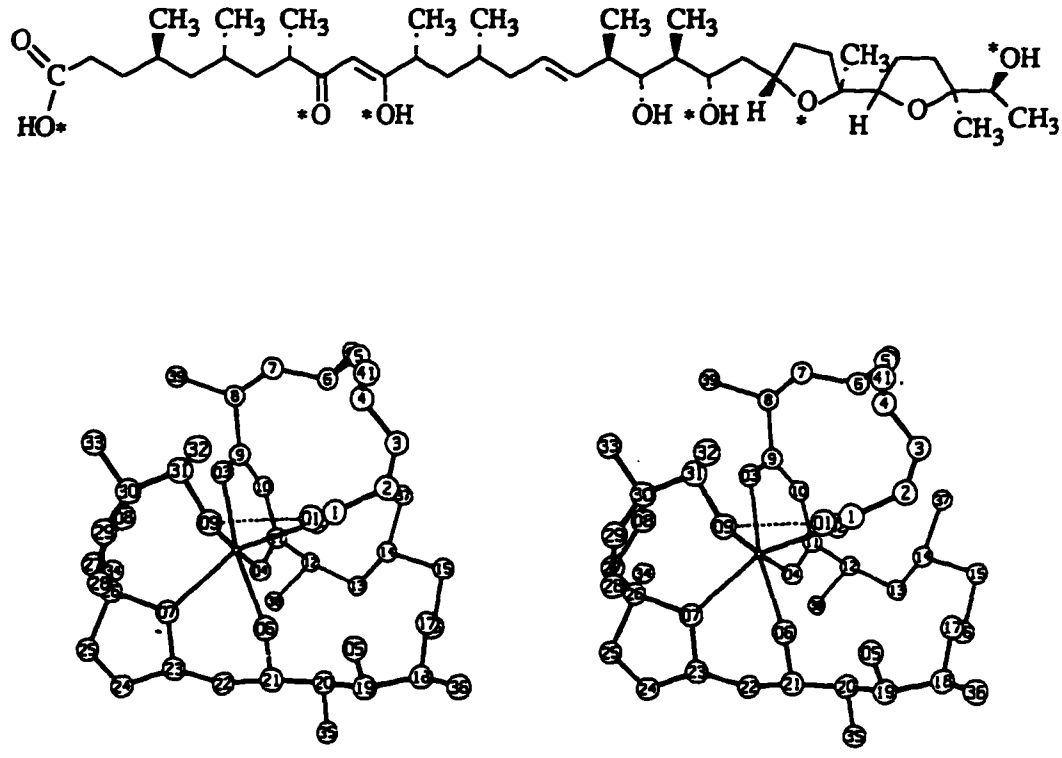

Figure 5.2 Structure of ionomycin (top) and stereoview of the crystal structure of the Ca(II) and Cd(II) complex of ionomycin (bottom).[35]

i) Spectral Properties

The UV-Vis and CD spectral properties of ionomycin have been studied in our laboratory earlier and the results have been published.[39,40] In 80% methanol-water solutions and between pH* values of 3.9-9.2, the UV-Vis spectrum of ionomycin shows a peak at 278 nm. This peak is characteristic of the enolic β-diketone moiety.[41] Increasing the pH* from 9.2 to 13.2 shifts the peak at 278 nm to 299 nm with an isosbestic point at 282 nm. The amplitude of the peak at 299 nm is approximately twice that of the peak at 278 nm. The absorbance-pH* behavior was found to be consistent

with the ionization of a single proton and is ascribed to the deprotonation of the β-diketone moiety. No discernible change was seen for the deprotonation of the carboxylic moiety in the wavelength range of 220-400 nm. The UV-Vis spectra of ionomycin as a function of pH* are shown in Figure 5.3. The figure also shows the CD spectra of ionomycin pertaining to each of its protonation states, H_2I, HI^-, and I^{2-}. The CD spectra for H_2I and HI^- are different in spite of the similar absorbance behavior of these forms between pH* = 3.9-9.2.(in the 220–400 nm range). This indicates that the ionophore undergoes a conformation change upon the loss of first proton. Information about the conformational change due to the loss of second proton could not be obtained from the available CD spectra. The differences in the CD spectrum of HI^- and I^{2-} are due to the differences in the absorbance of the two forms that are mirrored in the CD spectra.

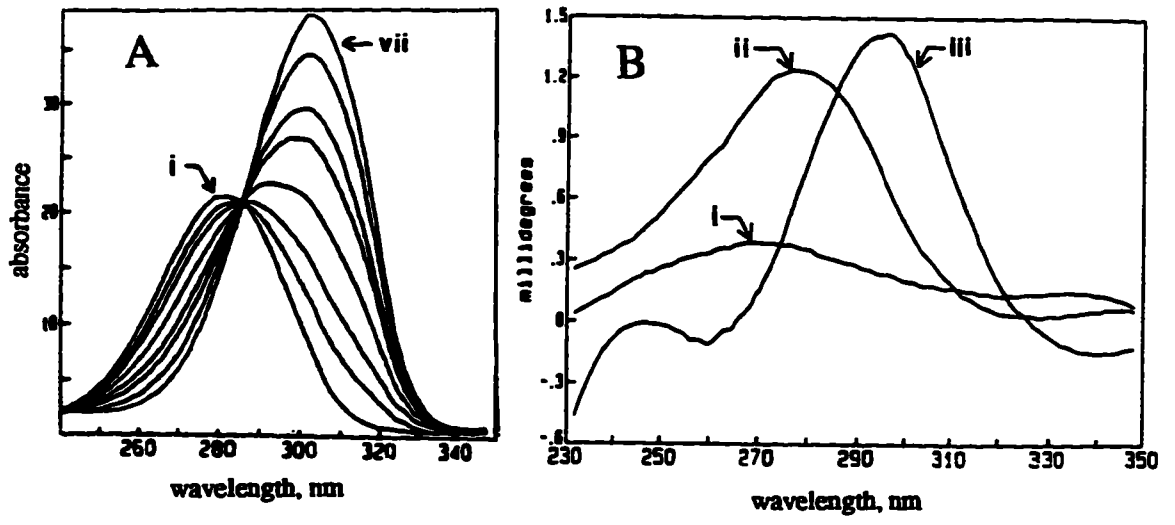

Figure 5.3. A: UV-Vis spectra of ionomycin as a function of pH*. The pH* values increase form 9.20 (i) to 13.14 (vii) in the sequence: 9.20, 11.00, 11.40, 11.75, 12.12, 12.29, 12.64, 13.4. B: CD spectra of ionomycin at (i) pH* = 3.86 (H_2I); (ii) pH* = 9.21 (HI^-); (iii) pH* = 13.04 (~I^{2-}).[40]

ii) Equilibrium and Complexation Properties

The protonation constants and complex formation constants for ionomycin were determined in 80% methanol-water earlier in our laboratory.[40] As mentioned previously, along with the carboxylic acid group, ionomycin also contains a β-diketone moiety that provides an additional site for proton dissociation. The acid-base equilibria of ionomycin are described by the set of equations given by

$$H^+ + I^{2-} \rightleftharpoons HI^-, \qquad K_{H1} = \frac{[HI^-]}{a^*_{H^+}[I^{2-}]} \tag{5.1}$$

$$H^+ + HI^- \rightleftharpoons H_2I, \qquad K_{H2} = \frac{[H_2I]}{a^*_{H^+}[HI^-]} \tag{5.2}$$

where I^{2-}, HI^- and H_2I represent the various forms of uncomplexed ionomycin, and, K_{H1} and K_{H2} are mixed-mode protonation constants. $a^*_{H^+}$ is defined by the equation,

$$a^*_{H^+} = 10^{-pH^*} \tag{5.3}$$

The values for log K_{H1} and log K_{H2} are 11.94 and 6.80, respectively. The former was determined spectrophotometrically, whereas the latter was determined potentiometrically. The equilibria represented by K_{H1} and K_{H2} are assigned to the protonation of the β-diketone moiety and the carboxylate moiety, respectively.

The carboxylic acid and β-diketone moieties of ionomycin can be modeled by the compounds 4-methylpentanoic acid (MPA) and 2,6-dimethyl-3,5-heptanedione (DMHD), respectively. Their structures are shown in Figure 5.4. The values of log K_H for MPA and DMHD in 80% methanol-water are 6.83 (potentiometric) and 11.38 (spectrophotometric), respectively.[40] It may be noted that the log K_{H1} value of the β-diketone moiety of ionomycin is ~0.6 log units higher than that of the DMHD. Based

on the electrostatic and steric features of the two ligands, a number of reasons may explain this difference: i) the presence of an ionized carboxylate functionality in ionomycin can make the dissociation of the β-diketone proton more difficult due to intramolecular interaction,[40] ii) the anion form of ionomycin is less stable because the bulky substituents force the molecule to take a conformation in which the two negatively charged oxygens are closer together, and iii) the bulky substituents can sterically hinder the solvation of the the β-diketone moiety. Reason (iii) has also been offered to explain the increase of 1.3 in the value of log K_H (in water) for methyl-t-butylneopentylacetic acid relative to the parent compound acetic acid.[42]

(i) (ii)

Figure 5.4. Structures of (i) 4-methylpentanoic acid and (ii) 2,6-dimethyl-3,5-heptanedione.

The complexation of ionomycin may be described by equation 5.3. Values of equilibrium constants (K_{MI}) for a series of divalent metal ions have been determined in 80% methanol-water system.[40] These equilibrium studies indicate that in the pH* range 6.5 to 8.5, an appreciable fraction of 1:1 metal-ionomycin complex (MI) exists as the protonated complex. The protonation constant (K_{MHI}) may be represented by equation 5.4. The values of K_{MI} and K_{MHI} for the complexes of ionomycin with selected divalent metal ions are summarized in Table 5.1. The selectivity order and relative affinities for the formation of the species MI are: Ni^{2+} (2000) > Zn^{2+} (600) > Co^{2+} (440) > Mn^{2+} (47) > Mg^{2+} (1.00) > Ca^{2+} (0.21) > Sr^{2+} (0.022).

$$M^{2+} + I^{2-} \rightleftharpoons MI, \quad K_{MI} = \frac{[MI]}{[M^{2+}][I^{2-}]} \tag{5.3}$$

$$MI + H^{+} \rightleftharpoons MHI^{+}, \quad K_{MHI} = \frac{[MHI^{+}]}{[MI][H^{+}]} \tag{5.4}$$

Table 5.1. Complexation Constants[a] for Ionomycin in 80% Methanol-Water Solutions at Ionic Strength = 0.050 M (Tetraethylammonium Perchlorate)

cation	log K_{MI}	log K_{MHI}
Sr^{2+}	5.30 ± 0.11	8.40 ± 0.13
Ca^{2+}	6.27 ± 0.04	8.32 ± 0.04
Mg^{2+}	6.95 ± 0.10	7.33 ± 0.03
Mn^{2+}	8.60 ± 0.03	6.34 ± 0.10
Co^{2+}	9.59 ± 0.11	6.08 ± 0.11
Ni^{2+}	10.25 ± 0.03	5.95 ± 0.10
Zn^{2+}	9.73 ± 0.12	6.47 ± 0.13

[a]Determined spectrophotometrically at 25.0 °C.[40]

iii) Mechanism of Metal Ion Transport

To undrestand the ionophore-catalyzed metal ion transport in a biological system is a challenging task due to the complexity of these systems. The mechanism involves multiple steps occurring in a heterogeneous medium. One approach to gain insight regarding the factors that control these processes, is to break the entire transport cycle into its basic components which may be studied individually. The results obtained from

the individual studies can be integrated to get a comprehensive picture of the transport mechanism. Two main components of the transport process are the interaction of the ionophore with the metal ion and the transport of the complex across the membrane. The latter process has been studied using a number of techniques to simulate membrane conditions. These range from simple artificial systems such as U-shaped tubes containing two aqueous phases separated from each other by an organic phase to using actual bilayer membrane systems such as liposomes or mitochondria.[28]

Although the intimate details of the mechanism of ion transport by ionomycin are still to be discovered, a general scheme has been hypothesized based on the transport studies.[43,44] It is illustrated in Figure 5.5. According to this scheme, the ionomycin molecule is first deprotonated at the inner membrane interface (shown as step 1 in the figure). The resultant anionic form has greater polarity and therefore is trapped at the polar interface. The anion complexes with the divalent metal ion M^{2+} (step 2) and loses another proton to make a neutral complex(step 3). This complex is able to break away from the polar interface, diffusing to the opposite side (outer side in this particular case, step 4). At the outer interface, the complex is protonated and then dissociates (steps 5 and 6). The anionic form of the ionomycin then picks up another proton (step 7) and the neutral molecule diffuses back to the inner interface for the next cycle (step 8). The net effect of the sequential reactions is illustrated in panel B of Figure 5.5 which shows the exchange of a divalent cation for two protons. In the overall cycle, the electroneutrality of the charge movements is maintained.

Ionophores other than ionomycin contain only one dissociable proton and therefore have to form 2:1 (ligand:metal) complexes with divalent metal ions to carry out electroneutral transport. The formation of 2:1 complexes has been proposed for the electroneutral transport of divalent metal ions by ionophores such as A23187 and monensin.[28,45]

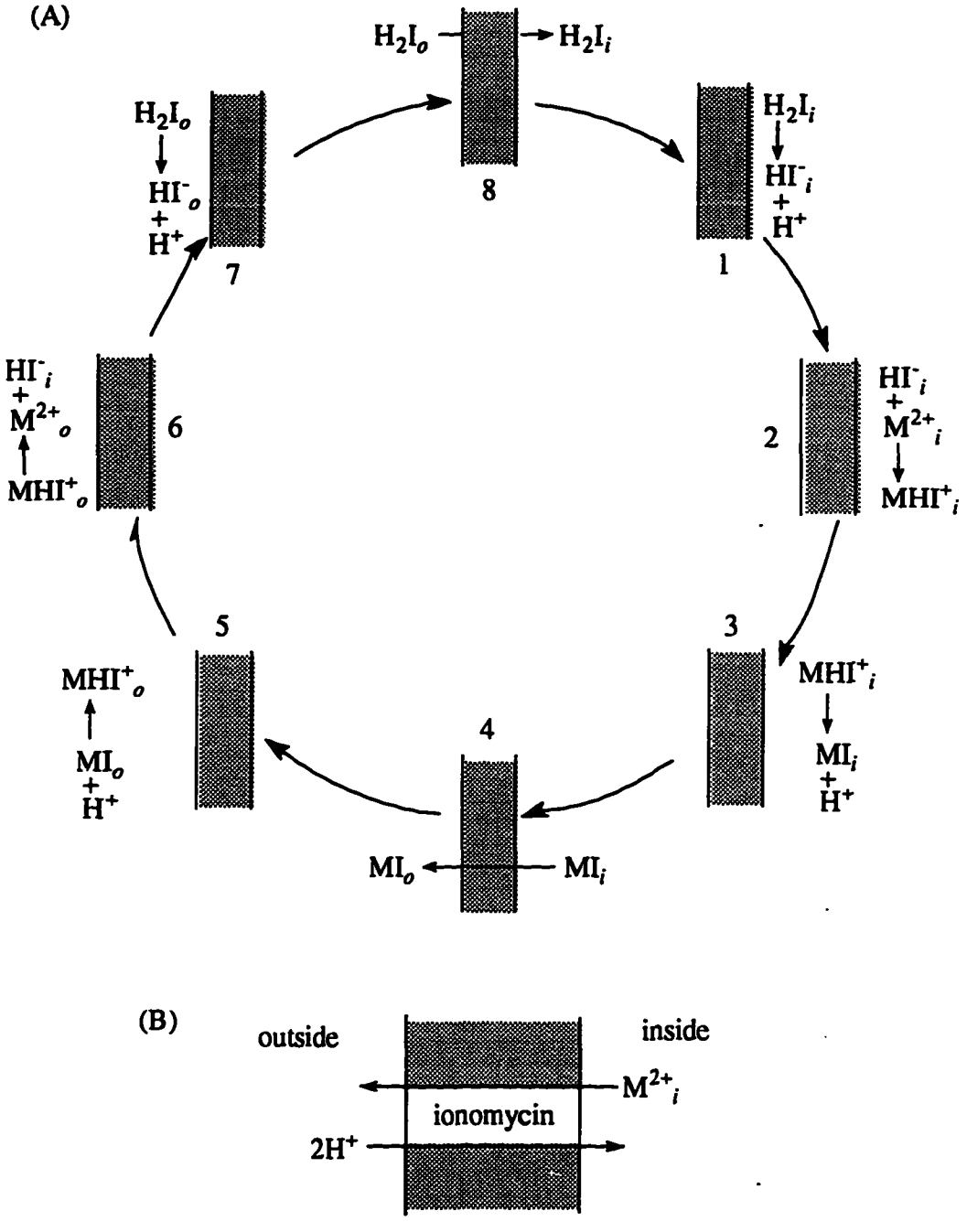

Figure 5.5. (A) The mechanism of divalent cation transport across the cell membrane catalyzed by ionomycin and (B) the net effect of the sequential reactions.[44] Shaded areas represent a section of bilayer membrane while the subscripts "i" and "o" refer to the inside and outside of the cell, respectively.

iv) Biological Applications of Ionomycin

There is increasingly wider use of ionomycin to selectively transport divalent cations across artificial and biological membranes.[28,46] It is frequently used in those studies, where the quantification and manipulation of Ca(II) or Mg(II) ions is required to understand the regulatory roles of these divalent metal ions. It is concluded from studies of mitochondrial respiration that ionomycin transports Ca(II) with a greater efficiency than A23187.[47] It was observed that the turnover number for the Ca(II) transport by ionomycin was 3- to 5-fold greater than that of A23187.

Ionomycin is a non-fluorescing compound. Thus it may be used in those studies where the fluorescence signal of the ionophore causes unwanted interference with other important signals, or in conjunction with other fluorescent ionophores to modulate and measure the intracellular concentration of divalent ions without complicating the fluorescence signal. These advantages of ionomycin along with its unique ability to make 1:1 charge neutral complexes with divalent cations (discussed earlier) have made it a popular choice.[48-51]

Recently, the properties of ionomycin in transporting Ni(II) into human epithelial kidney cells[52] and human platelets[53] have been reported. These studies have implications in understanding of the effect of Ni(II) compounds on humans. Nickel is a human carcinogen that mediates oxidative damage to DNA and chromatin, giving rise to pro-mutagenic products.[54] The carcinogenic potency of Ni(II) depends on its ability to permeate the target cells. It was observed that the presence of ionomycin in the system, increases Ni(II) uptake into the human epithelial kidney cells by 4- to 5-fold.[52] Knowledge of the mechanism and the kinetics of the reactions of ionomycin with Ni(II) would allow greater flexibility in the manipulation of the metal ion concentration in these studies.

E. Mechanism of Complex Formation Reactions of β-Diketones with Metal Ions

As discussed in the preceding sections, ionomycin contains a β-diketone moiety which participates in the binding of the metal ion. Therefore, in order to understand the mechanism of metal ion-ionomycin complexation, information about the properties of the β-diketone moiety would be helpful. The reactions of β-diketones with metal ions have been widely studied. These reactions are of practical interest because of their diverse applications. Metal-β-diketone complexes are used as catalysts for polymerization reactions, as insecticides for the control of soil-borne fungi, and in laser technology.[55] β-diketones also serve as excellent analytical reagents for detection and selective extraction of metal ions.[56] A review of the reactions of metal ions with β-diketones relevent to the current studies, is presented here.

The first study of the mechanism of metal complex formation of β-diketones was reported in 1959.[57] Since then, these reactions were investigated by several different groups[55,58-61] among which the contributions of Hynes *et al.*[55,62-78] are extensive. Reactions involving a wide variety of ligands and metals have been studied. A review article by Hynes presents an account of their common behavior.[60]

In this section, we will focus on the 1:1 metal-ligand complexes because of their relevance to the reported study. There are two unusual features of β-diketone ligands that complicate investigation of the metal complexation mechanism. First, these compounds exhibit keto/enol tautomerism and the consequent presence of three different forms of ligand (keto, enol and enolate) results in multiple pathways for complexation with metal. The metal ion can react with one, two or all three forms of the ligand. This complicates the reaction scheme and the corresponding rate law. Second, the slower rate of proton dissociation and the keto-enol interchange in β-diketones, compared to the rate of solvent exchange on the metal ions, disallows use of the dissociative interchange model

(described in Chapter I) for these ligands. Sutin *et al.*[59] have stated three properties of protonated multidentate ligands that may influence the rate of metal complexation. They are: i) the nature of the ligand as an entering group, ii) the rate of proton dissociation from the ligand, and iii) the effect of steric factors on ring closure. Which of these factors control the intimate mechanism of the reactions of metal ions with β-diketone ligands is still a matter of dispute.[60,61] The enol tautomers could be poor entering groups because of the intramolecular hydrogen bond which needs to be broken before the formation of the first bond between the ligand and the metal center. Although this argument is used to explain the nonreactivity of the protonated forms of certain aliphatic amino acids,[79] it cannot account for the lowering of the rate constant by three orders of magnitude which is frequently observed in β-diketones. It is also argued that if factor (iii) was responsible for the slow rate of complex formation of β-diketones, then the enolate form of the ligand also would react slowly. In most cases the rate constants measured for the reactions of the enolate form of the ligand with metal ions are two to three orders of magnitude greater than the corresponding rate constants for the enol form.[60,61] The rate constants for the enolate are close to those predicted on the basis of the dissociative interchange mechanism. Therefore, according to Hynes,[60] factor (iii) is not of great importance in determining the overall rate of complex formation with β-diketones.

Under the conditions where the enolate form of the β-diketone is negligible, a general mechanism considering the tautomerism phenomenon as well as the interaction of metal ion with both forms of the ligand, may be written as shown in Scheme 5.1. In this scheme, the keto and the enol forms of the ligand are represented by HK and HE, respectively, M^{n+} represents the metal ion and $[ML]^{(n-1)}$ represents the metal-β-diketone complex.

Scheme 5.1

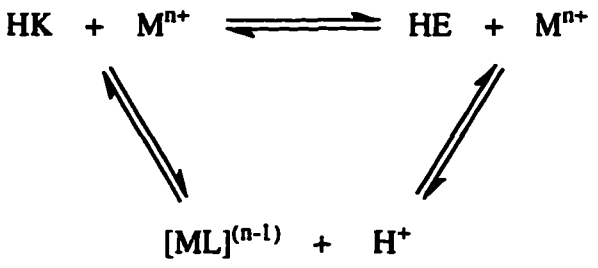

A noticeable feature of the reactivity of β-diketones is that the enol form is much more reactive than the keto form. This is expected, because deprotonation of the enol form occurs at oxygen compared to carbon in the case of the keto form. A perusal of the existing literature reveals that for all β-diketones studied so far, the keto form is unreactive with Ni(II); however, reactions of this form with Cu(II) and Fe(III) have been reported.[60] Although the reasons for the relative inertness of Ni(II) towards the keto form are still not clear, it may be ascribed to the difference in the ability of the metal ions to catalyze deprotonation of the keto form.[58]

F. Summary of Studies

An increasingly wider use of ionomycin as an ionophoric agent and its potential advantages over other divalent metal ionophores (discussed earlier) prompted us to examine the kinetics of this ionophore. These studies involve investigation of the components of the transport cycle which involve the interaction of the ligand and metal ion, i.e., steps 2, 3, 5 and 6 shown in Figure 5.5. All studies were performed in 80% methanol-water at 25.0 °C.

i) Keto-enol tautomerism of ligands

$$HK \underset{k_k}{\overset{k_e}{\rightleftharpoons}} HE \qquad K_{e/k} = \frac{k_e}{k_k} = \frac{[enol]}{[keto]} \tag{5.5}$$

The ratios ($K_{e/k}$) of enol to keto tautomers for ionomycin and DMHD were determined using NMR techniques. Kinetic studies were performed to determine the rate constants of keto-enol interconversion. Two different methods were employed: i) pH jump (explained in Chapter VI) and ii) rapid dissolution of concentrated (or neat) ligand in 80% methanol-water. The k_{obs} values for keto-enol interconversion were measured and the values for k_e and k_k were calculated. The effect of specific and general acid/base catalysis was studied in presence of EPPS and MES buffers.

ii) Metal-ligand reactions

Kinetic investigations were performed to study the reactions of Ni(II) and Mg(II) with ionomycin and DMHD. The reactions may be generally represented by equation 5.6 where H_nL represents the ligand consisting of keto (n = 1), enol (n = 1) and enolate (n = 0) forms.

$$M^{2+} + H_nL \rightleftharpoons ML^{(2-n)} + nH^+ \qquad (5.6)$$

The kinetic studies may be divided into two groups: 1) the reactions of ligands with Ni(II) in the presence of excess [H^+] to avoid the use of buffers, and 2) the reactions of ligands with Mg(II) in the presence of buffers.

In the first group, the formation and dissociation reactions were carried out under pseudo-first-order conditions using at least ten-fold excess [Ni^{2+}] and [H^+]. Under these conditions, the concentration of the enolate form is negligible and the reaction is expected to have a mechanism as shown in Scheme 5.1.

The objective of the second group was to investigate the kinetic behavior of ionomycin with a divalent metal ion under physiological conditions. Mg(II) was chosen as the metal ion for the following reasons: 1) Mg(II) is a biologically relevant metal ion, 2) the half-lives ($t_{1/2}$) for the reactions of Mg(II) with ionomycin were in the range that can be monitored on a stopped-flow instrument. The reactions of Ca(II), for example, are too fast ($t_{1/2} < 0.01$ sec) to be monitored on the same instrument. 3) Mg(II) does not form metal-hydroxides in the desired pH* range for the study (5.60 to 8.40). Ni(II) forms significant amounts of metal-hydroxides at pH* > 7.0 that complicate the mechanism of complexation.

The formation and dissociation of MgI were studied as a function of pH* and buffer concentration to investigate general or specific acid/base catalysis. The nature of the metal ion dependence was also studied by varying [Mg^{2+}] in the reactions. The formation reactions were performed in a pH* range of 7.60 to 8.20. At the higher pH* values, the contribution of the enolate form cannot be ignored in these reactions. The buffers used in the formation reactions are: 4-[2-hydroxyethyl]-1-piperazineethane-sulphonic acid (HEPES), 4-(2-hydroxyethyl)-1-piperazinepropane-sulfonic acid (EPPS),

and 2-[cyclohexylamino]ethanesulphonic acid (CHES). The dissociation reactions were studied in the pH range 5.60 to 6.40. The buffers used in the dissociation reactions are: *N,N,N'N'*-tetraethylethylenediamine (TEEDA), *N,N,N'N'*-tetraethylpropanediamine (TEPDA), and 4-morpholineethanesulphonic acid (MES). The mixed-mode log K_H values were determined for the buffers used in this study.

To calculate the formation rate constants from reverse rate constants obtained from the kinetic studies performed at low pH*, values of the equilibrium constants for the Ni(II)-ligand complexes were required. The value of the equilibrium constant for $Ni(DMHD)^+$ was obtained by potentiometric and spectrophotometric methods. For NiI, the value of the equilibrium constant is already known.[40]

All reactions of ionomycin were performed at an ionic strength of 0.050 M maintained with tetraethylammonium perchlorate. This was done in order to maintain consistency with the studies reported in the literature[28] that employ similar conditions. The reactions of DMHD with Ni(II), however, were also performed at the ionic strength 0.50 M maintained with $NaClO_4$. These conditions were employed by Hynes *et al.*[64] in their studies involving simple β-diketone systems similar to DMHD.

The data obtained from these studies are used to propose a mechanism for the interaction of ionomycin with a divalent metal ion such as Ni(II). The effect of buffers on these reaction was elucidated. To make these studies feasible, the conditions were altered from that of the natural biological systems, nevertheless, the information obtained may be conveniently extrapolated to the conditions of the natural biological systems. This information constitutes a vital part of a database of ionophore characteristics which can serve as a guide for their proper use. The information may also be used for the preparation and characterization of new ionophores with desired activities.

REFERENCES

1) Dobler, M. *Ionophores and Their Structures*; Wiley: New York, 1981.

2) Berger, J.; Rachlin, A. I.; Scott, W. E.; Sternbach, L. H.; Goldberg, M. W. *J. Am. Chem. Soc.* **1951**, *73*, 5295-5298.

3) Estrada-O., S.; Rightmire, B.; Lardy, H. A. *Antimicrob. Agents Chemother.* **1968**, 279-288.

4) Boyer, P. D.; Chance, B.; Ernster, L.; Mitchell, P.; Racker, E.; Slater, E. C. *Ann. Rev. Biochem.* **1977**, *46*, 955-1013.

5) Degani, H.; Shavit, N. *Arch. Biochem. Biophys.* **1972**, *152*, 339-346.

6) Pressman, B. C. *Fed. Proc.* **1973**, *32*, 1698-1703.

7) Semenoff, D.; Marzilli, L.; Strauss, H. W.; Harrison, K.; Rhodes, B. A.; Pitt, B. *J. Nucl. Med.* **1975**, *16*, 576.

8) Ruff, M. D. In *Polyether Antibiotics: Naturally Occuring Acid Ionophores*; Westley, J. W., Ed.; Marcel Dekker: New York, 1982; Vol. 1, pp 303-332.

9) Ammann, D.; Bissig, R.; Cimerman, Z.; Fiedler, U.; Guggi, M.; Morf, W. E.; Oehme, M.; Osswald, H.; Pretsch, E.; Simon, W. *Ion and Enzyme Electrodes in Biology and Medicine*; Urban and Schwarzenberg: Munich, 1976.

10) Gomperts, B. D.; Bennett, J. P.; Allan, D. *Eur. J. Biochem.* **1981**, *117*, 559-562.

11) Hilgenfeld, R.; Saenger, W. In *Structural Chemistry of Natural and Synthetic Ionophores and their Complexes with Cations*; Vogtle, F., Ed.; Springer-Verlag: New York, 1982; Vol. 101, pp 1-82.

12) Fyles, T. M. In *Biomimetic Ion Transport with Synthetic Transporters*; Dugas, H., Ed.; Springer-Verlag: New York, 1990; Vol. 1, pp 71-113.

13) Pedersen, C. J. *J. Am. Chem. Soc.* **1970**, *92*, 386-391.

14) Lehn, J. M. *Struct. Bond.* **1973**, *16*, 1-69.

15) Cram, D. J.; Cram, J. M. *Science* **1974**, *183*, 803-809.

16) Friedman, M. H. *Principles and Models of Biological Transport*; Springer-Verlag: New York, 1986.

17) Hladky, S. B.; Haydon, D. A. *Biochim. Biophys. Acta* **1972**, *274*, 294-312.

18) Mueller, P.; Rudin, D. O. *Curr. Top. Bioenerg.* **1969**, *3*, 157.

19) Pressman, B. C. *Ann. Rev. Biochem.* **1976**, *45*, 501-530.

20) Ovchinnikov, Y. A.; Ivanov, V. T.; Shkrob, A. M. *Membrane-Active Complexones*; Elsevier: New York, 1974.

21) Vogtle, F. *Top. Curr. Chem.*; Springer-Verlag: New York, 1982.

22) Westley, J. W. In *Polyether Antibiotics: Naturally Occuring Acid Ionophores*; Westley, J. W., Ed.; Marcel Dekker: New York, 1982; Vol. 1, pp 1-41.

23) Tsukube, H. *Cation-Binding by Macrocycles*; Marcel-Dekker: New York, 1990, p 497.

24) Dominguez, J.; Dunitz, J. D.; Gerlach, H.; Prelog, V. *Helv. Chim. Acta* **1962**, *45*, 129-138.

25) Brockmann, H.; Schmidt-Kastner, G. *Chem. Ber.* **1955**, *88*, 57-61.

26) Painter, G. R.; Pressman, B. C. *Top. Curr. Chem.* **1982**, *101*, 83-110.

27) Reed, P. W. In *Polyether Antibiotics: Naturally Occuring Acid Ionophores*; Westley, J. W., Ed.; Marcel Dekker: New York, 1982; Vol. 1, pp 185-302.

28) Taylor, R. W.; Kauffman, R. F.; Pfeiffer, D. R. In *Polyether Antibiotics: Naturally Occuring Acid Ionophores*; Westley, J. W., Ed.; Marcel Dekker: New York, 1982; Vol. 1, pp 103-184.

29) de Ligny, C. L.; Luykx, P. F. M.; Rehback, M.; Weineke, A. A. *Recl. Trav. Chim. Pays-Bas* **1960**, *79*, 699-736.

30) Gelsema, W. J.; de Ligny, C. L.; Remijnse, A. G.; Blijleven, H. A. *Recl. Trav. Chim. Pays-Bas* **1966**, *85*, 647-660.

31) Gelsema, W. J.; de Ligny, C. L.; Blijleven, H. A. *Recl. Trav. Chim. Pays-Bas* **1967**, *86*, 852-864.

32) Rorabacher, D. B.; Mackellar, W. J.; Shu, F. R.; Bonavita, S. M. *Anal. Chem.* **1971**, *43*, 561-573.

33) Liu, C.; Hermann, T. E. *J. Biol. Chem.* **1978**, *253*, 5892-5894.

34) Liu, W. C.; Slusarchyk, D. S.; Astle, G.; Trejo, W. H.; Brown, W. E.; Meyers, E. *J. Antibiot.* **1978**, *31*, 815-819.

35) Toeplitz, B. K.; Cohen, A. I.; Funke, P. T.; Parker, W. L.; Gougoutas, J. Z. *J. Am. Chem. Soc.* **1979**, *101*, 3344-3353.

36) Anteunis, M. J. O.; Verhegge, G. *Bull. Soc. Chim. Belg.* **1981**, *90*, 1153-1166.

37) Hanessian, S.; Cooke, N. G.; DeHoff, B.; Sakito, Y. *J. Am. Chem. Soc.* **1990**, *112*, 5276-5290.

38) Evans, D. A.; Dow, R. L.; Shih, T. L.; Takacs, J. M.; Zahler, R. *J. Am. Chem. Soc.* **1990**, *112*, 5290-5313.

39) Craig, M. E. *Ph.D. Thesis* **1990**, The University of Oklahoma, Norman, OK.

40) Stiles, M. K.; Craig, M. E.; Gunnell, S. L. N.; Pfeiffer, D. R.; Taylor, R. W. *J. Biol. Chem.* **1991**, *266*, 8336-8342.

41) Silverstein, R. M.; Bassler, G. C.; Morrill, T. C. *Spectrometric Identification of Organic Compounds*; 5th ed.; Wiley: New York, 1991, p 301.

42) Guter, G. A.; Hammond, G. S. *J. Org. Chem.* **1959**, *81*, 4686-4689.

43) Brasseur, R.; Nortedame, M.; Ruysschaert, J.-M. *Biochem. Biophys. Res. Commun.* **1983**, *114*, 632-637.

44) Erdahl, W. E.; Chapman, C. J.; Taylor, R. W.; Pfeiffer, D. R. *Biophys. J.* **1994**, *66*, 1678-1693.

45) Erdhal, W. L.; Chapman, C. J.; Wang, E.; Taylor, R. W.; Pfeiffer, D. R. *Biochemistry* **1996**, *35*, 13817-13825.

46) Woolley, G. A.; Pfeiffer, D. R.; Deber, C. M. In ; Kraicer, J. and Dixon, S. J., Eds.; Academic Press: Orlando, 1995; Vol. 27, pp 52-68.

47) Kauffman, R. F.; Taylor, R. W.; Pfeiffer, D. R. *J. Biol. Chem.* **1980**, *255*, 2735-2739.

48) Truneh, A.; Pearce, F. L. *Agents and Actions* **1984**, *14*, 179-184.

49) Nankova, B.; Hiremanglur, B.; Menezes, A.; Zeman, R.; Sabban, E. *Mol. Brain Res.* **1996**, *35*, 164-172.

50) Yamada, H. *Biochem. Biophys. Res. Comm.* **1996**, *225*, 215-218.

51) Capogna, M.; Gahwiler, B. H.; Thompson, S. M. *J. Neurophysiol.* **1996**, *75*, 2017-2028.

52) Refsvik, T.; Andreassen, T. *Carcinogenesis* **1995**, *16*, 1107-1112.

53) Azula, F. J.; Alonso, R.; Marino, A.; Trueba, M.; Macarulla, J. M. *Am. J. Physiol.* **1993**, *265*, C1681-C1688.

54) Tveito, G.; Hansteen, I.-L.; Dalen, H.; Haugen, A. *Cancer Research* **1989**, *49*, 1829-1835.

55) Blanco, C. A.; Hynes, M. J. *Can. J. Chem* **1992**, *70*, 2285-2289.

56) Koshimura, H. *Anal. Chim. Acta* **1970**, *49*, 67-75.

57) Taft, R. W.; Cook, E. H. *J. Am. Chem. Soc.* **1959**, *81*, 46-54.

58) Pearson, R. G.; Anderson, O. P. *Inorg. Chem.* **1970**, *9*, 39-46.

59) Jaffe, M. R.; Fay, D. P.; Cefola, M.; Sutin, N. *J. Am. Chem. Soc.* **1971**, *93*, 2878-2886.

60) Hynes, M. J. *Rev. Inorg. Chem.* **1990**, *11*, 21-78.

61) Hirsch, J.; Paulus, H.; Elias, H. *Inorg. Chem.* **1996**, *35*, 2343-2351.

62) Hynes, M. J.; O'Regan, B. D. *J. Chem. Soc., Dalton Trans.* **1976**, 1200-1202.

63) Hynes, M. J.; O'Regan, B. D. *Proc. Roy. Irish Academy* **1977**, *B77*, 285-294.

64) Hynes, J. M.; O'Regan, B. D. *J. Chem. Soc., Dalton Trans.* **1979**, 162-166.

65) Hynes, M. J.; O'Regan, B. D. *J. Chem. Soc., Dalton Trans.* **1980**, 7-13.

66) Hynes, M. J.; O'Mara, C.; Kelly, D. F. *Inorg. Chim. Acta* **1980**, *120*, 131-134.

67) Hynes, M. J.; O'Shea, M. T. *J. Chem. Soc., Dalton Trans.* **1983**, 331-336.

68) Hynes, M. J.; O'Shea, M. T. *Inorg. Chim. Acta* **1983**, *73*, 201-206.

69) Hynes, M. J.; Walsh, J. *J. Chem. Soc., Dalton Trans.* **1985**, 1543-1546.

70) Hynes, M. J.; Walsh, J. *J. Chem. Soc., Dalton Trans.* **1985**, 2565-2569.

71) Hynes, M. J.; Walsh, J. *J. Chem. Soc., Dalton Trans.* **1986**, 2243-2246.

72) Hynes, M. J.; Kelly, D., F. *Inorg. Chim. Acta* **1991**, *188*, 243-249.

73) Hynes, M. J.; Kelly, D. F. *Inorg. Chim. Acta* **1991**, *187*, 159-165.

74) Hynes, M. J.; Kelly, D. F. *Inorg. Chim. Acta* **1991**, *181*, 93-98.

75) Hynes, M. J.; Blanco, C. A.; Mooney, M. T. *J. Chem. Soc., Perkin Trans. 2* **1991**, 2055-2060.

76) Hynes, M. J. *J. Chem. Soc., Faraday Trans.* **1992**, *88*, 3533-3536.

77) Hynes, M. J.; Mooney, M. T.; Moloney, A. *J. Chem. Soc., Dalton Trans.* **1993**, 313-318.

78) Blanco, C.; Hynes, M., J. *Inorg. Chim. Acta* **1990**, *173*, 115-120.

79) Cassatt, J. C.; Wilkins, R. G. *J. Am. Chem. Soc.* **1968**, *90*, 6045-6050.

CHAPTER VI

EXPERIMENTAL

A. Reagents

The sources and purity of the following reagents are described in chapter II: nickel perchlorate, sodium perchlorate, sodium hydroxide, perchloric acid, ethylenediaminetetraacetic acid, 4-morpholineethanesulphonic acid (MES), 1,4-piperazinebis-[ethanesulphonic acid] (PIPES), 4-[2-hydroxyethyl]-1-piperazineethanesulphonic acid (HEPES) and 2-[cyclohexylamino]ethanesulphonic acid (CHES).

Ionomycin. The free acid form of ionomycin from *Streptomyces conglobatus* (Calbiochem) was used as received. The purity of the different lots of ionomycin ranged from 92% to 98% The ionophore was recovered from the shipping vials using distilled methanol as the solvent. The resulting solutions were stored in a refrigerator at ~4 °C and protected from light at all times. The mass spectrum (FAB) for ionomycin ($C_{41}H_{72}O_9$, M.W. = 709.0) showed peaks for the ions $(M+H)^+$ and $(M+Na)^+$ at m/e = 709.5 and m/e = 731.5, respectively. Ionomycin was standardized by performing spectrophotometric titrations with a standardized $Cu(ClO_4)_2$ solution in 80% methanol-water.[1,2] From the standardization experiments, the molar absorptivity of ionomycin was calculated in 80% methanol-water.

The molar absorptivity of ionomycin was also determined in ethanol, methanol,

chloroform and hexane (at 25.0 °C), using two identical sets of five solutions with concentrations 9.0, 18.0, 27.1, 36.1 and 45.1 μM. To make these solutions, the appropriate volume of standardized stock solution of ionomycin was placed in two sets of empty vials, and the solvent (80% methanol-water) was evaporated. The ionomycin in the first and the second set of vials was dissolved in methanol and hexane, respectively, to make the final concentrations. The solutions were equilibrated for at least a week and the absorbance was recorded. The solvents from the first and the second set of vials were evaporated and replaced with ethanol and chloroform, respectively. The absorbance was measured following the same procedure as for the previous set of solvents. The solvents (ethanol and chloroform) were evaporated again and replaced with 80% methanol-water. The absorbance was then measured to ensure that the loss (or degradation) of ionomycin during the experiment was less than 1%.

2,6-Dimethyl-3,5-heptanedione (DMHD). Commercially available DMHD (Parish Chemical Company) was light yellow in appearance when received. It was purified by distillation at low pressure at 26°C (lit.[3,4] b.p. = 94.0-94.5 at 20 mm; 62-63 at 3 mm). The colorless middle, distillation fraction was collected. Potentiometric titrations accounted for 92% of the weighed compound; owing to the high volatility of this compound, it is expected that a large fraction of the remaining 8% evaporated during the solution making process.

Magnesium Perchlorate. $Mg(ClO_4)_2$ (Aldrich, reagent grade) was standardized with EDTA using Eriochrome Black T as the indicator.[5] A few drops of a 0.4 percent solution of the indicator was used for each titration. The titration was performed in presence of NH_3/NH_4^+ buffer at pH = 10.0. The NH_4OH (Mallinckrodt) and NH_4Cl (Aldrich) used to make the buffer, were used as provided. The indicator changed color from wine red to

purple blue at the end point because of the following reaction.

$$\underset{\text{(wine red)}}{\text{Mg-Indicator}} + \text{EDTA} \rightleftharpoons \underset{\text{(purple blue)}}{\text{Indicator}} + \text{Mg-EDTA}$$

Calcium Perchlorate. $Ca(ClO_4)_2$ (G. Frederick Smith, reagent grade) was standardized with EDTA using Eriochrome Black T as the indicator in the presence of a known concentration of Mg(II).[5] The indicator does not form a strong complex with Ca(II) and therefore, the color change at the end point is sharper in the presence of Mg(II) ions. The procedure for the titration is the same as used for $Mg(ClO_4)_2$. The observed value of the volume of titrant used is corrected to account for the added Mg(II).

Copper Perchlorate. $Cu(ClO_4)_2$ (Aldrich) was standardized with EDTA using fast sulphon black (Sigma, 65%) as the indicator.[5] The indicator was prepared as a 5% solution in doubly-distilled water.

Tetraethylammonium hydroxide (Et_4NOH). Et_4NOH was purchased as a 20 wt. % solution in water (density = 1.041, Aldrich or Acros Organics) and was used as received.

Tetraethylammonium perchlorate (TEAP). TEAP was prepared by drop-wise addition of conc. $HClO_4$ (11.7 M) into a solution of 20% tetraethylammonium hydroxide. The pH of the reaction mixture was monitored using pH paper (Micro Essential) to minimize the addition of excess acid. The crude product was filtered and recrystallized twice from hot water. The crystals were dried at 70 °C under vacuum for 24 h and were stored in a desiccator over P_2O_5 (J. T. Baker).

For the earlier part of the study, commercially available TEAP (Eastman Kodak) was also used after double recrystallization from hot water.

4-(2-hydroxyethyl)-1-piperazinepropanesulfonic acid (EPPS). 99% pure EPPS (Aldrich) was used as provided.

N,N,N'N'-Tetraethylethylenediamine (TEEDA). 98% TEEDA (Aldrich) was used as provided. No extra peaks were seen in the ^1H NMR of this compound.

N,N,N'N'-Tetraethylpropanediamine (TEPDA). 97% TEPDA (Aldrich) was used as provided. No extra peaks were seen in the ^1H NMR of this compound.

Acetic acid. The stock solutions of CH_3COOH were made from concentrated acid (Fisher, glacial, ≥ 99%). The solutions were standardized against NaOH potentiometrically.

Solvents. The solubility of ionomycin in pure water is limited, therefore, all studies were performed using 80% methanol-water (w/w) as the solvent system. Solutions of 80% methanol-water were made using double-distilled water (see chapter II for the description of the distillation apparatus). Methanol (Fisher, reagent grade) was distilled prior to use. Chloroform (Fisher, reagent grade), ethanol (McCormick, absolute) and hexane (Aldrich, spectrophotometric grade) were used as provided.

The solvents used for the NMR studies are the following: methyl-d_3 alcohol-d (CD_3OD, Aldrich, 99.8 atom % D), methyl-d_3 alcohol (CD_3OH, Aldrich, 99 atom % D), deuterium oxide (D_2O, Aldrich, 99.96 atom % D), chloroform-d ($CDCl_3$, Cambridge Isotope, 99.8 atom % D) and benzene-d_6 (C_6D_6, Cambridge Isotope, 99.6 atom % D).

Glassware cleaning. All glassware used to prepare or store solutions of ionomycin was

submerged overnight in a mixture of 3:1 (v/v) sulfuric and nitric acids. The glassware was rinsed thoroughly with distilled and double-distilled water, and dried prior to use.

B. Measurement of Acidity

The operational pH* scales established by de Ligny *et al.*[6-8] for methanol-water mixtures were utilized to determine the acidity. pH* has the same meaning as the term pH when the latter is used in reference to an aqueous solution. pH* is defined by the relationship,

$$pH^* = -\log a^*_{H^+} = pH_{obs} - \delta \qquad (6.1)$$

where $a^*_{H^+}$ is the activity of hydrogen ion in the mixed solvent, pH_{obs} is the pH-meter reading, and δ is a correction factor. δ represents the difference between the liquid junction potential, E_j (in pH units), and the medium effect, $\log_m \gamma_H$.[9,10]

$$\delta = E_j - \log_m \gamma_H \qquad (6.2)$$

The value for the δ-factor for an electrode in 80% methanol-water solvent system was obtained by using the equation[11]

$$\delta = \log K^{m^*}_{H\ obs} - \log K^{m^*}_{H\ ref} \qquad (6.3)$$

where $K^{m^*}_{H\ obs}$ and $K^{m^*}_{H\ ref}$ are the values for the experimental and the reference mixed-mode protonation constants for acetic acid in 80% methanol-water, respectively; both

these constants, generally represented as K_H^{m*}, are defined by equation 6.4.

$$K_H^{m*} = \frac{[HL]}{a_{H^+}^{*}[L]} \tag{6.4}$$

Mean values of $K_{H\,ref}^{m*}$ at I = 0.050 M were calculated from the thermodynamic protonation constants, $K_{H\,ref}^{t*}$, reported by other workers.[11-13] The relationship between $K_{H\,ref}^{t*}$ and $K_{H\,ref}^{m*}$ is defined by the equation 6.5 where a_i^* represents the activity of species i in 80% methanol-water.

$$K_{H\,ref}^{t*} = \frac{a_{HL}^{*}}{a_{H^+}^{*}\,a_{L^-}^{*}} = K_{H\,ref}^{m*}\frac{\gamma_{HL}^{*}}{\gamma_{L}^{*}} \tag{6.5}$$

where a_i* and γ_i* represent the molal activity and the activity coefficient of the species i, respectively. The activity coefficients used for the calculations of $K_{H\,ref}^{m*}$ were obtained from the published literature.[14] The values for the activity coefficients of hydrochloric acid in methanol-water mixtures have been reported by Oiwa.[14] Although the data reported by Oiwa do not include activity coefficients for the conditions of our experiments (I = 0.050 M), these values were obtained by the interpolation and extrapolation of the reported data. The equations developed by Pitzer[15] were used to fit the data. A simplified expression for Pitzer equation may be represented by the expression[16]

$$\ln \gamma = -A_\psi\left[\frac{\sqrt{I}}{1+b\sqrt{I}} + \frac{2}{b}\ln(1+b\sqrt{I})\right]|z_M z_X| + (P_1)\,m + (P_2)m^2 \tag{6.6}$$

where z_M and z_X (electronic units) are the respective charges of the cation and the anion of the electrolyte, A_ψ is the Debye-Huckel coefficient for the osmotic function (A_ψ =

0.904, for 80% methanol-water system),[16] b is a parameter and its value is calculated to be 1.2,[16] m is the molality of the solution, I is the ionic strength in molal units (I = m, for cases where electrolyte consists of a monovalent cation and its anion such as Et_4N^+ and ClO_4^-), and, P_1 and P_2 are the parameters that are described elsewhere.[16]

Using a nonlinear least-squares fitting program, the values obtained for the parameters P_1 and P_2 for electrolytes consisting of monovalent ions in 80% methanol-water, are 2.5 and –6.6, respectively. These values may be used in equation 6.6 to calculate the activity coefficient at any ionic strength for the monovalent electrolytes in 80% methanol-water. Figure 6.1 shows the plot of activity coefficients versus molality in 80% methanol-water.[14] The activity coefficients for monovalent ions at ionic strength 0.050 M (0.059 molal) and 0.10 M (0.12 molal) were calculated to be 0.651 and 0.587, respectively. For the conversion of molality (mol kg^{-1}) to molarity (mol L^{-1}), the reported value of the specific gravity (ρ = 0.8425 g/mL)[14] for 80% methanol-water was used in the relationships,

$$M = \frac{m\,\rho}{1 - (0.001 \times m \times \text{Mol. Wt.})} \tag{6.7}$$

$$m = \frac{M}{\rho + (0.001 \times M \times \text{Mol. Wt.})} \tag{6.8}$$

where M and m are the molar and molal concentrations, respectively, and Mol Wt. is the molecular weight of the added elecrolyte.

Using the values for the activity coefficients obtained from equation 6.6 and the mean of the reported[11-13] values of log $K_{H\,ref}^{t*}$ (6.64), the value of log $K_{H\,ref}^{m*}$ in 80% methanol-water and I = 0.050 M was calculated to be 6.44. The value of log $K_{H\,obs}^{m*}$ was obtained from the potentiometric titration of 10.0 mM acetic acid (I = 0.050 M, TEAP) with 0.050 M Et_4NOH in 80% methanol-water. The titration data

were analyzed using the program PKAS[17,18] to calculate the value of log $K_{H}^{m*}{}_{obs}$. The PKAS program requires the value of autoprotolysis constant as an input. Equation 6.9 represents the protolysis of a solvent ROH, for which the autoprotolysis constants may be described by equations 6.8 to 6.10.

$$ROH \rightleftharpoons OR^- + H^+ \tag{6.9}$$

$$K_S^{t*} = a_{H^+}^{*} \cdot a_{OR^-}^{*}, \text{ (thermodynamic autoprotolysis constant)} \tag{6.10}$$

$$K_S^{m*} = a_{H^+}^{*} [OR^-] \text{ (mixed-mode autoprotolysis constant)} \tag{6.11}$$

$$K_S^{c*} = [H^+] [OR^-] \text{ (concentration autoprotolysis constant)} \tag{6.12}$$

The values of autoprotolysis constants at $I = 0.050$ and 0.10 M in 80% methanol-water are summarized in Table 6.1.

Table 6.1. Autoprotolysis Constants for 80% Methanol-Water

	log K_W^{x*}	
	($I = 0.050$ M)	($I = 0.10$ M)
[a] K_S^{t*}	14.42	14.42
[b] K_S^{m*}	14.23	14.19
[b] K_S^{c*}	14.05	13.96

[a] taken from the literature[19]

[b] calculated using values of activity coefficients from equation 6.6

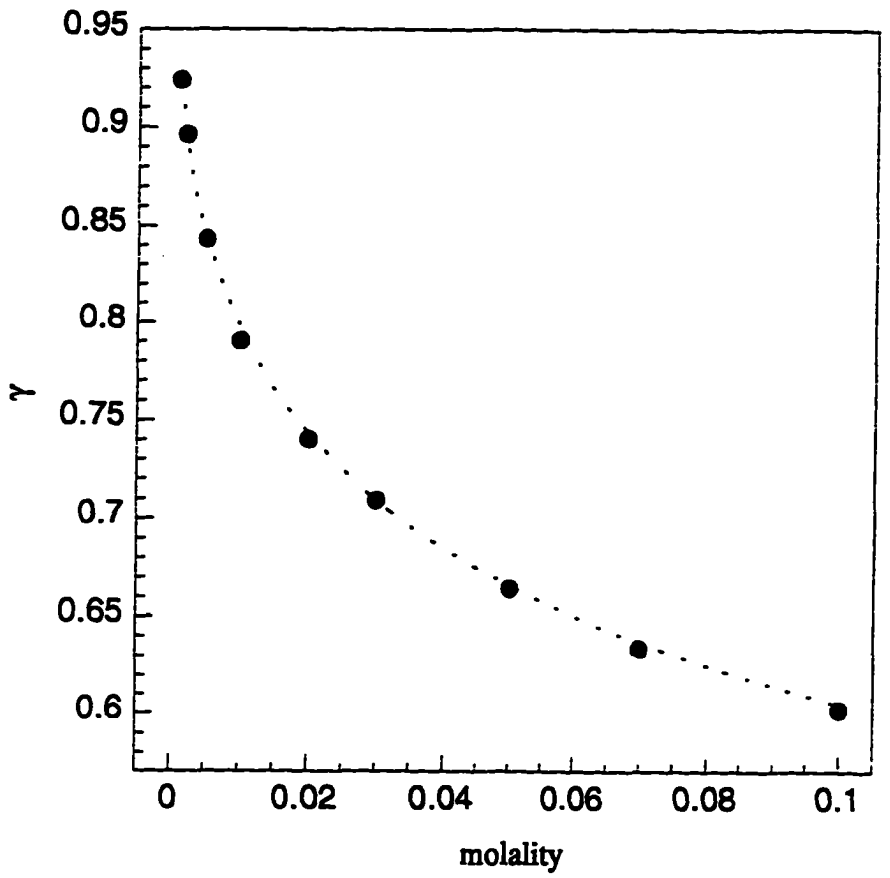

Figure 6.1. Plot of mean activity coefficient versus molality for HCl in 80% methanol-water solvent. The dotted line represents theoretical fit to the Pitzer's equation (equation 6.5).

The δ-factor for the electrode in 80% methanol-water at I = 0.050 M, was obtained by subtracting the value of log $K_H^{m*}{}_{ref}$ (= 6.44) from the experimentally determined value of log $K_H^{m*}{}_{obs}$ for acetic acid. The values for the δ-factors varied between -0.37 to -0.43 for the two Orion Ross 8103 electrodes used during the course of study. The internal filling solution used in these electrodes was a mixture of aqueous

3 M NaCl and MeOH (4:1, w/w). It was observed that the original filling solution recommended for the electrode (3 M KCl) caused precipitation at the surface of the electrode due to the formation of $KClO_4$.

The electrodes were used in conjunction with Corning model 125 or Fisher model 825MP pH meters. The pH-meter/electrode systems were calibrated using aqueous standard buffers (Gram-Pac®, Fisher) with nominal pH values of 4.01, 6.86 and 9.18. Subsequent to calibration, the electrodes were equilibrated in 80% methanol-water for at least 1 hour.

To measure pH* values lower than 4.0, calibration of the pH-meter/electrode system was performed using a series of standard solutions of $HClO_4$ in 80% methanol-water. The ionic strength of the $HClO_4$ solutions was adjusted to the same value (I = 0.10 or 0.050 M) as that of the solutions whose pH* values were to be determined. Standardization of $HClO_4$ was performed using aqueous NaOH solutions. To measure pH* values higher than 10.0, calibration of the pH-meter/electrode system was performed using a series of standard solutions of Et_4NOH (I = 0.050 M) in 80% methanol-water. Standardization of Et_4NOH was performed using standardized aqueous $HClO_4$. The concentration of Et_4NOH required to make a solution of particular pH* was calculated using equation 6.13 where K_S^{m*} and $a_{H^+}^*$ are described earlier in this section.

$$[OH^-] = \frac{K_S^{m*}}{a_{H^+}^*} \qquad (6.13)$$

pH* adjustments were made immediately before each experiment using concentrated Et_4NOH and/or $HClO_4$ solutions. During the pH* measurements, absorption of CO_2 into the solutions was minimized by passing solvent saturated nitrogen over the surface of the solutions.

C. Determination of Protonation Constants and Metal Complexation Constants for Buffers

The protonation constants for MES, EPPS, HEPES, CHES in 80% methanol-water and at $I = 0.050$ M (TEAP) were determined by potentiometric methods at 25 °C. Under the same conditions the constants for the second protonation step for TEEDA and TEPDA were also determined. A 10.0 mM solution of each buffer was titrated with 43.3 mM NaOH. The program PKAS was used to calculate the protonation constants.[17,18]

Complexation of Mg(II) with MES, HEPES, EPPS and CHES was studied using a potentiometric method. A 10.0 mM solution of each buffer was titrated with 43.3 mM NaOH at $I = 0.050$ M (TEAP) in the absence and presence of 5.0 mM Mg(II). The procedure for calculation of the metal ion complexation constants for the buffers is described in Chapter VII.

D. NMR studies of ionomycin and DMHD

The NMR studies were performed with the objective of studying the enol/keto ratios and the location of the enolic proton on the β-diketone moiety of ionomycin and DMHD in 80% methanol-water. ^{1}H and the ^{13}C NMR spectra of the ligands were obtained at 25.0 °C in 80% CD_3OD/D_2O (w/w) and 80% CD_3OH/H_2O (w/w), respectively. Since ionomycin is large molecule, additional, more sophisticated techniques were employed to facilitate peak assignment. These techniques are: DEPT (distortionless enhancement by polarization transfer)[20], COSY (correlated spectroscopy)[21] and HMQC (hetronuclear correlation through multiple quantum coherence).[21] The COSY and the HMQC spectra were obtained in 80% CD_3OD/D_2O

(w/w) and the DEPT spectrum was obtained in CD_3OH/H_2O (w/w).

In addition to the experiments described above, spin decoupling experiments in 80% CD_3OD/D_2O were also performed to ascertain ^1H–^1H connectivity.

The quantities of the keto and enol forms of the ligands were calculated from the area under the assigned peaks for the respective forms in the ^1H NMR spectra. The solutions of DMHD and ionomycin were prepared two days prior to the NMR measurement to ensure equilibration of tautomers.

To measure the enol content of neat DMHD, a set of two concentric tubes was used to acquire the NMR spectrum. The outer tube was filled with the compound while the inner tube contained C_6D_6 to acquire the lock signal.[22] All the NMR studies were performed using Varian XL 300-MHz or Varian Unityplus 500-MHz NMR spectrometers.

E. Determination of Complexation Constant for Ni(DMHD)$^+$

The complexation constant for the Ni(DMHD)$^+$ complex was determined by potentiometric as well as spectrophotometric methods in 80% methanol-water and $I = 0.050$ (TEAP). In the potentiometric measurements, a solution of 11.0 mM DMHD and 5.0 mM Ni(II) was titrated with 48.8 mM tetraethylammonium hydroxide. The data were obtained in the pH* range of 3.5 to 6.0. The data were analyzed using the program BEST to calculate the value of the formation constant.[18,23] The spectrophotometric titrations were carried out by adding small aliquots of concentrated Ni(II) to a solution containing 85.7 μM DMHD buffered at pH* = 5.10 using 5mM MES. The reaction mixture was equilibrated for 15 minutes before recording each spectrum. The absorbance (λ = 310 nm) versus [Ni^{2+}] data were fit to the equation derived for the conditional

complexation constant (described in the next chapter), using a nonlinear least-squares routine.

F. Kinetic Measurements

Kinetic measurements were made using the diode array UV-Vis spectrophotometer or the stopped-flow system which are described in chapter II. In the reaction chamber of the stopped-flow instrument, the concentrations of the reactant solutions are diluted by a factor of two. The concentrations of the reactants reported here are those obtained after mixing, unless otherwise mentioned. All reactions were performed at 25.0 °C.

For reactions where absorbance changes were very small ($\Delta A < 0.1$), the data for several runs were computer averaged to enhance the signal to noise ratio. For this purpose the data from the computer system of the stopped-flow instrument (Cromemco operating system) were transferred to an IBM compatible personal computer (CompuAdd® 320). The transfer of data was performed using Procom Plus communication software (version 2.0; Datastorm Tech., Inc.). From the IBM computer, the data were then imported into a Macintosh computer (Apple IIsi) using Apple File Exchanger software. The individual kinetic runs were averaged using the program Kaleidagraph (version 3.0.4, Abelbeck Software). Using this procedure of computer-averaging of the kinetic data, the reactions could be studied where the values for ΔA were as low as 0.01 absorbance units.

The kinetic data were fit to single and double exponential first-order expressions using the nonlinear least-squares routine of the Kaleidagraph program. The expression used for these fits are described in Chapter VII. For the reactions where the values for ΔA were more than 0.1, the program FOOLSii was used to calculate the pseudo first-order rate constants.

i) Kinetics of keto-enol tautomerism

NMR studies (reported in the next chapter) showed that, in 80% methanol-water, ionomycin and DMHD exist as mixtures of the enol and keto forms. We were interested in studying the kinetics of the interconversion of the tautomeric forms. Two methods were employed to initiate conversion of the enol to the keto form: i) pH jump and ii) rapid dissolution of concentrated ionomycin (in pure methanol) or neat DMHD, in an 80% methanol-water solution. These experiments were performed as a function of buffer concentration at different pH* values to investigate the possibility of general and specific acid-base catalysis.

In the pH-jump method, the ligand ([ionomycin] = 54 μM or [DMHD] = 36 μM) was dissolved in a highly basic solution of Et_4NOH (pH* = 12.5) where it exists predominantly in the enolate form. This solution was mixed with 10 mM EPPS buffer adjusted to a pH* that gave a final value between 7.0 and 8.0, after mixing. Upon mixing, the rapid decrease in the pH* resulted in conversion of enolate form of the ligand to its enol form at a rate comparable to the proton transfer reactions ($t_{1/2} \approx 10^{-10}$ s).[24] However, the rate of conversion of enol to keto form was comparable to the relaxation of other simple β-diketones ($t_{1/2} \approx$ 1 to 20 minutes).[25,26] This process was monitored on the stopped-flow instrument at λ = 278 nm for both ionomycin and DMHD. The reaction for the pH-jump experiment can be represented as shown in Scheme 6.1, where E^-, HE and HK represent the enolate, enol and the keto forms, respectively.

Scheme 6.1

$$E^- + H^+ \overset{\text{fast}}{\rightleftharpoons} HE \rightleftharpoons HK$$

The basis for the second method (rapid dissolution) is the fact that the keto/enol ratio for a β-diketone increases with the solvent polarity. In non-polar solvents, or in the neat compound, the enol form of the ligand is favored compared to the keto form since the former can be stabilized by intramolecular hydrogen bonding. In polar solvents the keto form of the compound can be stabilized by intermolecular bonds with the solvent. NMR experiments show that neat DMHD has a higher percentage of the enol form compared to a solution in 80% methanol-water. Therefore, on dilution of the ligand with 80% methanol-water, the equilibrium shifts toward the keto form, allowing the interconversion process to be studied. Small quantities (~0.01 μL) of pure DMHD were mixed with 3.0 mL of 80% methanol-water containing EPPS or CHES (5.0-20.0 mM) in a cuvette to make the final concentration of the ligand ~10^{-5} M. It is difficult to maintain the accuracy and precision in delivering very small volumes of ligand such as in this case; however, because keto-enol tautomerism is a first-order process, the rate constant can be calculated without the knowledge of the initial concentrations of the isomers.

The doubly protonated form of ionomycin is a solid. Therefore, concentrated solutions of ionomycin were made in pure methanol to perform the rapid dissolution experiments in 80% methanol-water solution.

ii) Reactions of Ni(II) with ionomycin and DMHD

All formation and dissociation reactions of NiI were monitored at 310 nm. The ionic strength was maintained at 0.050 M with TEAP. The concentration of the ligand in the formation reactions was 10.0 μM. The [Ni^{2+}] ranged from 0.01 to 8.0 mM. The series of solutions of NiI for the dissociation reactions consisted of 10.0 μM ionomycin and 2.0-16.0 mM Ni(II). The reactions were performed by mixing these solutions with 5.0-40.0 mM $HClO_4$.

The kinetics for the dissociation reaction of $Ni(DMHD)^+$ were studied at

conditions similar to the dissociation reactions of NiI. The reactions were monitored at 307 nm. The series of solutions of $Ni(DMHD)^+$ consisted of 31 μM DMHD and 2.0-16.0 mM Ni(II). The dissociation reactions were initiated by mixing these solutions with equal volumes (*ca.* 0.20 mL) of solutions containing 5.0-40.0 mM $HClO_4$.

The formation and dissociation of $Ni(DMHD)^+$ was also studied at ionic strength of I = 0.50 M with $NaClO_4$ in order to facilitate comparison of our results with the results obtained for the Ni(II)-(pentane-2,4-dione) system.[27] The concentration of the ligand in the formation reactions was 25 μM. The concentration of Ni(II) ion ranged from 2.0-45.0 mM. The dissociation reactions were carried out using a solution of the $Ni(DMHD)^+$ containing 22 μM DMHD and 20.0 mM Ni(II). These solutions were mixed with a series of solutions containing 5.0-50.0 mM $HClO_4$.

The initial pH* values of the solutions containing the metal-ligand complex were adjusted between 6.1 and 6.8. The pH* (3.3 to 4.0) for the formation reactions was maintained by adding at least ten-fold excess H^+ to ensure pseudo-first-order conditions.

iii) Reactions of Mg(II) with ionomycin and DMHD

All reactions of Mg(II) with ionomycin and DMHD were performed at I = 0.050 M maintained with TEAP.

a) Reactions of Mg(II) and ionomycin in presence of buffers: The complex formation reactions were studied as a function of buffer and metal ion concentration. The buffers chosen for these studies were HEPES, EPPS and CHES. The pH* of these reactions was maintained between 7.60 and 8.40. The concentrations of the reagents in these studies were: [I] = 10 μM, [Mg(II)] = 4.0 mM, [buffers] = 0.50-10.0 mM. The dependence of the formation reaction of MgI on metal ion concentration (1.0-12.0 mM) was studied in presence of 5.0 mM EPPS and in the pH* range 7.20 - 8.00. The concentration of ionomycin in these reactions was 9 μM.

Dissociation of MgI as a function of pH* and metal ion concentration was studied

using TEEDA, TEPDA or MES. The solution of MgI contained 20 μM ionomycin with varying [Mg^{2+}] (4.0-16.0 mM). Dissociation was initiated by mixing these solutions with a 20.0 mM buffer solution in the pH* range 5.60 - 6.37.

b) Reactions of Mg(II) with DMHD in the presence of buffers: The reactions of Mg(II) with DMHD were investigated in the presence of EPPS and CHES buffers at pH* = 8.40. The concentration of the buffers in these reactions was between 1.0 to 20.0 mM and the concentrations of DMHD and Mg(II) were 0.020 and 4.0 mM, respectively.

REFERENCES

1) Stiles, M. K.; Craig, M. E.; Gunnell, S. L. N.; Pfeiffer, D. R.; Taylor, R. W. *J. Biol. Chem.* **1991**, *266*, 8336-8342.

2) Drumhiller, J. A.; Laing, J. L.; Taylor, R. W. *Anal. Chim. Acta.* **1984**, *162*, 315-321.

3) Hammond, G. S.; Borduin, W. G.; Guter, G. A. *J. Am. Chem. Soc.* **1959**, *81*, 4682-4686.

4) Smith, L. I.; King, J. A. *J. Am. Chem. Soc.*. **1943**, *65*, 441-443.

5) Vogel, A. I. *Textbook of Quantitative Analysis*; 5th ed.; Wiley: New York, 1989, p 325.

6) de Ligny, C. L.; Luykx, P. F. M.; Rehback, M.; Weineke, A. A. *Recl. Trav. Chim. Pays-Bas* **1960**, *79*, 699-736.

7) Gelsema, W. J.; de Ligny, C. L.; Remijnse, A. G.; Blijleven, H. A. *Recl. Trav. Chim. Pays-Bas* **1966**, *85*, 647-660.

8) Gelsema, W. J.; de Ligny, C. L.; Blijleven, H. A. *Recl. Trav. Chim. Pays-Bas* **1967**, *86*, 852-864.

9) Popovych, O. *Crit. Rev. Anal. Chem.* **1970**, *1*, 73-117.

10) Bates, R. G.; Paabo, M.; Robinson, R. A. *J. Phys. Chem.* **1963**, *67*, 1833-1838.

11) Rorabacher, D. B.; Mackellar, W. J.; Shu, F. R.; Bonavita, S. M. *Anal. Chem.* **1971**, *43*, 561-573.

12) Shedlovsky, T.; Kay, R. L. *J. Phys. Chem.* **1965**, *60*, 151-155.

13) Bacarella, A. L.; Grunwald, E.; Marshall, H. P.; Purlee, E. L. *J. Org. Chem.* **1955**, *20*, 747-762.

14) Oiwa, I. T. *J. Phys. Chem.* **1956**, 754-759.

15) Pitzer, K. S. *J. Phys. Chem.* **1973**, *77*, 268-277.

16) Gupta, A. R. *J. Phys. Chem.* **1979**, *83*, 2986-2990.

17) Motekaitis, R. J.; Martell, A. E. *Can. J. Chem.* **1982**, 168-173.

18) Martell, A. E.; Motekaitis, R. J. *Determination and Use of Stability Constants*; 2nd ed.; Editor; VCH: New York, 1992.

19) Taylor, R. W. *Ph.D. Thesis* **1973**, Wayne State University, MI.

20) Atta-ur-Rahman *One and Two Dimensional Spectroscopy*; Elsevier: New York, 1989, pp 111-115.

21) Sanders, J. K. M.; Hunter, B. K. *Modern NMR Spectroscopy*; 2nd ed.; Oxford University Press: Oxford, 1993, pp 110-113.

22) Sanders, J. K. M.; Hunter, B. K. *Modern NMR Spectroscopy*; 2nd ed.; Oxford University Press: Oxford, 1993, pp 39-14.

23) Motekaitis, R. J.; Martell, A. E. *Can. J. Chem.* **1982**, *60*, 2403-2409.

24) Eigen, M. *Pure Appl. Chem.* **1963**, *6*, 97-115.

25) Hynes, M. J. *Rev. Inorg. Chem.* **1990**, *11*, 21-78.

26) Hernando, J. M.; Montero, O.; Blanco, C. *Collect. Czech. Chem. Commun.* **1984**, *55*, 1984-1991.

27) Hynes, J. M.; O'Regan, B. D. *J. Chem. Soc., Dalton Trans.* **1979**, 162-166.

CHAPTER VII

RESULTS

This chapter presents the results of the kinetic study of the reactions of ionomycin and the model compound, 2,6-dimethyl-3,5-heptanedione (DMHD), with the metal ions nickel(II) and magnesium(II). A detailed analysis of these reactions required information about the keto-enol tautomerism of the ligands. The results are presented from NMR spectroscopic studies performed to measure the enol/keto ratios for the ligands, and from kinetic studies performed to study the keto-enol interconversion mechanism. It was observed that the buffers used catalyze the processes of the keto-enol interconversion, as well as the metal-ligand complexation reactions. These catalytic effects are elucidated. Furthermore, values are reported for the stability constant for the Ni-DMHD complex and the protonation constants for the buffers that were used in the studies. All experiments were performed in 80% methanol-water solvent system and at 25.0 °C. The ionic strengths in all the studies were maintained at $I = 0.050$ with TEAP with the exception of the reactions of nickel(II) with DMHD, in which case, the studies were also performed at $I = 0.50$ M maintained using $NaClO_4$.

A. NMR Studies of Ionomycin and DMHD

i) ^{1}H NMR studies

^{1}H NMR studies of ionomycin and DMHD revealed that in 80% methanol-water, these compounds are present as mixtures of keto and enol forms. The structures of the keto and enol forms of the β-diketone moiety that is present in ionomycin and DMHD, are shown in Figure 7.1. The spectra for DMHD and ionomycin are shown in Figures 7.2 and 7.3, respectively, and the peak assignments are presented in Table 7.1.

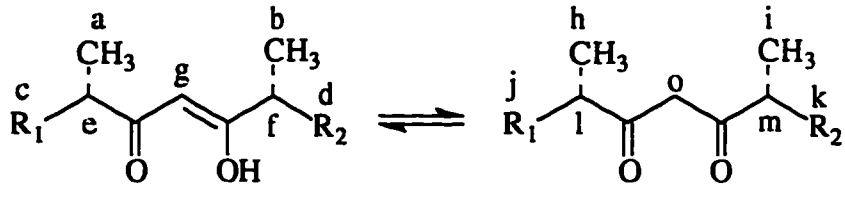

Figure 7.1. Isomeric forms of the β-diketone moieties of ionomycin and DMHD, enol (left) and keto (right). For DMHD, $R_1 = R_2 = CH_3$. R_1 and R_2 for ionomycin can be deduced from the ionophore structure shown in Table 7.2.

In the spectrum of DMHD, two sets of peaks were obtained that were assigned to the keto and the enol forms of the molecule. The peaks for the methine protons (at 2.52 and 2.73 ppm) appeared as septets due to the coupling of these protons with two equivalent methyl protons. The peaks for the methyl protons appeared as doublets due to coupling with the methine protons.

Compared to the spectrum of DMHD, the spectrum of ionomycin was much more difficult to analyze due to large number of overlapping peaks. However, the peaks for the two sets of methine protons of ionomycin that are labelled in Figure 7.1 as e, f, and,

l, m, were well-resolved. Their positions at 2.50 and 2.77 ppm, were very close to those of the methine protons of DMHD. These peaks appeared as multiplets due to second-order coupling with the adjoining methyl and methylene groups. To further substantiate the peak-assignments a Correlated Spectroscopy (COSY) spectrum was also obtained.

The COSY spectrum provides information about the ^{1}H-^{1}H connectivity.[1] The peaks for the protons appear along the diagonal as contours representing peak intensities. For the protons which are coupled to other protons, additional contours are observed off the diagonal. These off-diagonal contours are called crosspeaks. A vertical and a horizontal line drawn from a crosspeak will intercept the contours (on the diagonal) of the protons which are coupled to each other. The crosspeaks for the methine protons of the keto and enol forms of ionomycin (discussed above) can be seen in the COSY spectrum shown in Figure 7.4.

Table 7.1. Chemical Shifts for ^1H NMR Spectra of DMHD and Ionomycin in 80% CD_3OD/D_2O

proton label in Figure 7.1	chemical shift in ppm[a] (multiplicity, *J* Hz) ionomycin	DMHD
a, b	1.11 (doublet, 6.5 Hz)	1.13 (doublet, 7.1 Hz)
c, d	1.67 (multiplet)[b]	1.13 (doublet, 7.1 Hz)
e, f	2.50 (multiplet)	2.52 (septet, 7.0 Hz)
g[c]	5.65 (singlet)	5.63 (singlet)
h, i	1.06 (doublet)	1.09 (doublet, 7.1 Hz)
j, k	1.70 (multiplet)[b]	1.09 (doublet)
l, m	2.77 (multiplet)	2.73 (septet, 7.1 Hz)
o[c]	not observed[d]	3.78 (singlet)

[a]Peaks are assigned with respect to the methyl peak of $C(H)D_2OD$ referenced at 3.30 ppm. [b]Obtained from the COSY spectrum. [c]Peak disappears as the proton is replaced by the deuterium ion from the solvent. [d]Not observed due to: i) the low concentration of the keto form and ii) the fast exchange of the proton with the deuterium atom from the solvent.

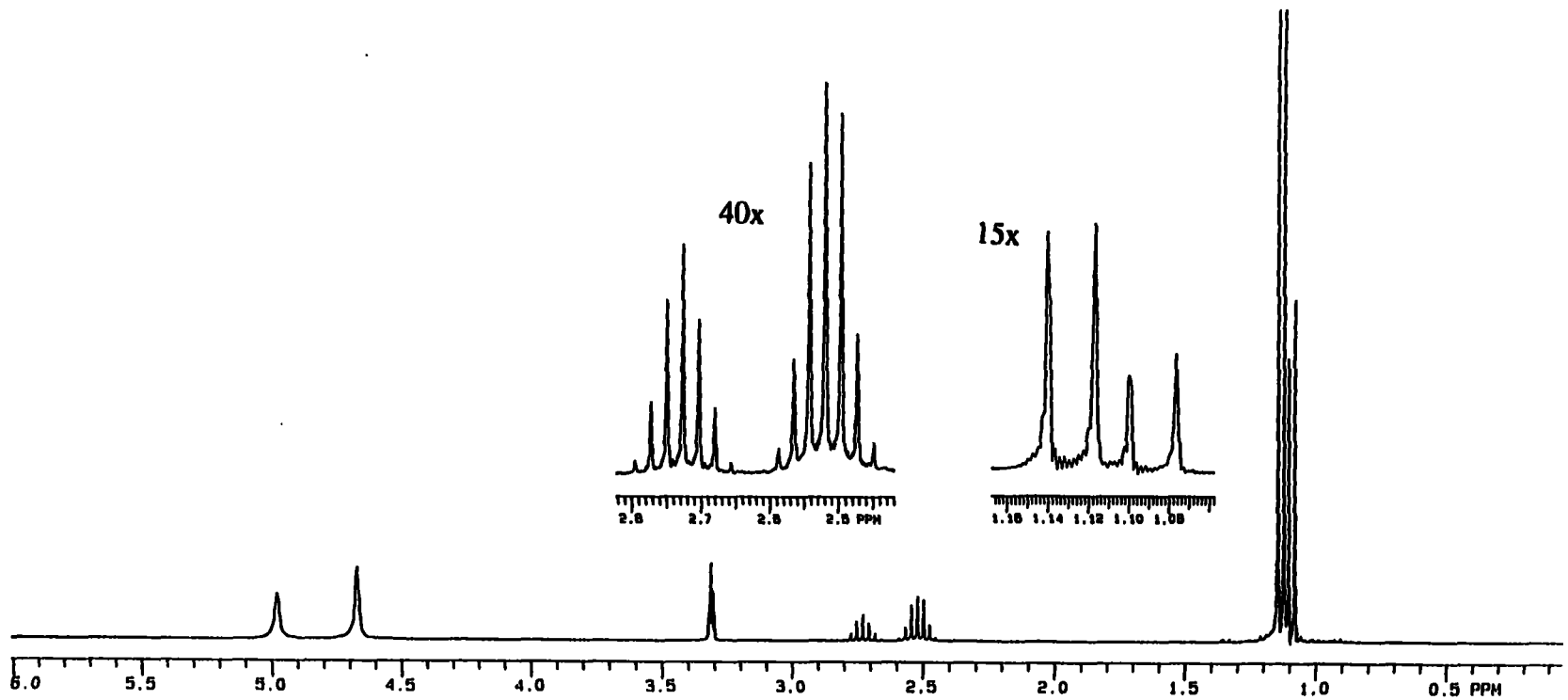

Figure 7.2. 300-MHz ^1H NMR spectrum of 2,6-dimethyl-3,5-heptanedione in 80% CD_3OD–D_2O (w/w).

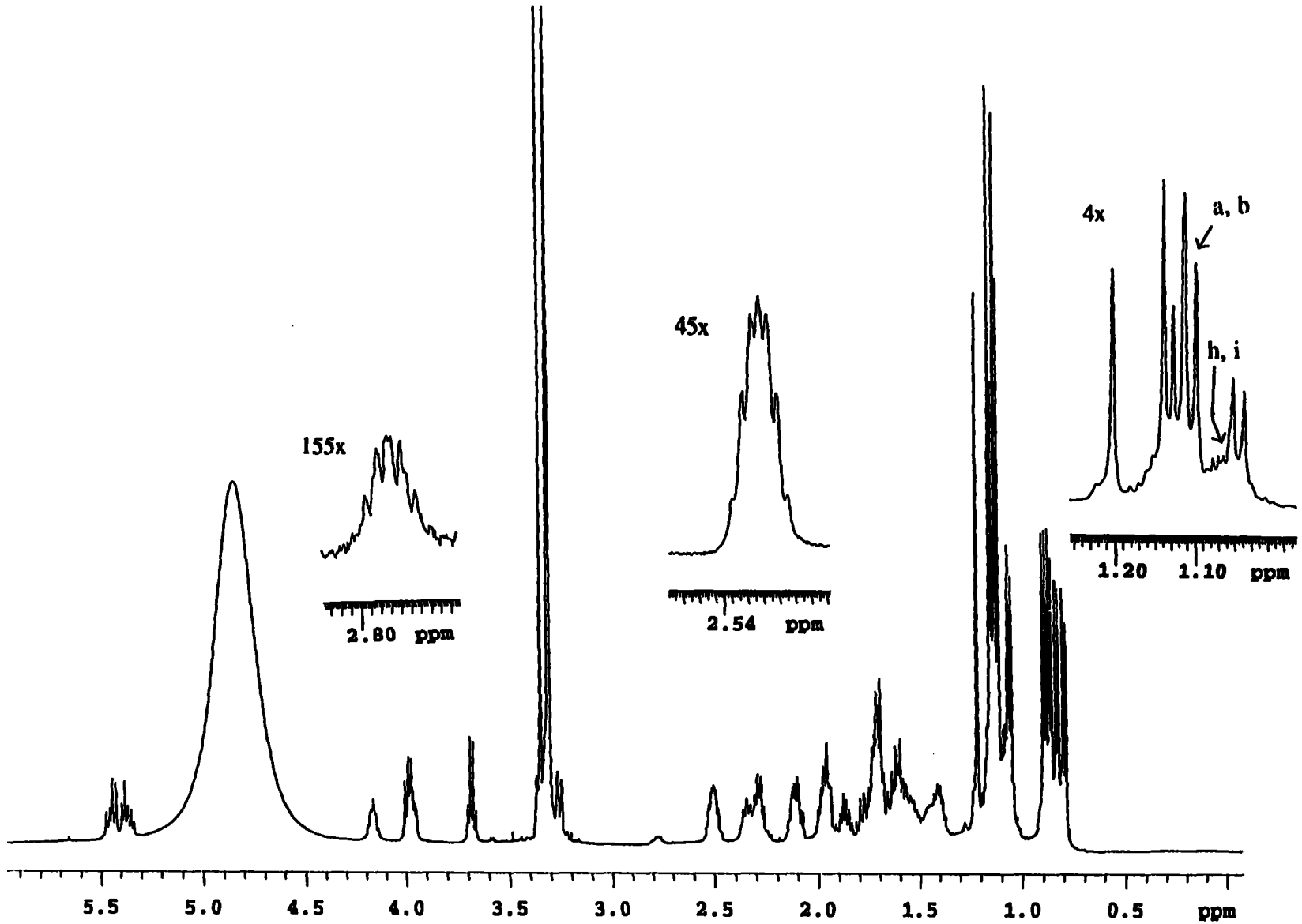

Figure 7.3. 500-MHz ^1H NMR spectrum of ionomycin in 80% CD_3OD–D_2O (w/w).

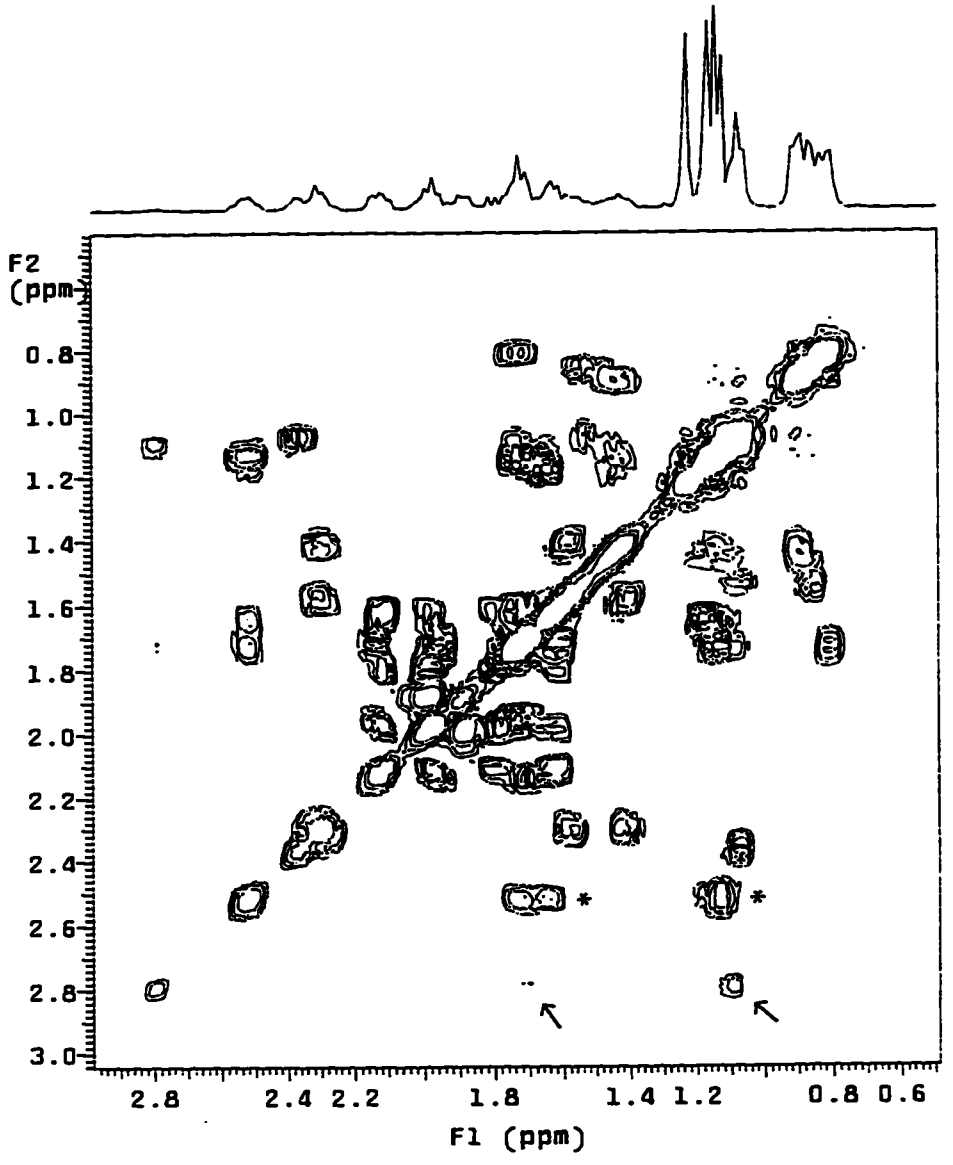

Figure 7.4. 500-MHz COSY spectrum of ionomycin in 80% CD_3OD–D_2O (w/w). The crosspeaks for the methine protons of the enol form (shown as e, f in Figure 7.1) are marked with asterisks and the crosspeaks for the corresponding proton for the keto form (shown as l, m in Figure 7.1) are marked with arrows.

ii) enol/keto ratios of ionomycin and DMHD

The values for the percentages of the enol and the keto forms of the two ligands were calculated using the relationships given by equations 7.1 and 7.2, respectively. In these equations, A_e and A_k represent the integrated area under the ^1H NMR peaks corresponding to the enol and the keto forms, respectively.

$$\% \text{ enol} = \frac{A_e}{A_e + A_k} \times 100 \qquad (7.1)$$

$$\% \text{ keto} = \frac{A_k}{A_e + A_k} \times 100 \qquad (7.2)$$

The calculations for DMHD were performed using the area under the methyl peaks. In the case of ionomycin, the analogous peaks are partially overlapped by other peaks and therefore, the peaks for the methine protons at 2.50 and 2.77 ppm were used to calculate the enol content. Three experiments were performed for each ligand to determine their enol content. The average values for the percentage of the enol form of DMHD and ionomycin were determined to be (74.7 ± 0.3) % and (88.0 ± 0.3) %, respectively. From the spectrum of neat DMHD, the percentage of the enol form was calculated to be (95.6 ± 0.2) %.

iii) ^{13}C NMR studies

The ^{13}C NMR spectra for ionomycin and DMHD are shown in Figures 7.5 and 7.6, respectively. The spectrum for DMHD showed peaks for both the enol and the keto forms of the ligand, whereas, the spectrum for ionomycin only showed peaks for the enol form. The absence of ketonic peaks in the latter case may be ascribed to either i) low concentration of the keto form (~12% of the total ligand), and/or ii) higher noise-level of

^{13}C NMR spectroscopy compared with ^{1}H NMR spectroscopy.

A heteronuclear correlation through multiple quantum coherence (HMQC) spectrum for ionomycin was also acquired.[1] The HMQC spectrum provides information about proton–carbon connectivity. The signals in an HMQC experiment are acquired via proton detection. The peak for a proton connected to another NMR active hetero-nuclei (^{13}C–for ionomycin), appears as an off-diagonal contour similar to those seen in a COSY experiment. The x- and the y- coordinates of the contour are the chemical shift values of the proton and the carbon in the ^{1}H and ^{13}C spectra, respectively. Two perpendicular lines, drawn from a contour to the ^{1}H and ^{13}C spectra drawn on x- and y- axis, respectively, would intercept the peaks of the atoms which are coupled to each other. The HMQC spectra for ionomycin was obtained in 80% CD_3OD/D_2O. The spectrum (not shown here), did not show any crosspeaks between the protons and carbon atoms corresponding to the keto form.

Tables 7.2 and 7.3 present the peak assignments for the ^{13}C spectra of ionomycin and DMHD, respectively. Since ionomycin is a large molecule that contains 41 carbon atoms, the peak assignment was facilitated by obtaining a Distortionless Enhancement by Polarization Transfer (DEPT) spectrum for this compound.[2] In the DEPT spectroscopic technique, the pulse sequences are modulated to obtain a set of three spectra. One of these spectra shows peaks for only –CH– carbon atoms while the other two spectra show peaks for $-CH_2-$, –CH– and $-CH_3$ carbon atoms. The difference in the nature of the latter two spectra is the opposite phasing of the $-CH_2-$ peaks. The quaternary carbon atoms are not seen in the DEPT spectrum. Comparison of the DEPT spectra with the ^{13}C spectra makes the assignment of all the peaks possible. The DEPT spectrum of ionomycin (not shown here) showed peaks for 10 methyl, 11 methylene, and 15 methine groups, that accounted for all the non-quaternary carbon atoms in the ionomycin molecule. The peaks for the quaternary carbons were assigned by comparing the DEPT

spectrum with the ^{13}C spectrum where the latter showed peaks for all the 41 carbon atoms present in the molecule.

Table 7.2. Chemical Shifts for ^{13}C NMR Spectra of Ionomycin

carbon number	carbon type	chemical shift in ppm[a]
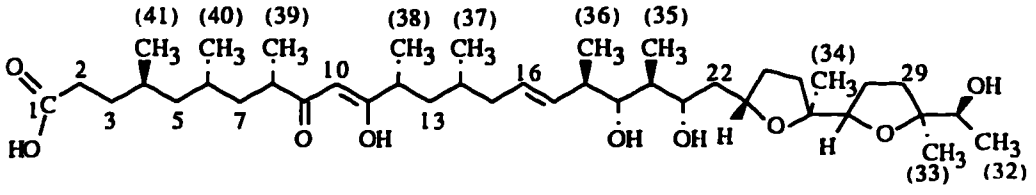		
32 to 41	$-CH_3$	10.9, 17.8, 18.9, 19.0, 19.4, 19.4, 19.51 19.7, 22.3, 25.6,
2, 3, 5, 7, 13, 15, 22, 24, 25, 28, 29	$-CH_2-$	28.1, 32.3, 32.7, 33.4, 33.5, 34.4, 39.1, 41.5, 42.1, 43.4, 45.7
4, 6, 8, 12, 14, 16, 17, 18, 19, 20, 21, 23, 27, 31	–CH–	29.1, 30.6, 32.1, 40.8, 41.2, 41.3, 43.4, 72.4, 73.8, 78.6, 80.9, 85.3, 130.4, 133.1
10	–CH–	99.1
9, 11	>C=O, =CO–	200.4, 200.8
26, 30	–CO–	85.6, 87.5
1	$-CO_2-$	178.3

[a]Peaks are assigned with respect to the methyl peak of CD_3OD referenced at 49.0 ppm.

Table 7.3. Chemical Shifts for ^{13}C NMR Spectra of DMHD

carbon type[a]	chemical shift in ppm[b]
$-CH_3$, (enol)	19.6
$-CH_3$, (keto)	18.0
–CH, (enol)	37.8
–CH, (keto)	42.7
=CH–, (enol)	96.2
$-CH_2-$, (keto)	53.1
>C=O, (enol)	201.2
=C–OH, (enol)	201.2
>C=O, (keto)	212.1

[a]Refer to Figure 7.1 for structures. [b]Peaks are assigned with respect to the methyl peak of CD_3OD referenced at 49.0 ppm.

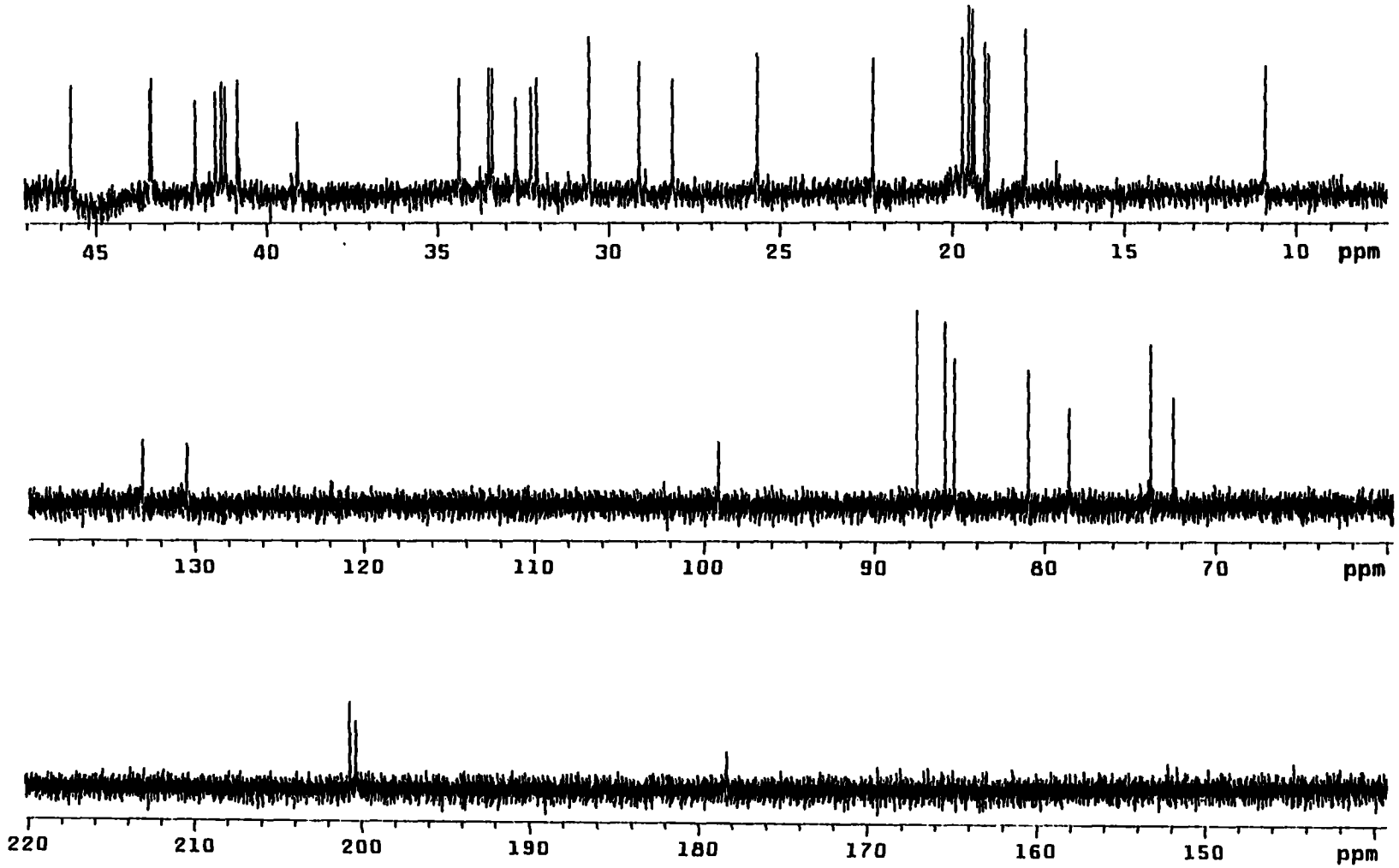

(147)

Figure 7.5. 125-MHz ^{13}C NMR spectrum of ionomycin in 80% CH_3OH–H_2O (w/w).

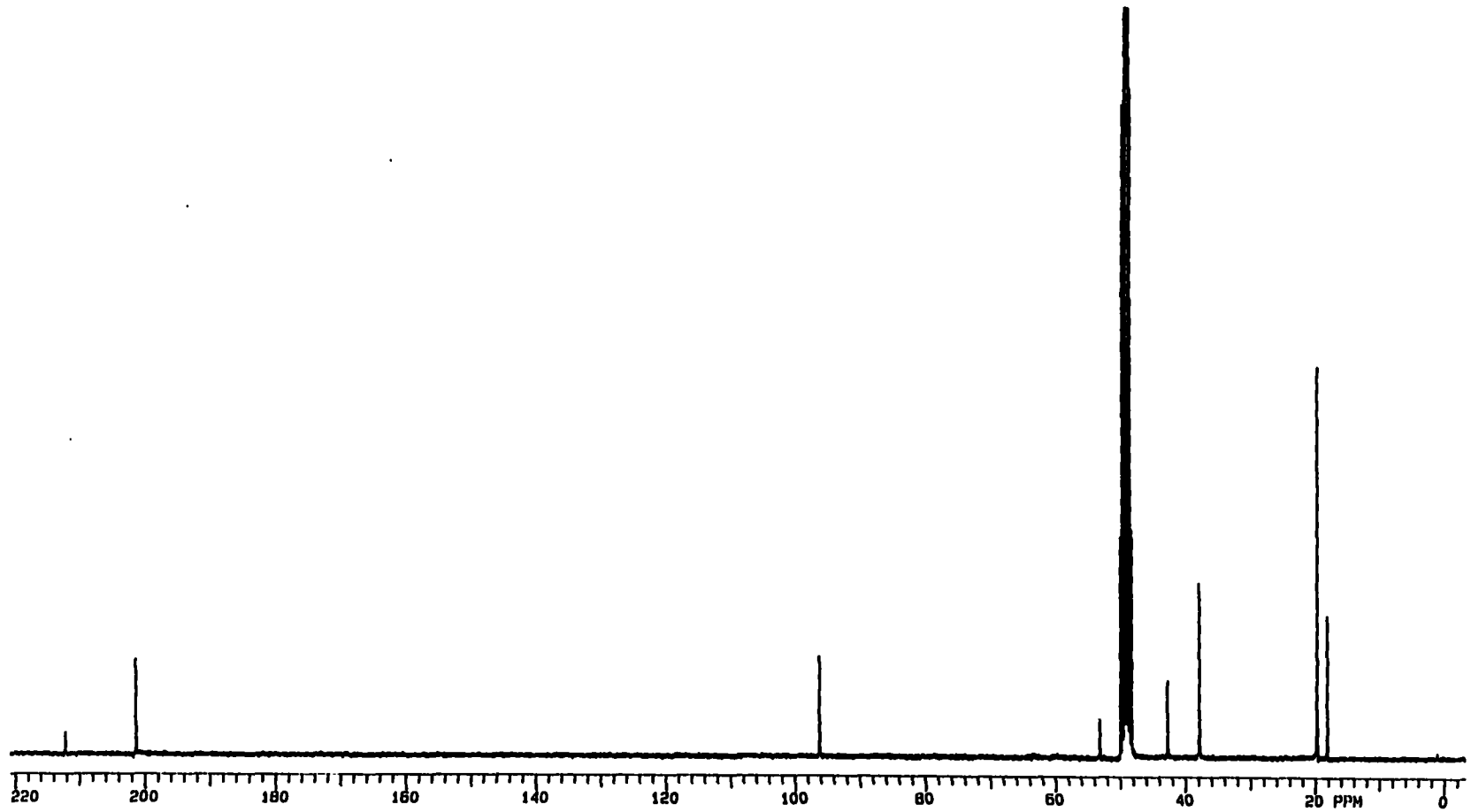

Figure 7.6. 75-MHz ^{13}C NMR spectrum of 2,6-dimethyl-3,5-heptanedione in 80% CH_3OH–H_2O (w/w).

B. Kinetics of Keto-Enol Isomerization

The keto-enol isomerization process may be represented by Scheme 7.1 in which HE and HK represent the enol and the keto forms of the ligand, respectively, and, k_e and k_k represent the forward and reverse rate constants for enolization, respectively. The observed rate constant, k_{obs}, for the interconversion process is described by equation 7.3.[3] The equilibrium constant, $K_{e/k}$, for the process is defined by the equation 7.4. The values of $K_{e/k}$ for the ligands can be obtained from their enol/keto ratios. From the NMR experiments these values for ionomycin and DMHD are calculated to be 7.33 and 2.95, respectively.

Scheme 7.1.

$$HK \underset{k_k}{\overset{k_e}{\rightleftharpoons}} HE$$

$$k_{obs} = k_e + k_k \tag{7.3}$$

$$K_{e/k} = \frac{k_e}{k_k} = \frac{[HE]}{[HK]} \tag{7.4}$$

We investigated the feasibility of several methods to initiate the keto-enol interconversion for ionomycin. The usual bromination technique used by several investigators to study simple β-diketone systems[4-6] did not meet with success. The FAB mass spectrum showed that the ionomycin molecule breaks down into smaller fragments (at m/e < 400) upon reaction with bromine. The methods we used are: i) pH-jump and ii) rapid dissolution of the ligands into 80% methanol-water. The general methodology for these is described in Chapter VI.

i) pH-jump experiments

When highly basic solutions of ionomycin or DMHD containing the enolate form (E^-) of the ligand were mixed with EPPS buffer at ~neutral pH*, a rapid absorbance-jump was observed at 278 nm. This initial jump in absorbance was followed by a comparatively slower first-order decrease. These absorbance changes were ascribed to the following two processes: i) rapid conversion of E^- to HE, and ii) the slow approach to equilibrium between HE and HK. The absorbance-time data for the slow process were fit to the first-order expression described by equation 7.5, where A_0 and A_∞ are the initial and final values of the absorbance and A_i is the instantaneous value for the absorbance at any time t.

$$[A_i - A_\infty] = [A_0 - A_\infty] \exp (-k_{obs}t) \qquad (7.5)$$

A nonlinear least-squares routine was used to fit the data and the values of A_0, A_∞ and k_{obs} were obtained for each run. The values of k_{obs} as a function of buffer concentration are summarized in Table 7.4 where n represents the number of replicates. The plots of k_{obs} against the concentration of the conjugate base form of the EPPS buffer were linear. These plots for ionomycin and DMHD are shown in Figures 7.7 and 7.8, respectively. The behavior shown by these plots indicates general-base catalysis of the keto-enol interconversion process. The buffer independent rate constants were obtained from the intercepts of these plots; the values for ionomycin and DMHD obtained from the least-squares fits are $(2.50 \pm 0.03) \times 10^{-1}$ s^{-1} and $(4 \pm 5) \times 10^{-3}$ s^{-1}, respectively.

From the analysis of the absorbance-time data, the values of $K_{e/k}$ can also be obtained using the relationship described by equation 7.6,

$$K_{e/k} = \frac{A_\infty}{\Delta A(1 + K_{H1}a^*_{H^+})} \qquad (7.6)$$

where ΔA is the absorbance change ($A_\infty - A_0$), K_{H1} is the first protonation constant, and $a^*_{H^+}$ is the hydrogen ion activity of the ligand solution before mixing with the buffer. The derivation of this equation is shown in Appendix I, part C. From the values of $K_{e/k}$, the average percentages of the enol form for ionomycin and for DMDH were calculated to be 89% and 76%, respectively. These values are in reasonable agreement with those obtained from the NMR experiments.

Table 7.4. Observed Rate Constants for Keto-Enol Interconversion of Ionomycin and DMHD, Initiated by pH-Jump,[a] in 80% Methanol-Water

initial pH*	final pH*	k_{obs} (s^{-1})	n	10^3 [EPPS]$_{base}$, (M)[b]	% [HE]
ionomycin[c]					
12.44	6.99	0.279 ± 0.004	8	1.80	87.5
12.44	7.44	0.315 ± 0.006	12	3.81	88.6
12.44	7.90	0.355 ± 0.007	13	6.40	88.9
					88.3 ± 0.7 (mean)
DMHD[d]					
12.44	6.99	0.0307 ± 0.0003	6	1.80	77.3
12.44	7.44	0.0677 ± 0.0004	10	3.81	75.2
12.44	7.90	0.1048 ± 0.0009	8	6.40	76.7
					76 ± 1 (mean)

[a] λ = 278 nm, T = 25 °C. [b]Conjugate base form of EPPS calculated from the total [EPPS] = 10.0 mM after mixing, using the mixed-mode value of log K_H = 7.65. [c][ionomycin] = 27 μM after mixing. [d][DMHD] = 36 μM after mixing.

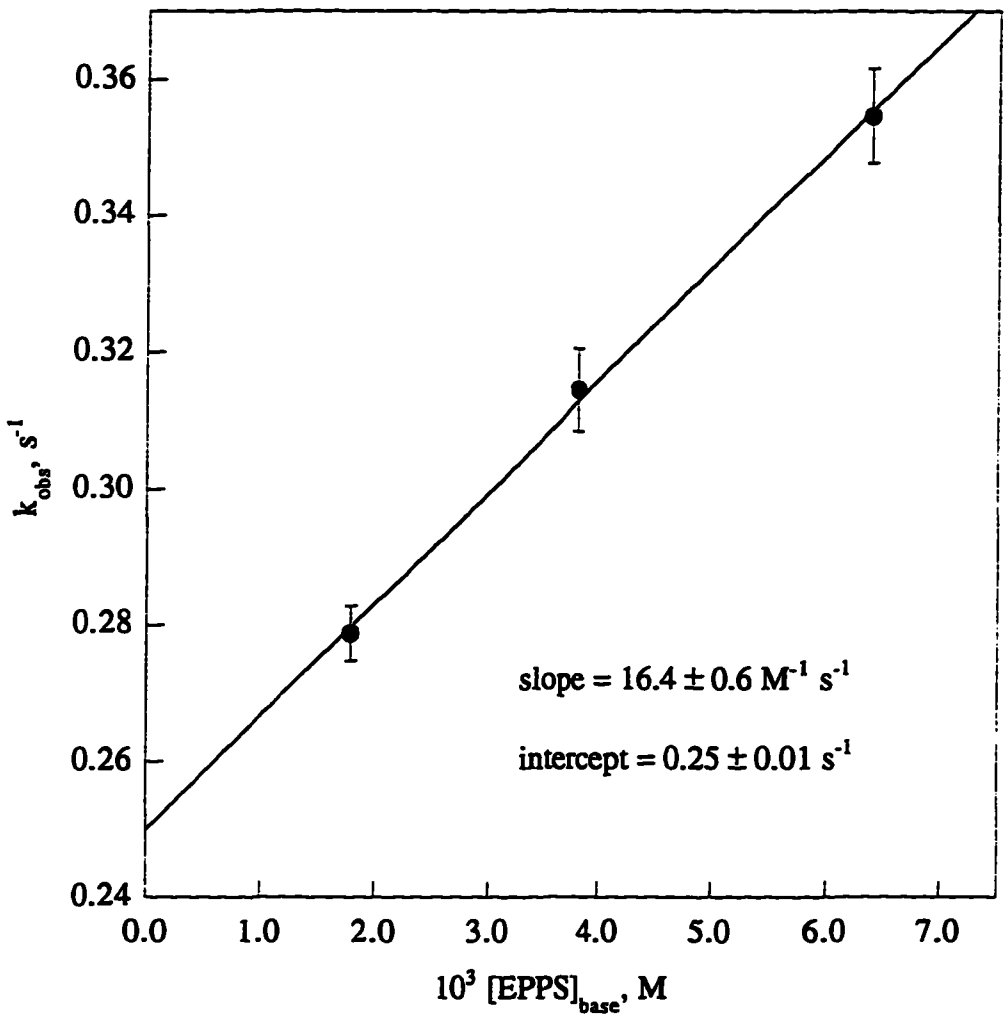

Figure 7.7. Plot of k_{obs} for the keto-enol interconversion for ionomycin determined from the pH-jump experiment, versus the concentration of the conjugate base form of EPPS buffer. The error bars represent the mean ± 1 S.D.

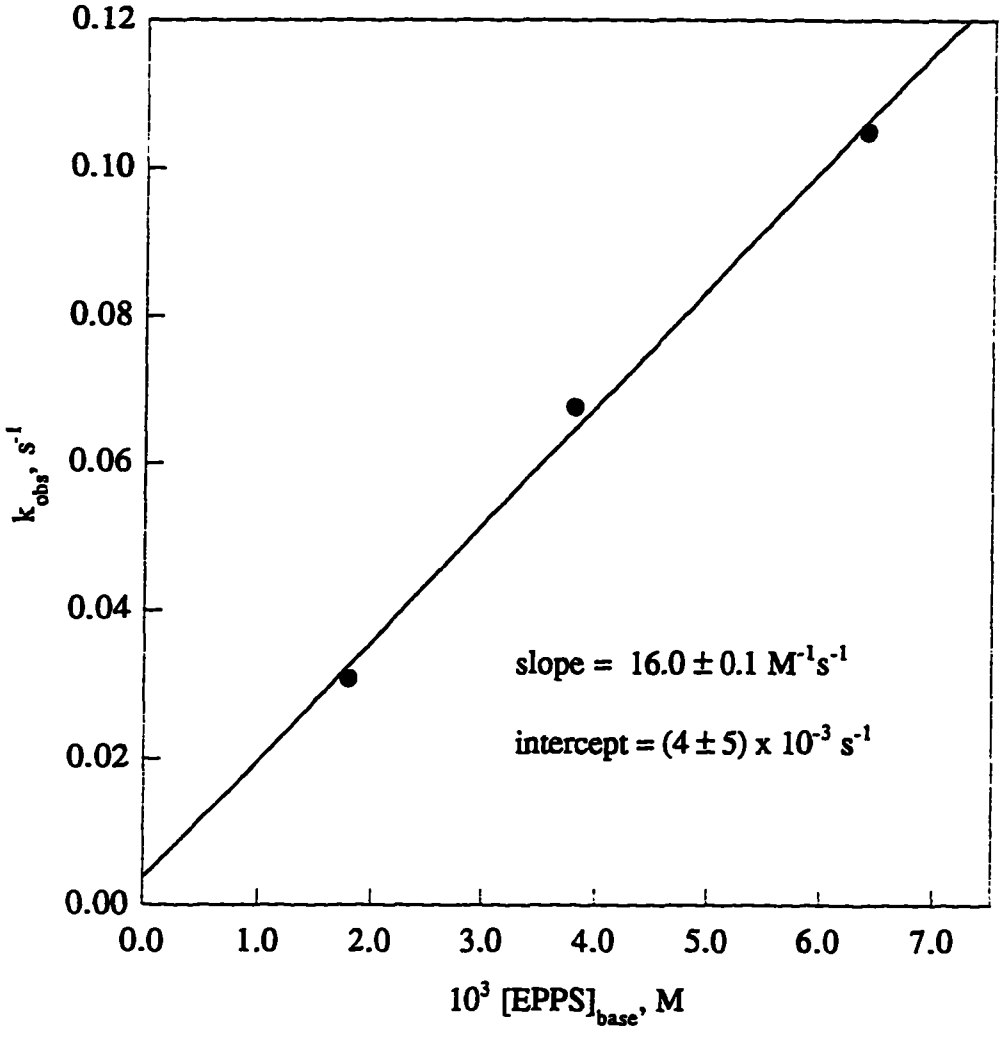

Figure 7.8. Plot of k_{obs} for the keto-enol interconversion of DMHD determined from the pH-jump experiment, versus the concentration of the conjugate base form of EPPS buffer. The errors in k_{obs} (mean ± 1 S.D.) are contained within the symbols.

ii) Rapid-dissolution experiments

Following dissolution of neat DMHD in buffered 80% methanol-water solutions, a decrease in absorbance at 278 nm was observed. This change resulted from the conversion of the enol form of the ligand to the keto form, that is driven by the increased solvent polarity compared to the neat ligand. The experiments were performed as a function of buffer concentration (EPPS or MES) at different pH* values. The observed processes obeyed first-order kinetics and the absorbance-time data were fit to equation 7.5 using a nonlinear least-squares method to obtain values for k_{obs}, A_0 and A_∞. Equation 7.7 was used to calculate the percentage of enol form (% [HE]) in 80% methanol-water. The derivation of this equation is based on the assumption that the absorbance of the keto form is negligible at the wavelength used to monitor the interconversion process. The value for % $[HE]_0$ for DMHD was calculated to be 95.6 from the results of the NMR experiments.

$$\% [HE] = \frac{A_\infty (\% [HE]_0)}{A_0} \tag{7.7}$$

The values of k_{obs} and %[HE] as a function of pH* and buffer concentration are summarized in Table 7.5. It can be seen that the enol/keto ratio is independent of the concentration or the nature of the buffer. The plots of k_{obs} against the concentration of the conjugate base form of the buffer gave straight lines; these plots are shown in Figures 7.10 and 7.11. The behavior seen in these plots is indicative of general-base catalysis, consistent with the results of the pH-jump experiments. From the intercept of these plots the buffer-independent values of k_{obs} for the interconversion process were obtained. These values are $(4 \pm 3) \times 10^{-3}$ and $(1.7 \pm 0.2) \times 10^{-3}$ s^{-1} for experiments using EPPS and MES buffers, respectively.

Rapid-dilution experiments were also performed with ionomycin. In these

experiments, concentrated solutions of ionomycin in pure methanol were diluted with buffered 80% methanol-water solutions. The absorbance changes in these experiments were very small ($\Delta A \sim 0.01$ AU) and were too rapid to be monitored by the technique employed. However, in the absence of the buffers and at low pH* values, the absorbance changes were slow enough to be measured accurately. From the absorbance-time data the value of k_{obs} for ionomycin at pH* = 3.22 was calculated to be $(1.9 \pm 0.1) \times 10^{-3}\ s^{-1}$.

Table 7.5. Observed Rate constants for Keto-Enol Interconversion of DMHD as a Function of Total Concentration of Buffer, in 80% Methanol-Water at $I = 0.050$ M (TEAP)

10^3 [buffer]$_{tot}$, (M)	pH*	$10^2 k_{obs}$ (s^{-1})	n	% [HE]
EPPS				
5.0	7.00	2.2 ± 0.1	3	72.6
5.0	7.34	3.7 ± 0.4	3	71.9
5.0	7.61	5.8 ± 0.4	3	71.3
10.0	7.00	4.1 ± 0.1	3	73.3
10.0	7.34	6.8 ± 0.3	3	74.3
10.0	7.60	10.0 ± 0.7	3	72.1
20.0	7.00	7.5 ± 0.3	3	74.2
MES				
2.0	5.00	0.21 ± 0.02	3	72.0
2.0	5.29	0.23 ± 0.02	3	72.9
2.0	6.02	0.40 ± 0.02	1	73.4
2.0	6.37	0.46 ± 0.02	1	75.3
2.0	7.00	0.53 ± 0.01	3	73.8
10.0	5.00	0.33 ± 0.01	3	73.8
20.0	5.00	0.52 ± 0.04	3	74.9
				73 ± 1 (mean)

[a][DMHD] varied between 5 and 30 μM, λ = 278 nm, T = 25 °C.

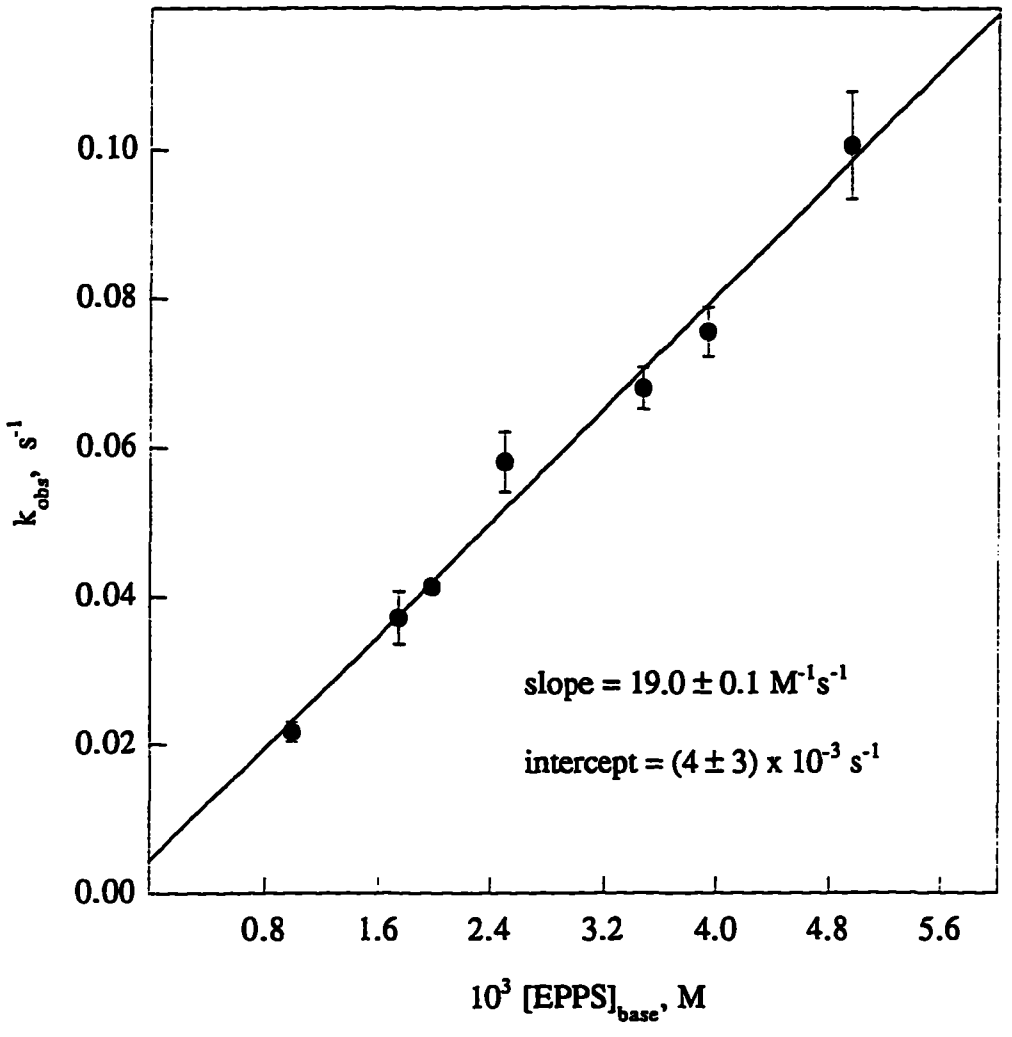

Figure 7.9. Plot of k_{obs} for the keto-enol interconversion of DMHD determined from the rapid-dilution experiment, versus the concentration of the conjugate base form of EPPS buffer. The error bars represent the mean ± 1 S.D.

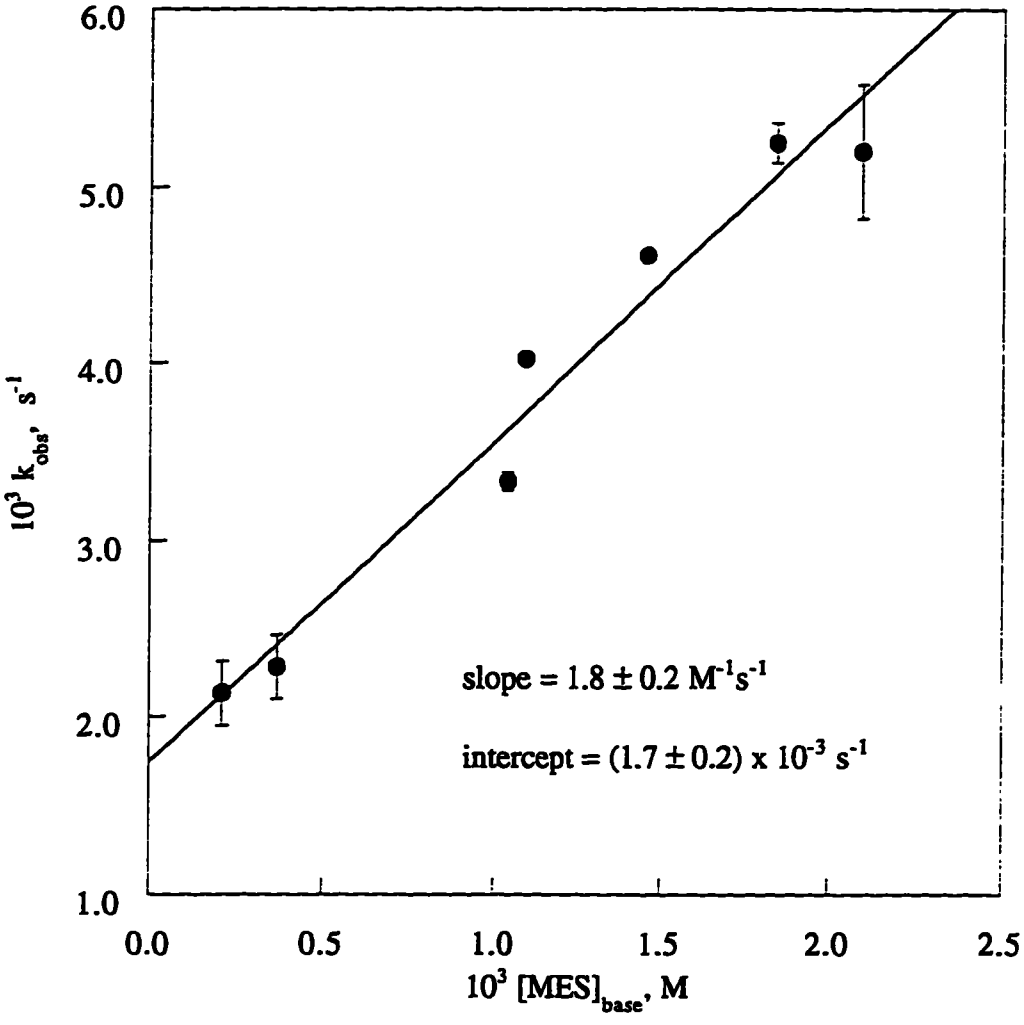

Figure 7.10. Plot of k_{obs} for the keto-enol interconversion of DMHD determined from the rapid-dilution experiment, versus the concentration of the conjugate base form of MES buffer. The error bars represent the mean ± 1 S.D.

C. Equilibrium Constants for Metal-Ligand Complexation

The complexation constant (K_{NiL}) for the $Ni(DMHD)^+$ complex, described by equation 7.8, was determined experimentally using spectrophotometric and potentiometric methods. Equation 7.9 describes the conditional stability constant (K'_{NiL}) for the $Ni(DMHD)^+$ complex at a given pH*. In these equations, L^- and HL represent the deprotonated and protonated forms of DMHD, respectively.

$$K_{NiL} = \frac{[NiL^+]}{[Ni^{2+}]\,[L^-]} \tag{7.8}$$

$$K'_{NiL} = \frac{[NiL^+]}{[Ni^{2+}]\,\{[L^-] + [HL]\}} \tag{7.9}$$

The spectrophotometric data {absorbance, $[Ni^{2+}]$}, were fit to equation 7.10 using a nonlinear least-squares routine to give values of K'_{NiL}, A_0 and A_{sat}

$$A_i = \frac{A_0 + A_{sat}\,K'_{NiL}\,[Ni^{2+}]}{1 + K'_{NiL}\,[Ni^{2+}]} \tag{7.10}$$

where A_0 and A_{sat} are initial and maximum absorbance values, respectively and A_i is the measured absorbance at each $[Ni^{2+}]$. Except for minor differences in the terminology, equation 7.10 is same as equation 3.16 which is derived in Appendix I, part B. The value of K'_{NiL} at pH* = 5.10 was determined to be 254 ± 3. Using this value of the conditional constant and the protonation constant (K_H) in equation 7.11, the value of log K_{NiL} was calculated to be 8.63.

$$\log K_{NiL} = \log \{ K'_{NiL} (1+K_H a_{H^+}) \} \quad (7.11)$$

The values of log K_{NiL} obtained from two different potentiometric runs were 8.61 and 8.60. Table 7.6 summarizes the equilibrium constants for the complexes of ionomycin and DMHD with Ni(II) along with the values of the acid dissociation constants for both the ligands.

It is noteworthy that the log K_H value for the NiI complex is 5.95 and at mildly acidic pH* values, a significant fraction of the complex is present in its protonated form. The protonation constant, K_{NiHL}, is defined by equation 7.12. Using the constants for the Ni(II)-ionomycin system presented in Table 7.6, a species distribution diagram was constructed for this system. This diagram is shown in Figure 7.11. The concentrations of metal and ligand used to construct this diagram are approximately the average concentrations used in the kinetic studies.

$$K_{NiHL} = \frac{[NiHI^+]}{a^*_{H^+} [NiI]} \quad (7.12)$$

Table 7.6. Nickel(II) Complexation Constants and Protonation Constants for Ionomycin and DMHD in 80% Methanol-Water Solutions at 25 °C and $I = 0.050$ M (TEAP)

	ionomycin	DMHD
log K_{NiL}, M^{-1}	10.25[a]	8.61, 8.60 (potentiometric) 8.63 (spectrophotometric) 8.61 (mean value)
log K_H, M^{-1}[a, b]	11.94 (K_{H1}) 6.80 (K_{H2})	11.33[c]
log K_{NiHL}[a, b]	5.95	

[a]From earlier work in this laboratory.[7] [b]Mixed-mode values are reported. [c]Average of the values obtained from the potentiometric (11.27) and the spectrophotometric (11.38) methods.

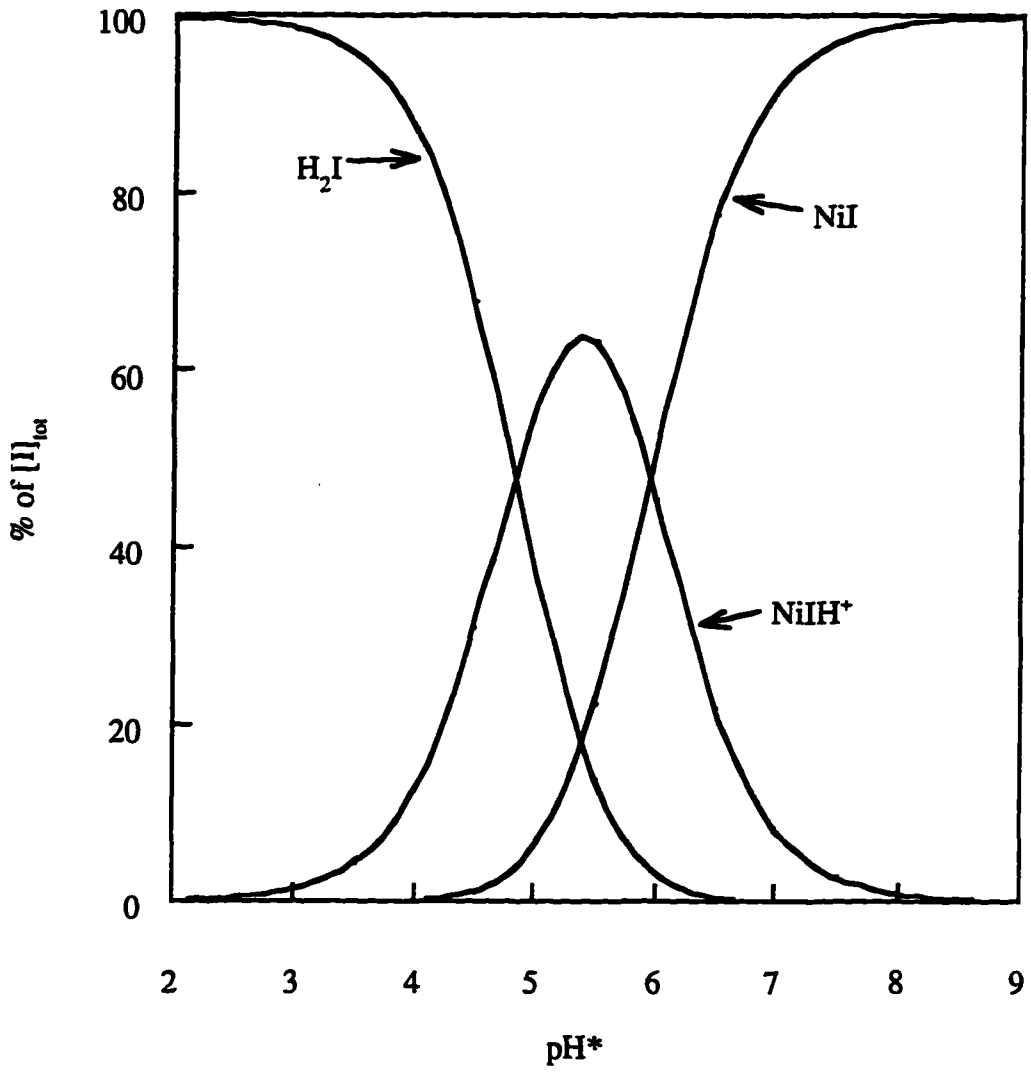

Figure 7.11. Species distribution diagram for Ni(II)-ionomycin in 80% methanol water. [ionomycin $]_{tot}$ = 5.0 x 10^{-6} M and $[Ni^{2+}]$ = 5 x 10^{-3} M.

D. Kinetics of the reaction of Ni(II) with Ionomycin and DMHD

The complexation of Ni(II) with ionomycin and DMHD causes a band shift from 280 nm to 302 nm, and 278 nm to 302 nm, respectively. The UV-Vis spectra of ionomycin and its complex with Ni(II) are shown in Figure 7.12. The UV-Vis spectra of DMHD and $Ni(DMHD)^+$ are very similar to the corresponding spectra of ionomycin and NiI which indicates that the β-diketone moiety in both cases is involved in complex formation. The reaction kinetics for both ligands were monitored at wavelengths between 305 to 310 nm. In this wavelength range, the ratio of the absorbance change to the background absorbance was optimal.

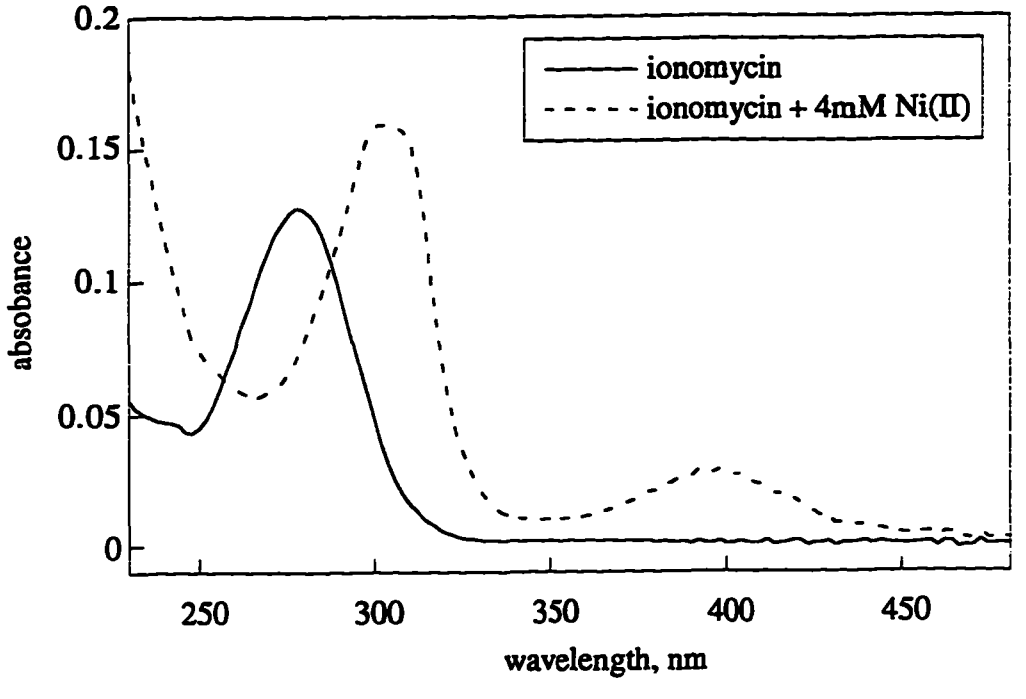

Figure 7.12. UV-Vis spectral change of ionomycin caused by addition of Ni(II) at mildly acidic conditions in 80% methanol-water.

i) General mechanism for the reactions of β-diketones with metal ions

In order to propose a mechanism consistent with the kinetic data obtained for the reactions of Ni(II) with ionomycin and DMHD, we first considered the general scheme proposed by several investigators for the reactions of simple β-diketones with metal ions.[4,6,8-10] It is shown as Scheme 7.2. This scheme involves three coupled pathways: i) interconversion of the keto (HK) and enol (HE) forms of the ligand, ii) reaction of the metal ion with the keto form of the ligand and iii) reaction of the metal ion with the enol form of the ligand. The rate constants for these pathways are labelled as follows: k_e for the conversion of the keto form to the enol form, k_k for the conversion of the enol form to the keto form, k_{HE} and k_{-HE} for the formation and dissociation of the complex involving the enol form, respectively, and, k_{HK} and k_{-HK} for the formation and dissociation of the complex involving the keto form of the ligand, respectively.

Scheme 7.2

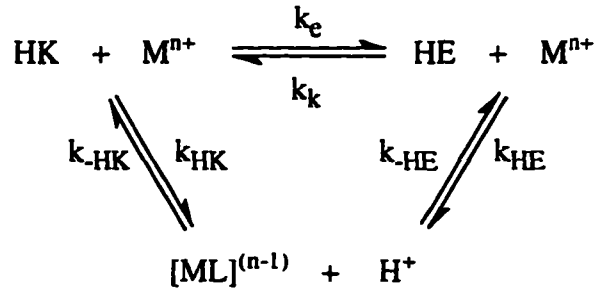

Since the enolate form of the ligand is not included in this scheme, its validity is limited to the cases where the concentration of the enolate form is negligible. Considering the values of the protonation constants for DMHD and ionomycin, it is clear that the concentration of the enolate forms of both ligands was negligible (~10 ppb) in our investigation of the reactions of Ni(II) with these ligands at pH* < 4. This permitted us to test the consistency of Scheme 7.2 with the kinetic data.

The mathematical treatment required to derive the rate law for Scheme 7.2, can be simplified by applying pseudo first-order conditions. One way to achieve this is by taking $[M^{n+}]$ and $[H^+]$ in great excess compared to [HL]. These conditions for the reactions of Ni(II) with DMHD and ionomycin, were employed. Under these conditions, the pseudo-first-order rate constants for the pathways involving $[ML]^{(n-1)}$ in Scheme 7.2 can be described by equations 7.12–7.15.

$$k'_{HE} = k_{HE}[M^{n+}] \tag{7.12}$$

$$k'_{-HE} = k_{-HE}[H^+] \tag{7.13}$$

$$k'_{HK} = k_{HK}[M^{n+}] \tag{7.14}$$

$$k'_{-HK} = k_{-HE}[H^+] \tag{7.15}$$

The rate laws can be described by equations 7.16–7.18.

$$\frac{d[HK]}{dt} = -k_e[HK] - k'_{HK}[HK] + k_k[HE] + k'_{-HK}[ML]^{(n-1)} \tag{7.16}$$

$$\frac{d[HE]}{dt} = k_e[HK] - k_k[HE] - k'_{HE}[HE] + k'_{-HE}[ML]^{(n-1)} \tag{7.17}$$

$$\frac{d[ML]^{(n-1)}}{dt} = k'_{HK}[HK] + k'_{HK}[HK] + k'_{HE}[HE] + k'_{-HK}[ML]^{(n-1)} \tag{7.18}$$

Integration of these rate laws may be accomplished by the method of matrices.[11-15] The derivation of the solution is shown in Appendix I, part D. The general solution yields

equations 7.19–7.21 as the expressions for the three roots.

$$\lambda_1 = 0 \tag{7.19}$$

$$\lambda_2 = p - \frac{b}{p} \tag{7.20}$$

$$\lambda_3 = \frac{b}{p} \tag{7.21}$$

Of these roots, only the latter two are meaningful and the quantities b and p are related to the rate constants in Scheme 7.2 by equations 7.22 and 7.23.

$$p = k_e + k_k + (k_{HE} + k_{HK})[M^{n+}] + (k_{-HE} + k_{-HK})[H^+] \tag{7.22}$$

$$b = k_e\{k_{HE}[M^{n+}] + (k_{-HK} + k_{-HE})[H^+]\} + k_{HK}[M^{n+}]\{k_k + k_{HE}[M^{n+}] + k_{-HE}[H^+]\} + k_k(k_{-HE} + k_{-HK})[H^+] + k_{HE}k_{-HE}[M^{n+}][H^+] \tag{7.23}$$

Substitution of the quantities p and b into equations 7.20 and 7.21 yields,

$$\lambda_2 = k_e + k_k + (k_{HE} + k_{HK})[M^{n+}] + (k_{-HE} + k_{-HK})[H^+] - \left[\frac{k_e\{k_{HE}[M^{n+}] + (k_{-HK} + k_{-HE})[H^+]\} + k_{HK}[M^{2+}] + \{k_k + k_{HE}[M^{2+}] + k_{-HE}[H^+]\} + k_k(k_{-HE} + k_{-HK})[H^+] + k_{HE}k_{-HK}[M^{2+}][H^+]}{k_e + k_k + (k_{HE} + k_{HK})[M^{n+}] + (k_{-HE} + k_{-HK})[H^+]}\right] \tag{7.24}$$

and,

$$\lambda_3 = \left[\frac{k_e\{k_{HE}[M^{n+}] + (k_{-HK} + k_{-HE})[H^+]\} + k_{HK}[M^{2+}] + \{k_k + k_{HE}[M^{2+}] + k_{-HE}[H^+]\} + k_k(k_{-HE} + k_{-HK})[H^+] + k_{HE}k_{-HK}[M^{2+}][H^+]}{k_e + k_k + (k_{HE} + k_{HK})[M^{n+}] + (k_{-HE} + k_{-HK})[H^+]}\right] \tag{7.25}$$

The expressions for the roots λ_2 and λ_3 can be further simplified based on the fact that the keto form of β-diketones reacts very slowly with metal ions, and is almost inert towards Ni(II), compared to the enol form.[16] Thus, the pathway involving the reaction of the keto form with metal ion can be ignored and the terms containing rate constants associated with this pathway, namely k_{HK} and k_{-HK}, can be neglected in the expressions for λ_2 and λ_3. When these simplifications are incorporated in equations 7.24 and 7.25, equations 7.26 and 7.27 are obtained, respectively.

$$\lambda_2 = k_e + k_k + k_{HE}[M^{n+}] + k_{-HE}[H^+] - \left[\frac{k_e k_{HE}[M^{n+}] + (k_e + k_k)k_{-HE}[H^+]}{k_e + k_k + k_{HE}[M^{n+}] + k_{-HE}[H^+]}\right] \quad (7.26)$$

$$\lambda_3 = \left[\frac{k_e k_{HE}[M^{n+}] + (k_e + k_k)k_{-HE}[H^+]}{k_e + k_k + k_{HE}[M^{n+}] + k_{-HE}[H^+]}\right] \quad (7.27)$$

The general solution for Scheme 7.2 shows that: i) under pseudo-first-order conditions, this system is biphasic in nature, irrespective of the overall direction of the reaction (complex formation or complex dissociation), and ii) the observed rate constants for a reaction following this mechanism are given by λ_2 and λ_3 as shown above. Since p, b, λ_2 and λ_3 are positive quantities, it is clear from equations 7.20 and 7.21 that the value for λ_2 is always greater than that of λ_3. Consequently, equations 7.26 and 7.27 represent the faster and slower processes, respectively. In this dissertation, the observed rate constants λ_2 and λ_3 are represented by the terms $k_{obs(f)}$ and $k_{obs(s)}$, respectively. Although the general solution of Scheme 7.2 implies a biphasic nature for this system, it is not uncommon to observe only one process due to the negligible contribution of the other.[17,18]

ii) Analysis of the kinetic data for the dissociation of NiI and Ni(DMHD)$^+$ complexes

The dissociation of both NiI and Ni(DMDH)$^+$ complexes was studied as a function of [H^+] and [Ni^{2+}]. These reactions occurred as single, first-order processes. The values of k_{obs} were obtained by fitting the absorbance-time data to equation 7.5. The data are summarized in Tables 7.7 and 7.8 for NiI and Ni(DMHD)$^+$, respectively. It can be seen that changing the Ni(II) concentration has very little effect on the value of k_{obs}. The plots of k_{obs} versus [H^+] were linear. These plots are shown in Figures 7.13 and 7.15 (for clarity only the data at the lowest and highest [Ni^{2+}] are plotted).

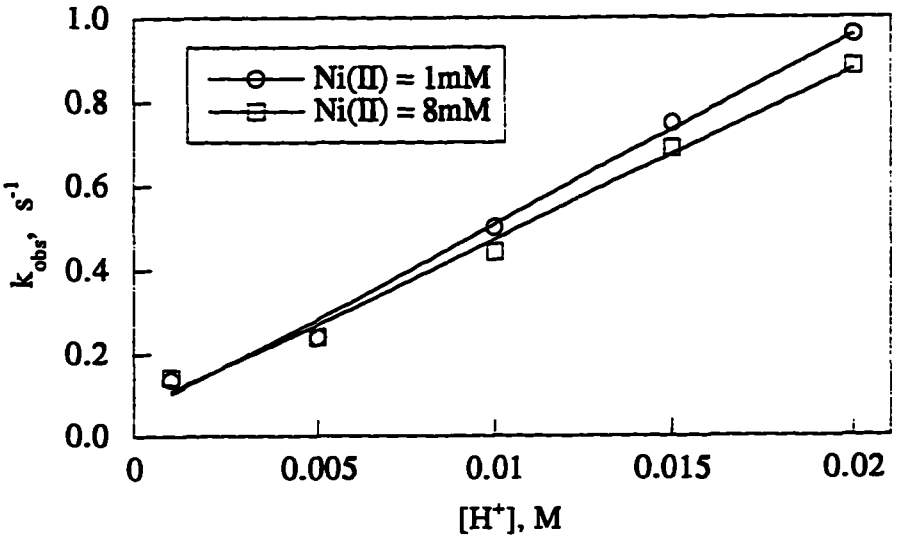

Figure 7.13. The effect of [H^+] and [Ni^{2+}] on k_{obs} for the dissociation of NiI.

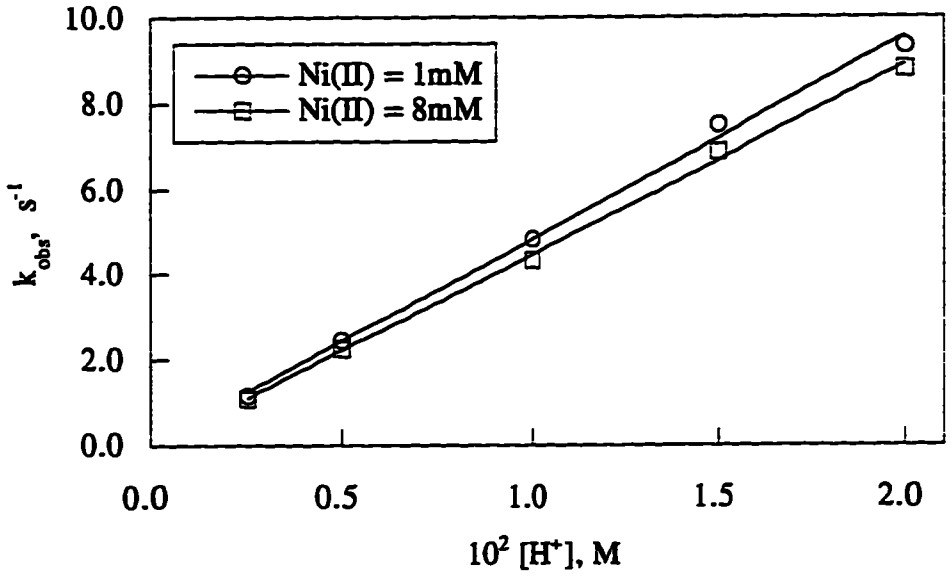

Figure 7.14. The effect of $[H^+]$ and $[Ni^{2+}]$ on k_{obs} for the dissociation of $Ni(DMHD)^+$.

The data for the dissociation reactions were found to be consistent with the expression for λ_2 (equation 7.26) representing the faster process for Scheme 7.2. The expression for this root may be written by replacing λ_2 and M^{n+} with $k_{obs(f)}$ and $[Ni^{2+}]$, respectively, to yield,

$$k_{obs(f)} = k_e + k_k + k_{HE}[Ni^{2+}] + k_{-HE}[H^+] - \left[\frac{k_e k_{HE}[Ni^{2+}] + (k_e + k_k)k_{-HE}[H^+]}{k_e + k_k + k_{HE}[Ni^{2+}] + k_{-HE}[H^+]}\right] \quad (7.28)$$

Expansion of equation 7.28 by taking a common denominator over the entire right hand side gives,

$$k_{obs(f)} = \frac{\begin{array}{c}(k_e + k_k)^2 + 2(k_e + k_k)k_{HE}[Ni^{2+}] + 2(k_e + k_k) \\ k_{-HE}[H^+] + (k_{HE}[Ni^{2+}])^2 + 2k_{HE}k_{-HE}[Ni^{2+}][H^+] + \\ (k_{-HE}[H^+])^2 - k_e k_{HE}[Ni^{2+}] - (k_e + k_k)k_{-HE}[H^+]\end{array}}{(k_e + k_k) + k_{HE}[Ni^{2+}] + k_{-HE}[H^+]} \qquad (7.28)$$

The value of the equilibrium constant for the enolic pathway ($K_E = k_{HE}/k_{-HE}$) for DMHD and ionomycin is ~ 10^{-3} (see Table 7.9); therefore, the condition $k_{HE} >> k_{-HE}$ is valid. Also, the values of $(k_e + k_f)$ for DMHD and ionomycin are very small ($\sim 10^{-3}$ s^{-1}). Therefore, the terms in k_{HE} and $(k_e + k_f)$ may be neglected in the equation 7.28 yielding equation 7.29.

$$k_{obs(f)} = \frac{(k_e + k_k)k_{-HE}[H^+] + 2k_{HE}k_{-HE}[Ni^{2+}][H^+] + (k_{-HE}[H^+])^2}{k_{-HE}[H^+]} \qquad (7.29)$$

Cancelling $k_{-HE}[H^+]$ from the numerator and the denominator of the right hand side, neglecting the term $(k_e + k_f)$, and dividing both sides of equation 7.29 by $[Ni^{2+}]$, gives equation 7.30.

$$\frac{k_{obs(f)}}{[Ni^{2+}]} = k_{-HE}\frac{[H^+]}{[Ni^{2+}]} + 2k_{HE} \qquad (7.30)$$

For both ionomycin and DMHD, the data fits equation 7.30. The plots of $k_{obs}/[Ni^{2+}]$ versus $[H^+]/[Ni^{2+}]$ were linear. These plots for ionomycin and DMHD are shown in Figures 7.15 and 7.16. The slopes gave k_{-HE} values of 49.0 ± 0.6 M^{-1} s^{-1} and 480 ± 7 M^{-1} s^{-1} for NiI and $Ni(DMHD)^+$, respectively. The values of the intercepts ($2k_{HE}$) are not considered due to large errors associated with them (-22 ± 65 and 3 ± 4 for DMHD and ionomycin, respectively). Therefore, these values were not used to calculate the values of k_{HE}. However, the values of k_{HE} were calculated using a procedure described in the next section.

Table 7.7. Observed Rate constants for the Dissociation Reactions[a] of NiI in 80% Methanol-Water at $I = 0.050$ M (TEAP)

10^3 [Ni^{2+}][b] (M)	10^3 [H^+][b] (M)	k_{obs} (s^{-1})	n	[H^+]/[Ni^{2+}]	10^{-1} k_{obs}/[Ni^{2+}] ($M^{-1}s^{-1}$)
1.0	2.5	0.138 ± 0.005	5	2.50	13.8
1.0	5.0	0.239 ± 0.007	3	5.00	23.9
1.0	10.0	0.501 ± 0.004	3	10.0	50.1
1.0	15.0	0.75 ± 0.02	5	15.0	74.9
1.0	20.0	0.96 ± 0.01	3	20.0	95.9
2.5	2.5	0.151 ± 0.006	4	1.00	6.02
2.5	5.0	0.248 ± 0.007	4	2.00	9.93
2.5	10.0	0.50 ± 0.01	5	4.00	20.2
2.5	15.0	0.772 ± 0.005	4	6.00	30.9
2.5	20.0	1.08 ± 0.02	6	8.00	43.1
5.0	2.5	0.158 ± 0.001	3	0.50	3.15
5.0	5.0	0.226 ± 0.006	5	1.00	4.53
5.0	10.0	0.50 ± 0.01	5	2.00	10.1
5.0	15.0	0.75 ± 0.03	7	3.00	15.0
5.0	20.0	0.92 ± 0.04	5	4.00	18.4
8.0	2.5	0.143 ± 0.004	4	0.30	1.79
8.0	5.0	0.24 ± 0.01	4	0.62	3.01
8.0	10.0	0.44 ± 0.01	4	1.25	5.54
8.0	15.0	0.69 ± 0.01	7	1.88	8.61
8.0	20.0	0.88 ± 0.01	6	2.50	11.0

[a]Dissociation was initiated with $HClO_4$; $[H_2I]_{tot} = 5.0$ μM after mixing; $\lambda = 310$ nm.
[b]Concentrations after mixing.

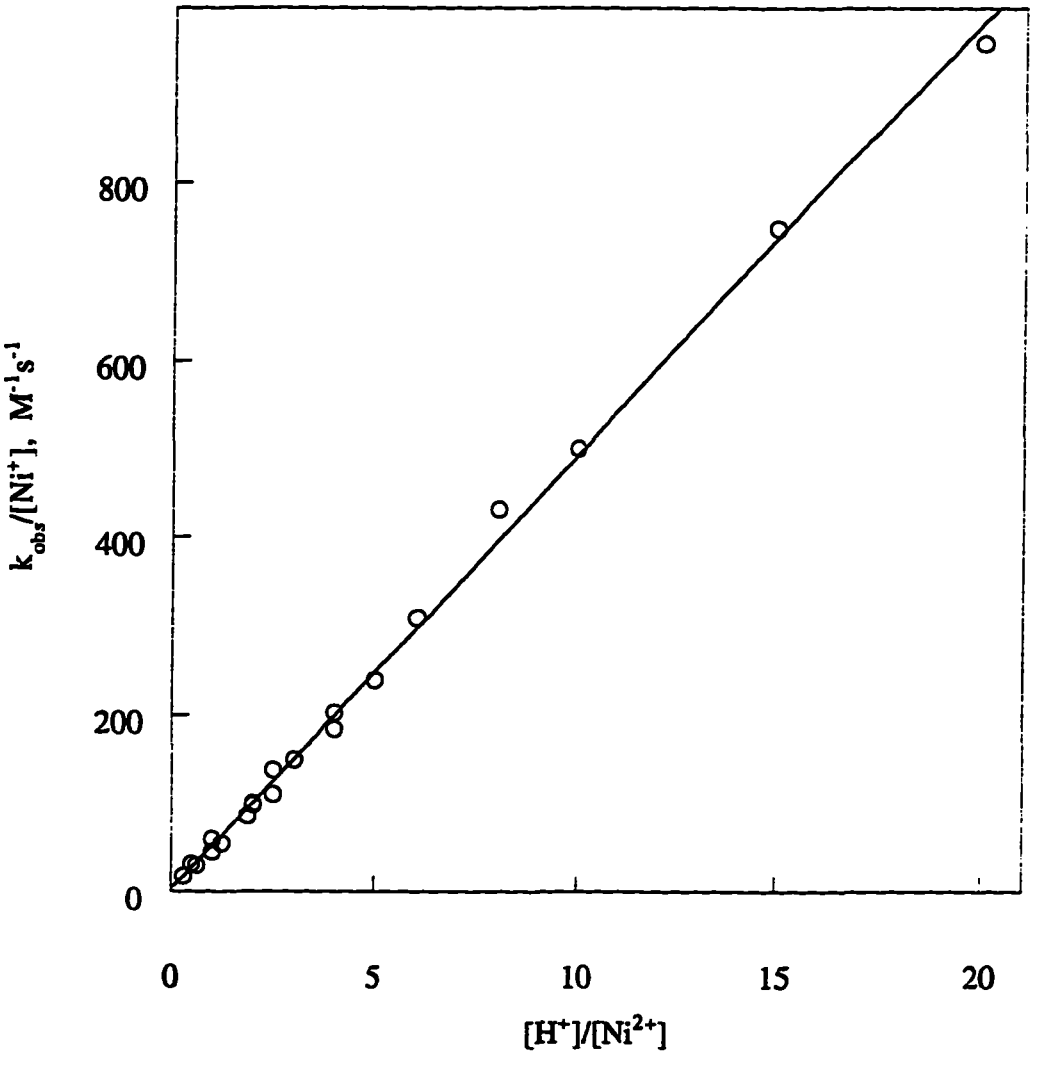

Figure 7.15 Plot of equation 7.30 for the data obtained from the dissociation of NiL.

Table 7.8. Observed Rate Constants for the Dissociation Reactions[a] of $Ni(DMHD)^+$ in 80% Methanol-Water at $I = 0.050$ M (TEAP)

10^3 $[Ni^{2+}]^b$ (M)	10^3 $[H^+]^b$ (M)	k_{obs} (s^{-1})	n	$[H^+]/[Ni^{2+}]$	10^{-2} $k_{obs}/[Ni^{2+}]$ (M^{-1}s^{-1})
1.0	2.5	1.15 ± 0.04	7	2.50	11.5
1.0	5.0	2.42 ± 0.02	6	5.00	24.2
1.0	10.0	4.82 ± 0.04	7	10.0	48.2
1.0	15.0	7.51 ± 0.10	6	15.0	75.1
1.0	20.0	9.32 ± 0.08	11	20.0	93.2
8.0	2.5	1.09 ± 0.02	9	0.31	1.36
8.0	5.0	2.25 ± 0.01	9	0.62	2.81
8.0	10.0	4.32 ± 0.06	9	1.25	5.40
8.0	15.0	6.87 ± 0.04	9	1.88	8.59
8.0	20.0	8.80 ± 0.04	7	2.50	11.0

[a]Dissociation was initiated with $HClO_4$; [DMHD] = 15.8 μM, after mixing; λ = 307 nm.
[b]Concentrations after mixing.

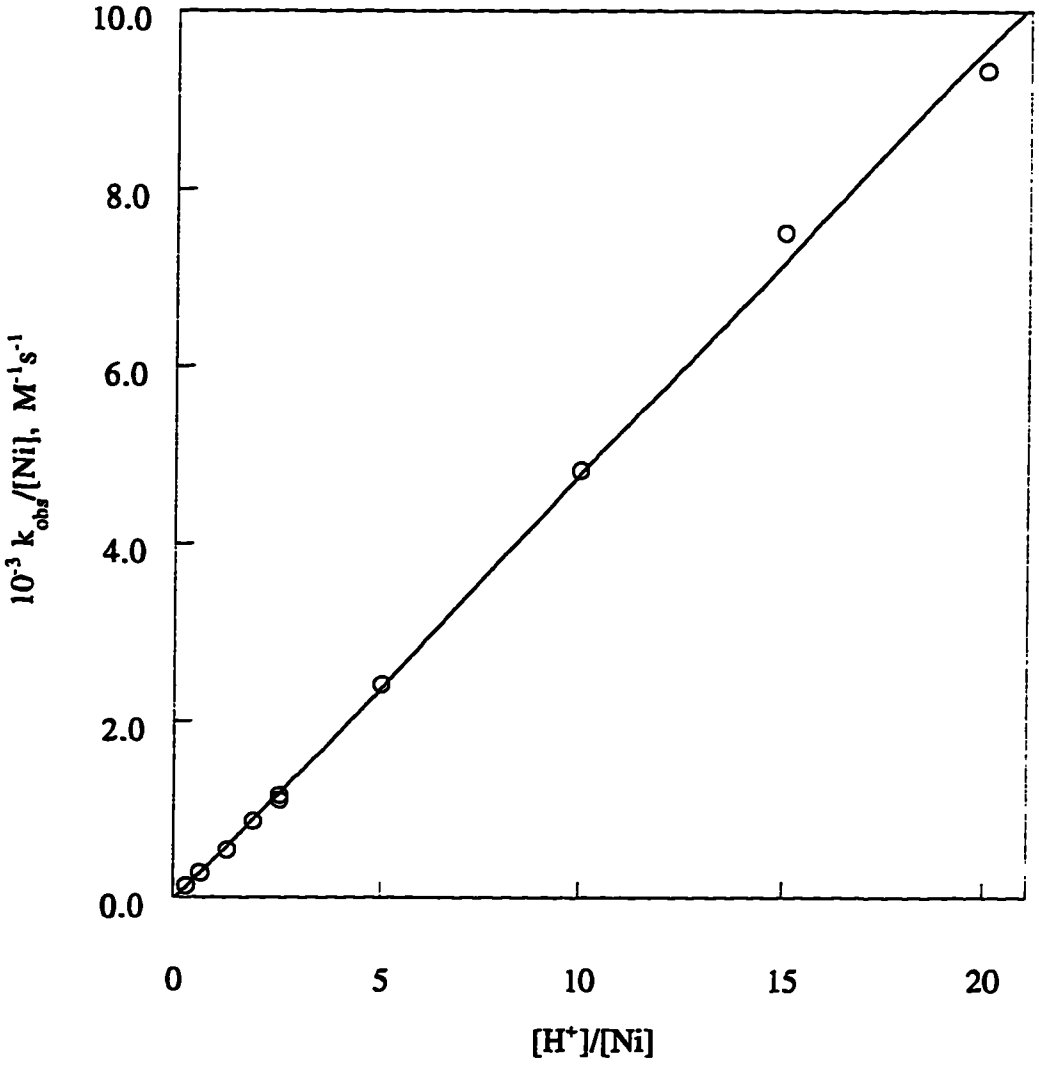

Figure 7.16 Plot showing the validity of equation 7.30 for the data obtained from the dissociation of Ni(DMHD)$^{+}$.

iii) Calculation of k_{HE}

The values for k_{HE} can be calculated using the values of the equilibrium constant for the enolic pathway, K_E, that is defined by equation 7.31.

$$K_E = \frac{k_{HE}}{k_{-HE}} \tag{7.31}$$

If the enolic pathway is shown by equation 7.32, then K_E is expressed by equation 7.33. Similarly, if the ketonic pathway is shown by equation 7.34, then the equilibrium constant for the ketonic pathway, K_K, can be defined by equation 7.35.

$$HE + Ni^{2+} \rightleftharpoons NiL^{+} + H^{+} \tag{7.32}$$

$$K_E = \frac{[NiL^{+}][H^{+}]}{[Ni^{2+}][HE]} \tag{7.33}$$

$$HK + Ni^{2+} \rightleftharpoons NiL^{+} + H^{+} \tag{7.34}$$

$$K_K = \frac{[NiL^{+}][H^{+}]}{[Ni^{2+}][HK]} \tag{7.35}$$

To calculate the value of K_E (or K_K), a relationship may be established between $K_{e/k}$, K_E and K_T. The equilibrium constant K_T, for the reaction of the total ligand (HL) with Ni(II) shown by equation 7.36, is defined by equation 7.37. The equilibrium constant for the keto-enol interconversion, $K_{e/k}$, is defined by equation 7.38.

$$HL + Ni^{2+} \rightleftharpoons NiL^{+} + H^{+} \tag{7.36}$$

$$K_T = \frac{[NiL^+][H^+]}{[Ni^{2+}][HL]} = \frac{K_{NiL}}{K_H^c} \tag{7.37}$$

$$K_{e/k} = \frac{[HE]}{[HK]} = \frac{K_K}{K_E} \tag{7.38}$$

The value for K_H^c can be obtained from the mixed-mode value of K_H listed in Table 7.6. using the relationship described by equation 7.39 for the *i*th ionizable proton. γ_{H^+} is the activity coefficient described by equation 6.6 in Chapter VI and its value is calculated to be 0.651 for this system (I = 0.050 M, T = 25 °C, solvent = 80% methanol-water).

$$K_{Hi}^c = \gamma_{H^+} K_{Hi} \tag{7.39}$$

The experimentally accessible values of K_T and $K_{e/k}$ may be used to calculate K_E and K_K as described below.

If the total ligand concentration, [HL], is given by equation 7.40,

$$[HL] = [HK] + [HE] \tag{7.40}$$

then using equations 7.37 and 7.38, the relationship between K_T, K_E and K_K can be derived.

$$\frac{1}{K_T} = \frac{1}{K_K} + \frac{1}{K_E} \tag{7.41}$$

Furthermore, using equations 7.38 and 7.41, the following relationships can be derived.

$$K_E = \left(\frac{1}{K_{e/k}} + 1\right) K_T \qquad (7.42)$$

$$K_K = (K_{e/k} + 1)\, K_T \qquad (7.43)$$

Using known values of K_H^c, K_{NiL} and $K_{e/k}$, the values of K_T and K_E for DMHD were calculated to be 2.9 x 10^{-3}, and 3.9 x10^{-3}, respectively. Using equation 7.31, the value of k_{HE} for the reaction of DMHD with Ni(II) was calculated to be 1.9 $M^{-1}s^{-1}$.

In order to obtain the value of k_{HE} for the formation of NiI complex, the species distribution diagram shown in Figure 7.11 needs to be considered first. This diagram shows, that at pH* = 6.0, which is the initial pH of the NiI solution in the dissociation reactions, a significant fraction of the complex exists in the protonated form ($NiHI^+$). Observation of only a single, first-order process for the dissociation reaction suggests that the step involving the protonation of the NiI complex is fast and the removal of the metal ion may be the rate-determining step. The dissociation process may be summarized as shown in Scheme 7.3.

Scheme 7.3

$$NiI + H^+ \overset{\text{(fast)}}{\rightleftharpoons} NiHI^+$$

$$NiHI^+ + H^+ \rightleftharpoons Ni^{2+} + H_2I$$

The equilibrium constant (K_T) for the formation of $NiHI^+$ is defined by equation 7.44. Its value (using the information in Table 7.6) was calculated to be 4.5 x 10^{-3}. The values

of K^c_{H1} and K^c_{H2} were obtained from their corresponding mixed-mode values using the relationship described by equation 7.39.

$$K_T = \frac{[NiHI^+][H^+]}{[Ni^{2+}][H_2I]} = \frac{K_{NiL} K_{NiHL}}{K^c_{H1} K^c_{H2}} \qquad (7.44)$$

Using this value of K_T and the value of $K_{e/k}$ for ionomycin, K_E was calculated to be 5.1 x 10^{-3}. Finally, using equation 7.31 the value of k_{HE} for the reaction of ionomycin with Ni(II) was calculated to be 0.25 s^{-1} M^{-1}. Table 7.9 summarizes the values of the equilibrium and rate constants for the Ni(II)-I and Ni(II)-DMHD systems.

Table 7.9. Keto-Enol Equilibrium Constants, Complexation Constants, and Rate Constants for Ni(II)-Ionomycin and Ni(II)-DMHD Systems in 80% Methanol-Water Solutions at 25.0 °C and I = 0.050 M (TEAP)

	ionomycin	DMHD
$K_{e/k}$[a]	7.33	2.95
K_T	4.47 x 10^{-3}	1.93 x 10^{-3}
K_E	5.10 x 10^{-3}	3.92 x 10^{-3}
K_K	3.72 x 10^{-2}	1.16 x 10^{-2}
k_{-HE}, M^{-1} s^{-1}	49.0	4.8 x 10^2
k_{HE}, M^{-1} s^{-1}	0.25	1.9

[a]Values used are from NMR experiments since these are subject to least error compared to values obtained from pH-jump or rapid-dilution experiments.

iii) Formation and dissociation kinetics of the $Ni(DMDH)^+$ complex at $I = 0.50$ M

The reactions for the formation and dissociation of the $Ni(DMDH)^+$ complex were also studied at an ionic strength of $I = 0.50$ M maintained with $NaClO_4$. These conditions were employed to facilitate comparison of our results with kinetic studies of other β-diketones. The formation and dissociation data are shown in Table 7.10. The data are consistent with the model described by equation 7.30. The plot of $k_{obs}/[Ni^{2+}]$ versus $[H^+]/[Ni^{2+}]$, shown in Figure 7.18, gives a straight line with the value of the slope (k_{-HE}) equal to $1119 \pm 7\ M^{-1}s^{-1}$. This value is approximately two times larger than the value of k_{-HE} obtained at $I = 0.050$ M. In order to calculate the value of k_{HE}, the value of K_E was corrected for ionic strength using the activity coefficients calculated from Pitzer's equation.[19,20] The corrected value of K_E at $I = 0.50$ M is 2.1×10^{-3}. The value of k_{HE} was determined to be $2.3\ M^{-1}s^{-1}$ using equation 7.31.

Table 7.10. Observed Rate Constants for the Reaction of Ni^{2+} with DMHD in 80% Methanol-Water at $I = 0.50$ M ($NaClO_4$)[a]

10^3 [Ni^{2+}][b] (M)	10^3 [H^+][b] (M)	k_{obs}[c] (s^{-1})	n	[H^+]/[Ni^{2+}]	10^{-3} k_{obs}/[Ni^{2+}] ($M^{-1}s^{-1}$)
Data for Complex Formation[d]: Ni^{2+} + DMHD ⇌ $Ni(DMHD)^+$ + H^+					
10.0	0.25	0.32 ± 0.08	4	0.025	0.032
20.0	0.25	0.34 ± 0.02	24	0.012	0.017
25.0	0.25	0.36 ± 0.01	13	0.010	0.014
30.0	0.25	0.38 ± 0.01	17	0.008	0.013
35.0	0.25	0.39 ± 0.01	11	0.007	0.011
40.0	0.25	0.40 ± 0.01	14	0.006	0.010
45.0	0.25	0.42 ± 0.02	15	0.005	0.009
Data for Complex Dissociation[e]: $Ni(DMHD)^+$ + H^+ ⇌ Ni^{2+} + DMHD					
2.5	2.5	3.4 ± 0.2	9	1.0	1.344
5.0	2.5	5.5 ± 0.2	9	2.0	2.200
10.0	2.5	10.6 ± 0.4	9	4.0	4.240
15.0	2.5	17.1 ± 0.6	8	6.0	6.836
20.0	2.5	22.6 ± 0.5	9	8.0	9.044
2.5	5.0	3.6 ± 0.2	7	0.5	0.730
5.0	5.0	5.7 ± 0.1	7	1.0	1.142
10.0	5.0	10.2 ± 0.2	7	2.0	2.030
15.0	5.0	16.4 ± 0.2	9	3.0	3.286
20.0	5.0	22.1 ± 0.4	9	4.0	4.413
25.0	5.0	27.5 ± 0.7	9	5.0	5.492
2.5	10.0	3.2 ± 0.1	12	0.3	0.316
5.0	10.0	5.8 ± 0.2	9	0.5	0.578
10.0	10.0	11.3 ± 0.3	8	1.0	1.134
15.0	10.0	17.6 ± 0.3	8	1.5	1.762
20.0	10.0	23.7 ± 0.3	11	2.0	2.366
25.0	10.0	27.9 ± 0.6	9	2.5	2.791
2.5	20.0	3.4 ± 0.1	9	0.1	1.170

Table 7.10 continued...

10^3 [Ni^{2+}]^b (M)	10^3 [H^+]^b (M)	k_{obs}^{c} (s^{-1})	n	[H^+]/[Ni^{2+}]	10^{-3} k_{obs}/[Ni^{2+}]
5.0	20.0	5.3 ± 0.2	8	0.3	0.265
15.0	20.0	14.9 ± 0.3	7	0.8	0.743
25.0	20.0	25.8 ± 0.7	9	1.3	1.291
2.5	45.0	3.4 ± 0.1	8	0.1	0.077
5.0	45.0	6.0 ± 0.1	9	0.1	0.134
10.0	45.0	10.4 ± 0.2	9	0.2	0.233
15.0	45.0	16.4 ± 0.4	9	0.3	0.365
20.0	45.0	22.8 ± 0.6	7	0.4	0.508
25.0	45.0	28.3 ± 0.6	6	0.6	0.628

$^a\lambda$ = 307 nm. ^{b}Concentrations after mixing. ^{c}Values of k_{obs} given as mean ± 1 S.D. for n replicates. ^{d}[DMHD] = 25 μM after mixing. ^{e}Dissociation was initiated with $HClO_4$; [DMHD] = 11.5 μM after mixing.

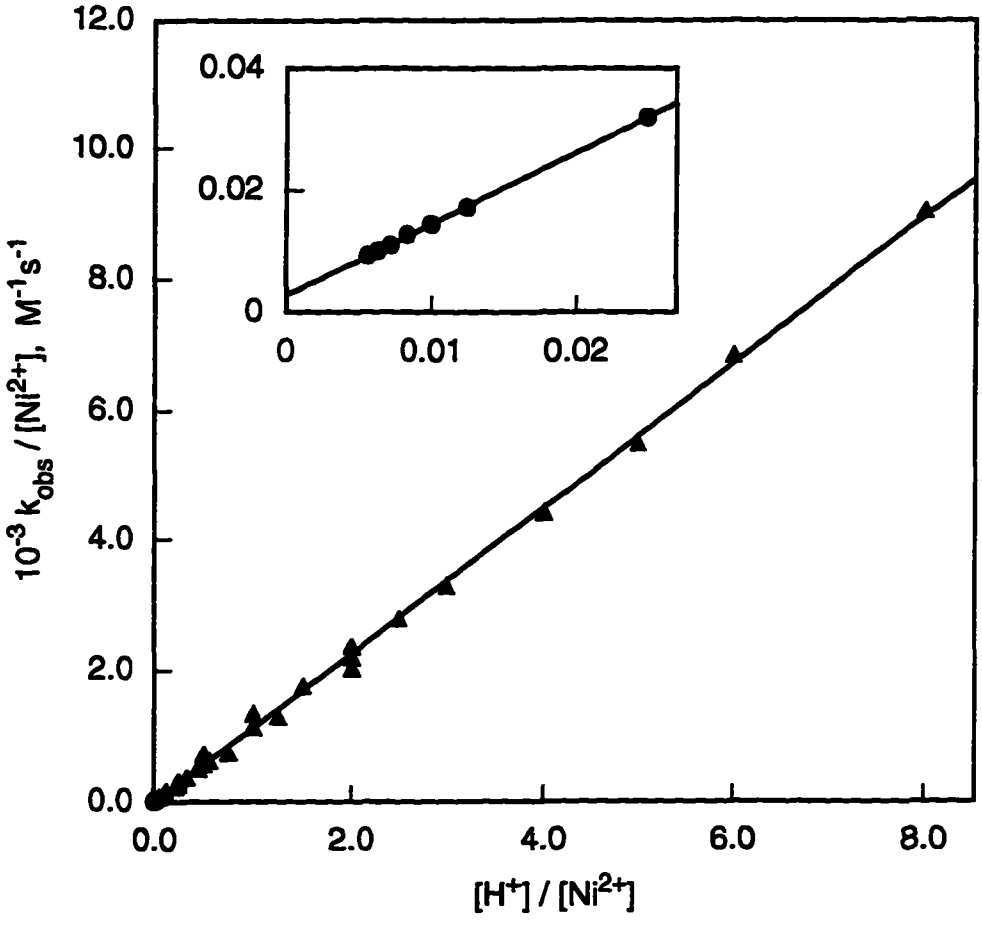

Figure 7.17 Plot showing the validity of equation 7.30 derived for the reaction of the enol form of DMHD with Ni(II) at I = 0.50 M ($NaClO_4$). The inset shows the formation data which lie in the region very close to the intercept.

iv) Kinetics of the of NiI complex

The reactions of the formation of NiI complex were performed in the pH* range 3.50 to 3.92. The species distribution diagram (Figure 7.12) shows that under the experimental conditions employed in these reactions, only a small fraction of the ligand reacted with the metal ion. Therefore, the absorbance changes in these reactions were very small. To obtain meaningful rate constants from the absorbance versus time curves, the absorbance-time data from several runs were averaged. Signal averaging increased the signal to noise ratio significantly and facilitated analysis of the data. The kinetic data for the formation reactions of the NiI complex were biphasic in nature. This behavior is predicted by the mathematical solution of Scheme 7.2. Figure 7.18 shows a plot of signal-averaged absorbance-time data for the formation of NiI. The noise level associated with this curve is relatively low, considering the small magnitude of the absorbance change (only 0.06 AU). The data were fit to a double exponential expression shown by equation 7.45, where A_i is the absorbance at any time t, A_∞ the absorbance at t = 8 half-lives, A_{01} and A_{02} are the initial and the final absorbance values of the fast processes, respectively, $k_{obs(f)}$ and $k_{obs(s)}$ are the observed rate constants for the fast and the slow processes, respectively, and $(A_{02} - A_{01})$ and $(A_\infty - A_{02})$ are the amplitudes of the absorbance changes for the fast and the slow processes, respectively. The absorbance changes for the fast and slow process may be represented as ΔA_f and ΔA_s, respectively.

$$[A_\infty - A_i] = [(A_{02} - A_{01}) \exp(-k_{obs(f)}t)] + [(A_\infty - A_{02}) \exp(-k_{obs(s)}t)] \quad (7.45)$$

The kinetic data for the formation of NiI complex are summarized in Table 7.11. The observed rate constants for the fast process showed linear dependence on the $[Ni^{2+}]$ and no dependence on $[H^+]$. Due to the very small absorbance change in these reactions, rate constants obtained for the slow process had large errors associated with them and

thus were not considered.

It can be seen from Table 7.11, that the values of ΔA_f decrease with increasing pH and the opposite trend is observed for ΔA_s. Extrapolation of the ΔA_f versus $[H^+]$ trend indicates that below pH 3.2, only the fast process will be seen. This conclusion is consistent with the kinetic data for the dissociation of NiI, obtained at pH* values less than 2.5, where only the fast process was observed.

Table 7.11. Observed Rate Constants for the Formation Reactions of NiI in 80% Methanol-Water at $I = 0.050$ M (TEAP)[a]

-log $[H^+]$	10^3 $[Ni^{2+}]$	$k_{obs(f)}$ (s^{-1})	n	$k_{obs(s)}$ (s^{-1})	ΔA_f (%)	ΔA_s (%)
3.35	8.0	0.130 ± 0.009	8	0.017 ± 0.009	79.4	20.6
3.56	8.0	0.110 ± 0.006	10	0.014 ± 0.003	70.2	29.7
3.62	8.0	0.123 ± 0.006	10	0.011 ± 0.005	63.0	37.0
3.95	8.0	0.136 ± 0.007	8	0.017 ± 0.001	47.2	52.8
3.56	4.0	0.055 ± 0.002	6			
3.56	5.0	0.066 ± 0.002	8			
3.56	6.0	0.073 ± 0.001	7			
3.56	8.0	0.110 ± 0.006	10			
3.62	4.0	0.069 ± 0.002	9			
3.62	6.0	0.093 ± 0.002	9			
3.62	8.0	0.123 ± 0.006	10			

[a] $[H_2I] = 10.0$ μM, $\lambda = 310$ nm. For cases where both fast and slow processes were observed, the rate constants were obtained by fitting absorbance-time data to equation 7.45. In the cases where the absorbance change for the slow process was very small, the rate constants for only the fast process were obtained by fitting the initial portion of the absorbance-time data to equation 7.5.

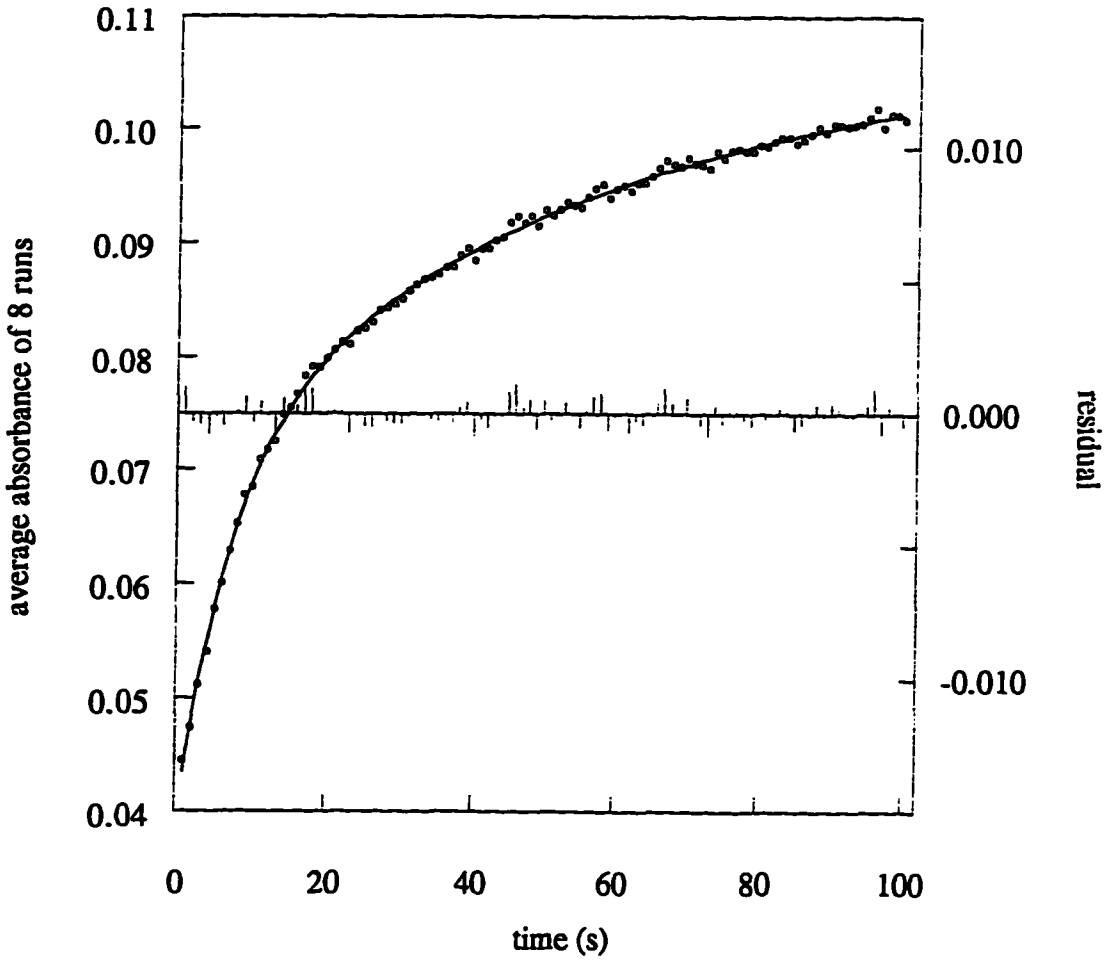

Figure 7.18. Averaged absorbance versus time data for formation of the NiI complex at pH* = 3.95, I = 0.050 (TEAP). The absorbance, A_i, versus time data fit the expression for two, single first-order reactions (equation 7.45). The solid line represents the theoretical fit. The values for $k_{obs(f)}$ and $k_{obs(s)}$ are $(1.4 \pm 0.1) \times 10^{-1}$ and $(1.7 \pm 0.1) \times 10^{-2}$ s^{-1}, respectively.

E. Kinetics of the Reactions of Mg(II) with Ionomycin and with DMHD in Buffered Solutions

The complexation of ionomycin and DMHD with Mg(II) results in a band shift from 280 to 310 nm. The kinetics of formation and dissociation of the complex was observed at 305 nm where the ratio of the absorbance change to the background absorbance is optimal. The ionic strength in all these reaction was maintained at 0.050 M using TEAP. The reactions were carried out in the pH* range of 5.00 to 8.40 where the use of buffers is required to maintain constant $[H^+]$ during the course of the reaction. In order to estimate the buffering ranges of different buffers, their protonation constants (K_H) were determined in 80% methanol-water and $I = 0.050$.

i) Determination of the protonation constants (K_H) for the buffers

The values for K_H for all buffers used in these reactions were determined potentiometrically. The log K_H values are summarized in Table 7.12. In order to evaluate the degree of interaction between Mg(II) and the buffers, potentiometric titrations of buffer solutions were performed in the absence and presence of Mg(II). An example of the titration curves obtained for EPPS buffer is shown in Figure 7.9. How closely the two curves obtained for each buffer coincided was indicative of the degree of complexation of the metal ion by the buffer. The complex formation reaction is described by equation 7.46, where $[Mg^{2+}]$, $[B^-]$ and $[MgB^+]$ represent the concentrations of the magnesium ion, the anionic form of the buffer and the buffer-metal complex, respectively, and K_{MB} represents the metal-buffer binding constant. The estimates of the binding constants were obtained from equation 7.47, where, K_H and K_H' are the protonation constants of the buffer calculated from the titration curves obtained in the absence and presence of metal ion, respectively.

$$Mg^{2+} + B^{-} \rightleftharpoons MgB^{+} \qquad K_{MB} = \frac{[MgB^{+}]}{[Mg^{2+}]\,[B^{-}]} \tag{7.46}$$

$$K_{MB} = \frac{(K_H/K_H^{'}) - 1}{[Mg^{2+}]} \tag{7.47}$$

In the pH* range from 5.0 to 9.5 the titration curve for each buffer coincided with the corresponding curve obtained in the presence of Mg(II). The value of K_{MB} was calculated to be less than 15 for all the buffers studied. These values indicate that the complexation between the buffer and Mg(II) is not significant (e.g., $[MgB^{+}] \leq 13\%$, when the buffer concentration is 10 mM).

Table 7.12. Mixed-Mode log K_H Values for Different Buffers in 80% Methanol-Water at $I = 0.050$ M (TEAP)

Buffer	log K_H	n
MES	6.00 ± 0.03[a]	2
HEPES	7.21 ± 0.03[b]	4
EPPS	7.65 ± 0.06[b]	3
CHES	8.86	1
TEEDA[c]	4.9 ± 0.1[a]	2
TEPDA[c]	6.95	1

[a]Values represent mean ± average deviation. [b]Values represent the mean ± 1 S.D.
[c]The reported value is the constant for the second protonation step
($BH^{+} + H^{+} \rightleftharpoons BH_2^{2+}$).

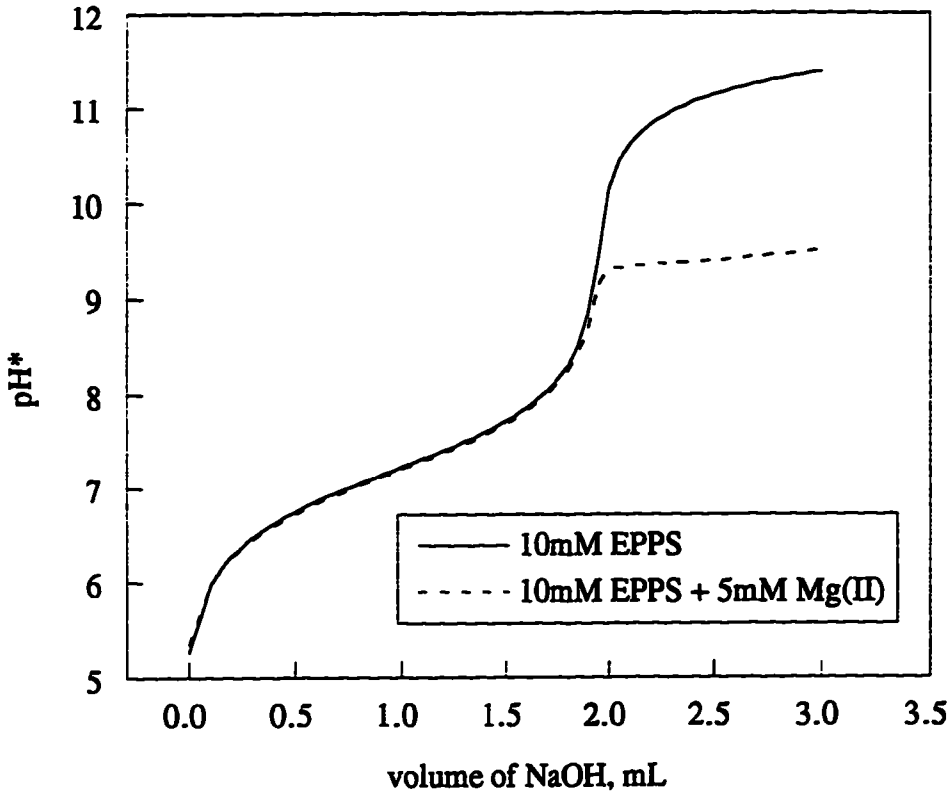

Figure 7.19. Potentiometric titration of EPPS in the absence and presence of Mg(II).

ii) Formation of the MgI complex

Kinetic studies of the formation reactions of Mg(II) with ionomycin were carried out in buffered solutions using at least a ten-fold excess of Mg(II) with respect to the ligand concentration. The reactions were performed using three different buffers, HEPES, EPPS and CHES, and were studied as a function of pH* and buffer concentration. In the pH* range 7.20 to 8.40 a single, first-order process was observed in each case. The values for k_{obs} were determined from the linear least-squares fits of the

absorbance-time data to the expression for the first-order process (equation 7.5). The values of k_{obs} as a function of the total buffer concentration are summarized in Tables 7.13, 7.14 and 7.15 for HEPES, EPPS and CHES, respectively. Plots of k_{obs} versus total buffer concentration for these buffers are shown in Figures 7.20 to 7.22. Saturation type behavior is seen in these plots which is consistent with the mathematical expression shown by equation 7.48, where p_1, p_2 and p_3 are the parameters.

$$k_{obs} = \frac{p_1 + p_2 [x]}{1 + p_3 [x]} \tag{7.48}$$

Behavior consistent with equation 7.48 is also observed when k_{obs} is plotted against the concentration of the conjugate base form of the buffers. The plots of k_{obs} versus the concentration of the conjugate base form of buffer as a function of pH* for EPPS and HEPES are shown in Figures 7.23 and 7.24, respectively. By interpolation and extrapolation of the data in these plots the values of k_{obs} are calculated at total buffer concentrations of 0.005, 0.01, and 0.02 M at each pH*. Plots of these calculated values of k_{obs} against $[OH^-]$ are linear (see Figures 7.25 and 7.26). This behavior is indicative of specific base catalysis.

When the values of k_{obs} obtained at pH* = 8.00 for the three buffers are plotted against the product of the protonation constant and concentration of the base form of the buffer ($K_H[buffer]_B$), a single curve is obtained as shown in Figure 7.27. This behavior is indicative of general-base catalysis by the buffers.

Table 7.13. Observed Rate Constants for the Formation Reaction of the MgI Complex as a Function of $[HEPES]_{tot}$, in 80% Methanol-Water at $I = 0.050$ M (TEAP)[a]

pH*	10^3 $[HEPES]_{tot}$, (M)[b]	k_{obs} (s^{-1})	n
7.20	5.0	16.6 ± 0.5	9
7.20	10.0	18.3 ± 0.6	10
7.20	20.0	19.6 ± 0.5	10
7.60	1.0	13.3 ± 0.3	10
7.60	3.0	15.7 ± 0.2	9
7.60	5.0	17.7 ± 0.3	9
7.60	10.0	18.8 ± 0.2	9
7.60	20.0	20.1 ± 0.3	11
8.00	1.0	15.0 ± 0.3	9
8.00	3.0	20.2 ± 0.3	10
8.00	5.0	22.7 ± 0.4	10
8.00	10.0	25.0 ± 0.4	10
8.00	20.0	28.2 ± 0.5	10
8.40	1.0	22.4 ± 0.3	9
8.40	3.0	27.8 ± 0.3	10
8.40	5.0	32.7 ± 0.7	9
8.40	10.0	38.7 ± 0.9	11
8.40	20.0	43.7 ± 0.9	9

[a][Mg(II)] = 4.0 mM, [ionomycin] = 10.0 μM after mixing, λ = 310 nm.
[b]Concentrations after mixing.

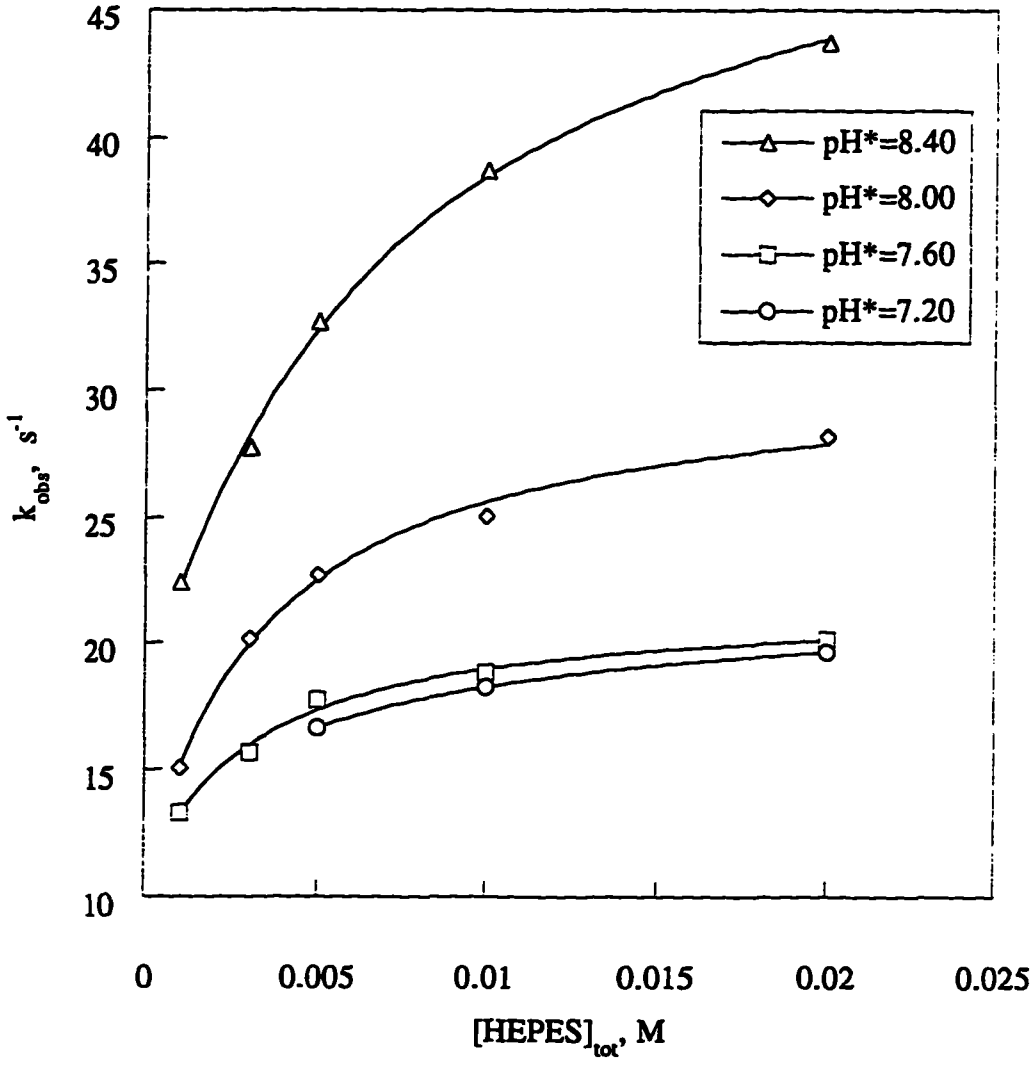

Figure 7.20 Plots of k_{obs} versus $[HEPES]_{tot}$ for the formation reaction of the MgI complex. The error bars represent the mean ± 1 S.D.

Table 7.14. Observed Rate Constants for the Formation Reaction of the MgI Complex as a Function of $[EPPS]_{tot}$, in 80% Methanol-Water at $I = 0.050$ M (TEAP)[a]

pH*	10^3 $[EPPS]_{tot}$, (M)[b]	k_{obs} (s^{-1})	n
7.20	1.0	14.1 ± 0.2	7
7.20	3.0	16.1 ± 0.2	10
7.20	5.0	16.5 ± 0.3	10
7.20	10.0	18.2 ± 0.2	9
7.20	20.0	19.0 ± 0.3	11
7.60	1.0	15.0 ± 0.1	9
7.60	3.0	16.6 ± 0.1	9
7.60	5.0	18.5 ± 0.2	9
7.60	10.0	20.2 ± 0.2	9
7.60	20.0	21.9 ± 0.3	10
8.00	1.0	17.2 ± 0.2	9
8.00	3.0	22.9 ± 0.2	10
8.00	5.0	24.6 ± 0.2	9
8.00	10.0	27.4 ± 0.2	11
8.00	20.0	31.8 ± 0.3	10
8.40	1.0	20.4 ± 0.2	10
8.40	3.0	34.2 ± 0.3	8
8.40	5.0	36.6 ± 0.3	10
8.40	10.0	43.8 ± 0.3	11
8.40	20.0	50.7 ± 0.4	10

[a][Mg(II)] = 4.0 mM, [ionomycin] = 10.0 μM after mixing, $\lambda = 310$ nm.
[b]Concentrations after mixing.

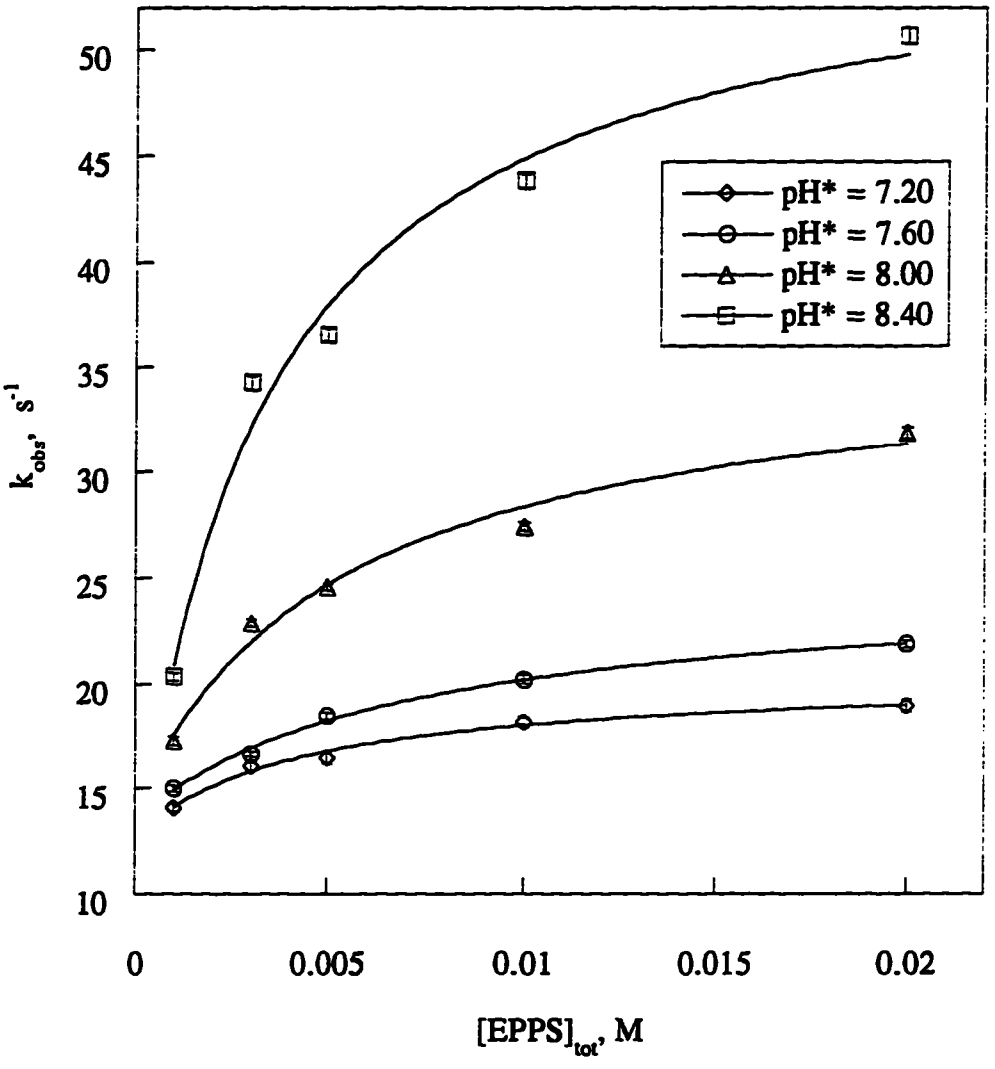

Figure 7.21 Plots of k_{obs} versus $[EPPS]_{tot}$ for the formation reaction of the MgI complex. The error bars represent the mean ± 1 S.D.

Table 7.15. Observed Rate Constants for the Formation Reaction of the MgI Complex as a Function of $[CHES]_{tot}$, in 80% Methanol-Water at $I = 0.050$ M (TEAP)[a]

pH*	10^3 $[CHES]_{tot}$, (M)[b]	k_{obs} (s^{-1})	n
8.00	1.0	19.6 ± 0.2	10
8.00	2.0	25.1 ± 0.3	10
8.00	5.0	31.0 ± 0.3	9
8.00	10.0	38.8 ± 0.5	9
8.00	20.0	43.7 ± 0.5	9
8.40	1.0	37.8 ± 0.4	9
8.40	2.0	46.2 ± 0.6	5
8.40	5.0	64.1 ± 0.6	10
8.40	10.0	69.9 ± 0.7	9
8.40	20.0	89.7 ± 0.8	10
8.80	1.0	58.2 ± 0.4	8
8.80	2.0	81.4 ± 0.6	10
8.80	5.0	98.9 ± 1.2	11
8.80	10.0	117.4 ± 2.1	12
8.80	20.0	119.7 ± 2.9	6

[a][Mg(II)] = 4.0 mM, [ionomycin] = 10.0 μM after mixing, λ = 310 nm.
[b]Concentrations after mixing.

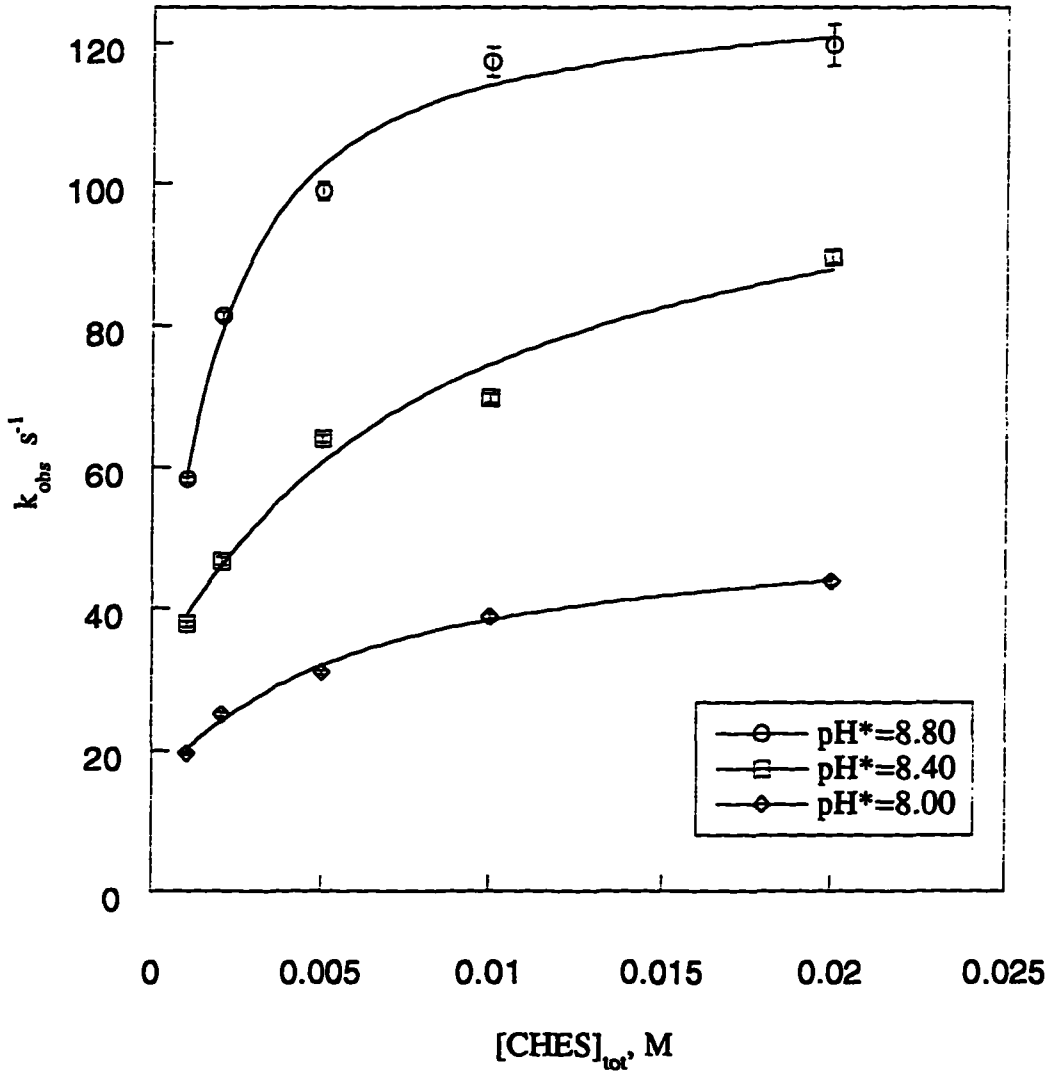

Figure 7.22 Plots of k_{obs} versus $[CHES]_{tot}$ for the formation reaction of the MgI complex. The error bars represent the mean ± 1 S.D.

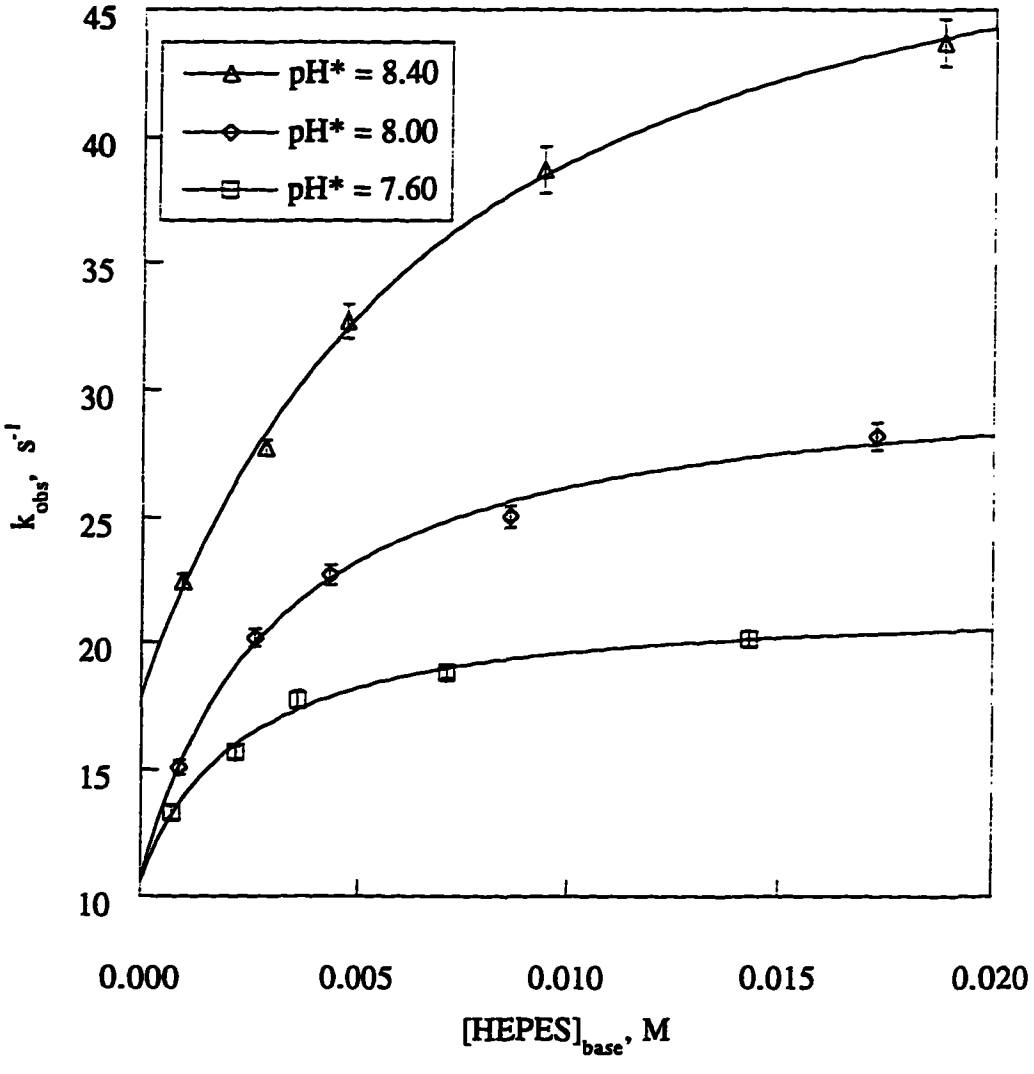

Figure 7.23. Plots of k_{obs} versus the conjugate base form of HEPES buffer for the formation reaction of the MgI complex. The error bars represent the mean ± 1 S.D.

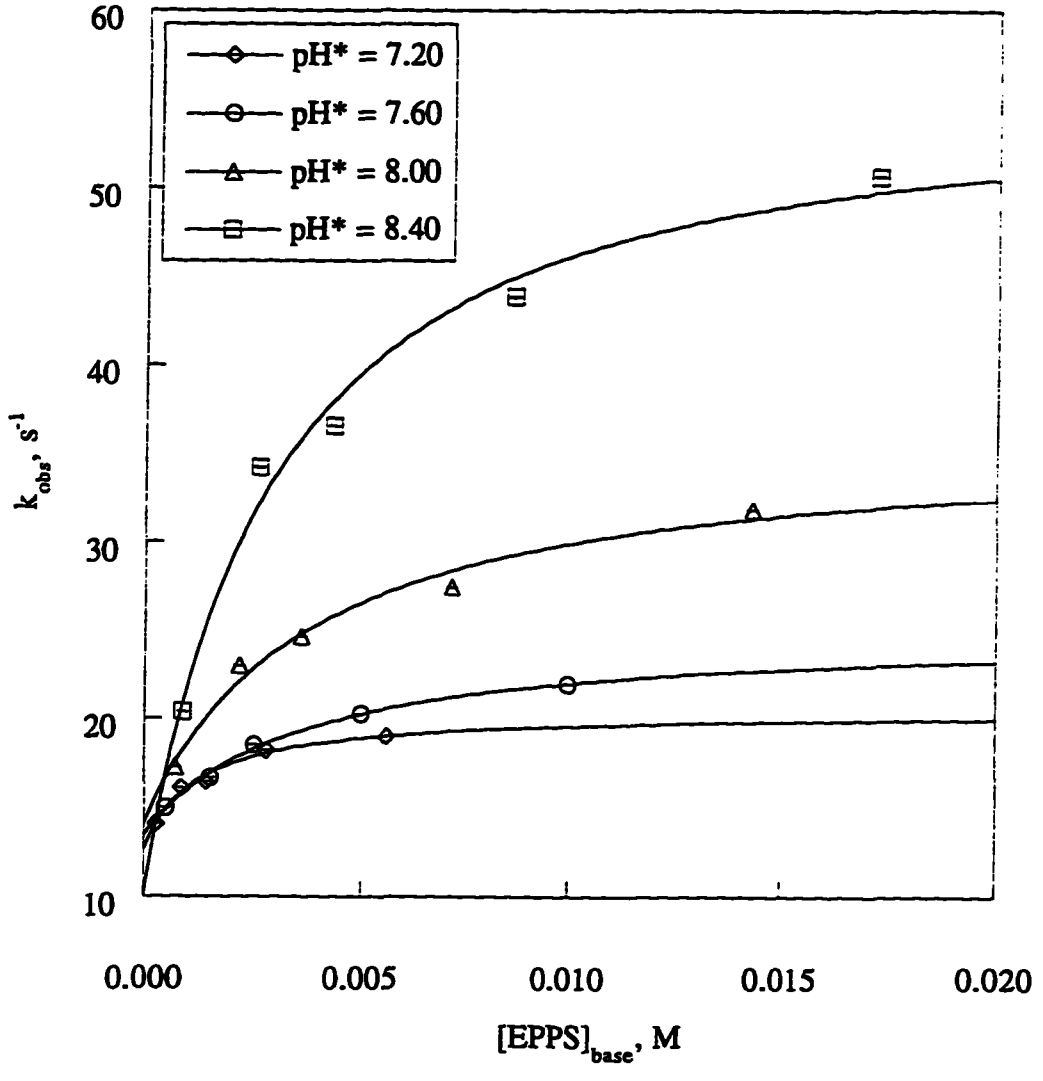

Figure 7.24. Plots of k_{obs} versus the conjugate base form of EPPS buffer for the formation reaction of the MgI complex. The error bars represent the mean ± 1 S.D.

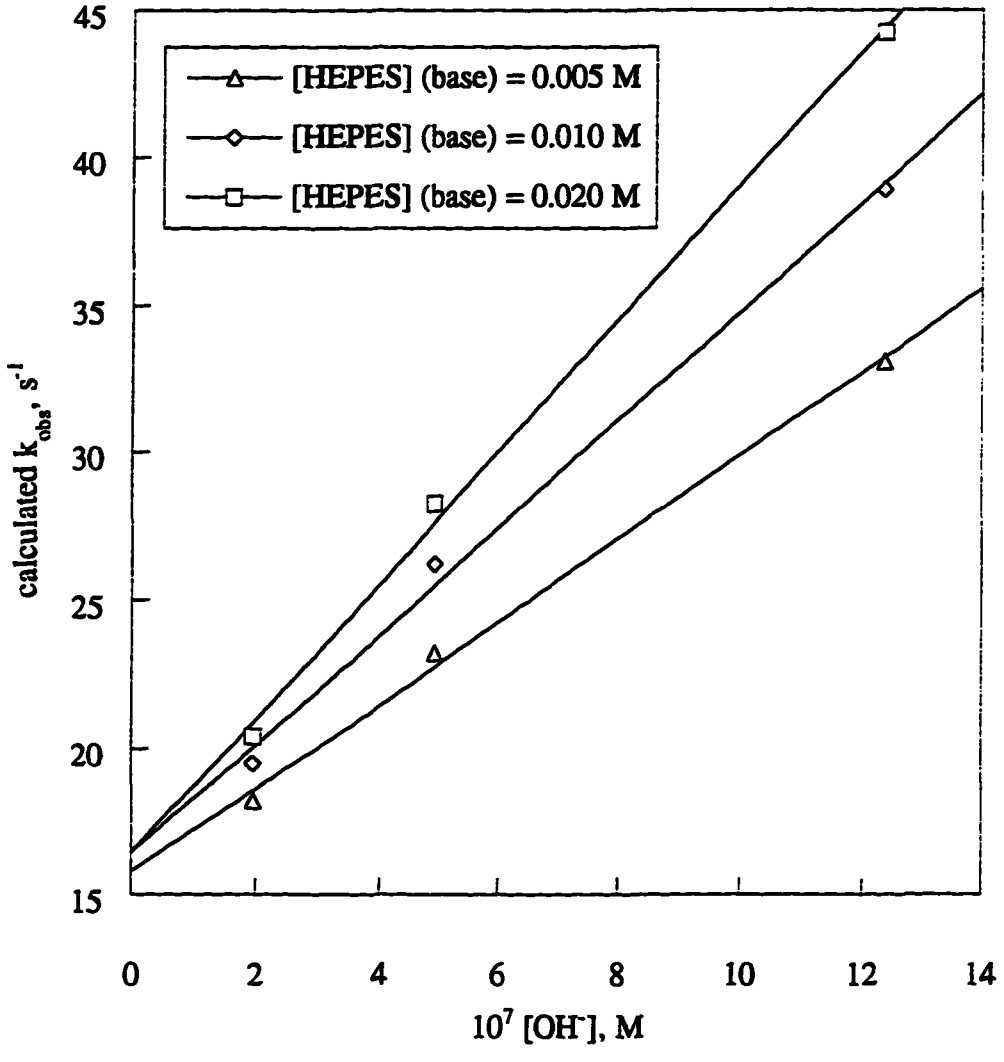

Figure 7.25 Plots of calculated k_{obs} versus [OH^-] for varying concentrations of the conjugate base form of HEPES buffer for the formation reaction of MgI complex.

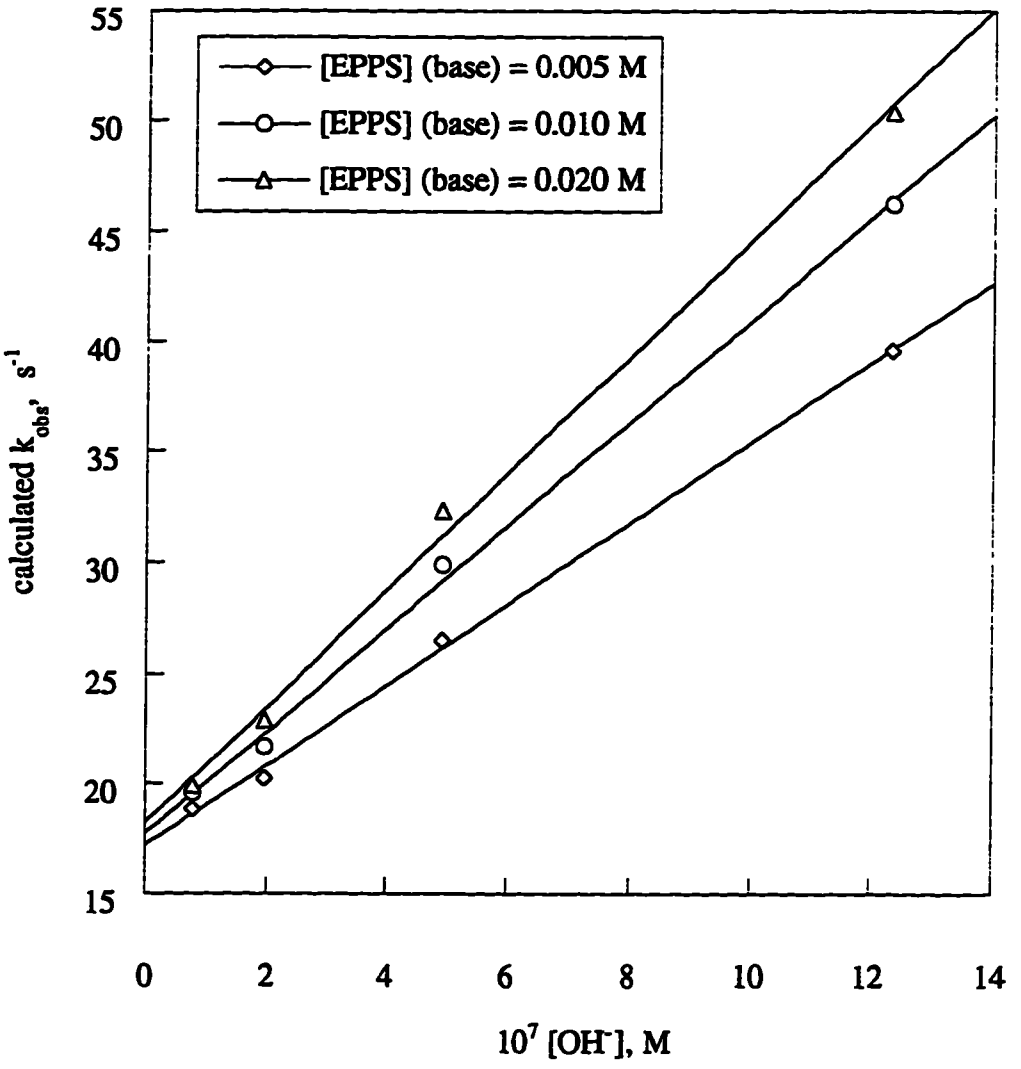

Figure 7.26 Plots of calculated k_{obs} versus [OH^-] for varying concentrations of the conjugate base form of EPPS buffer for the formation reaction of MgI complex.

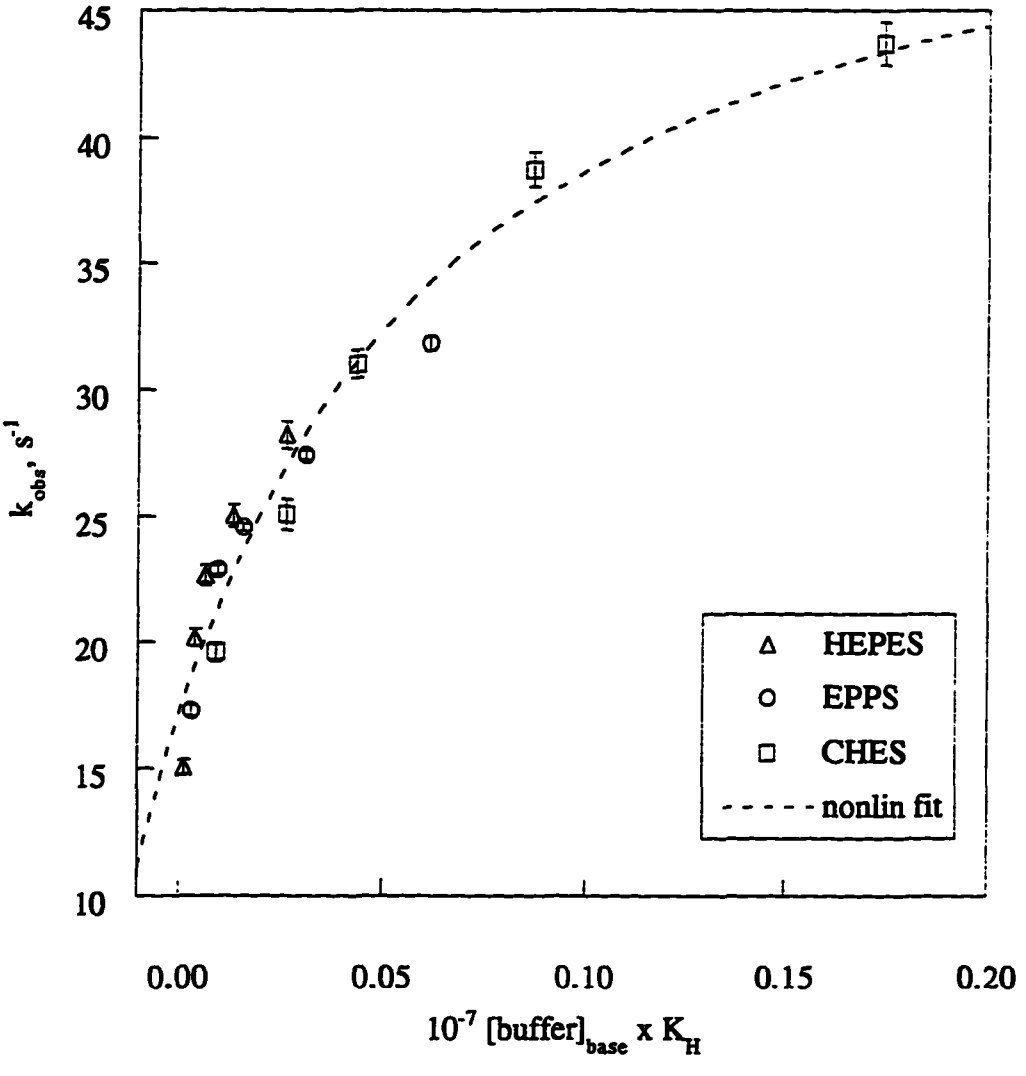

Figure 7.27 Plot of k_{obs} versus {[buffer]$_{base}$ x K_H}for the formation of the MgI complex at pH* = 8.00. The dashed line represents the fit to an expression of the form $k_{obs} = (m_1 + m_2[\text{Buffer}]_{base})/(1 + m_3[\text{Buffer}]_{base})$.

iii) Dissociation of the MgI complex

The dissociation of the MgI complex was studied in the pH* range 5.00 to 6.50 in three different buffers: MES, TEPDA and TEEDA. The reactions were studied as a function of pH* and $[Mg^{2+}]$. The data are summarized in Table 7.16. Figure 7.28 shows a plot of k_{obs} versus the total buffer concentration for TEPDA. Figure 7.29 shows the plot for k_{obs} versus $\{K_a \times [buffer]_{acid}\}$ at pH* = 6.00 for MES, TEPDA and TEEDA, where K_a is the acid dissociation constant ($1/K_H$). This behavior is suggestive of general acid-catalysis.

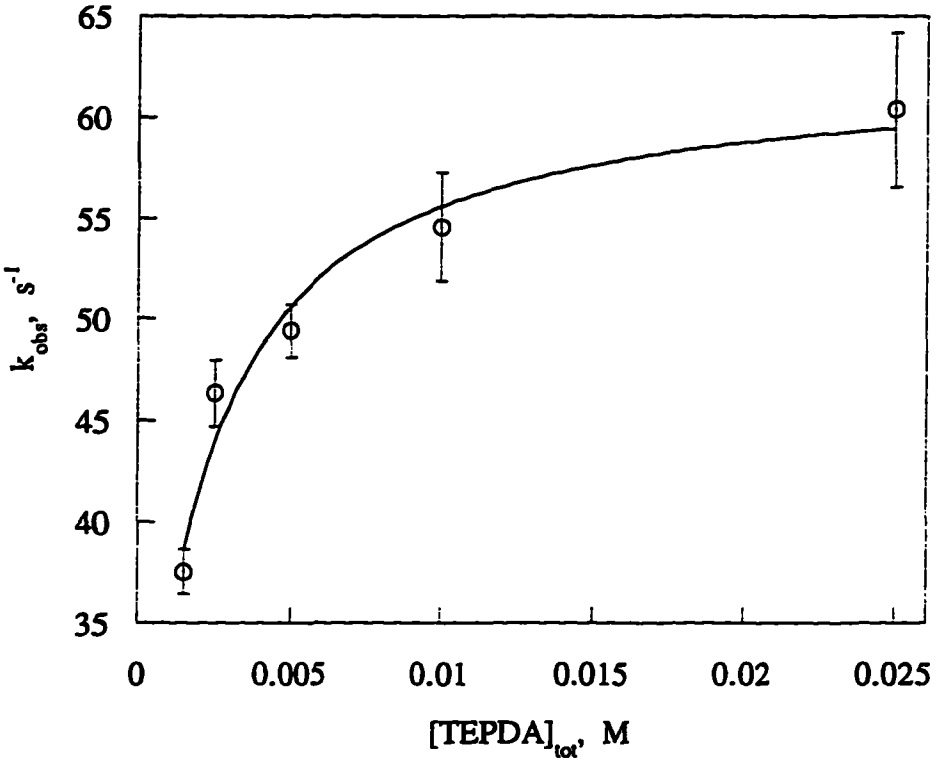

Figure 7.28. Plot of k_{obs} versus total concentration of TEPDA buffer for the dissociation of the MgI complex at pH* = 6.00 and $[Mg^{2+}] = 10^{-4}$ M.

Table 7.16. Observed Rate Constants for the Dissociation Reaction of the MgI Complex as a Function of $[buffer]_{tot}$ in 80% Methanol-Water at $I = 0.050$ M (TEAP)[a]

pH*	10^3 $[buffer]_{tot}$, (M)[b]	10^3 $[Mg^{2+}]$, (M)	k_{obs} (s^{-1})	n
TEPDA				
6.00	1.5	0.10	37.6 ± 1.1	9
6.00	2.5	0.10	46.3 ± 1.6	6
6.00	5.0	0.10	49.4 ± 1.3	7
6.00	10.0	0.10	54.6 ± 2.7	8
6.00	25.0	0.10	60.8 ± 3.8	6
6.00	10.0	2.0	55.5 ± 0.9	10
6.00	10.0	5.0	56.2 ± 1.5	11
6.00	10.0	8.3	58.9 ± 1.4	11
6.37	10.0	0.10	33.3 ± 1.1	8
5.60	10.0	0.10	91.7 ± 4.0	11
MES				
6.00	5.0	0.10	52.0 ± 2.4	7
6.00	10.0	0.10	57.0 ± 2.4	9
6.00	10.0	2.0	55.7 ± 1.1	9
6.00	10.0	5.0	57.3 ± 1.0	11
6.00	10.0	8.3	57.5 ± 0.7	11
6.37	10.0	0.10	32.7 ± 1.0	10
5.60	10.0	0.10	89.6 ± 3.6	11
TEEDA				
6.00	1.5	0.10	47.4 ± 1.1	7
6.00	2.5	0.10	52.2 ± 1.7	7
6.00	5.0	0.10	58.4 ± 2.9	7
6.00	10.0	0.10	59.5 ± 2.3	8
6.00	10.0	2.0	52.6 ± 1.0	10
6.00	10.0	5.0	53.4 ± 1.0	9
6.00	10.0	8.3	55.2 ± 0.9	11
6.37	10.0	0.10	30.1 ± 0.9	10
5.60	10.0	0.10	88.9 ± 3.0	11

[a][ionomycin] = 10.0 μM after mixing; $\lambda = 304$ nm; [b]Concentrations after mixing

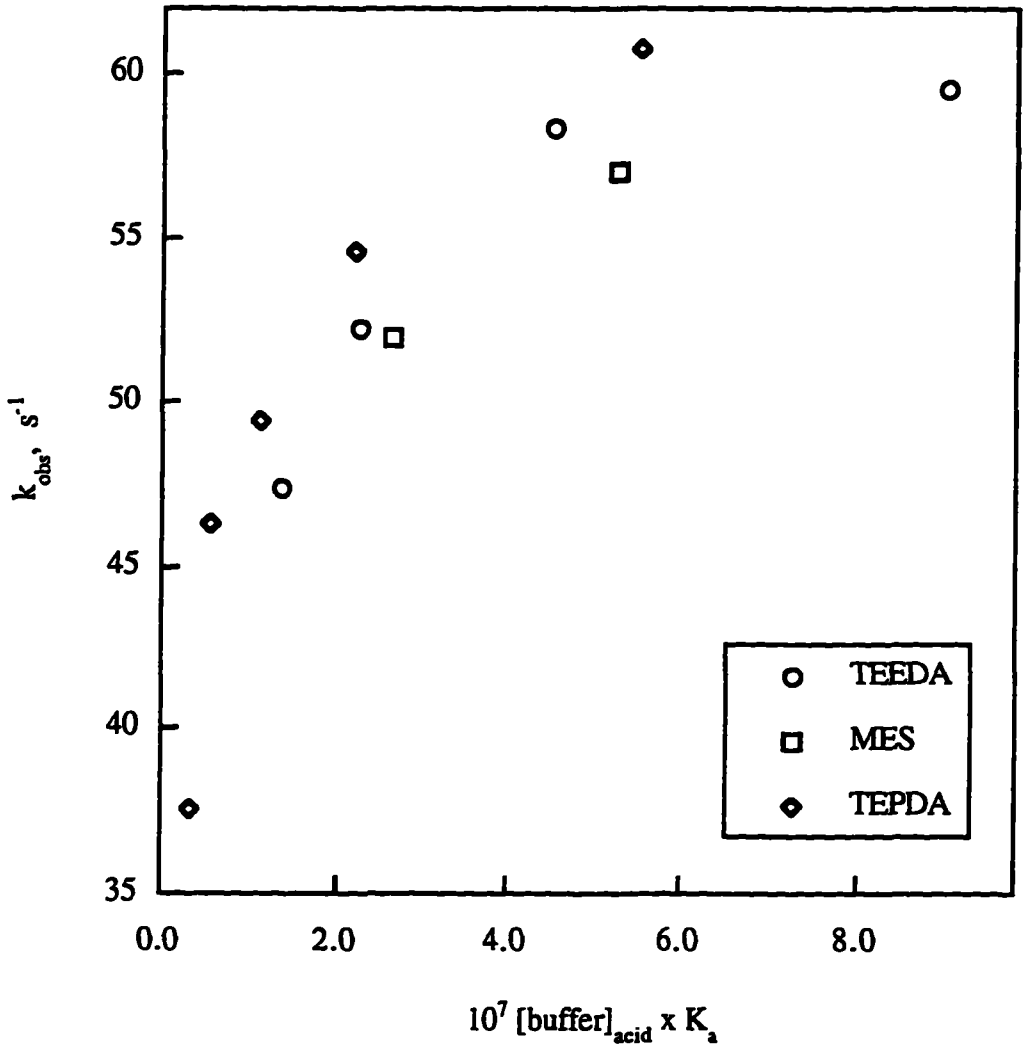

Figure 7.29 Plot of k_{obs} versus {[buffer]$_{acid}$ x K_a} for the dissociation of the MgI complex at pH* = 6.00 and $[Mg^{2+}] = 10^{-4}$ M.

iv) Formation of the $Mg(DMHD)^+$ complex

The reactions of excess Mg(II) with DMHD at pH* = 8.40, in the presence of CHES buffer, were observed to be biphasic in nature. The rate constants for the fast step showed a saturation-type behavior with increasing concentration of the buffer, which is similar to that observed for the formation of the MgI complex. However, the rate constants for the slow step increased linearly with increasing concentration of the buffer. The kinetic data are summarized in Table 7.17. Figure 7.30 shows the effect of buffer concentration on the fast and slow processes.

The reactions of Mg(II) with DMHD were also performed in EPPS buffer where biphasic behavior similar to that with EPPS was observed. However, these studies were only qualitative in nature and so the data are not shown here.

Table 7.17. Observed Rate Constants for the Formation Reaction of the $Mg(DMHD)^+$ Complex as a Function of [CHES] at pH* = 8.40, in 80% Methanol-Water at I = 0.050 M (TEAP)[a]

10^3 $[CHES]_{total}$, (M)[b]	$k_{obs,(f)}$ (s^{-1})	n	10^2 $k_{obs,(s)}$ (s^{-1})	n
1.0	14.9 ± 0.2	5	5.7 ± 0.1	2
2.5	17.2 ± 0.2	4	7.5 ± 0.1	3
5.0	-		10.3 ± 0.3	4
10.0	18.2 ± 0.5	3	16.2 ± 0.6	5
20.0	18.7 ± 0.2	6	29.0 ± 0.1	3

[a][DMHD] = 20.0 μM after mixing; $[Mg^{2+}]$ = 4mM after mixing; λ = 304 nm;
[b]Concentrations after mixing.

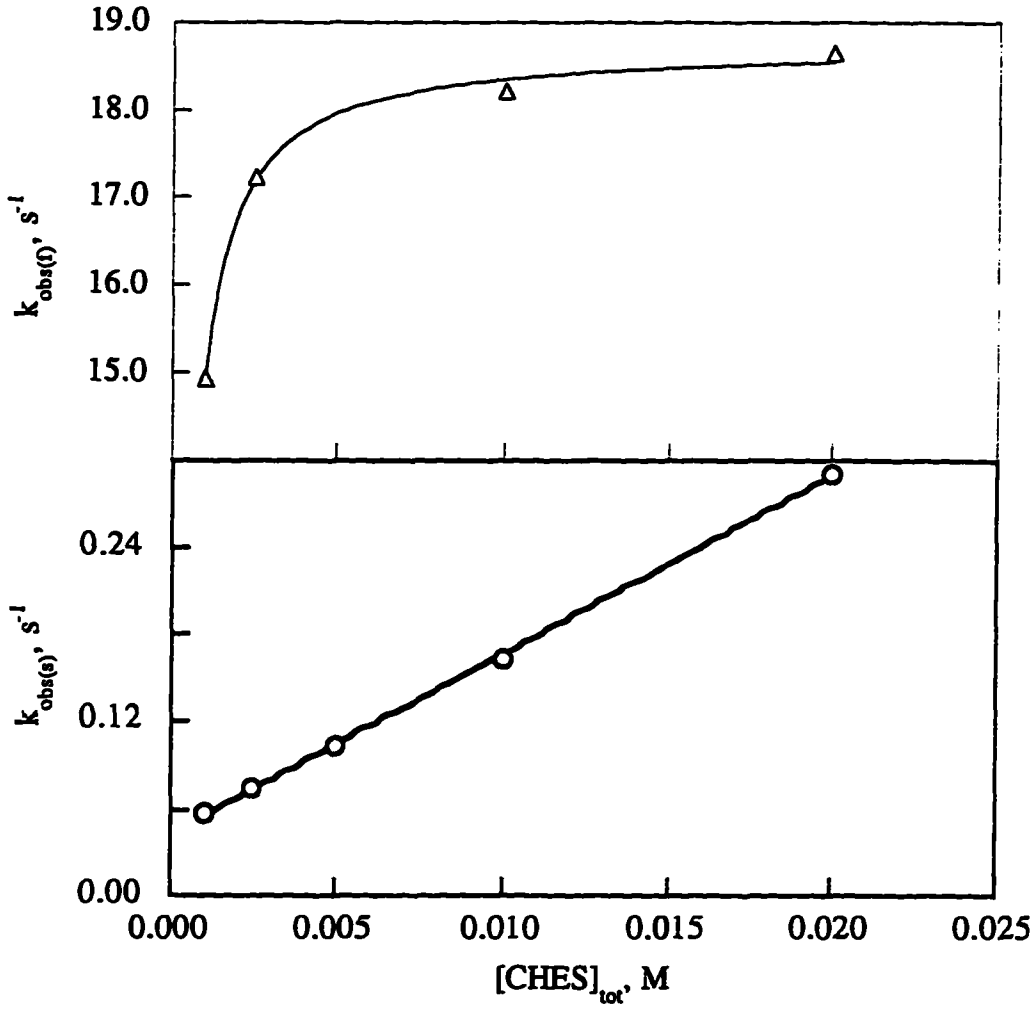

Figure 7.30. Plots of k_{obs} versus the total CHES concentration for the fast (above) and slow (bottom) processes of the formation of the $Mg(DMHD)^+$ complex at pH* = 8.40. The data for the fast process are consistent with equation 7.48, that was used to generate the solid line.

v) Studies of the formation of MgI complexes as a function of $[Mg^{2+}]$

The formation of MgI was studied in the pH* range of 7.20 to 8.00 as a function of $[Mg^{2+}]$ under pseudo-first-order conditions where the concentration of the metal ion was at least in ten-fold excess over $[I]_{tot}$. The data are presented in Table 7.19 and plots of k_{obs} versus $[Mg^{2+}]$ are shown in Figure 7.31. Saturation-type behavior was observed for the values of k_{obs} with increasing $[Mg^{2+}]$.

The nonlinear least-squares fit of the data to the expression 7.49 gave the values of p_1 and p_2 summarized in Table 7.18. The significance of these parameters is discussed in the next chapter.

$$k_{obs} = \frac{p_1 [Mg^{2+}]}{1 + p_2 [Mg^{2+}]} \qquad (7.49)$$

Table 7.18. Values for Parameters from Nonlinear Least-Squares Fit of Equation 7.49, for Formation Kinetics of MgI in 80% Methanol-Water

pH*	$10^{-4}\, p_1$	$10^{-2}\, p_2$	$\frac{p_1}{p_2}$
7.20	0.7 ± 0.4	2.0 ± 1.0	35
7.60	1.0 ± 0.1	2.2 ± 0.2	45
8.00	1.3 ± 0.4	2.0 ± 0.8	65

Table 7.19. Observed Rate Constants for the Formation Reaction of the MgI complex as a Function of $[Mg^{2+}]$, in 80% Methanol-Water at $I = 0.050$ M (TEAP)[a]

pH*	10^3 $[Mg^{2+}]$, (M)	k_{obs} (s^{-1})	n
7.20	2.0	12.5 ± 0.5	7
7.20	4.0	16.8 ± 0.4	7
7.20	6.0	20.6 ± 0.5	7
7.20	8.0	24.2 ± 0.5	9
7.20	10.0	25.5 ± 0.6	10
7.20	12.0	25.2 ± 0.6	10
7.60	1.0	6.0 ± 0.5	7
7.60	2.5	14.0 ± 0.3	9
7.60	4.0	19.4 ± 0.3	10
7.60	7.0	25.7 ± 0.5	8
8.00	2.0	14.2 ± 0.3	11
8.00	4.0	24.5 ± 0.4	10
8.00	6.0	34.1 ± 0.5	9
8.00	8.0	39.5 ± 0.6	10
8.00	10.0	43.7 ± 0.6	10
8.00	12.0	44.4 ± 0.9	9

[a]Reactions were carried out in 5 mM EPPS buffer. [ionomycin] = 9.0 μM after mixing. $\lambda = 310$ nm.

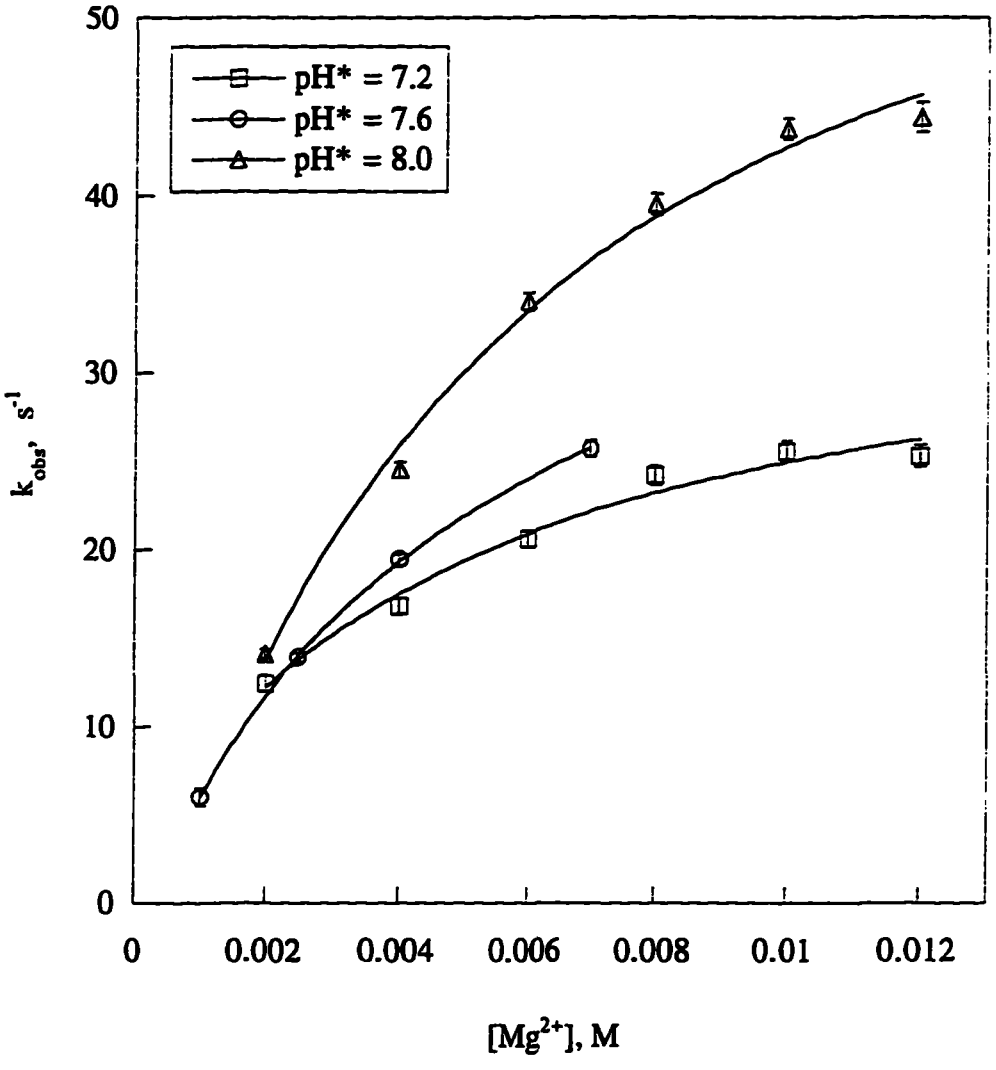

Figure 7.31. Plots of k_{obs} versus $[Mg^{2+}]$ for formation of the MgI complex at different pH* values. The error bars represent the mean ± 1 S.D.

F. Molar Absorptivity of Ionomycin

The molar absorptivity of ionomycin was calculated in different solvents from plots of absorbance versus concentration. In the UV-Vis region, ionomycin showed a peak at 278 nm in the solvents methanol, 80% methanol-water, ethanol and hexane. However in chloroform, a shoulder at 278 nm and two new peaks at 264 and 271 nm were observed. The shape of the spectrum in the wavelength region 250 to 320 was restored when the chloroform was removed and the sample was redissolved in 80% methanol-water. Table 7.20. gives the values of the molar absorptivity of ionomycin in different solvents.

Table 7.20. Molar Absorptivity Constants of Ionomycin at 278 nm in Different Solvents

solvent	$10^{-4}\,\varepsilon_{278}$
80% methanol-water	1.29 ± 0.001
methanol	1.32 ± 0.001
ethanol	1.28 ± 0.001
hexane	1.24 ± 0.002
chloroform	1.59 ± 0.003

REFERENCES

1) Sanders, J. K. M.; Hunter, B. K. *Modern NMR Spectroscopy*; 2nd ed.; Oxford University Press: Oxford, 1993, pp 110-113.

2) Atta-ur-Rahman *One and Two Dimensional Spectroscopy*; Elsevier: New York, 1989, pp 111-115.

3) Wilkins, R. G. *Kinetics and Mechanism of Reactions of Transition Metal Complexes*; 2nd ed.; VCH: New York, 1991, pp 1-55.

4) Jaffe, M. R.; Fay, D. P.; Cefola, M.; Sutin, N. *J. Am. Chem. Soc.* **1971**, *93*, 2878-2886.

5) Hirsch, J.; Paulus, H.; Elias, H. *Inorg. Chem.* **1996**, *35*, 2343-2351.

6) Hynes, M. J. *J. Chem. Soc., Faraday Trans.* **1992**, *88*, 3533-3536.

7) Craig, M. E. *Ph.D. Thesis* **1990**, The University of Oklahoma, Norman, OK.

8) Blanco, C.; Hynes, M. *Bull. Soc. Chim. Fr.*, **1989**, 611-614.

9) Pearson, R. G.; Anderson, O. P. *Inorg. Chem.* **1970**, *9*, 39-46.

10) Hynes, M. J.; Mooney, M. T.; Moloney, A. *J. Chem. Soc., Dalton Trans.* **1993**, 313-318.

11) Matsen, F. A.; Franklin, J. L. *J. Am. Chem. Soc.* **1950**, *72*, 3337-3341.

12) Lowry, T. M.; John, W. T. *J. Chem. Soc.* **1910**, *97*, 2634-2637.

13) Lewis, E. S.; Johnson, M. D. *J. Am. Chem. Soc.* **1960**, *82*, 5399-5404.

14) Frost, A. A.; Pearson, R. G. *Kinetics and Mechanism*; Wiley: New York, 1953, pp 160-164.

15) Kells, L. M. *Differential Equations, A Brief Course with Aplications*; McGraw-Hill: New York, 1968, pp 135-168.

16) Hynes, M. J. *Rev. Inorg. Chem.* **1990**, *11*, 21-78.

17) Hynes, M. J.; Kelly, D. F. *J. Chem. Soc., Dalton Trans.* **1988**, 905-908.

18) Hynes, M. J.; Blanco, C. A.; Mooney, M. T. *J. Chem. Soc., Perkin Trans. 2* **1991**, 2055-2060.

19) Gupta, A. R. *J. Phys. Chem.* **1979**, *83*, 2986-2990.

20) Pitzer, K. S. *J. Phys. Chem.* **1973**, *77*, 268-277.

CHAPTER VIII

DISCUSSION

A. Keto-Enol Tautomerism of Ionomycin and DMHD

i) Enol/keto ratios

The results described in the previous chapter show that both ionomycin and the model compound 2,6-dimethyl-3,6-heptanedione (DMHD) exist in keto and enol forms. This observation is not surprising since most β-diketones behave in similar manner.[1,2] The values for the percentage of the enol form in ionomycin and DMHD obtained in 80% methanol-water solution, are summarized in Table 8.1. It can be seen that the values obtained for the % enol form of ionomycin from ^{1}H NMR and pH-jump experiment are not significantly different. The values obtained for the % enol form of DMHD from different techniques listed in Table 8.1, are all within 2%.

Generally, the enol/keto ratio of β-diketones is dependent on the intermolecular and the intramolecular hydrogen bonding of the ligand.[3-6] Intermolecular bonding can exist between ligand molecules or between ligand and solvent molecules. In non-polar solvents or in the neat form of the compound, the intramolecular hydrogen bonding and intermolecular hydrogen bonding between the ligand molecules are predominant, favoring the enol form. The enol form is further stabilized by the presence of conjugation in the molecule. For example in acetylacetone, the intramolecular hydrogen bonding stabilizes the enol tautomer by 5 to 10 kcal and the conjugation further stabilizes this tautomer by 2 to 3 kcal.[4] However, as the solvent polarity increases, the more polar keto

form is favored[7] and the percentage of enol form decreases.

Table 8.1. Percentage of Enol Form of Ionomycin and DMHD Present in 80% Methanol-Water Solution Measured by Different Techniques

technique	ionomycin	DMHD
^{1}H NMR	88.0 ± 0.3	74.7 ± 0.3
pH-jump	88.3 ± 0.7	76 ± 1
rapid-dilution	–	73 ± 1

The results of the ^{1}H-NMR experiments with DMHD are consistent with this general behavior of β-diketones. It was observed that the concentration of the enol form of DMHD decreases from 96% in the neat compound to 75% in 80% methanol-water. The enol content of pure ionomycin was not determined. Since ionomycin is crystalline in its pure form, such a task would require the use of the solid-state ^{1}H-NMR technique. The large sample requirements for this experiment (~400 mg) makes the cost prohibitive.

Why does ionomycin have greater percentage of enol form than DMHD? It is proposed that the keto-enol equilibrium in β-diketones shifts more towards the enol form as the alkyl substituents get bulkier.[6,8] To understand this steric effect, one may consider the possible conformations of a β-diketone molecule. The structures for various conformers are shown in Figure 8.1 where I, II and III represent the keto forms and IV, V and VI represent the enol forms. It can be seen that bulky substituents (R_1 and R_2) on conformers I and II will introduce strain that can be released by adopting a conformation

shown by structure III. This conformer has a greater tendency to enolize compared to I or II because the electrostatic repulsion between the two carbonyls in III can be minimized by forming an intramolecular hydrogen bond. Since ionomycin has bulkier R_1 and R_2 groups compared to DMHD, the above argument may be presented to explain the greater percentage of the enol content of the former in 80% methanol-water.

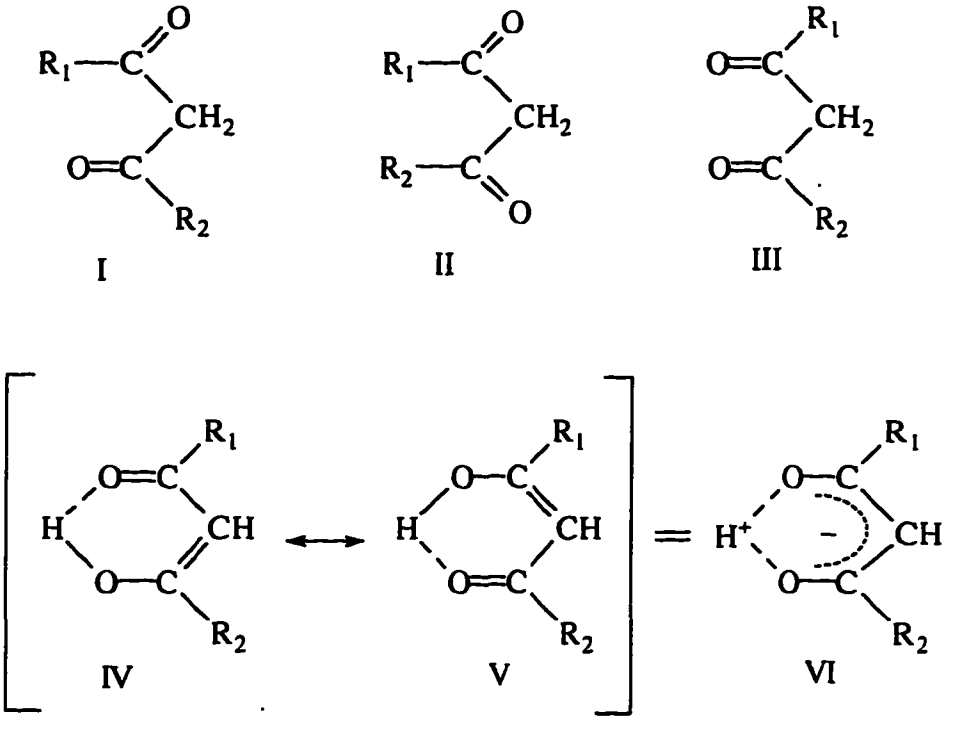

Figure 8.1. The structures of keto (top) and enol (bottom) forms of a β-diketone with substituents R_1 and R_2.

The effect of buffers on the enol/keto ratios ($K_{e/k}$) may be analyzed from the data shown in Table 8.1. Comparison of the NMR data to that of the rapid-dilution and pH-jump experiments shows, that the concentration and the nature of buffer have no significant effect on the enol/keto ratios of ionomycin and DMHD. The ligand solutions used in the NMR experiments contained no buffer, whereas the pH-jump and the rapid-

dilution experiments were performed in the presence of buffers. The rapid-dilution experiments were performed in the presence of two different buffers at varying concentrations. The values of $K_{e/k}$ obtained for ionomycin from NMR and pH-jump experiments are identical within the experimental error. The values of $K_{e/k}$ for DMHD obtained from three different experiments are within 2% of each other. Similar behavior was observed by Hynes *et al.*[9] who reported no change in the enol/keto ratio of an aqueous solution of pentane-2,4-dione upon addition of the cacodylate buffer.

The NMR experiments were performed with ~millimolar concentrations of ionomycin. At these concentrations the carboxylate group is almost completely protonated ($\geq$ 98.1%, for [ionomycin] = 1mM; calculated using log K_H^I = 6.43). However, at the final pH* of the pH-jump experiments (~7.0) more than half of the ionomycin carboxylate groups are deprotonated. Despite the variation of the pH* in these experiments, the percentage of the enol form of ionomycin obtained from the two experiments is identical. This indicates that the protonation state of the carboxylate group does not significantly influence the enol/keto ratio of ionomycin in solution.

ii) Conformation of the enol form of ionomycin

From the results of the ^{13}C NMR experiments, a notable feature about the structure of the enol form of ionomycin may be inferred. In these experiments the two quaternary carbon atoms of the β-diketone moiety of ionomycin appear only 0.4 ppm apart. Such a small difference in the chemical shift of these carbon atoms suggests that they are nearly equivalent. The corresponding carbon atoms in DMHD are found to be identical since the spectrum shows a single peak for these carbon atoms. These results indicates that the double bonds in the β-diketone moiety of both the ligands are delocalized over the three carbon atoms and the proton is shared by the two oxygen atoms; this structure is shown as VI in Figure 8.1. If the double bond in the β-diketone moiety of ionomycin was localized in a single position (Figure 8.1, IV or V), the

difference in the chemical shifts for >C=O and =C–OH carbon atoms would be expected to be greater than 0.4 ppm.[10] For example, in the naturally occurring compounds aurantoside A and B, both of which contain β-diketone moieties with localized double bonds, the difference in the chemical shifts for the >C=O and =C–OH carbon atoms is ~20 ppm.[11] Another example is the naturally occurring compound citrinin, which shows peaks for the corresponding carbon atoms ~10 ppm apart.[12]

The small difference in the chemical shifts of the two quaternary carbon atoms in ionomycin may be caused by two factors: i) the difference in the structure of the side chains (four carbon atoms away), and/or ii) the difference in the local environment of the two carbon atoms; different polar groups in the ionomycin molecule may hydrogen bond with the two oxygen atoms of the β-diketone moiety. It can be seen that the side chains on the quaternary carbon atoms of DMHD are identical and therefore the peaks for these two carbon atoms overlap.

iii) Calculation of protonation constants for the keto and the enol forms

The individual and the overall protonation reactions for the enol form (K_{He}) and the keto form (K_{Hk}) of the ligands are given by equations 8.1 to 8.3, where, E represents the enolate form of the ligand, HL represents the total ligand, and HE and HK represent the enol and the keto forms of the ligand, respectively. In these equations, the formal charge on the ligands is omitted for the convenience of using the same set of equations for DMHD and ionomycin. The values for the protonation constants are calculated using the known values of the enol/keto ratios ($K_{e/k}$) and the protonation constants (K_H). Using equations 8.1-8.4, the set of equations shown by 8.5 to 8.6 may be derived to obtain the values of K_{He} and K_{Hk}; these values are summarized in Table 8.2. The calculated values of log K_{HE} for ionomycin and DMDH are required for subsequent treatment of the metal complexation kinetic data for these ligands.

$$E + H^+ \rightleftharpoons HL;\ K_H \tag{8.1}$$

$$E + H^+ \rightleftharpoons HE;\ K_{He} \tag{8.2}$$

$$E + H^+ \rightleftharpoons HK;\ K_{Hk} \tag{8.3}$$

$$[HL] = [HE] + [HK] \tag{8.4}$$

$$K_{e/k} = \frac{[HE]}{[HK]} = \frac{K_{He}}{K_{Hk}} \tag{8.5}$$

$$K_H = K_{Hk} + K_{He} \tag{8.6}$$

Table 8.2. Mixed-Mode Protonation Constants for Keto and Enol Tautomers

	ionomycin[a]	DMHD
$K_{e/k}$	2.95	7.33
log K_H[b]	11.94	11.33
log K_{He}	11.88	11.20
log K_{Hk}	11.02	10.73

[a]The reported values of the protonation constants are for the β-diketone moiety.
[b]From ref. (13).

iv) Kinetics of keto-enol tautomerism

Scheme 8.1

$$HE \underset{k_e}{\overset{k_k}{\rightleftharpoons}} HK$$

The keto-enol tautomerism is shown in Scheme 8.1, where k_k and k_e are the rate constants for the formation of the keto and the enol forms, respectively. The kinetics of keto-enol tautomerism was studied using the pH-jump and the rapid-dilution techniques. The experiments were performed in the pH* range 5.00 to 7.60. The plots of k_{obs} versus the concentration of the conjugate base form of the buffer gave straight lines (see Figures 7.7-7.10 in Chapter VII). The slope and the intercept of these lines did not change with varying pH*. These results indicate that the keto-enol interconversion of ionomycin and DMHD is general base catalyzed and the contributions from the specific acid/base catalysis are comparatively negligible.

The intercepts of the k_{obs} versus $[buffer]_{base}$ plots, represent the buffer-independent values of k_{obs} for the keto-enol interconversion. For ionomycin, this value is $0.248 \pm 0.001\ s^{-1}$ as obtained form the pH-jump experiment performed in the presence of EPPS buffer. For DMHD, three different experiments were performed. The values obtained are: $(4 \pm 5) \times 10^{-3}\ s^{-1}$ from pH-jump in EPPS, $(4 \pm 3) \times 10^{-3}\ s^{-1}$ from rapid-dilution experiment in EPPS and $(1.7 \pm 0.2) \times 10^{-3}\ s^{-1}$ from rapid-dilution experiment in MES. From the values of k_{obs} and $K_{e/k}$, the values of k_e and k_k may be calculated using the relationships $k_{obs} = k_e + k_k$ and $K_{e/k} = k_e/k_k$. The calculations for DMHD were performed using the value of $k_{obs} = 1.7 \times 10^{-3}\ s^{-1}$, since that result has the lowest associated error. The k_e and k_k values for ionomycin and DMHD are summarized in Table 8.3.

Table 8.3. Resolved Rate Constants for Keto-Enol Interconversion of Ionomycin and DMHD

rate constant	ionomycin	DMHD
k_e, s^{-1}	2.2×10^{-1}	1.3×10^{-3}
k_k, s^{-1}	3.0×10^{-2}	4.3×10^{-4}

The values of k_e and k_k for ionomycin are approximately two orders of magnitude larger than the corresponding values for DMHD. It is proposed that the higher values of these rate constants for ionomycin are due to intramolecular base catalysis, shown by the mechanism in Scheme 8.2. In this mechanism the rate-limiting deprotonation of the β-diketone moiety is assisted by the carboxylate group which interacts with the proton electrostatically. Evidence for such an interaction comes from the fact that the value of the second proton dissociation constant for ionomycin is ~0.6 log units higher than the value of the dissociation constant for DMHD.[13] The difference in the values for these constants is attributed to the presence of the carboxylic group in ionomycin. While the interaction of the carboxylate with the proton makes its dissociation from the molecule more difficult, on the other hand it weakens the O–H bonding between the proton and the β-diketone oxygen. This argument supports the existence of the mechanism proposed here.

Scheme 8.2

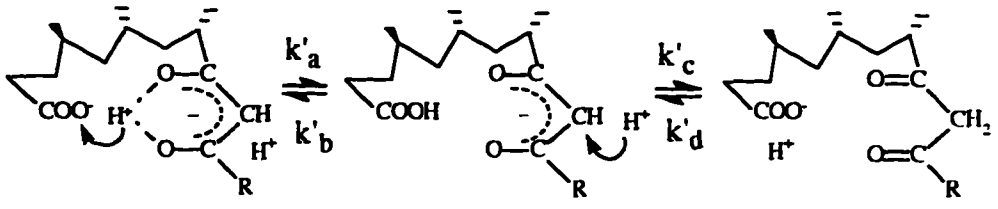

In the mechanism shown in Scheme 8.2, the formation of an enolate intermediate is suggested. This situation is similar to the tautomerization of simple β-diketones. Eigen proposed that the interconversion of β-diketones does not proceed by the direct transfer of a proton from carbon to oxygen,[14] but proceeds via a mechanism in which the enolate intermediate is formed as shown in Scheme 8.3 where, k_a, k_b, k_c and k_d represent the rate constants for the steps shown.

Scheme 8.3

$$HE \underset{k_b}{\overset{k_a}{\rightleftharpoons}} H^+ + E^- \underset{k_d}{\overset{k_c}{\rightleftharpoons}} HK$$

The values of k_b and k_c for acetylacetone have been determined to be 3×10^{10} and 1×10^7 $M^{-1}s^{-1}$, respectively.[14] Since $k_b >> k_c$, this condition is used to derive the relationships given by equation 8.7 and 8.8 that relate the overall rate constants for the formation of keto and enol forms (k_k and k_e shown in Scheme 8.1) with the rate constants for the individual steps shown in Scheme 8.3.

$$k_k = \frac{k_a k_c}{k_b + k_c} \approx \frac{k_a k_c}{k_b} \tag{8.7}$$

$$k_e = \frac{k_d k_b}{k_b + k_c} \approx k_d \tag{8.8}$$

Similar relationships can be derived for Scheme 8.2 also, where k_a, k_b, k_c and k_d are replaced by k'_a, k'_b, k'_c and k'_d, respectively. It can be seen from equation 8.7, that a faster rate of deprotonation (step k_a in Scheme 8.3 or step k'_a in Scheme 8.2) will increase the value of k_k. Similarly, equation 8.8 shows that a faster rate of deprotonation from the keto form (step k_d in Scheme 8.3 or step k'_d in scheme 8.2) will increase the value of k_e.

From the available data, an intimate tautomerization mechanism like that shown in Scheme 8.3 cannot be established for DMHD; however, it is likely that such a mechanism exists for this system also.

The intermolecular base catalysis of the tautomerism of ionomycin is expected to be negligible under the conditions of our experiments. The concentration of ionomycin in these experiments is too low (~10 μM) to produce such catalytic effects. However, additional experiments may be performed in varying amounts of acetate buffer, to resolve the possible effects of intermolecular base catalysis.

B. Mechanism of Ni(II) Complexation with Ionomycin and DMHD

i) Interpretation of the data from the dissociation kinetic studies

The kinetic data obtained for the dissociation reactions of the Ni(II) complexes of ionomycin and DMHD are consistent with a mechanism shown in Scheme 8.4; k_e, k_k, k_{HE} and k_{-HE} are the rate constants for the steps shown in this scheme.

Scheme 8.4.

$$HK + Ni^{2+} \underset{k_k}{\overset{k_e}{\rightleftharpoons}} HE + Ni^{2+} \underset{k_{-HE}}{\overset{k_{HE}}{\rightleftharpoons}} NiL^{+} + H^{+}$$

According to this mechanism, the formation of the metal-ligand complex takes place through the enol form of the ligand. Many other β-diketone systems follow this mechanism.[15-20] For example, the complexation of 1,1,1-trifluoropentane-2,4-dione and 4,4,4-Trifluoro-1-(2-thienyl)-butane-1,3-dione with Ni(II) takes place exclusively through the enol form of the ligand, despite the fact that in solution 99% of the ligand exists in the keto form.[15,17,18] The fact that the data for both ionomycin and DMHD fit the general solution (equation 7.30) for Scheme 8.4 suggests that the metal complexation behavior of ionomycin is similar to that of simple β-diketones. It is expected that under the conditions employed (pH* < 4), product formation through the pathway involving the enolate form of the ligand is negligible. The basis of this assumption is treated in detail in section C.

The much greater reactivity of the enol form of the ligand compared to the keto form is attributed to a more facile dissociation of the proton from the oxygen atom in the former compared to the more sluggish dissociation of a proton from the α carbon atom, in the keto form.[1] However, there are examples of reactions[16,21,22] where the metal

complexation of the β-diketones takes place through the keto form also, although the rate constants for these reactions are two to three orders of magnitude smaller than the reactions of corresponding enol forms. It is proposed that the reactivity of the keto form to some extent may depend on the nature of metal ion.[1] Metal ions which are either very labile or which form relatively stable complexes, e.g., Fe(III), Cu(II) and $[UO_2]^{2+}$, react with the keto form; whereas, metal ions which form complexes of relatively low stability and which are relatively inert, e.g., Ni(II), do not react with the keto form. The reduction potential of the metal ion is sometimes considered important for its ability to react with the keto form.[20] Metal ions with high reduction potential ($M^{n+} \rightarrow M^0$), such as Fe(III) (-0.04 V) and Cu(II) (+0.35 V), react with the keto form; whereas the metal ions with low reduction potential, such as Ni(II) (-0.25 V), do not react with the keto form.

ii) Interpretation of the data from the formation kinetic studies

Two first-order processes were observed for the complexation of ionomycin with Ni(II) in the pH* range 3.3 to 4.0. This behavior is predicted by the general solution of Scheme 8.4 (see Chapter VII for detailed mathematical treatment). The observed rate constants for both processes (fast and slow) were found to be independent of pH* within experimental error. The rate constants for the fast process ($k_{obs(f)}$) show a linear dependence on $[Ni^{2+}]$. Metal ion dependence of the rate constants for the slow process ($k_{obs(s)}$) was not analyzed; large errors were associated with these numbers due to the small magnitudes of the absorbance changes.

Analysis of the values for the absorbance changes for the fast and slow processes shows that the faster process predominates at lower pH* values. This observation is consistent with the fact that the data for the dissociation of NiI performed at low pH* (< 2.5), fit the solution for the fast process. From the behavior of the two processes as a

function of pH*, it may be concluded that the slow process will be predominant at physiological pH.

The kinetic data for the formation of $Ni(DMHD)^+$ are consistent with the mechanism shown in Scheme 8.4. The slope for the plot of $k_{obs}/[Ni^{2+}]$ versus $[H^+]/[Ni^{2+}]$ obtained from the formation data is same (within the experimental error) as the slope for a similar plot obtained from the dissociation data.

iii) Metal complexation behavior of DMHD and ionomycin

Table 8.4 shows that for the reactions of Ni(II) with DMHD, the values of k_{HE} and k_{-HE} lie within the typical range of values obtained for similar reactions of other β-diketones; however, the values of the rate constants for ionomycin are approximately an order of magnitude smaller.

To gain an insight into the intimate details of the mechanism of metal complexation of ionomycin and DMHD, the experimental values of k_{HE} may be compared with their predicted values from the dissociative-interchange (I_d) model for ligand substitution described in chapter I. The values of k_{HE} for these reactions are four to five orders of magnitude smaller than the calculated value ($\sim 10^4\ M^{-1}s^{-1}$) for the I_d model. This situation is similar to those observed for the reactions of several β-diketones with various divalent metal ions.[1] The disagreement between the experimental and predicted values of k_{HE} shows that the metal complexation of β-diketones does not proceed through dissociative-interchange mechanism in which the rate-determining step is the first bond formation. It is expected that the rate determining step is the second bond formation. Slow ring closure or steric hinderance is ruled out to be a cause for this anomaly; if these factors were causing the lowering of the rates, then one would expect both enol and enolate forms to behave in a similar manner. However, it is observed that the values of the rate constants for enolate-metal complexation are comparable to those calculated from the dissociative-interchange model. Some examples of the rate constants for the reactions of

Table 8.4. Rate Constants for the Reactions of Enol Form of β-diketones with Ni(II)[a, b]

ligand	solvent[c]	k_{HE} ($M^{-1}s^{-1}$)	10^{-3} k_{-HE} ($M^{-1}s^{-1}$)	reference
ionomycin[d]	80% MeOH/H2O	0.25	0.049	this work
DMHD[d]	80% MeOH/H_2O	1.88	0.48	this work
DMHD	80% MeOH/H_2O	2.30	1.1	this work
1-phenylbutane-1,3-dione	66% MeOH/H_2O	3.21	0.9	23
pentane-2,4-dione	88% MeOH/H_2O	17.0	0.6	24
pentane-2,4-dione	H_2O	19.3	4.1	24
heptane-3,5-dione	H_2O	10.0	14.9	25

[a]The ionic strength in all studies except for two[d] was maintained at 0.50 M with $NaClO_4$. [b]The uncertainties in all reported rate constants are < 2.5%. [c]The percentage of methanol in the MeOH/H_2O solvent systems is expressed by weight. [d]I = 0.050 M (Et_4NClO_4).

Ni(II) with the enol and the enolate form of some β-diketones are summarized in Table 8.5.

The value of k_{HE} for the NiI complex (0.16 $M^{-1}s^{-1}$) is approximately eight times smaller than that of the $Ni(DMHD)^+$ complex. The smaller value of the rate constant in the former case can be attributed to the steric hinderance faced by the metal ion in approaching the β-diketone moiety. It is observed that an increase in the chain length of the substituents on the β-diketone, results in a slower reaction with the metal ion. For example, a reduction by a factor of two is observed in the rate constant for the reaction of Ni(II) with the enol tautomer of heptane-3,5-dione (HD) compared with the enol tautomer

of pentane-2,4-dione (PD) (see table 8.3). While the HD molecule is only two carbon atoms longer than PD, the ionomycin molecule is 25 carbon atoms longer than DMHD. Moreover, in solution ionomycin can adopt a conformation in which the β-diketone moiety is blocked by the polar oxygen containing groups (carboxylate, alcohol and furan) that can hydrogen bond with the β-diketone moiety. Such a conformation will make ionomycin a poor incoming ligand; thus it would be expected that the formation of the metal complexes of ionomycin will be slower than that of DMHD.

Table 8.5. Formation Rate Constants for Reaction of the Enol and the Enolate forms of β-Diketones with Ni(II)

ligand	rate constants ($M^{-1}s^{-1}$) enol (k_{HE})	enolate (k_E)	reference
4,4,4-trifluoro-1-(2-thienyl)butane-1,3-dione	2.3	1×10^4	18
1,1,1-trifluoropentane-2,4-dione	1.7	3.4×10^3	15
1-phenylbutane-1,3-dione	3.2	2.7×10^4	23

Ionomycin is unique among the group of carboxylic acid ionophores in that it contains a β-diketone moiety in its structure. One effect of this group can be seen by comparing the formation rate constants for NiI and $Ni(A23187)^+$ complexes. The reaction of the protonated form of carboxylic acid ionophore A23187, proceeds with a rate constant of ~90 $M^{-1}s^{-1}$ in 80% methanol-water.[26] In ionomycin, where the β-diketone moiety is present, the rate constant is three orders of magnitude lower. Thus,

it can be concluded that the β-diketone group participates in the rate determining step and is responsible for the slower rate of metal complexation of ionomycin compared to other carboxylic acid ionophores that do not contain this functionality.

In accord with the I_d mechanism, the carboxylate form of ionophores such as A23187 and Lasalocid react much faster than their neutral forms. The structures of these ionophores are shown in Figure 5.1, Chapter V. The deprotonated form of A23187 reacts with Ni(II) with a rate constant of 3.3×10^6 in 80% methanol-water. The rate constant for the formation of the complexes of Ni(II) with deprotonated form of the carboxylic acid ionophore Lasalocid A is 6.0×10^5 $M^{-1}s^{-1}$ (in methanol).[27] Much lower values are expected for a similar reaction involving monoprotonated form ionomycin because of the presence of the β-diketone moiety.

The values of dissociation rate constant (k_{-HE}) for NiI and $Ni(DMHD)^+$ were calculated to be 49.0 and 480 $M^{-1}s^{-1}$, respectively. The difference in these values can be explained by the difference in the denticity of ionomycin and DMHD. Since octahedral geometry is common for Ni(II) compounds,[28] it is reasonable to assume that the structure of NiI complex is very similar to the structure of CaI shown in Figure 5.2, Chapter V. In this structure, ionomycin acts as a hexadentate ligand containing several linked chelate rings. On the other hand, DMHD forms simple bidentate chelate complexes. Before the dissociation of the β-diketone moiety in ionomycin, the necessity to open successive linked chelate rings, particularly those containing donor atoms that cannot be protonated (i.e., pyran and the alcohol oxygen atoms) is most likely responsible for smaller value of k_{-HE}.

iv) Effect of ionic strength on metal-β-diketone complexation

From the kinetic data obtained for the reactions of DMHD with Ni(II), the effect of the ionic strength on these reactions may be analysed. It is a well-recognized trend that the rate constant increases with increasing ionic strength when the reactants have charges of the same sign and the rate constant decreases with increasing ionic strength when the reactants have charges of opposite sign.[29,30] The value of k_{-HE} increases by a factor of 2.3 as the ionic strength increases from 0.050 to 0.50 M. This observation may be explained based on the fact that the electrolyte reduces the electrostatic repulsion between the two reacting ions having charges of the same sign (H^+, Ni-DMHD$^+$).

The value of k_{HE} increases 1.9 times as the ionic strength increases from 0.050 to 0.50 M. This change is unexpected due to the neutral charge of the ligand. However, the difference in the type of electrolyte used for the two studies ($NaClO_4$ versus Et_4NClO_4) may be a reason for this anomaly. It is possible that Na^+ forms an adduct with DMHD, such as shown in Figure 8.2, which will make the reacting ligand species positively charged.

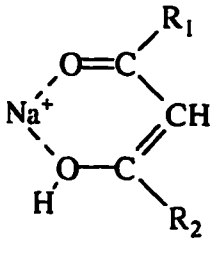

Figure 8.2. Proposed NaDMHD$^+$ adduct.

C. Reactivity of the Enolate Form of β-Diketones

To avoid the use of buffers and to maintain pseudo-first order conditions, most studies of β-diketones have been performed at very low pH* (or pH) values.[9,15-25,31-43] At such low pH* values the presence of the enolate form in most β-diketones systems is usually negligible. However, if the pKa of the enol form is low (< 4), the contribution by the enolate in the metal complexation reactions becomes significant. In such cases, the reactions of metal ions with the enol form of β-diketones generally proceed by a pathway with an inverse dependence on acid concentration which proceeds parallel to the acid-independent pathway. The mechanism for these reactions is shown in Scheme 8.6. This mechanism is an extension of the mechanism shown in Scheme 8.4. In this scheme $[ME^*H]^{n+}$ and $[ME^*]^{(n-1)+}$ are the intermediates in which only one end of the β-diketone is attached to the metal center. If the equilibria between these intermediates as well as HE and E^- are maintained, an expression for the acid dependence of k_{HE} can be derived as shown by equation 8.9.[18]

Scheme 8.6

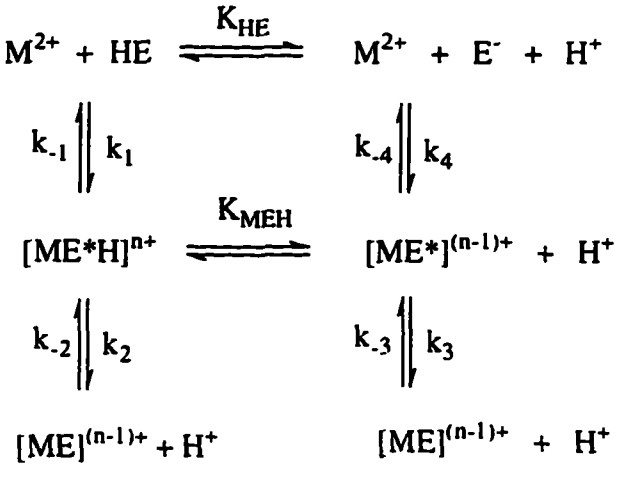

$$k_{HE} = \frac{k_1 + K_{HE}k_4/[H^+]}{1 + \dfrac{k_{-1} + K_{MEH}k_{-4}/[H^+]}{k_2 + K_{MEH}k_3/[H^+]}} \qquad (8.9)$$

Analysis of the above expression can be simplified by considering its two limiting forms.[18] If $(k_2 + K_{MEH}k_3/[H^+]) >> (k_{-1} + K_{MEH}k_{-4}/[H^+])$, then equation 8.9 takes the form of equation 8.10, and if $(k_2 + K_{MEH}k_3/[H^+]) << (k_{-1} + K_{MEH}k_{-4}/[H^+])$, then equation 8.9 takes the form of equation 8.11. Both equations 8.10 and 8.11 predict a linear relationship between k_{HE} and $1/[H^+]$.

$$k_{HE} = k_1 + \frac{K_{HE}k_4}{[H^+]} \qquad (8.10)$$

$$k_{HE} = \frac{k_1k_2}{k_{-1}} + \frac{K_{HE}(k_4/k_{-4})k_3}{[H^+]} \qquad (8.11)$$

If the enolate form of the β-diketone participates in the metal complex formation, then according to equations 8.7 and 8.8, an inverse-acid dependence is observed. Such behavior is seen for the reaction of 4,4,4-trifluoro-1-(2-thienyl)butane-1,3-dione (HTTA) with Ni(II).[18] The value for the pKa of the enol form of HTTA is 4.0. The plot of k_{HE} versus $1/[H^+]$ is a straight line where the values for the rate constants for Ni(II) complexation by enol (2.3 $M^{-1}s^{-1}$) and the enolate (1 x 10^4 $M^{-1}s^{-1}$) forms are calculated from the intercept and the slope of the plot, respectively. It can be seen that the enolate form of HTTA reacts approximately four orders of magnitude faster than the enol form. Similar results are obtain for the reaction of 1-phenylbutane-1,3-dione with Ni(II) in methanol-water where the formation rate constant for the enolate form (2.7 x 10^4 M^{-1} s^{-1}) is approximately four orders of magnitude higher than that for the enol form

(3.21 $M^{-1}s^{-1}$).[23] Generally, the rate constants for metal complexation of the enolate form are close to those predicted by the I_d mechanism.[1]

For ionomycin and DMHD, the inverse acid dependence of k_{HE} was not observed. The values of log K_{He} calculated for these ligands are 11.88 and 11.20, respectively (see Table 8.2). These values suggest that the concentration of the enolate form of the ligand was negligible (10 ppb) in the kinetic studies of ionomycin and DMHD with Ni(II).

D. Reactions of Ionomycin with Mg(II) and the Effect of Buffers on these Reactions

The reactions of ionomycin with Mg(II) may be envisaged to proceed through three possible pathways. These pathways, as shown in Scheme 8.7, are: i) the reaction of Mg(II) with doubly protonated ligand H_2I, ii) the reaction of Mg(II) with the monoprotonated ligand HI^-, and iii) the reaction of Mg(II) with unprotonated ligand, I^{2-}.

Pathway (i) is expected to be much slower than pathways (ii) and (iii) because it involves the neutral form of the ligand (H_2I). It is speculated that the carboxylate group in the carboxylic acid ionophores serves as an initial point of attachment in the metal complexation process.[44] The terminal location of this group on the backbone of the ionomycin molecule, as opposed to the inner cavity location, supports such a role of this moiety. In H_2I, the carboxylate group is protonated and therefore, the electrostatic attraction for the metal ion is minimal; consequently, it is not as efficient in performing the role of metal-catching as its ionized form. It was pointed out earlier that for A23187 the rate constant for the pathway involving the unprotonated form of ligand is 3×10^4 times greater than that for the pathway involving the protonated form.

Scheme 8.7

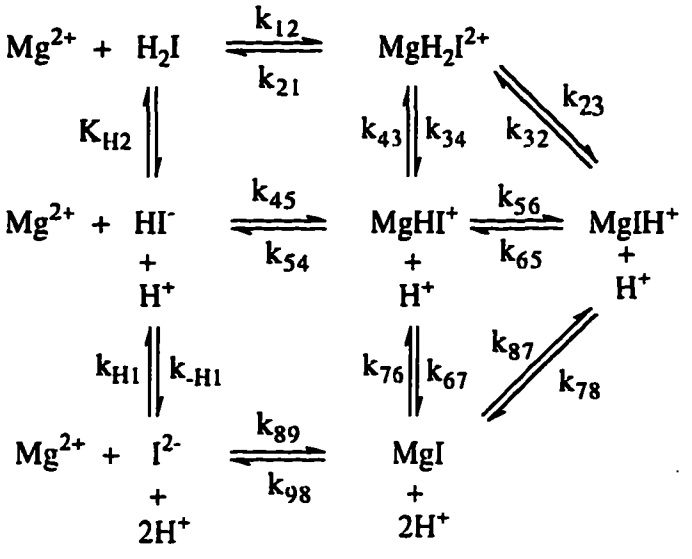

Additional support for the above argument comes from the comparison of the k_{obs} values for the reactions Ni(II) with ionomycin and Mg(II) with ionomycin. The former reactions were performed at low pH* where most of the ligand (> 99.9%) is present as H_2I. With Mg(II), the reactions were performed at mildly basic pH* values where a significant amount (86% to 99%) of the total ligand is present as HI^-. It was observed that the reaction of H_2I with Ni(II) proceeds with k_{obs} values (at $[H_2I] \approx 10\ \mu M$ and $[M^{2+}] \approx 1$ mM) that are at least 100 times smaller than the k_{obs} values for the reactions of ionomycin (mostly HI^-) with Mg(II). Although, the nature of the metal ion and the pH* conditions for the two types of reactions are different, neither of these factors is expected to affect k_{obs} by two orders of magnitude. The results from our studies show that k_{obs} values for the reaction of Ni(II) with ionomycin are independent of the pH* in the range 3.3 to 5.0. And it is reported that the nature of the metal ion does not effect the kinetics of metal-β-diketone systems significantly.[1] From these findings it can be concluded that the reactivity of H_2I is much lower then that of HI^-.

Which pathway (ii or iii) predominates, depends on the comparative rates of conversion of HI^- to I^{2-} versus the consumption of HI^- through pathway (ii). To analyze these pathways would require the value of k_{45} which, unfortunately, cannot be obtained from the available data. However, some calculations may be performed to speculate on the contribution of the two pathways. Under the conditions of our study (pH* < 8.8), 99.92 % of the total ligand exists in the HI^-. The rate constant for the deprotonation of HI^-, k_{-H1}, is estimated to be ~0.01 s^{-1} from the values of the protonation constant K_{H2} (8.3 x 10^{11} M^{-1}) and the rate constant for protonation of the enolate form ($k_{H1} = 10^{10}$ $M^{-1}s^{-1}$). Therefore, although pathway (iii) is expected to be very rapid ($k_{89} \approx 10^6$ $M^{-1}s^{-1}$ based on the I_d mechanism), product formation through this pathway is dependent on the conversion of HI^- to I^{2-} which is comparatively slow.

Although the extent of the contribution from pathways (ii) and (iii) are not clear, we found that the features of the kinetic data observed can be explained based on a mechanism where pathway (ii) is predominant. Before a more elaborate version of this pathway is discussed, it is useful to summarize the results of the kinetic studies. The summary is presented as follows.

1) The values of k_{obs} increase with increasing $[OH^-]$. At a constant concentration of the conjugate base form of the buffer, the plots of k_{obs} versus $[OH^-]$ were linear in the pH* range of 7.6 to 8.4. The straight lines obtained for the different concentrations of the buffers converge as $[OH^-]$ approaches 0.

2) The values of k_{obs} increase with increasing concentration of the conjugate base form of the buffer, $[B^-]$. At constant pH* values, the plots of k_{obs} versus $[B^-]$ show saturation behavior. The curves obtained at different pH* values converge towards a common value as $[B^-]$ approaches 0. When the observed rate constants at a given pH* value are plotted as a function of $K_H[B^-]$ (where K_H is the protonation

constant of the buffer), a single saturation type curve is obtained regardless of the type of buffer.

3) At a given pH*, the plots of k_{obs} versus $[Mg^{2+}]$ showed saturation type of behavior consistent with equation 8.12, where p_1 and p_2 are the two parameters.

$$k_{obs} = \frac{p_1 [Mg^{2+}]}{1 + p_2 [Mg^{2+}]} \qquad (8.12)$$

The preceding observations are consistent with the mechanism shown in Scheme 8.8. According to this scheme, the ionomycin molecule undergoes a rearrangement prior to reacting with the metal ion. k_r and k_{-r} represent the rate constants for the forward and reverse paths for the rearrangement step.

Scheme 8.8

$$HI^- \underset{k_{-r}}{\overset{k_r}{\rightleftharpoons}} [HI^-]^*$$

$$Mg^{2+} + [HI^-]^* \underset{k_{54}}{\overset{k_{45}}{\rightleftharpoons}} MgHI^+ \xrightarrow{k_{67}} MgI + H^+$$

Assuming a steady-state for the intermediates $[HI^-]^*$ and $[MgHI^+]$, the rate law for Scheme 8.8 is given by equation 8.13. Under pseudo-first-order conditions of excess $[Mg^{2+}]$, the value of k_{obs} is given by equation 8.14. The expression for k_{obs} has a form that is consistent with the behavior observed for the metal ion dependence for these reactions.

$$\frac{d[MgI]}{dt} = \frac{k_r k_{45} k_{67} [Mg^{2+}] [HI]_{tot}}{k_{-r}(k_{54} + k_{67}) + (k_{45} k_{67} [Mg^{2+}])} \tag{8.13}$$

$$k_{obs} = \frac{\frac{k_r k_{45} k_{67}}{(k_{54} + k_{67}) k_{-r}} [Mg^{2+}]}{1 + \frac{k_{45} k_{67}}{(k_{54} + k_{67}) k_{-r}} [Mg^{2+}]} \tag{8.14}$$

The behavior observed as a function of $[OH^-]$ may be explained based on a specific-base catalysis of the rearrangement step. The possibility for such a catalysis originates from the fact that in order for the metal ion to bind to the β-diketone moiety of ionomycin, the hydrogen bond between the proton and the oxygen atom has to break. This process can be catalyzed by the hydroxide ion. The value for the rate constant k_r for the step [HI]–>[HI]* may be obtained by evaluating p_1/p_2, where the values of p_1 and p_2 are obtained from the nonlinear least-square fitting of the k_{obs}, $[Mg^{2+}]$ data to equation 8.12. The values obtained for p_1/p_2 are summarized in Table 7.18 of Chapter VII. These values have a linear dependence on $[OH^-]$.

The activated ligand molecule [HI]*, binds to the metal ion to give a protonated metal-ligand complex, $MgHI^+$. The results obtained from the study of the metal-ligand equilibria are consistent with the existence of $MgHI^+$.[13] It is believed that the basic form of buffer catalyzes the abstraction of proton from the $MgHI^+$ intermediate, i.e., the step represented by the rate constant k_{67}. According to equation 8.14, under the conditions where $k_{67} >> k_{54}$, the value of k_{obs} becomes independent of k_{67}. This fact is consistent with the kinetic data which show that the value of k_{obs} becomes constant at higher buffer concentrations.

The mechanism presented here for the reactions of ionomycin with Mg(II) also explains the converging behavior of the plots of k_{obs} versus the concentration of specific or general base. The plots show that at very low $[OH^-]$, the general base catalysis is

negligible. This is true, because at low [OH^-], the step [HI]–>[HI]* becomes rate-limiting. Similarly, in the absence of [B^-] the step [$MgHI^+$]–>[MgI] becomes rate-limiting and the effect of OH^- catalysis becomes negligible. At the higher concentrations of [B^-], the deprotonation of [$MgHI^+$] becomes faster than the preceding step of the formation of $MgHI^+$ and thus the values of k_{obs} show a saturation type behavior.

It is seen that the principle of microscopic reversibility is observed for the buffer catalyzed step. According to this principle, if a certain series of steps constitutes the mechanism of a forward reaction, the mechanism of the reverse reaction is given by the same steps traversed backwards.[45,46] This means that, since the forward reactions of the formation of the metal complex is general-base catalyzed, the dissociation is expected to be general-acid catalyzed. This is observed to be true since the plots of k_{obs} for the dissociation reactions versus K_a[HB] (where K_a is the acid dissociation constant) for different buffers gave a single curve. Although to apply the principle of microscopic reversibility, the forward and the reverse reactions need to be performed under the same conditions, in our studies the pH* conditions were different. Nevertheless, the qualitative behavior of the catalytic effects on these reactions is not expected to change as a function of pH* and thus the above arguments are valid.

Conclusion

It is found that ionomycin exists in both enol and keto forms in the polar solvent systems. In 80% methanol-water the enol content is 88%. The keto-enol interconversion is catalyzed by the conjugate base form of the buffers. In addition, an intramolecular base-catalyzed mechanism is proposed. The reactions of ionomycin with Ni(II) at low pH* proceed through the enol form of the ligand. This mechanism is similar to that of

DMHD which shows that at low pH* values ionomycin behaves as a simple β-diketone. The formation and dissociation rate constants for NiI complex are approximately one order of magnitude smaller than that of DMHD. The smaller values of k_{HE} and k_{-HE} for ionomycin compared to DMHD are explained on the basis of steric effects and denticity of the ligands.

A mechanism is proposed for the reaction of ionomycin with Mg(II). This mechanism is based on the kinetic data that was obtained at pH* values close to physiological pH*. Thus, this mechanism may be operative in biological systems. According to this mechanism the metal-ligand product formation takes place through a pathway in which the monoprotonated form of ionomycin (HI^-) reacts with the metal ion. The reaction proceeds through the formation of a metal-ligand precursor complex, $MgHI^+$. The existence of a protonated metal-ligand complex is consistent with the equilibrium studies. The reactions are found to be specific- and general-base catalyzed. These results provide a note of caution for studies where buffers are present when ionomycin is used as an ionophore.

REFERENCES

1) Hynes, M. J. *Rev. Inorg. Chem.* **1990**, *11*, 21-78.

2) Toullec, J. In *The Chemistry of Functional Groups*; Rappoport, Z., Ed.; John Wiley: New York, 1990, pp 323-398.

3) Sawyer, D. T.; Heineman, W. R.; Beebe, J. M. *Chemistry Experiments for Instrumental Methods*; Wiley: New York, 1984, pp 298-299.

4) Burdett, J. L.; Rogers, M. T. *J. Am. Chem. Soc.* **1964**, *86*, 2105-2109.

5) Kabachnik, M. I.; Ioffe, S. T.; Popov, E. M.; Vatsuro, K. V. *Tetrahedron* **1961**, *12*, 76-94.

6) Schweitzer, G. K.; Benson, E. W. *J. Chem. Eng. Data* **1968**, *13*, 452-453.

7) Allen, G.; Dwek, R., A. *J. Chem. Soc. (B)* **1966**, 161-163.

8) Koshimura, H.; Saito, J.; Okubo, T. *Bull. Chem. Soc. Japan* **1979**, *46*, 632-634.

9) Hynes, M. J.; Mooney, M. T.; Moloney, A. *J. Chem. Soc., Dalton Trans.* **1993**, 313-318.

10) Pretsch, E.; Seibl, J.; Simon, W.; Clarc, T. *Spectral Data for Structure Determination of Organic Compounds*; Springer-Verlag: New York, 1983, p C90.

11) Matsunaga, S.; Fusetani, N.; Kato, Y. *J. Am. Chem. Soc.* **1991**, *113*, 9690-9692.

12) Turner, W. B.; Aldridge, D. C. *Fungal Metabolites II*; Academic: New York, 1983, p 824.

13) Stiles, M. K.; Craig, M. E.; Gunnell, S. L. N.; Pfeiffer, D. R.; Taylor, R. W. *J. Biol. Chem.* **1991**, *266*, 8336-8342.

14) Eigen, M. *Pure Appl. Chem.* **1963**, *6*, 97-115.

15) Hynes, M. J.; O'Shea, M. T. *J. Chem. Soc., Dalton Trans.* **1983**, 331-336.

16) Hynes, M. J.; Blanco, C. A.; Mooney, M. T. *J. Chem. Soc., Perkin Trans. 2* **1991**, 2055-2060.

17) Hynes, M. J.; Kelly, D. F. *J. Chem. Soc., Dalton Trans.* **1988**, 905-908.

18) Jaffe, M. R.; Fay, D. P.; Cefola, M.; Sutin, N. *J. Am. Chem. Soc.* **1971**, *93*, 2878-2886.

19) Hynes, M. J.; O'Mara, C.; Kelly, D. F. *Inorg. Chim. Acta* **1986**, *120*, 131-134.

20) Blanco, C. A.; Hynes, M. J. *Can. J. Chem* **1992**, *70*, 2285-2289.

21) Hynes, M. J.; O'Regan, B. D. *J. Chem. Soc., Dalton Trans.* **1980**, 7-13.

22) Hynes, M. J.; O'Regan, B. D. *Proc. Roy. Irish Academy* **1977**, *B77*, 285-294.

23) Hynes, M. J.; Mooney, M. T. *Proc. Roy. Irish Acad.* **1989**, *89B*, 441-451.

24) Hynes, J. M.; O'Regan, B. D. *J. Chem. Soc., Dalton Trans.* **1979**, 162-166.

25) Blanco, C.; Hynes, M. *Bull. Soc. Chim. Fr.*, **1989**, 611-614.

26) Thomas, T. P. *Ph.D. Thesis* **1991**, The University of Oklahoma, Norman, OK.

27) Garcia-Rosas, J.; Schneider, H. *Inorg. Chim. Acta* **1982**, *70*, 183-187.

28) Cotton, F. A.; Wilkinson, G. *Advanced Inorganic Chemistry*; Wiley: New Delhi, 1988, pp 892-901.

29) Wilkins, R. G. *Kinetics and Mechanism of Reactions of Transition Metal Complexes*; 2nd ed.; VCH: New York, 1991, pp 110-116.

30) Schmid, R.; Sapunov, V. N. *Non-Formal Kinetics*; Verlag: Florida, 1982, pp 152-154.

31) Hynes, M. J.; Kelly, D., F. *Inorg. Chim. Acta* **1991**, *188*, 243-249.

32) Hynes, M. J.; Kelly, D. F. *Inorg. Chim. Acta* **1991**, *187*, 159-165.

33) Hynes, M. J.; Kelly, D. F. *Inorg. Chim. Acta* **1991**, *181*, 93-98.

34) Hynes, M. J. *J. Chem. Soc., Faraday Trans.* **1992**, *88*, 3533-3536.

35) Hynes, M. J.; O'Mara, C.; Kelly, D. F. *Inorg. Chim. Acta* **1980**, *120*, 131-134.

36) Hynes, M. J.; O'Shea, M. T. *Inorg. Chim. Acta* **1983**, *73*, 201-206.

37) Blanco, C.; Hynes, M., J. *Inorg. Chim. Acta* **1990**, *173*, 115-120.

38) Hynes, M. J.; Walsh, J. *J. Chem. Soc., Dalton Trans.* **1985**, 1543-1546.

39) Hynes, M. J.; Walsh, J. *J. Chem. Soc., Dalton Trans.* **1986**, 2243-2246.

40) Hynes, M. J.; O'Regan, B. D. *J. Chem. Soc., Dalton Trans.* **1976**, 1200-1202.

41) Blanco, C. A.; Hernando, J. M.; Mateo, M. *Int. J. Chem. Kinet.* **1992**, *24*, 533-540.

42) Hynes, M. J.; Walsh, J. *J. Chem. Soc., Dalton Trans.* **1985**, 2565-2569.

43) Hernando, J. M.; Montero, O.; Blanco, C. *Collect. Czech. Chem. Commun.* **1984**, *55*, 1984-1991.

44) Painter, G. R.; Pressman, B. C. *Top. Curr. Chem.* **1982**, *101*, 83-110.

45) Burwell, R. L.; Pearson, R. G. *J. Phy. Chem.* **1966**, *70*, 300-303.

46) Krupka, R. M.; Kaplan, H.; Laidler, K. J. *Trans. Faraday Soc.* **1966**, *62*, 2754-2759.

APPENDIX I

A. Derivation of Equations 3.6 and 3.8

Scheme 3.1

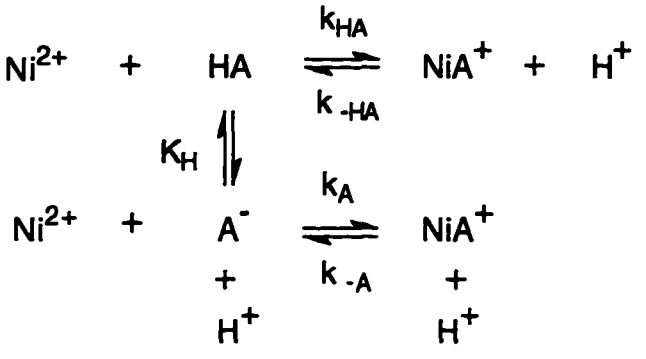

In the scheme 3.1, k_{HA} and k_A represent the rate constants for the forward reaction of the protonated and the deprotonated forms of the ligand, respectively, k_{-HA} and k_{-A} represent the rate constants for the reverse reaction of the protonated and the deprotonated forms of the ligand, respectively, and K_H represents the protonation constant for hydroxamic acid.

If $[HA]_{tot}$ is the total concentration of the free hydroxamic acid (HA + A^-), the rate of disappearance of ligand may be described by

$$\frac{-d[HA]_{tot}}{dt} = k_{HA}[Ni^{2+}][HA] + k_A[A^-][Ni^{2+}] - k_{-HA}[NiA^+][H^+] - k_{-A}[NiA^+] \qquad (A.1)$$

The mass balance equation for hydroxamic acid is

$$[HA]_{tot,0} + [NiA^+]_0 = [HA]_{tot} + [NiA^+] = [HA]_{tot,\infty} + [NiA^+]_\infty \qquad (A.2)$$

where the subscripts 0 and ∞ refer to the initial and equilibrium concentrations of a species, respectively, and absence of those subscripts denote instantaneous concentrations.

From equation A.2, it follows that

$$[NiA^+] = [HA]_{tot,\infty} + [NiA^+]_\infty - [HA]_{tot} \qquad (A.3)$$

By using relations, $K_H = \dfrac{[HA]}{[H^+]\,[A^-]}$, and $[HA]_{tot} = [HA] + [A^-]$, following equations may be derived,

$$[HA] = K_H\,[H^+]\,[A^-] \text{ and } [A^-] = \frac{[HA]_{tot}}{1 + K_H\,[H^+]} \qquad (A.4)$$

Substituting the expressions for [HA], $[A^-]$ and $[NiA^+]$ in equation A.1 yields

$$\frac{-d[HA]_{tot}}{dt} = \left[\frac{(k_A + k_{HA}\,K_H\,[H^+])\,[Ni^{2+}]}{1 + K_H\,[H^+]}\right][HA]_{tot} - (k_{-HA}\,[H^+] + k_{-A}) \times ([HA]_{tot,\infty} + [NiA^+]_\infty - [HA]_{tot}) \qquad (A.5)$$

or,

$$\frac{-d[HA]_{tot}}{dt} = \alpha\,[HA]_{tot} - \beta\,([HA]_{tot,\infty} + [NiA^+]_\infty - [HA]_{tot}) \qquad (A.6)$$

where $\alpha = \left[\dfrac{(k_A + k_{HA}\,K_H\,[H^+])\,[Ni^{2+}]}{1 + K_H\,[H^+]}\right]$ and $\beta = k_{-HA}\,[H^+] + k_{-A}$

At equilibrium, the overall rate = 0 and $[HA]_{tot} = [HA]_{tot,\infty}$; therefore,

$$\alpha\,[HA]_{tot} - \beta\,[NiA^+]_\infty = 0;\ \text{or,}\ [NiA^+]_\infty = \frac{\alpha\,[HA]_{tot,\infty}}{\beta}$$

Substituting the expression for $[NiA^+]_\infty$ in equation A.6 yields,

$$\frac{-d[HA]_{tot}}{dt} = \alpha\,[HA]_{tot} - \beta\left[[HA]_{tot,\infty} + \frac{\alpha\,[HA]_{tot,\infty}}{\beta} - [HA]_{tot}\right] \qquad (A.7)$$

$$= \alpha\,[HA]_{tot} - \beta\,[HA]_{tot,\infty} - \alpha\,[HA]_{tot,\infty} + \beta\,[HA]_{tot}$$

$$= (\alpha + \beta)\,([HA]_{tot} - [HA]_{tot,\infty})$$

Substituting the expressions for $[\alpha]$ and $[\beta]$ yields the final rate law (equation 3.8),

$$\frac{-d[HA]_{tot}}{dt} = \left[\frac{(k_A + k_{HA}K_H[H^+])[Ni^{2+}]}{1 + K_H[H^+]} + k_{-A} + k_{-HA}[H^+]\right]([HA]_{tot} - [HA]_{tot,\infty}) \qquad (A.8)$$

Under conditions, where $[Ni^{2+}] > 10\,[HA]_{tot}$ (*i.e.*, pseudo-first-order-conditions) and when $[H^+]$ is kept constant with buffers, the term in square brackets in expression A.8 is a constant, k_{obs}, for a given value of $[Ni^{2+}]$,

$$\frac{-d[HA]_{tot}}{dt} = k_{obs}([HA]_{tot} - [HA]_{tot,\infty}) \qquad (A.9)$$

Rearrangement of equation A.9 yields

$$\frac{d[HA]_{tot}}{([HA]_{tot} - [HA]_{tot,\infty})} = - k_{obs}\, dt \qquad (A.10)$$

Integration of equation A.10 is represented by equation A.11.

$$\int_{t=0}^{t=t} \frac{d[HA]_{tot}}{([HA]_{tot} - [HA]_{tot,\infty})} = - k_{obs} \int_{t=0}^{t=t} dt \qquad (A.11)$$

The left hand side of equation A.11 represents the integral function of the type shown by equation A.12 (CRC handbook, 67th edition, CRC press: Florida, p. A-21), where a and b are constants,

$$\int \frac{dx}{(a+b)} = \frac{1}{b} \ln (a + bx) \qquad (A.12)$$

If $x = [HA]_{tot}$, $a = - [HA]_{tot,\infty}$ and $b = 1$, then equation A.11 becomes

$$\ln ([HA]_{tot} - [HA]_{tot,\infty}) \Big|_{t=0}^{t=t} = - k_{obs}\, t \Big|_{t=0}^{t=t} \qquad (A.13)$$

Evaluating equation A.13 between the limits $t = 0$ to $t = t$ yields

$$\ln ([HA]_{tot} - [HA]_{tot,\infty}) - \ln ([HA]_{tot,0} - [HA]_{tot,\infty}) = - k_{obs}\, t \qquad (A.14)$$

The absorbance A_i of the reacting solution at any time, in a observation cell of path length 1 cm, is given by the relationship

$$A_i = \varepsilon_{A^-} [A^-] + \varepsilon_{HA} [HA] + \varepsilon_{NiA} [NiA^+] + A_x \qquad (A.15)$$

where, ε_i is the molar absorptivity of the species i and, A_x represents the contributions to the absorbance from buffers or excess Ni^{2+}. Since the concentrations of buffers or Ni^{2+} does not vary significantly during the reaction, A_x is a constant quantity.

Using equations A.3 and A.4, the quantities for $[NiA^+]$, [HA] and $[A^-]$ may be replaced in equation A.15, yielding the following relationship,

$$A_i = \varepsilon_{A^-}\left[\frac{[HA]_{tot}}{1 + K_H [H^+]}\right] + \varepsilon_{HA}\left[\frac{K_H [H^+] [HA]_{tot}}{1 + K_H [H^+]}\right] + \varepsilon_{NiA^+} ([HA]_{tot,0} + [NiA^+]_0 - [HA]_{tot}) + A_x \qquad (A.16)$$

Rearranging A.16 yields

$$A_i = \left[\frac{\varepsilon_A - \varepsilon_{HA} K_H [H^+]}{1 + K_H [H^+]} - \varepsilon_{NiA^+}\right] [HA]_{tot} + \varepsilon_{NiA} ([HA]_{tot,0} + [NiA^+]_0) + A_x \qquad (A.17)$$

At $t = 0$, $A_i = A_0$ and $[HA]_{tot} = [HA]_{tot,0}$, and therefore

$$A_0 = \left[\frac{\varepsilon_A - \varepsilon_{HA} K_H [H^+]}{1 + K_H [H^+]} - \varepsilon_{NiA^+} \right] [HA]_{tot,0} + \varepsilon_{NiA} ([HA]_{tot,0} + [NiA^+]_0) + A_x \tag{A.18}$$

At $t = \infty$, $A_i = A_\infty$ and $[HA]_{tot} = [HA]_{tot,\infty}$, and therefore

$$A_\infty = \left[\frac{\varepsilon_A - \varepsilon_{HA} K_H [H^+]}{1 + K_H [H^+]} - \varepsilon_{NiA^+} \right] [HA]_{tot,\infty} + \varepsilon_{NiA} ([HA]_{tot,0} + [NiA^+]_0) + A_x \tag{A.19}$$

Using equations A.17, A.18 and A.19, the expressions for $(A_i - A_\infty)$ and $(A_0 - A_\infty)$ can be evaluated, as shown by equations A.20 and A.21.

$$(A_i - A_\infty) = \left[\frac{\varepsilon_A - \varepsilon_{HA} K_H [H^+]}{1 + K_H [H^+]} - \varepsilon_{NiA^+} \right] ([HA]_{tot} + [HA]_{tot,\infty}) \tag{A.20}$$

$$(A_0 - A_\infty) = \left[\frac{\varepsilon_A - \varepsilon_{HA} K_H [H^+]}{1 + K_H [H^+]} - \varepsilon_{NiA^+} \right] ([HA]_{tot,0} + [HA]_{tot,\infty}) \tag{A.21}$$

Taking natural log on both sides of the equations A.20 and A.21 and then subtracting equation A.20 from equation A.21 yields

$$\ln (A_i - A_\infty) - \ln (A_0 - A_\infty) = \ln ([HA]_{tot} + [HA]_{tot,\infty}) - \ln ([HA]_{tot,0} + [HA]_{tot,\infty}) \quad (A.22)$$

Combining equations A.14 and A.22 gives,

$$\ln (A_i - A_\infty) - \ln (A_0 - A_\infty) = -k_{obs}\, t \quad (A.23)$$

If the intermediates of the reaction are assumed to be in steady-state, then

$$\frac{-d[HA]_{tot}}{dt} = \frac{d[NiA^+]}{dt}$$

and equation A.24 (or equation 3.6) may be written where the square brackets represent the absolute value of the enclosed quantity.

$$\ln [A_i - A_\infty] - \ln [A_0 - A_\infty] = -k_{obs}\, t \quad (A.24)$$

B. Derivation of Equation 3.15

The conditional stability constant for 1:1 Ni(II)-hydroxamate complex, K'_{NiA}, is defined as

$$K'_{NiA} = \frac{[NiA^+]_\infty}{[Ni^{2+}]_\infty [HA]_{tot,\infty}} \tag{A.25}$$

where $[HA]_{tot,\infty} = [A^-]_\infty + [HA]_\infty$.

In the mass balance equation for hydroxamic acid $[NiA^+]_0 = 0$ and, therefore,

$$[HA]_{tot,0} = [HA]_{tot,\infty} + [NiA^+]_\infty \tag{A.26}$$

From equations A.25 and A.26,

$$[HA]_{tot,\infty} = \frac{[HA]_{tot,0}}{1 + K'_{NiA}[Ni^{2+}]_\infty} \tag{A.27}$$

and

$$[NiA^+] = \frac{K'_{NiA}[Ni^{2+}]_\infty [HA]_{tot,0}}{1 + K'_{NiA}[Ni^{2+}]_\infty} \tag{A.28}$$

The value of A_∞ at a given $[Ni^{2+}]$, is given by the equation

$$A_{\infty,Ni} = \varepsilon_{HA}[HA]_{tot,\infty} + \varepsilon_{NiA^+}[NiA^+] \tag{A.29}$$

Substituting the expressions for $[HA]_{tot,\infty}$ and $[NiA^+]$ from equations A.27 and A.28 yields

$$A_{\infty, Ni} = \frac{\varepsilon_{HA} [HA]_{tot, 0}}{1 + K'_{NiA} [Ni^{2+}]_\infty} + \frac{\varepsilon_{NiA^+} [HA]_{tot, 0} K'_{NiA} [Ni^{2+}]_\infty}{1 + K'_{NiA} [Ni^{2+}]_\infty} \quad (A.30)$$

Now, $\varepsilon_{HA} [HA]_{tot,0} = A_0$ and $\varepsilon_{NiA^+} [HA]_{tot,0} = A_{sat}$, where A_0 and A_{sat} are the initial ($[Ni^{2+}] = 0$) and the maximum (saturated with $[Ni^{2+}]$) absorbance values, respectively, and therefore,

$$A_{\infty, Ni} = \frac{A_0 + A_{sat} K'_{NiA} [Ni^{2+}]_\infty}{1 + K'_{NiA} [Ni^{2+}]_\infty} \quad (A.31)$$

Subtracting A_0 from both sides of equation A.31 will yield

$$A_{\infty, Ni} - A_0 = \frac{(A_{sat} - A_0) K'_{NiA} [Ni^{2+}]_\infty}{1 + K'_{NiA} [Ni^{2+}]_\infty} \quad (A.32)$$

If ΔA_{Ni} is the value for the total absorbance change during a reaction at a given $[Ni^{2+}]$ and ΔA_{sat} is the value for the total absorbance change for the reaction at saturating levels of Ni^{2+}, these terms can be substituted for $A_{\infty, Ni} - A_0$ and $A_{sat} - A_0$ in equation A.32, respectively, to yield the final expression

$$\Delta A_{Ni} = \frac{\Delta A_{sat} K'_{NiA} [Ni^{2+}]_\infty}{1 + K'_{NiA} [Ni^{2+}]_\infty} \quad (A.33)$$

C. pH-Jump Method, Derivation of Equation 7.6

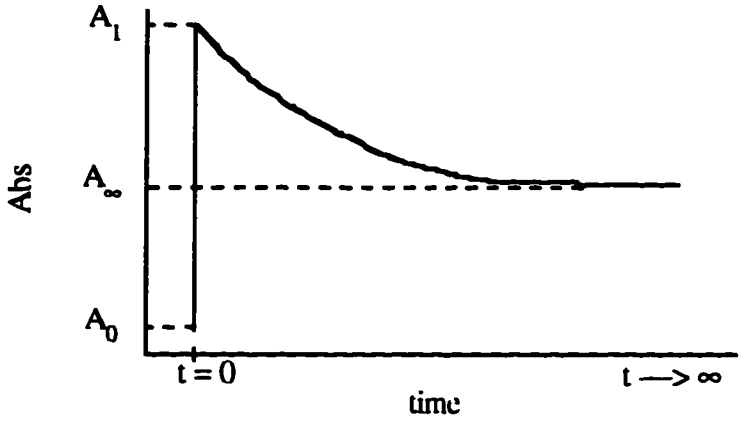

Figure A.1 The change in absorbance with time, in a pH-jump experiment for ionomycin or DMHD, when the process is monitored at the λ_{max} of the peak for the enol form of the ligand.

The following Scheme describes the pH-jump process, initiated by mixing a buffer (HB) and the enolate form of a ligand that exhibits keto-enol tautomerism. E^-, HE and HK represent the enolate, enol and the keto form of the ligand, respectively.

$$E^- + HB \underset{}{\overset{\text{(fast)}}{\rightleftharpoons}} HE + B^- \overset{\text{(slow)}}{\rightleftharpoons} HK + B^-$$

As illustrated in Figure A.1, the absorbance of the reaction mixture changes from A_0 to A_1, during the fast process, and from A_1 to A_∞, during the slow process. The concentration of the various forms of the ligand (L = E^-, HE, HK) may be represented by $[L]_0$ and $[L]_1$, where the subscripts "0" and "1" describe the time at which those concentrations are present. $[L]_\Delta$ represents the change in concentration of the ligand

between t = 1 to t = ∞.

At equilibrium, if the ratio of the concentrations of enol to keto form of the ligand is described by $K_{e/k}$, the following holds true,

$$K_{e/k} = \frac{[HE]_0}{[HK]_0} = \frac{[HE]_\infty}{[HK]_\infty} = \frac{[HE]_0 + [HE]_\Delta}{[HK]_0 + [HK]_\Delta} = \frac{[HE]_\Delta}{[HK]_\Delta} \qquad (A.34)$$

If the absorbance of the keto form of the ligand is negligible at the wavelength at which the process is being monitored, A_1 and A_∞ are given by equations A.35 and A. 36 where ε_{HE} is the molar absorptivity constant for the enol form of the ligand.

$$A_1 = \varepsilon_{HE}[HE]_0 + \varepsilon_{HE}[HE]_\Delta + \varepsilon_{HE}[HK]_\Delta \qquad (A.35)$$

$$A_\infty = \varepsilon_{HE}[HE]_0 + \varepsilon_{HE}[HE]_\Delta \qquad (A.36)$$

The mixed-mode protonation constant for the ligand is described by equation A.37.

$$K_{H1} = \frac{[HE]_0 + [HK]_0}{[E^-]\, a_{H^+}} \qquad (A.37)$$

Substituting $[HK]_0 = \frac{[HE]_0}{K_{e/k}}$, and $[E^-] = [HE]_\Delta + \frac{[HE]_\Delta}{K_{e/k}}$, and cancelling the common terms from the numerator and the denominator will give equation A.38.

$$[HE]_0 = (K_{H1}\, a_{H^+})\, [HE]_\Delta \qquad (A.38)$$

Substituting the right-hand side of equation A.38 for $[HE]_0$ in equations A.35 and A.36, and rearranging gives equations A.39 and A.40, respectively.

$$\varepsilon_{HE}[HE]_{\Delta} = \frac{A_1}{(1 + \frac{1}{K_{e/k}} + K_{H1}\, a_{H^+})} \tag{A.39}$$

$$\varepsilon_{HE}[HE]_{\Delta} = \frac{A_{\infty}}{(1 + K_{H1}\, a_{H^+})} \tag{A.40}$$

Equating the right hand sides of equations A.39 and A.40 to each other, rearranging, and substituting $(A_1 - A_{\infty}) = \Delta A$, yields the final expression given by equation A.41.

$$K_{e/k} = \frac{A_{\infty}}{\Delta A(1 + K_{H1}a_{H^+})} \tag{A.41}$$

D. General Solution for Scheme 7.2

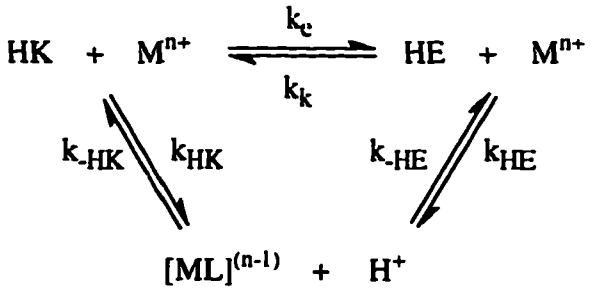

In the above scheme, if k_e, k_k, k_{HE}, k_{-HE}, k_{HK} and k_{-HK} are the rate-constants for the pathways shown in the scheme and if k'_{HE}, k'_{-HE}, k'_{HK} and k'_{-HK} are the pseudo-first order rate constants described by equations A.42–A.45, then the rate-laws may be written as given by equations A.46–A.48.

$$k'_{HE} = k_{HE}\,[M^{n+}] \tag{A.42}$$

$$k'_{-HE} = k_{-HE}\,[H^+] \tag{A.43}$$

$$k'_{HK} = k_{HK}\,[M^{n+}] \tag{A.44}$$

$$k'_{-HK} = k_{-HE}\,[H^+] \tag{A.45}$$

Rate laws:

$$\frac{d[HK]}{dt} = -k_e[HK] - k'_{HK}[HK] + k_k[HE] + k'_{-HK}[ML]^{(n-1)} \tag{A.46}$$

$$\frac{d[HE]}{dt} = k_e[HK] - k_k[HE] - k'_{HE}[HE] + k'_{-HE}[ML]^{(n-1)} \tag{A.47}$$

$$\frac{d[ML^{(n-1)}]}{dt} = k'_{HK}[HK] + k'_{HE}[HE] - k'_{-HK}[ML]^{(n-1)} - k'_{-HE}[ML]^{(n-1)} \tag{A.48}$$

The solution for the set of differential equations (A.46–A.48) may be obtained by solving the secular equation A.41, where λ represents the roots of the equations.[1]

$$\begin{bmatrix} k_e + k'_{HK} - \lambda & - k_k & - k'_{-HK} \\ - k_e & k_k + k'_{HE} - \lambda & - k'_{-HE} \\ - k'_{HK} & - k'_{HE} & k'_{-HK} + k'_{-HE} - \lambda \end{bmatrix} = 0 \tag{A.49}$$

Equation A.49 may be simplified by adding row 2 and row 3 to row 1, which yields

$$\begin{bmatrix} - \lambda & - \lambda & - \lambda \\ - k_e & k_k + k'_{HE} - \lambda & - k'_{-HE} \\ - k'_{HK} & - k'_{HE} & k'_{-HK} + k'_{-HE} - \lambda \end{bmatrix} = 0 \tag{A.50}$$

[1]The method is described in: Kell, L. M. *Differntial Equations, A brief Course with Applications* McGraw-Hill: New York, 1968; Chapter 7.

or,

$$-\lambda \begin{bmatrix} 1 & 1 & 1 \\ -k_e & k_k + k'_{HE} - \lambda & -k'_{-HE} \\ -k'_{HK} & -k'_{HE} & k_{-'HK} + k'_{-HE} - \lambda \end{bmatrix} = 0 \qquad \text{(A.51)}$$

According to equation A.51, either $\lambda = 0$, or,

$$\begin{bmatrix} 1 & 1 & 1 \\ -k_e & k_k + k'_{HE} - \lambda & -k'_{-HE} \\ -k'_{HK} & -k'_{HE} & k'_{-HK} + k'_{-HE} - \lambda \end{bmatrix} = 0 \qquad \text{(A.52)}$$

solving equation A.52 yields,

$$\{(k_k + k'_{HE} - \lambda)(k'_{-HK} + k'_{-HE} - \lambda) - k'_{HE}k'_{-HE}\} - \{-k_e(k'_{-HK} + k'_{-HE} - \lambda) - k'_{HK}k'_{-HE}\} + \{k_e k'_{HE} + k'_{HK}(k_k + k'_{HE} - \lambda)\} = 0 \qquad \text{(A.53)}$$

Rearrangement of equation A.53 yields,

$$\lambda^2 - (k_e + k_k + k'_{HK} + k'_{-HK} + k'_{HE} + k'_{-HE})\lambda + (k_e k'_{-HK} + k_e k'_{HE} + k_e k'_{-HE} + k'_{HK} k_k + k'_{HK} k'_{HE} + k'_{HK} k'_{-HE} + k_k k'_{-HK} + k_k k'_{-HE} + k'_{-HK} k'_{HE}) = 0 \quad \text{(A.54)}$$

Equation A.54 is a quadratic of the form $\lambda^2 + p\lambda + b = 0$, where the parameters p and b are defined by equations A.55 and A.56, respectively.

$$p = k_e + k_k + k'_{HK} + k'_{-HK} + k'_{HE} + k'_{-HE} \quad \text{(A.55)}$$

$$b = k_e k'_{-HK} + k_e k'_{HE} + k_e k'_{-HE} + k'_{HK} k_k + k'_{HK} k'_{HE} + k'_{HK} k'_{-HE} + k_k k'_{-HK} + k_k k'_{-HE} + k'_{-HK} k'_{HE} \quad \text{(A.56)}$$

Replacement of the psuedo-first-order rate constants in equations A.47 and A.48 using equations A.42–A.45, gives equations A.57 and A.58.

$$p = k_e + k_f + (k_{HE} + k_{HK})[M^{n+}] + (k_{-HE} + k_{-HK})[H^+] \quad \text{(A.57)}$$

$$b = k_e\{k_{HE}[M^{n+}] + (k_{-HK} + k_{-HE})[H^+]\} + k_{HK}[M^{n+}]\{k_f + k_{HE}[M^{n+}] + k_{-HE}[H^+]\} + k_f(k_{-HE} + k_{-HK})[H^+] + k_{HE}k_{-HE}[M^{n+}][H^+] \quad \text{(A.58)}$$

The roots of the quadratic equation A.54 are given by equation A.59, where q is given by equation A.60.

$$\lambda_{2,3} = 0.5\,(p \pm q) \tag{A.59}$$

$$q = (p^2 - 4b)^{1/2} \tag{A.60}$$

The binomial expansion of equation A.60 is given by

$$q = p\left[1 - \frac{1}{2}\left(\frac{4b}{p^2}\right) - \frac{1}{8}\left(\frac{4b}{p^2}\right)^2 + - - -\right] \tag{A.61}$$

If only the first two terms are retained, the value of the quantity q is given by equation

$$q = p - \frac{2b}{p} \tag{A.62}$$

Substitution of equation A.62 intp equation A.63 enables us to obtain the expressions for the roots of the equation A.54

$$\lambda_2 = p - \frac{b}{p} \tag{A.63}$$

$$\lambda_3 = \frac{b}{p} \tag{A.64}$$

APPENDIX II

Table A.1. Kinetic Data Obtained from the Stopped-Flow Experiments for the Reactions of Ni(II) with PNBHA Performed at 25 °C and $I = 0.010$ M ($NaClO_4$)

10^3 [Ni^{2+}]^a (M)	k_{obs} (s^{-1})	A_0	$A_{\infty, Ni}$	ΔA_{Ni}	n^b
pH = 5.43 (±0.01)					
2.0	25.9 ± 0.2	0.129 ± 0.001	0.180 ± 0.001	0.051 ± 0.001	7
3.0	26.8 ± 0.4	0.127 ± 0.002	0.200 ± 0.001	0.073 ± 0.001	7
4.0	29.4 ± 0.3	0.150 ± 0.008	0.239 ± 0.006	0.089 ± 0.002	8
5.0	29.6 ± 0.4	0.129 ± 0.002	0.241 ± 0.001	0.112 ± 0.001	10
8.0	34.8 ± 1.0	0.152 ± 0.026	0.299 ± 0.009	0.146 ± 0.020	7
10.0	36.5 ± 0.3	0.129 ± 0.004	0.308 ± 0.002	0.180 ± 0.004	8
15.0	43.8 ± 0.3	0.129 ± 0.005	0.354 ± 0.001	0.225 ± 0.005	9
pH = 5.60 (±0.01)					
1.0	16.6 ± 0.9	0.060 ± 0.002	0.107 ± 0.003	0.046 ± 0.002	4
2.0	20.0 ± 0.1	0.058 ± 0.002	0.146 ± 0.003	0.088 ± 0.002	4
3.0	21.4 ± 0.6	0.052 ± 0.005	0.176 ± 0.000	0.124 ± 0.005	4
4.0	21.9 ± 0.5	0.051 ± 0.002	0.208 ± 0.001	0.157 ± 0.002	4
5.0	23.7 ± 0.4	0.047 ± 0.001	0.225 ± 0.002	0.178 ± 0.004	4
7.5	27.4 ± 0.5	0.041 ± 0.002	0.270 ± 0.001	0.229 ± 0.002	4
10.0	30.3 ± 0.2	0.039 ± 0.002	0.308 ± 0.001	0.270 ± 0.002	4

Table A.1. Continued...

10^3 [Ni^{2+}][a] (M)	k_{obs} (s^{-1})	A_0	$A_{\infty, Ni}$	ΔA_{Ni}	n[b]
pH = 6.00 (±0.01)					
1.0	8.87 ± 0.06	0.109 ± 0.001	0.198 ± 0.002	0.090 ± 0.002	8
2.0	10.60 ± 0.04	0.111 ± 0.001	0.257 ± 0.001	0.146 ± 0.002	8
3.0	12.23 ± 0.06	0.114 ± 0.002	0.302 ± 0.001	0.188 ± 0.002	7
4.0	13.72 ± 0.08	0.117 ± 0.003	0.331 ± 0.002	0.214 ± 0.003	8
5.0	15.50 ± 0.08	0.118 ± 0.003	0.363 ± 0.001	0.244 ± 0.002	8
8.0	20.3 ± 0.2	0.138 ± 0.002	0.418 ± 0.001	0.280 ± 0.002	9
10.0	23.7 ± 0.1	0.135 ± 0.002	0.440 ± 0.001	0.305 ± 0.002	8
15.0	31.2 ± 0.1	0.146 ± 0.003	0.481 ± 0.001	0.334 ± 0.002	9
pH = 6.30 (±0.01)					
1.0	6.35 ± 0.03	0.106 ± 0.002	0.252 ± 0.002	0.145 ± 0.002	7
2.0	8.18 ± 0.04	0.101 ± 0.003	0.313 ± 0.005	0.212 ± 0.002	8
3.0	9.59 ± 0.05	0.104 ± 0.001	0.353 ± 0.002	0.250 ± 0.002	8
4.0	12.48 ± 0.05	0.134 ± 0.003	0.406 ± 0.002	0.271 ± 0.002	8
5.0	14.0 ± 0.1	0.106 ± 0.006	0.425 ± 0.002	0.326 ± 0.002	9
8.0	19.7 ± 0.1	0.118 ± 0.004	0.465 ± 0.001	0.347 ± 0.003	9
10.0	23.7 ± 0.1	0.122 ± 0.003	0.481 ± 0.001	0.358 ± 0.004	10
15.0	32.6 ± 0.2	0.138 ± 0.004	0.506 ± 0.001	0.368 ±0.004	9

[a] concentrations after mixing

[b] number of runs for which the values were averaged

Table A.2. Kinetic Data Obtained from the Stopped-Flow Experiments for the Reactions of Ni(II) with *t*-CHA Performed at 25 °C and $I = 0.010$ M ($NaClO_4$)

10^3 [Ni^{2+}]^a (M)	k_{obs} (s^{-1})	A_0	$A_{\infty, Ni}$	ΔA_{Ni}	n^b
pH = 5.43 (±0.01)					
1.09	26.6 ± 0.6	0.065 ± 0.002	0.154 ± 0.002	0.089 ± 0.002	8
2.06	27.1 ± 0.5	0.076 ± 0.010	0.249 ± 0.008	0.173 ± 0.007	11
3.12	28.8 ± 0.2	0.060 ± 0.006	0.300 ± 0.006	0.240 ± 0.008	11
5.14	32.6 ± 0.4	0.072 ± 0.010	0.439 ± 0.020	0.367 ± 0.013	16
10.3	41.3 ± 0.8	0.054 ± 0.020	0.580 ± 0.010	0.526 ± 0.007	9
15.4	51.0 ± 0.7	0.039 ± 0.010	0.695 ± 0.010	0.656 ± 0.010	11
pH = 6.30 (±0.01)					
1.0	6.82 ± 0.05	0.106 ± 0.005	0.621 ± 0.010	0.515 ± 0.005	11
2.0	8.94 ± 0.08	0.115 ± 0.008	0.826 ± 0.010	0.711 ± 0.006	10
3.0	11.10 ± 0.06	0.094 ± 0.004	0.852 ± 0.010	0.759 ± 0.010	9
5.0	15.3 ± 0.2	0.118 ± 0.010	1.059 ± 0.030	0.942 ± 0.030	10
8.0	22.3 ± 0.3	0.206 ± 0.020	1.207 ± 0.020	1.000 ± 0.010	10
10.0	27.4 ± 0.2	0.202 ± 0.020	1.266 ± 0.010	1.064 ± 0.020	9
15.0	35.6 ± 0.5	0.245 ± 0.030	1.335 ± 0.020	1.089 ± 0.030	11

Table A.2. Continued...

10^3 [Ni^{2+}]^a (M)	k_{obs} (s^{-1})	A_0	$A_{\infty, Ni}$	ΔA_{Ni}	n^b
pH = 6.70 (±0.01)					
1.09	6.13 ± 0.15	0.128 ±0.005	0.760 ± 0.003	0.632 ± 0.006	7
2.06	8.24 ± 0.10	0.133 ± 0.005	0.913 ± 0.010	0.780 ± 0.009	7
3.12	11.16 ± 0.08	0.181 ± 0.008	1.023 ± 0.010	0.842 ± 0.01	6
5.14	16.40 ± 0.2	0.144 ± 0.006	1.104 ± 0.007	0.960 ± 0.01	7
8.20	24.04 ± 0.3	0.173 ± 0.006	1.160 ± 0.06	0.987 ± 0.01	7
10.3	10.27 ± 0.7	0.209 ± 0.010	1.219 ± 0.005	1.009 ± 0.01	8
15.4	15.40 ± 1.0	0.206 ± 0.02	1.193 ± 0.004	0.987 ± 0.02	10

^{a}concentrations after mixing
^{b}number of runs for which the values were averaged

Table A.3. Kinetic Data Obtained from the Stopped-Flow Experiments for the Reactions of Ni(II) with 1-NHA Performed at 25 °C and $I = 0.010$ M ($NaClO_4$)

10^3 [Ni^{2+}]^a (M)	k_{obs} (s^{-1})	A_0	$A_{\infty, Ni}$	ΔA_{Ni}	n^b
pH = 5.70 (±0.01)					
2.0	22.3 ± 1.9	0.231 ± 0.01	0.294 ± 0.007	0.063 ± 0.006	15
3.0	23.2 ± 1.5	0.209 ± 0.005	0.304 ± 0.003	0.094 ± 0.005	18
4.0	24.2 ± 1.5	0.217 ± 0.008	0.334 ± 0.008	0.118 ± 0.006	25
5.0	25.2 ± 1.6	0.223 ± 0.008	0.364 ± 0.004	0.142 ± 0.007	18
8.0	29.6 ± 1.1	0.223 ± 0.010	0.416 ± 0.006	0.193 ± 0.007	21
10.0	31.0 ± 1.6	0.237 ± 0.020	0.462 ± 0.009	0.225 ± 0.01	19
15.0	37.0 ± 2.2	0.246 ± 0.020	0.520 ± 0.030	0.274 ± 0.01	26
pH = 6.00 (±0.01)					
1.0	11.5 ± 0.8	0.234 ± 0.005	0.296 ± 0.003	0.062 ± 0.005	8
2.0	12.5 ± 0.2	0.222 ± 0.004	0.340 ± 0.001	0.118 ± 0.004	8
3.0	15.0 ± 0.5	0.277 ± 0.040	0.415 ± 0.030	0.138 ± 0.010	7
4.0	15.0 ± 0.4	0.221 ± 0.005	0.404 ± 0.006	0.183 ± 0.007	5
5.0	16.8 ± 0.4	0.189 ± 0.007	0.400 ± 0.005	0.211 ± 0.008	16
8.0	21.1 ± 0.4	0.198 ± 0.008	0.460 ± 0.004	0.262 ± 0.008	9
10.0	22.7 ± 0.6	0.208 ± 0.014	0.497 ± 0.009	0.290 ± 0.008	11
15.0	30.1 ± 0.7	0.252 ±0.017	0.571 ±0.007	0.318 ± 0.010	11

Table A.3. Continued...

10^3 [Ni^{2+}][a] (M)	k_{obs} (s^{-1})	A_0	$A_{\infty, Ni}$	ΔA_{Ni}	n[b]
pH = 6.30 (±0.01)					
1.0	8.30 ± 0.2	0.222 ± 0.01	0.319 ± 0.006	0.097 ± 0.010	10
2.0	9.92 ± 0.30	0.213 ± 0.005	0.376 ± 0.006	0.162 ± 0.005	9
3.0	11.5 ± 0.30	0.224 ± 0.006	0.431 ± 0.008	0.207 ± 0.006	14
4.0	13.0 ± 0.2	0.221 ± 0.004	0.460 ± 0.003	0.238 ± 0.005	14
5.0	14.4 ± 0.2	0.221 ± 0.004	0.489 ± 0.002	0.268 ± 0.005	11
8.0	18.7 ± 0.4	0.239 ± 0.008	0.559 ± 0.010	0.321 ± 0.010	15
10.0	21.6 ± 0.5	0.243 ± 0.010	0.585 ± 0.008	0.342 ± 0.009	16
15.0	29.0 ± 0.6	0.252 ± 0.010	0.618 ± 0.10	0.365 ± 0.010	13

[a]concentrations after mixing
[b]number of runs for which the values were averaged

Table A.4. Kinetic Data Obtained from the Stopped-Flow Experiments for the Reactions of Ni(II) with BHA Performed at 25 °C and $I = 0.010$ M ($NaClO_4$)

10^3 [Ni^{2+}]^a (M)	k_{obs} (s^{-1})	A_0	$A_{\infty, Ni}$	ΔA_{Ni}	n^b
pH = 5.60 (±0.01)					
2.0	26.1 ± 1.8	0.091 ± 0.003	0.163 ± 0.001	0.073 ± 0.002	8
3.0	27.4 ± 1.1	0.092 ± 0.004	0.188 ± 0.002	0.095 ± 0.005	9
5.0	29.6 ± 0.4	0.070 ± 0.002	0.213 ± 0.001	0.142 ± 0.002	8
8.0	35.7 ± 0.8	0.087 ± 0.005	0.284 ± 0.002	0.197 ± 0.003	5
10.0	38.8 ± 0.6	0.098 ± 0.003	0.333 ± 0.006	0.235 ± 0.006	10
15.0	45.2 ± 0.9	0.066 ± 0.008	0.362 ± 0.005	0.296 ± 0.005	11
pH = 5.75 (±0.01)					
2.0	22.3 ± 0.7	0.109 ± 0.004	0.194 ± 0.002	0.085 ± 0.003	10
3.0	24.2 ± 1.2	0.124 ±0.020	0.235 ± 0.008	0.111 ± 0.009	10
5.0	25.4 ± 0.8	0.082 ± 0.006	0.252 ± 0.002	0.170 ± 0.006	13
8.0	30.6 ± 1.0	0.101 ± 0.010	0.326 ± 0.007	0.225 ± 0.006	17
10.0	35.9 ± 0.8	0.135 ± 0.005	0.386 ± 0.004	0.251 ± 0.003	7
15.0	41.1 ± 0.7	0.100 ± 0.020	0.393 ± 0.005	0.293 ± 0.020	15

Table A.4. Continued...

10^3 [Ni^{2+}][a] (M)	k_{obs} (s^{-1})	A_0	$A_{\infty, Ni}$	ΔA_{Ni}	n[b]
pH = 6.00 (±0.01)					
2.0	14.30 ± 0.2	0.087 ± 0.004	0.221 ± 0.003	0.134 ± 0.002	5
3.0	15.94 ± 0.4	0.085 ± 0.003	0.265 ± 0.002	0.180 ± 0.004	10
5.0	18.64 ± 0.6	0.056 ± 0.006	0.304 ± 0.005	0.248 ± 0.009	10
8.0	23.82 ± 1.2	0.067 ± 0.010	0.375 ± 0.004	0.308 ± 0.010	8
10.0	28.01 ± 0.6	0.100 ± 0.006	0.431 ± 0.003	0.332 ± 0.007	6
15.0	34.35 ± 0.9	0.056 ± 0.007	0.439 ± 0.004	0.383 ± 0.007	8
pH = 6.30 (±0.01)					
1.0	8.51 ± 0.20	0.138 ± 0.003	0.271 ± 0.004	0.132 ±0.003	8
2.0	9.92 ± 0.13	0.115 ± 0.001	0.315 ± 0.002	0.200 ± 0.002	8
3.0	11.6 ± 0.24	0.114 ± 0.001	0.315 ± 0.002	0.200 ± 0.002	8
5.0	14.6 ± 0.26	0.084 ± 0.010	0.406 ± 0.020	0.322 ± 0.006	9
8.0	20.2 ± 0.2	0.102 ± 0.005	0.483 ±0.004	0.380 ± 0.007	8
10.0	25.4 ± 0.5	0.128 ± 0.007	0.523 ± 0.007	0.395 ± 0.009	9
15.0	32.1 ± 0.5	0.095 ± 0.010	0.511 ±0.010	0.416 ± 0.001	6

[a]concentrations after mixing

[b]number of runs for which the values were averaged

Table A.5. Kinetic Data Obtained from the Stopped-Flow Experiments for the Reactions of Ni(II) with PMBHA Performed at 25 °C and $I = 0.010$ M ($NaClO_4$)

10^3 [Ni^{2+}]^a (M)	k_{obs} (s^{-1})	A_0	$A_{\infty, Ni}$	ΔA_{Ni}	n^b
pH = 5.60 (±0.01)					
4.0	39.5 ± 1.9	0.050 ± 0.003	0.121 ± 0.001	0.070 ± 0.004	7
5.0	37.03 ± 1.0	0.046 ± 0.009	0.130 ± 0.006	0.084 ± 0.008	10
8.0	43.86 ± 0.7	0.054 ± 0.009	0.180 ± 0.004	0.126 ± 0.005	10
10.0	46.0 ± 1.4	0.070 ± 0.006	0.201 ± 0.002	0.131 ± 0.005	11
15.0	54 ± 1	0.053 ± 0.012	0.247 ± 0.003	0.195 ± 0.009	9
pH = 6.00 (±0.01)					
1.0	16.1 ± 0.7	0.110 ± 0.070	0.140 ± 0.060	0.030 ± 0.010	7
2.0	17.6 ± 0.9	0.074 ± 0.004	0.158 ± 0.004	0.083 ± 0.006	13
3.0	18.8 ± 0.4	0.077 ± 0.003	0.194 ± 0.002	0.116 ± 0.002	9
5.0	19.9 ± 0.4	0.081 ± 0.004	0.222 ± 0.006	0.141 ± 0.006	11
8.0	23.3 ± 0.6	0.082 ± 0.003	0.247 ± 0.004	0.165 ± 0.005	12
10.0	25.9 ± 0.7	0.087 ± 0.005	0.337 ± 0.001	0.249 ± 0.005	10

Table A.5. Continued...

10^3 [Ni^{2+}]^a (M)	k_{obs} (s^{-1})	A_0	$A_{\infty, Ni}$	ΔA_{Ni}	n^b
pH = 6.30 (±0.01)					
1.0	9.1 ± 0.2	0.080 ± 0.006	0.153 ± 0.006	0.071 ± 0.004	10
2.0	11.5 ± 0.3	0.093 ± 0.008	0.217 ± 0.007	0.123 ± 0.004	12
3.0	13.7 ± 0.3	0.10 ± 0.010	0.260 ± 0.004	0.152 ± 0.009	16
5.0	14.2 ± 0.2	0.074 ± 0.008	0.270 ± 0.010	0.200 ± 0.009	12
8.0	15.1 ± 0.2	0.071 ± 0.006	0.320 ± 0.010	0.250 ± 0.020	12
10.0	20.1 ± 0.4	0.078 ± 0.005	0.361 ± 0.004	0.282 ± 0.006	11
15.0	33 ± 1	0.120 ± 0.020	0.440 ± 0.070	0.310 ± 0.020	13

^{a}concentrations after mixing
^{b}number of runs for which the values were averaged

Table A.6. Kinetic Data Obtained from the Stopped-Flow Experiments for the Reactions of Ni(II) with *N*-PBHA Performed at 25 °C and $I = 0.010$ M ($NaClO_4$)

10^3 [Ni^{2+}]^a (M)	k_{obs} (s^{-1})	A_0	$A_{\infty, Ni}$	ΔA_{Ni}	n^b
pH = 5.40 (±0.01)					
1.925	6.842 ± 0.2	0.10693	0.16750	0.06057	5
4.815	8.844 ± 0.1	0.10499	0.22110	0.11611	5
9.630	12.32 ± 0.3	0.10529	0.27084	0.16555	5
14.44	16.78 ± 0.07	0.27815	0.30103	0.02288	5
pH = 5.75 (±0.01)					
0.963	3.662 ± 0.2	0.11234	0.17653	0.06419	5
1.925	4.238	0.11698	0.22185	0.10487	5
2.895	5.000	0.11661	0.24795	0.13134	5
4.815	8.844 ± 0.1	0.11174	0.28735	0.17561	5
7.225	8.797 ± 0.3	0.11725	0.31426	0.19701	5
9.630	12.32 ± 0.3	0.11812	0.34294	0.22482	5
12.04	12.26 ± 0.1	0.12431	0.35853	0.23422	5
14.44	13.91 ± 0.2	0.12684	0.36856	0.24171	5

Table A.6 Continued...

10^3 [Ni^{2+}]^a (M)	k_{obs} (s^{-1})	A_0	$A_{\infty, Ni}$	ΔA_{Ni}	n^b
pH = 6.05 (±0.01)					
0.963	2.880 ± 0.03	0.10983	0.20901	0.09919	5
1.925	3.768 ± 0.01	0.10897	0.25727	0.14830	5
4.815	6.338 ± 0.02	0.11647	0.32514	0.20867	5
9.630	10.90 ± 0.08	0.12984	0.37059	0.24075	5
12.04	13.94 ± 0.8	0.12362	0.36754	0.24392	5
14.44	14.90 ± 0.1	0.13675	0.39469	0.25795	5
pH = 6.34 (±0.01)					
0.963	2.663 ± 0.002	0.11954	0.26680	0.14735	5
1.925	3.880 ± 0.04	0.12072	0.31337	0.19264	5
4.815	7.160 ± 0.05	0.13216	0.36452	0.23236	5
9.630	13.05 ± 0.3	0.13349	0.38722	0.25373	5
12.04	15.3 ± 0.2	0.13969	0.39469	0.25500	5
14.44	17.60 ± 0.03	0.15152	0.39794	0.24642	5

Table A.6. Continued...

10^3 [Ni^{2+}][a] (M)	k_{obs} (s^{-1})	A_0	$A_{\infty, Ni}$	ΔA_{Ni}	n[b]
pH = 5.75 (±0.01)					
0.963	2.896 ± 0.003	0.13678	0.31966	0.18289	5
1.925	4.692 ± 0.1	0.13854	0.35754	0.21899	5
2.895	6.518 ± 0.1	0.13563	0.37059	0.23496	5
4.815	10.29 ± 0.3	0.14714	0.38722	0.24007	5
7.225	14.37 ± 0.1	0.15526	0.39577	0.24051	5
9.630	18.92 ± 0.1	0.18369	0.40012	0.21643	5
12.04	22.98 ± 0.02	0.16550	0.40340	0.23790	5
14.44	25.12 ± 3.6	0.17928	0.41794	0.23865	5

[a]concentrations after mixing
[b]number of runs for which the values were averaged